THE UNIVERSITY OF MANITOBA

LATERAL STABILITY OF UNRESTRAINED REINFORCED CONCRETE BEAMS

BY

ALLEN LESLIE STRANG

A THESIS

SUBMITTED TO THE FACULTY OF GRADUATE STUDIES

IN PARTIAL FULFILLMENT OF THE REQUIREMENTS OF THE DEGREE

OF

MASTER OF SCIENCE

DEPARTMENT OF CIVIL ENGINEERING

WINNIPEG, MANITOBA

APRIL, 1976

"LATERAL STABILITY OF UNRESTRAINED REINFORCED CONCRETE BEAMS"

by

ALLEN LESLIE STRANG

A dissertation submitted to the Faculty of Graduate Studies of the University of Manitoba in partial fulfillment of the requirements of the degree of

MASTER OF SCIENCE

ABSTRACT:

The lateral stability of reinforced concrete beams was investigated experimentally and analytically. A total of 14 small scale rectangular beams were load tested with support conditions including unrestrained cantilever, simple-support and overhung. Of the 14 test specimens, 11 failed by lateral buckling.

It is concluded that current building code provisions which use the slenderness ratio L/b are incorrect and that the ratio Ld/b^2 should be used. For unrestrained cantilevers, a maximum value of $Ld/b^2 = 600$ is recommended pending further investigation.

ACKNOWLEDGEMENTS

The experimental portion of this study was carried out in the Civil Engineering Testing Laboratory at the University of Manitoba with the financial assistance of the National Research Council of Canada.

The writer wishes to express his thanks to all who assisted him in the work and especially to G.A. Morris, his Advisor, to R.B. Pinkney and A.H. Shah for their advice, to Sandy McKinnon who typed the final manuscript and to Victoria for her encouragement.

PAGE

CONTENTS

LIST OF FIGURES

LIST OF TABLES

LIST OF PHOTOGRAPHS

NOTATION:

X, Y, Z	- Global axes of a beam, corresponding to the unloaded position
ξ, η, ζ	- Local axes of a beam cross-section in the deformed position
A	- Area
A_s	- Area of tensile reinforcement
A_s'	- Area of compressive reinforcement
A_t	- Area of one leg of a vertical stirrup
B	- Lateral flexural rigidity ($B = EI_\eta$)
B_1	- Vertical flexural rigidity ($B_1 = EI_\xi$)
C	- Torsional rigidity
C_w	- Warping rigidity
E	- Young's Modulus (Elastic modulus)
E_s	- Elastic modulus of steel
E_{sec}	- Secant modulus of concrete
F	- Force
G	- Modulus of rigidity
G_c	- Modulus of rigidity of concrete
G_c'	- Reduced modulus of rigidity of concrete
G_s	- Modulus of rigidity of steel
I	- Moment of inertia (second moment of area)
I_{sy}	- Moment of inertia of the reinforcement about the Y Axis

I_1, I_2	- Moment of inertia of the reinforcement (about the Y Axis) at one face (top or bottom) of the beam ($I_{sy} = I_1 + I_2$)
I_ξ	- Moment of inertia in the strong direction of the beam
I_ζ	- Moment of inertia in the weak direction
L	- Length of a beam
M	- Bending moment
M_X, M_Y, M_Z	- Bending moments in the directions of the global axes of the beam
M_ξ M_η M_ζ	- Bending moments with respect to the local axes
M_e	- Moment required to produce an extreme fiber stress of $0.85f_c'$ on a transformed elastic section having a modular ratio n = 15
M_u	- Ultimate flexural moment
P	- Load
P_{cr}	- Critical lateral buckling load of a beam
P^*_{cr}	- Ideal critical load, at $0.85f_c'$
S	- Scale factor, ratio of prototype size to model size
a	- Depth of the rectangular concrete stress block at ultimate moment
b	- Width of a rectangular beam
b_s	- Width out to out of reinforcement
b_1	- Width enclosed by a stirrup

c	- Depth from compressive face to neutral axis at ultimate moment
d	- Depth of a rectangular beam from compressive face to centroid of tensile reinforcement
d'	- Total depth of a rectangular beam
d_1	- Depth enclosed by a stirrup
f'_c	- Compressive strength of a 3" x 6" concrete cylinder specimen
f_T	- Stress in the tensile reinforcement in an over-reinforced flexural member at ultimate moment
f_{yC}	- Yield stress in the compressive reinforcement
f_{yT}	- Yield stress in the tensile reinforcement
h_1	- Height of load application above or below the centroid of a beam
h	- Distance between centroids of tensile and compressive reinforcement
k_1, k_2 --	- Constants
n	- Modular ratio of concrete ($n = E_s/E_{sec}$)
p	- Tensile reinforcement ratio ($p = (A_s - A'_s)/bd$)
p_s	- Pitch of vertical stirrups
q	- A numerical factor dependent upon f'_c in the expression for "a"
s	- A measure of length
t_s	- Thickness of reinforcement parallel to Y direction
u, v	- Deflections of a beam in the X and Y directions respectively

$\bar{y}$	- Distance from the compressive face of a beam to the neutral axis of its transformed section
σ	- Stress
σ_{cr}	- Critical stress at lateral buckling
σ_s	- Average stress in the tensile reinforcement in a transformed section
ε	- Strain
ε_s	- Tensile reinforcement strain
ε_s'	- Compressive reinforcement strain
Ø	- Twist angle about the Z axis
Δ	- Deflection
ν	- Poisson's ratio
β	- A factor dependent upon d'/b
γ	- A factor dependent upon d_1/b_1

CHAPTER 1

INTRODUCTION

The introduction of high strength concrete and reinforcement have made the use of deep, slender concrete beam elements practical and economical in many structures. At some point, the slenderness of such beams is limited by lateral instability, but the phenomenon is referred to only briefly in available building codes(1)(2). The commentary on the ACI Code suggests that there is no problem of lateral instability for beams of reasonable proportions. The code writers appear, in this regard, to be thinking in terms of beams supported at two or more points and provided with ample lateral restraint. In the case of cantilevered beams, the restraint is considerably less and lateral instability may become a problem. This study was undertaken to explore the effects of lateral instability on the load-carrying capacity of slender cantilevered concrete beams.

A review of available literature indicates that very little has been written on the subject of lateral instability of concrete beams in general and almost nothing on cantilevered concrete beams. All of the experimental data reported have been for simply-supported beams tested under various loading conditions. As a result of the lack of experimental data for cantilevered beams, it was decided to proceed with an experimental program with the objective of measuring the lateral buckling loads for cantilevered concrete beams and correlating these buckling loads with parameters related to the beam geometry.

The study was carried out using fourteen small-scale reinforced concrete beam specimens. Ten specimens were loaded as laterally-unsupported cantilevers. Two were tested as overhung beams (laterally unsupported beams with loaded overhanging ends) to illustrate the most unstable case likely to be found in practice. Finally, two were tested as center-point-loaded simply-supported beams (as models of a larger beam referred to in the literature).

Initially, the study was to be confined to the consideration of under-reinforced beams, to be consistent with the prevailing ultimate strength design philosophy that all flexural members should fail in a ductile manner. A shortage of mild steel reinforcement forced a change, however, and some of the test specimens were over-reinforced. As a second objective, an attempt was made to establish geometric limits (in the form of a slenderness ratio) which would preclude a lateral buckling failure before a flexural failure occurred.

1.1 Relationship to Previous Studies

A survey of literature on the subject of lateral instability of beams was prepared by Lee[3]. This literature survey listed 142 articles beginning with a thesis written by Prandtl in 1899, considered to be the original work on the subject, and continued to the end of 1959. The survey dealt with metal beams under various loadings but did not consider concrete beams.

The first paper dealing with the stability of concrete beams, Marshall[4] gave a theoretical treatment of the problem without experimental results. Marshall concluded that code provisions which treat lateral instability of beams on the basis of the ratio L/b are inadequate; instead, the ratio Ld/b^2 should be used. The most recent codes[1][2] use the L/b criterion. (L = Length, d = depth, b = width)

The first record of test data for slender concrete beams was published in 1954 by Vasarhelyi and Turkalp[5]. Three beams with L/b ratios of 36 were tested. Although lateral deflections were observed, Vasarhelyi and Turkalp concluded that the strengths of their beams were not reduced by lateral instability.

Hansell and Winter[6] published the results of tests of ten beams with L/b ratios in the range 28.8 to 86.4. The specimens were tested as simple beams, loaded at their quarter points. The load points were designed to allow lateral deflection of the beam. No reduction was found in the ultimate strengths of the beams, and Hansell and Winter concluded that no lateral instability had occurred. They demonstrated that lateral instability occurred at an L/b ratio of 106 and concluded that the then current code provisions, requiring L/b not to exceed 32, were too restrictive. They further demonstrated that the secant modulus E_{sec}, corresponding to the extreme fibre strain, should be used for lateral instability computations for concrete beams.

Smith[7], in a discussion of Hansell and Winter's paper, reported on the testing of twelve simply-supported center-point-loaded microconcrete beams. His discussion was the first published report of concrete beam specimens which failed by lateral buckling. In addition, he discussed lateral stability of the test specimens in terms of the slenderness ratio Ld/b^2 proposed by Marshall(4).

Siev(8) reported on the testing of ten beams, six of which were rectangular and four of which were L-shaped in cross-section. Lateral instability was observed in all of the tests. In addition, Siev carried out a theoretical investigation of the flexural and torsional rigidity of beams in various states of loading, ranging from elastic uncracked to plastic cracked sections.

Sant and Bletzacker(9) tested eleven reinforced concrete beams with L/b ratios of 96 and d/b ratios in the range 3.78 to 12.45. The specimens were simply-supported and center-point-loaded, with rotation and lateral deflection allowed at the load point. Sant and Bletzacker concluded that there was a critical slenderness ratio of the form Ld/b^2 (and dependent upon the material properties and loading configuration) above which lateral buckling occurred. They suggested that the slenderness of the beam should be limited in terms of the maximum reinforcement ratio and plotted this criterion in the form of an interaction curve relating the slenderness ratio Ld/b^2 to the reinforcement ratio and yield strength, $(p)(f_{sy})$. Sant and Bletzacker plotted their results as well as those of Smith(7) and Hansell and Winter(6) on the interaction diagram and added those of Siev(8) in the discussion in a later publication(10).

Two specimens tested in the present study were scale models of Sant and Bletzacker's specimen B_{24}-1. They were used to determine the similarity between the results of model tests and prototype behaviour of laterally buckling beams.

In 1967, Massey[11] published the results of the tests of thirteen specimens which were simply-supported and loaded in pure bending. Of the thirteen specimens, eleven buckled laterally. Massey developed analytical expressions for the lateral flexural rigidity, the torsional rigidity and the warping rigidity of slender rectangular concrete beams and determined the reduced modulus of rigidity of concrete as a function of the bending moment. Massey's procedures are used later in this study to compute the theoretical buckling loads of the test specimens.

In a literature survey[12] published in 1969, Marshall analyzed the published results of Hansell and Winter[6], Sant and Bletzacker[9], Massey[11] and others not previously published. Marshall concluded, as he had done earlier[4], that lateral stability was a function of the slenderness ratio Ld/b^2 and, in addition, that the bending moment at lateral buckling was a function of the ratio $f_c' b^3 d/L$ (in which f_c' is the compressive strength of the concrete).

Marshall[4][12], Smith[7] and Sant and Bletzacker[9] have pointed out that the slenderness ratio for the lateral buckling of rectangular beams should be written in the form Ld/b^2 rather than in the form L/b used in current building codes[1][2]. Their argument is as follows:

In simplified form, ignoring the warping rigidity, the elastic critical load, at which a rectangular beam buckles laterally, is given by[13]:

$$P_{cr} = K_1 \sqrt{BC}/L^2 \quad \text{--} \quad (1.1)$$

The constant k_1 is dependent upon the loading condition and the amount of lateral restraint, having the value 4.013 for an unrestrained tip-loaded cantilever and 16.94 for an unrestrained center-point-loaded simply-supported beam. The lateral flexural rigidity is given by:

$$B = k_2 d\ b^3 E_{sec} \quad \text{--} \quad (1.2)$$

The constant k_2 has the value 1/12 for an elastic uncracked section in which the reinforcement is ignored. The cross-sectional dimensions are given by b and d, and the secant modulus E_{sec} is used after Hansell and Winter[6]. The torsional rigidity is given by:

$$C = k_3 d\ b^3 G \quad \text{--} \quad (1.3)$$

The constant k_3 has the value 1/3 for a very narrow rectangular cross-section and G is the modulus of rigidity. For simplicity, the modulus of rigidity is assumed to equal:

$$G = k_4 E_{sec} \quad \text{--} \quad (1.4)$$

In which k_4 is an arbitrary constant. By substituting Equations (1.2) through (1.4) into Equation (1.1), and collecting all constant terms into one term, (k_5), the following is obtained.

$$P_{cr} = k_5 b^3 d\ E_{sec}/L^2 \qquad (1.5)$$

If the usual expression for flexural stress at any point in the beam (My/I) is written in terms of the buckling load, the following expression results:

$$\sigma_{cr} = k_6 P_{cr} L/k_7 bd^2 \qquad (1.6)$$

The constant k_6 depends on the loading configuration, and is 1.0 for a cantilever. The denominator is in the form of a section modulus (k_7 reflects the amount of cracking). By combining Equations (1.5) and (1.6) and writing all constant terms into one constant, (k_8), the stress at lateral buckling is given by:

$$\sigma_{cr} = \frac{k_8 E_{sec}}{Ld/b^2} \qquad (1.7)$$

Equation (1.7) indicates that the critical stress at lateral buckling is a function of the secant modulus of the concrete and the loading and restraint geometry (as the summation of the effects of the constant terms) and the slenderness ratio Ld/b^2. It is based upon assumed linear behaviour, which assumption is inaccurate for reinforced concrete. It does, however, point out the nature of the governing geometric parameter for the discussion of lateral stability of rectangular beams.

Sant and Bletzacker assumed an under-reinforced rectangular cross-section and argued that the member should reach its ultimate flexural moment at or before the instant of lateral buckling. For these conditions, Equation (1.6) is rewritten with the reinforcement yield stress as the critical stress and the section modulus in terms of the tensile reinforcement, as follows:

$$f_y = k_5 PL/(k_9 d)(bdp) \quad (1.8)$$

In Equation (1.8), the term $(k_9 d)$ is the distance between the tensile and compressive stress resultants and the parameter p is the tensile reinforcement ratio (as a fraction of the cross-section area). Combining Equations (1.5) and (1.8):

$$pf_y = \frac{k_{10} E_{sec}}{Ld/b^2} \quad (1.9)$$

Equation (1.9) relates the reinforcement ratio and yield strength to the slenderness ratio of the beam. The term k_{10} reflects the loading and restraint geometry and the term E_{sec} reflects the concrete properties. This equation provides the basis for a code provision which limits the tensile reinforcement as a function of the beam slenderness.

In contrast to Sant and Bletzacker, Marshall(4)(12) approached the problem on the assumption of a balanced section and argued that the moment in the member should be limited to the point at which the concrete reached its compressive strength at the instant of lateral buckling. This approach is not well suited to use with the current ultimate strength design philosophy which requires that flexural members be under-reinforced.

Some work has been carried out to determine the laterally deflected shape of unrestrained elastic cantilevers. Piotrowski and Zihrul[14] used Moiré photography techniques and found that their results compared favourably with a numerical example published by Swann and Godden[15]. Woolcock and Trahair[16] published deflection measurements for a narrow rectangular cantilever, an I-shaped cantilever and an I-shaped simply-supported beam, all of steel. They also published theoretical results which agreed closely with the measured deflections.

Numerical and analytical analyses of the problem of lateral buckling of elastic beams have been published by several authors[13][15][16]. The linear-elastic analysis given by Timoshenko and Gere[13] was used as a basis for the theoretical discussion in this study.

1.2 Assumptions and Limitations in the Present Study

The experimental portion of this study consisted of the load testing of ten small-scale reinforced concrete members as laterally unsupported cantilevers and two as overhung beams. The cross-sections were kept constant and only the length was changed. The experimental work was, therefore, limited to a very small portion of the large range of possibilities of unstable beams.

The experimental data used in this study are based upon the testing of small-scale beams. It is assumed that the conclusions drawn from these data apply to full-sized members with similar loading and restraint conditions. Such an assumption is valid only if the test specimens are flexurally similar models of the full-sized (prototype) members. The general theory of model similitude has been presented by Charlton(17) and the modelling of reinforced concrete structures has been discussed by Harris, Sabnis and White(18) and Petri(19).

In a direct model, similar (or identical) materials are used and all linear dimensions are scaled by the same factor. That is:

$$L_i = SL_i' \quad \text{---} \quad (1.10)$$

In Equation (1.10), S is the scale factor, the primed (') symbol refers to the model and the subscript i refers to any particular dimension. For flexural similarity, the deflections of the model and prototype are related by the same scale factor:

$$\Delta_i = S\Delta_i' \quad \text{---} \quad (1.11)$$

From model similitude theory(17), it can be demonstrated that the condition of flexural similarity occurs only when the strain in the model equals the prototype strain at every point.

$$\varepsilon_i = \varepsilon_i' \quad \text{---} \quad (1.12)$$

For Equation (1.12) to be valid, the elastic modulii (Young's modulus, the modulus of rigidity, the secant modulus and Poisson's ratio) and the tensile and compressive strengths for the model and prototype materials must be equal. In other words, the materials must have identical stress-strain behaviour and strength. With the exception of the concrete stress-strain curve, in which case the model concrete curve was flatter than generally observed prototype curves, the properties of the materials used in this study approximated these requirements. It can be shown that, to a first approximation, the conditions of flexural similarity are met with stress-strain curves of similar shape. Thus the differences in the concrete stress-strain curves have not been considered, and flexural similarity has been assumed.

It can also be shown that the model and prototype loads (forces) are related by:

$$P = S^2 P' \qquad (1.13)$$

By using Equations (1.10) and (1.13), and by applying dimensional analysis to the relationships previously developed it is possible to relate the data derived from small-scale tests to full-sized structures. In particular, Equation (1.9) will be used in Chapter 6 in the discussion of a design criterion. Since the left side of this equation has dimensions of force/length^2, the scale factor S cancels out when Equations (1.10) and (1.13) are applied. Thus, Equation (1.9) is unaltered by scale and the experimental data can be applied to any size of member, assuming the conditions of flexural similarity are met.

CHAPTER 2

THEORETICAL CONSIDERATIONS

This chapter discusses the elastic lateral stability of an unrestrained cantilevered beam and the ultimate flexural strength of a reinforced concrete beam.

In Section 2.1, the equation giving the lateral buckling load of an unrestrained, homogeneous, linearly elastic cantilever is developed. In Section 2.2, the rigidity co-efficients required to compute the buckling load are developed for a reinforced concrete member. The combined result of Sections 2.1 and 2.2 is an elastic analysis modified to approximate non-homogeneous non-linear inelastic behaviour. Such an approach has the disadvantage that the computed buckling loads will be inaccurate to the extent that the simplifying assumptions are inaccurate. The analysis of the actual buckling behaviour of a reinforced concrete beam is complex in the extreme and has not been attempted in this study. The modified elastic analysis is used, in Chapter 5, to compute buckling loads for the test specimens.

The final section in the chapter presents the analysis of the ultimate flexural strength of a reinforced concrete beam to give a basis for the computation, in Chapter 5, of the ultimate flexural capacity of the test specimens.

2.1 Lateral Buckling of an Unrestrained Cantilevered Beam

An unrestrained cantilevered beam is one which is fixed at one end and free to translate and rotate along the remainder of its length. This discussion is limited to the case of an elastic beam of uniform cross-section which is loaded through its centroid at the free end and which is initially straight, as shown in Figure 2.1. The co-ordinate system shown has its origin at the centroid of the cross-section at the end. The Z-axis is coincident with the longitudinal axis of the beam and the X and Y axes are coincident with the principal axis of the cross-section.

The beam is subjected to a load P at its free end and a small lateral deflection is assumed, as shown in the figure. At some distance z from the origin, a section mn is taken and a local co-ordinate system drawn with the ζ-axis tangent to the deflected beam axis and the ξ and η axes coincident with the principal axes of the cross-section. The twist angle ϕ about the Z-axis is shown positive and, as a result, the deflection components u and v in the X and Y directions respectively are negative.

A free body of the beam segment to the right of section mn is shown in Figure 2.1(b). The moments M_ξ, M_η, and M_ζ acting on the left end of the segment are shown in the positive directions assumed by Timoshenko and Gere(13). Since the deflections are assumed to be small, the curvature in the ξ-ζ plane is assumed equal to the curvature in the X-Z plane and the curvature in the η-ζ plane is assumed equal to that in

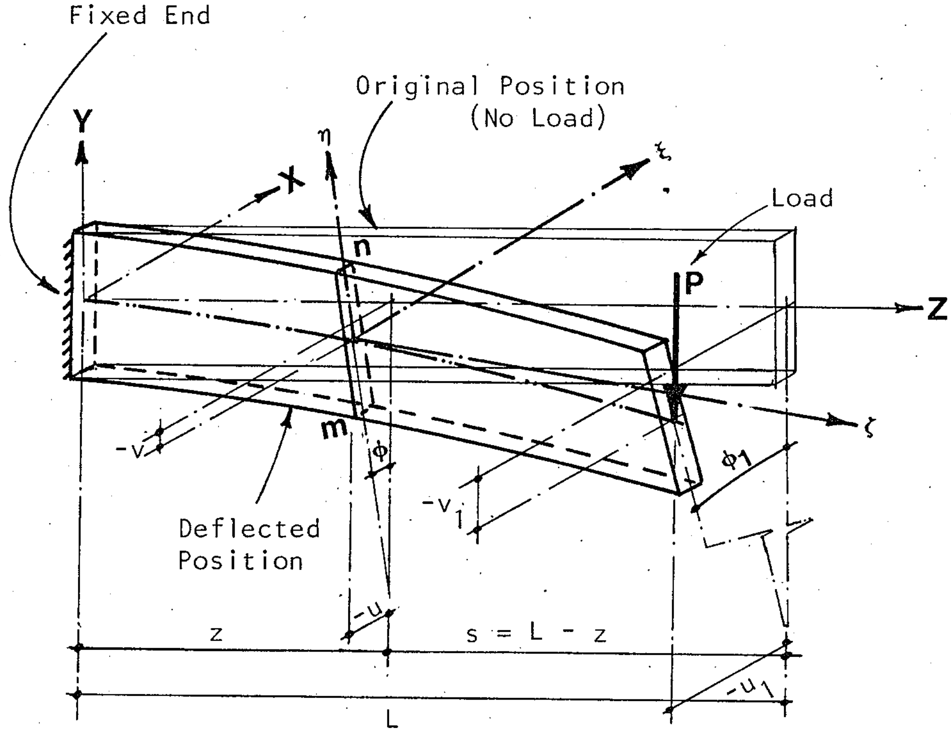

DEFLECTED CONFIGURATION

(a)

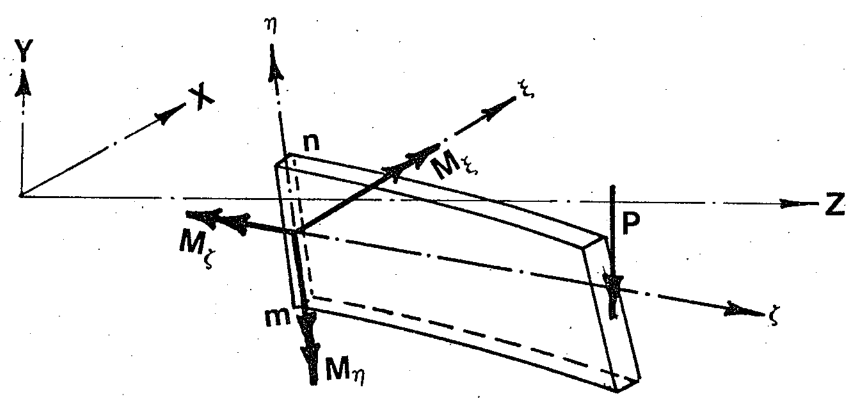

FORCES ACTING ON A BEAM SEGMENT

(b)

LATERAL BUCKLING OF AN UNRESTRAINED CANTILEVERED BEAM

FIGURE 2.1

the Y-Z plane. The equations of bending of the beam segment in Figure 2.1(b) then become[13]:

$$B_1 \frac{d^2v}{dz^2} = M_\xi \qquad (2.1)$$

$$B \frac{d^2u}{dz^2} = M_\eta \qquad (2.2)$$

$$C \frac{d\phi}{dz} - C_w \frac{d^3\phi}{dz^3} = M_\zeta \qquad (2.3)$$

Equations (2.1) and (2.2) are derived from beam bending theory. The term B_1 is the strong-direction bending rigidity (EI_ξ) and the term B is the weak-direction bending rigidity (EI_η). Equation (2.3) is derived from torsional theory. The term C is the St Venant torsional rigidity and the term C_w is the warping rigidity.

Considering the free body in Figure 2.1(b) and taking moments in the directions of the X, Y and Z axes at the centroid of the cut cross-section, the following are obtained:

$$M_X = -P(L - z) \qquad (2.4)$$

$$M_Y = 0 \qquad (2.5)$$

$$M_Z = P(-u_1 + u) \qquad (2.6)$$

Again, the moments are taken positive in the directions assumed by Timoshenko and Gere, in which M_X and M_Y are positive when they produce curvatures such that the normal to the concave side points in the positive direction of the respective axis and M_Z is positive when it rotates the cross-section clockwise. For small values of ϕ, u and v, the X-, Y- and Z- axes are related to the ξ-, η- and ζ- axes by the direction cosines given in Table 2.1.

Table 2.1

Direction Cosines Relating Global and Local Axes

	X	Y	Z
ξ	1	ϕ	$-\frac{du}{dz}$
η	$-\phi$	1	$-\frac{dv}{dz}$
ζ	$\frac{du}{dz}$	$\frac{dv}{dz}$	1

Using these direction cosines, considering the assumed positive directions and ignoring second-order small quantities, the following expressions are obtained for the moment components in the local co-ordinate system:

$$M_\xi = -P(L - z) \quad \text{------------} \quad (2.7)$$

$$M_\eta = -P(L - z)\phi \quad \text{------------} \quad (2.8)$$

$$M_\zeta = P(L - z)\frac{du}{dz} - P(u_1 - u) \quad \text{------------} \quad (2.9)$$

Substituting Equations (2.7) to (2.9) into Equations (2.1) to (2.3), the following expressions are obtained:

$$B_1 \frac{d^2v}{dz^2} + P(L - z) = 0 \quad \text{------------} \quad (2.10)$$

$$B \frac{d^2u}{dz^2} + P(L - z)\phi = 0 \quad \text{------------} \quad (2.11)$$

$$C_w \frac{d^3\phi}{dz^3} - C \frac{d\phi}{dz} + P(L - z) \frac{du}{dz} - P(u_1 - u) = 0 \quad \text{---------------} \quad (2.12)$$

To obtain an expression for the angle of twist, Equation (2.12) is differentiated with respect to "z" and the result combined with Equation (2.11). The result is as follows:

$$C_w \frac{d^4\phi}{dz^4} - C \frac{d^2\phi}{dz^2} + P(L - z) \frac{d^2u}{dz^2} = 0 \quad \text{------------------------} \quad (2.13)$$

From Equation (2.11):

$$\frac{d^2u}{dz^2} = - \frac{P(L - z)\phi}{B} \quad \text{--} \quad (2.14)$$

Substituting (2.14) into (2.13), the following expression results:

$$C_w \frac{d^4\phi}{dz^4} - C \frac{d^2\phi}{dz^2} - \frac{P^2(L - z)^2\phi}{B} = 0 \quad \text{-------------------------} \quad (2.15)$$

To simplify Equation (2.15), the variable $s = (L - z)$ is introduced, resulting in:

$$\frac{d^4\phi}{ds^4} - \frac{C}{C_w} \frac{d^2\phi}{ds^2} - \frac{P^2s^2\phi}{C_wB} = 0 \quad \text{----------------------------------} \quad (2.16)$$

For the case of the unrestrained cantilevered beam shown in Figure 2.1(a), the following boundary conditions apply to Equation (2.16):

$$\text{At } s = 0; \quad M_\zeta = 0 = C \frac{d\phi}{ds} - C_w \frac{d^3\phi}{ds^3} \quad \text{--------------------------} \quad (2.17)$$

$$\frac{d^2\phi}{ds^2} = 0 \quad \text{--} \quad (2.18)$$

$$\text{At } s = L; \quad \phi = 0 \qquad (2.19)$$

$$\frac{d\phi}{ds} = 0 \qquad (2.20)$$

To obtain the critical load at which the beam buckles laterally, Equation (2.16) must be solved for the boundary conditions in Equations (2.17) to (2.20). Timoshenko and Gere[13] give an approximate solution, for large values of $\frac{L^2C}{C_w}$ as:

$$P_{cr} = \frac{4.013\sqrt{BC}}{\left\{1-\sqrt{\frac{C_w}{L^2C}}\right\}^2 L^2} \qquad (2.21)$$

Equation (2.21) gives the load P_{cr} at which an unrestrained beam buckles laterally, in terms of the length L, the lateral flexural rigidity B, the torsional rigidity C and the warping rigidity C_w. Expressions for the three rigidity terms are developed in the following section.

For the case of the overhung beams, Equation (2.21) may be used to compute the buckling load by introducing the concept of effective length. Kerensky, Flint and Brown[20] give the effective lengths of cantilevered beams with various types of restraint using the effective length of an unrestrained cantilever as 1.0L. For the case of the overhung beam, they give an effective length of 2.7L based upon a theoretical analysis and of

2.95L based upon test measurements.

For the simply-supported beam, the development of the critical load equation is similar to that for the cantilevered beam. Timoshenko and Gere[13] give the following solution, for a narrow rectangular cross-section in which the warping rigidity is assumed to be zero, and for loading through the centroid at mid-span as:

$$P_{cr} = 16.94 \frac{\sqrt{BC}}{L^2} \quad \text{(2.22)}$$

For non-zero values of the warping rigidity, Timoshenko and Gere provide a table of factors to be used in place of the 16.94 multiplier.

2.2 Parameters in the Critical Load Equation

To determine the critical buckling load for any given beam, it is necessary to compute the values of the three rigidity terms, B, C and C_w for substitution into Equation (2.21) or (2.22). In the sections which follow, expressions developed by Massey[11] for the three terms are used.

2.2.1 Lateral Flexural Rigidity - B

On the assumption that the concrete below the neutral axis does not contribute to the lateral flexural rigidity, Massey[11] gives the following expression for B:

$$B = \frac{\bar{y}b^3}{12} E_{sec} + \sum I_{sy} E_s \quad \text{(2.23)}$$

Where:

$\bar{y}$ = the depth from the compressive face of the beam to the neutral axis

b = the width of the beam

E_{sec} = the secant modulus determined from the stress of the extreme concrete fiber at the point of maximum moment (after Hansell and Winter[6])

$\sum I_{sy}$ = the moment of inertia of the reinforcement with respect to the Y-axis

E_s = the elastic modulus of steel.

2.2.2 Torsional Rigidity - C

Massey[11] gives the following expression for the value of torsional rigidity:

$$C = \beta d^3 d' G_c' + 1/3(G_s - G_c') \sum b_s^3 t_s + \frac{\gamma b_1^2 d_1 A_t E_s}{2\sqrt{2}\, p_s} \qquad (2.24)$$

Where:

C = torsional rigidity

β = a parameter dependent upon the ratio d'/b_1

G_c' = the reduced modulus of rigidity of concrete

G_s = the modulus of rigidity of steel

γ = a parameter dependent upon the ratio d_1/b_1

A_t = the area of one leg of a stirrup

E_s = the elastic modulus of steel

p_s = the pitch, center to center, of stirrups.

The cross-section and reinforcement dimensions b, d', b_s, t_s, b_1 and d_1 are shown on Figure 2.2.

The third term in Equation (2.24) is the contribution of the closed vertical stirrups.

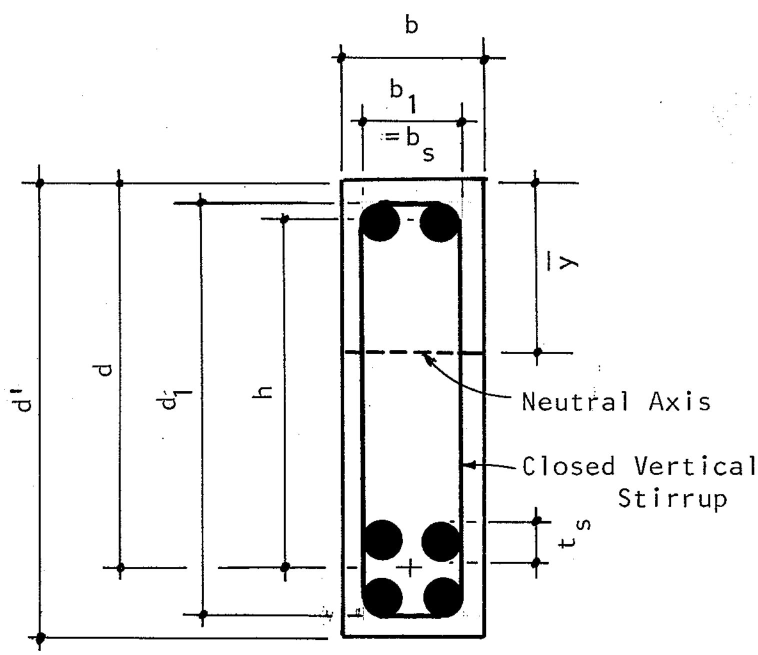

SYMBOLS FOR LATERAL FLEXURAL AND TORSIONAL RIGIDITY

FIGURE 2.2

2.2.3 Warping Rigidity - C_w

Massey[11] gives the following expression for warping rigidity:

$$C_w = E_s h^2 \frac{I_1 I_2}{(I_1+I_2)} \quad \text{--} \quad (2.25)$$

Where:

C_w = Warping rigidity;

E_s = Elastic modulus of steel;

I_1 = Moment of inertia of compressive reinforcement with respect to the Y-axis; and

I_2 = Moment of inertia of the tensile reinforcement with respect to the Y-axis.

Massey concludes that Equation (2.25) underestimates the actual value of warping rigidity and suggests that there is an interaction between the reinforcing steel and the concrete which contributes additional bending resistance. There is not sufficient information in Massey's paper to determine what the actual value of warping rigidity should be for the beams tested in this project. The value of warping rigidity has therefore been computed using Equation (2.25).

2.3 Flexural Analysis of Beams

Section 2.2 dealt with the lateral buckling mode of failure. Equally important is the flexural mode of failure in which the beam remains in its vertical plane and fails by yielding of the reinforcement or by crushing of the concrete.

Failure of the beam is assumed to occur when the strain at the extreme concrete fiber reaches 0.003 inches/inch (at which time the concrete crushes). If the average strain in the tensile reinforcement reaches yield level as the limiting concrete strain is reached, the reinforcement is said to be balanced. If yielding occurs before the concrete strain reaches 0.003, the beam is under-reinforced. To insure against the possibility of brittle failure, code provisions[1][2] specify that beams be under-reinforced by limiting the tensile reinforcement to 75% of the balanced reinforcement.

The strain distribution in an under-reinforced beam at failure is shown in Figure 2.4(b). The corresponding concrete stress distribution is shown in broken lines on Figure 2.4(c).

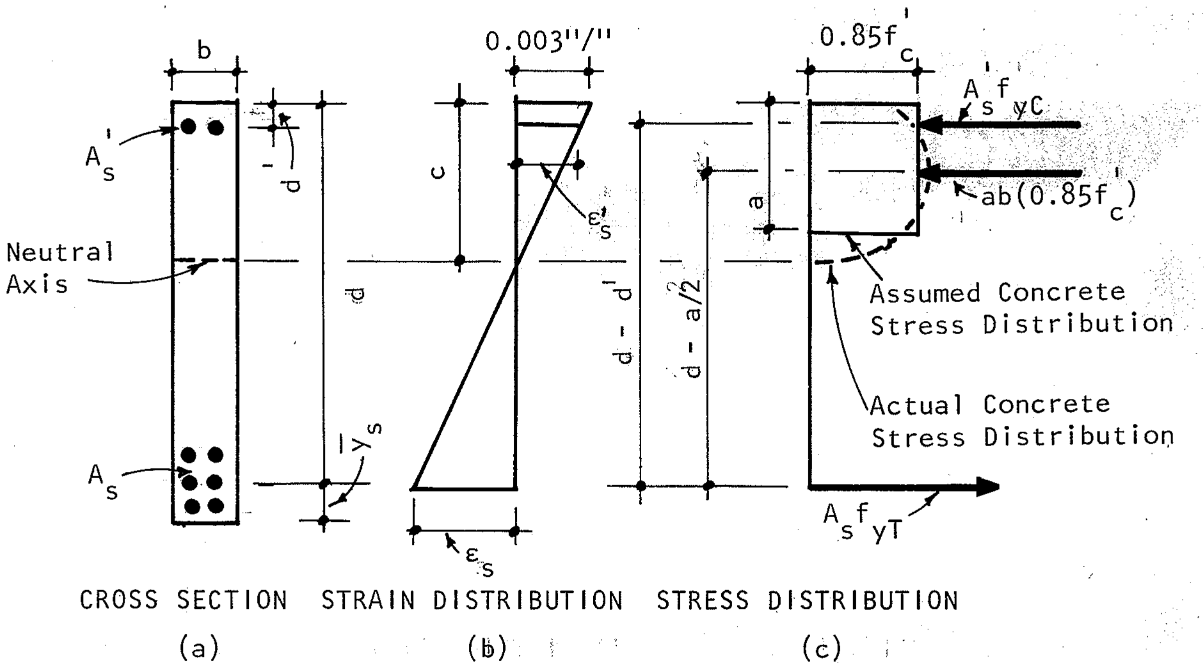

ULTIMATE STRENGTH ANALYSIS OF AN UNDER-REINFORCED FLEXURAL SECTION

FIGURE 2.3

The various terms shown on Figure 2.3 are defined on pages 24 and 25.

For the purpose of analysis, the actual concrete stress distribution is replaced by the commonly assumed rectangular stress block, as shown in Figure 2.3(c). The block has a depth given by[2]:

$$a = c(0.85 - q) \qquad (2.26)$$

Where:

$q = 0$ for f_c' less than 4000 psi.

$q = (f_c' - 4000)(0.00005)$ for f_c' equal to or greater than 4000 psi.

Since the tensile reinforcement yields, the force $A_s f_{yT}$ is known and constant. Similarly, the force $A_s' F_{yC}$ in the compressive reinforcement is known and constant if the reinforcement is assumed to have yielded. The force in the concrete compressive zone is then computed by statics, and is the volume of the concrete stress block. The stress block height a and the moment arms of the two compressive forces about the centroid of the tensile reinforcement are then computed and the ultimate flexural moment found.

In equation form:

$$M_u = \left\{ d - \frac{1}{2} \frac{(A_s f_{yT} - A_s' f_{yC})}{(0.85 f_c' b)} \right\} (A_s f_{yT} - A_s' f_{yC}) + A_s' F_{yC}(d - d') \qquad (2.27)$$

In which:

M_u = Ultimate flexural moment

A_s = Area of tensile reinforcement

A_s' = Area of compressive reinforcement

b = Width of rectangular cross-section or width of compression flange in a T-beam

d = Depth compression face to centroid of tensile reinforcement

d' = Depth compression face to centroid of compressive reinforcement

f'_c = Compressive strength of concrete

f_{yC} = Yield stress of compressive reinforcement

f_{yT} = Yield stress of tensile reinforcement

To verify that both the compressive and tensile reinforcement have yielded, the neutral axis is located by rewriting Equation (2.26) as follows:

$$c = \frac{2(A_s f_{yT} - A'_s f_{yC})/0.85 f'_c b}{(0.85 - q)} \quad \text{------------} \quad (2.28)$$

The tensile reinforcement strain is then computed as:

$$\varepsilon_s = 0.003((d - c)/c) \quad \text{------------} \quad (2.29)$$

and the compressive reinforcement strain as:

$$\varepsilon'_s = 0.003((c - d')/c) \quad \text{------------} \quad (2.30)$$

If the tensile and compressive reinforcement strains are both above yield level, the assumptions made are valid and the moment computed by Equation (2.27) is the ultimate value.

In the event that one or both of the reinforcements do not yield, the values of one or both of the reinforcement forces are variable with strain and the analysis is much more complicated. The analysis is easiest handled by a trial and error procedure in which the location of the neutral axis is assumed and the equilibrium of the section checked.

CHAPTER 3

EXPERIMENTAL STUDIES

3.1 Introduction

The experimental portion of this study consisted of the testing of 14 concrete beam specimens with cross-sections ½ inch wide by 5 inches deep, of varying length, with three types of loading configuration. This Chapter describes the construction of the beam specimens, the loading apparatus and the test instrumentation.

The first configuration was simply-supported center-point loading. Two specimens were built as models of a beam (Specimen B_{24}-1) testing by Sant and Bletzacker[9], and tested under similar loading conditions to determine the comparison between small-scale models and prototype beams. Ten specimens were tested as unrestrained cantilevers, having lengths varying from 32 inches to 48 inches. In the unrestrained cantilevers, three reinforcement types were used (because the supply of the original type ran out and no more could be found). The final two specimens were tested as overhung beams, with the loaded end cantilevered over a support which was free to rotate about all three axes.

The specimens in each of the three series of tests are outlined in Table 3.1, and the loading configurations are shown in Figure 3.1. The reinforcement patterns for the various specimens are shown in Figure 3.2.

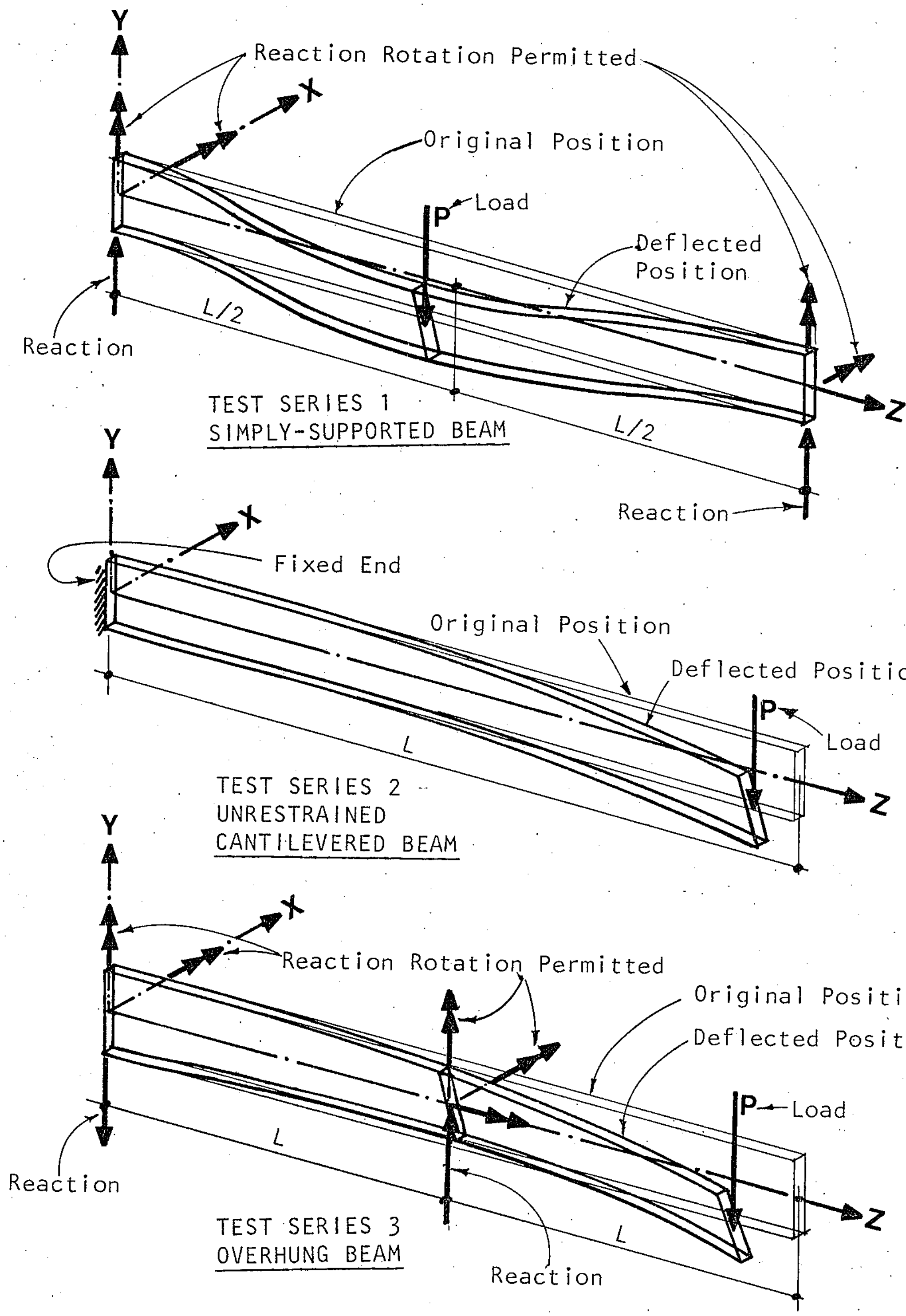

TEST TYPES AND LOADING CONFIGURATIONS

FIGURE 3.1

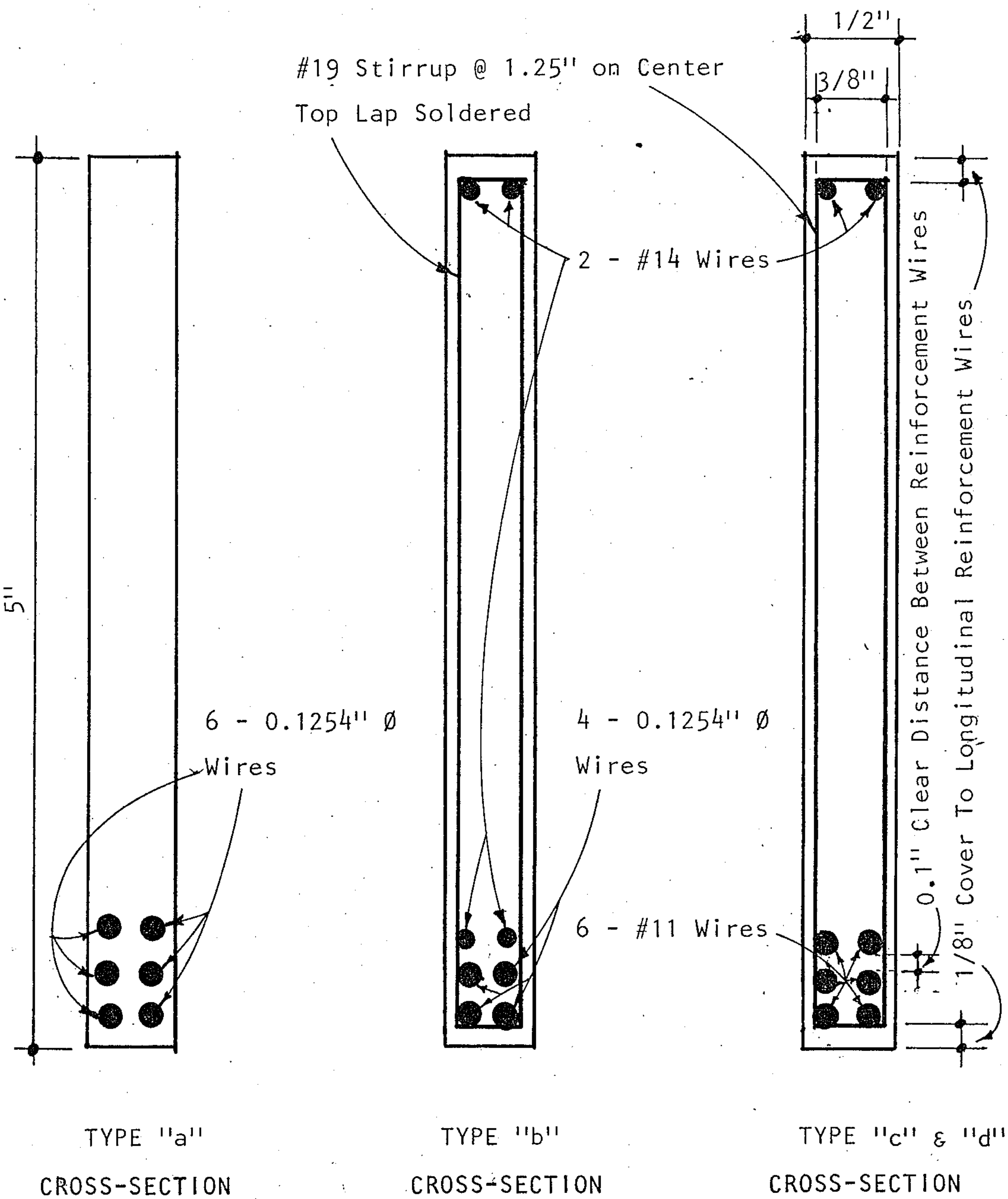

SPECIMEN REINFORCEMENT TYPES

FIGURE 3.2

The specimens were designated by a four-character code which denoted the loading type, the length and the reinforcement.

Table 3.1

Summary of the Test Specimens

Test Series 1

Simply-supported, center-point loaded beam, strain-hardened mild steel reinforcement, 1/2 inch by 5 inch cross-section.

S48a - No. 1   48 inch length
S48a - No. 2   48 inch length

Test Series 2

Unrestrained cantilever beam loading, 1/2 inch by 5 inch cross-section.

(i) Strain-hardened mild steel reinforcement

C44b   44 inch length
C40b   40 inch length
C36b   36 inch length
C32b   32 inch length

(ii) High-strength reinforcement

C48c   48 inch length
C44c   44 inch length
C40c   40 inch length
C36c   36 inch length
C32c   32 inch length

(iii) Cold-drawn mild steel wire

C32d   32 inch length

Test Series 3

Overhung beam loading, strain-hardened mild steel reinforcement, 1/2 inch by 5 inch cross-section.

O19b   19 inch length
O14b   14 inch length

The first character in the designation was an upper case letter, "S" for the simply-supported beams, "C" for the unrestrained cantilevered beams and "O" for the overhung beams. The second two digits were the beam length in inches (corresponding to the dimension "L" in Figure 3.1). The last lower case letter denoted the reinforcement type and pattern (as in Figure 3.2). Type "a" reinforcement consisted of 6-0.1254 inch wires, strain-hardened to 55 ksi, on the tension side with no stirrups or compressive reinforcement. In the case of the type "b", "c" and "d" reinforcement, #19 wire stirrups at 1-1/4 inch centers and 2-#14 wires (strain-hardened to 60 ksi) compressive reinforcement were used. Type "b" tensile reinforcement was 4-0.1254 inch wires and 2-#14 (0.008 inch) wires strain-hardened to 60 ksi. Type "c" tensile reinforcement was 6-#11 (0.117 inch diameter) "bright steel" wire - a high-strength carbon steel. Type "d" reinforcement consisted of 6 mild steel wires which were cold-drawn to reduce their diameter from 0.1254 inch to 0.117 inch. The resulting yield-point was approximately 70 ksi.

In all cases except the simply-supported beams, where there were two identical specimens, the four character code differentiated completely among the specimens. In the case of the simply-supported beams the specimens were differentiated by numbering them.

3.2 Design of the Test Beams

The criteria for the selection of the cross-section, for the series 2 beams, were that the beam should conform to the requirements of current building codes[1][2] (except for lateral stability provisions), and that lateral buckling failures should occur at reasonable beam lengths. A cross-section 1/2 inch wide by 5 inches deep, with 0.056 square inches of tensile reinforcement, was chosen. Material properties were assumed as $f_c' = 5000$ psi, and fy = 65,000 psi. To prevent disintegration of the beam at failure, nominal compressive reinforcement was provided and stirrups were placed at 1-1/4 inch centers. The reinforcement pattern chosen is shown on Figure 3.2 as the type "b" cross-section.

With the substitution of high-strength reinforcement in the type "c" cross-section, the cross-section became over-reinforced. In the case of the cold-drawn reinforcement (type "d"), the cross-section was not over-reinforced but it exceeded the maximum 75% of balanced reinforcement with $f_c' = 5000$ psi. In each case, the area of reinforcement was kept as nearly equal to that in the type "b" cross-section as was practical.

In the Test Series 1 beams, which were the models of one of Sant and Bletzacker's tests, the cross-section width (and thus the linear scale factor) was fixed by the mould size for the Series 2 beams. With the scale fixed, a reinforcement pattern (Figure 3.2.(b)) was chosen to give a scaled area equivalent to the prototype cross-section.

3.3 Reinforcement Wire

Reinforcement for the test beams was fabricated from steel wire. In general, three types of reinforcement were used.

The first type was strain-hardened mild steel wire, which was used in the type "a" and type "b" cross-sections. The wire was preloaded to raise the yield-point to the desired level, (55 ksi in the case of type "a" and 60 ksi in type "b"). To simulate the effect of the deformations on prototype reinforcement, indentations were made on four sides by pulling the wire through two sets of knurled rolls[18]. An indentation depth of 1/20 the wire diameter and 34 indentations per inch gave an area of indentation per unit length equivalent to that of prototype reinforcement[21].

For the type "c" cross-section, high-strength carbon steel "bright wire" was used as tensile reinforcement. (The compressive reinforcement was strain-hardened mild steel). In this case, the wires were also deformed.

In the case of the type "d" cross-section, the tensile reinforcement was made by cold-drawing mild steel wire to reduce its diameter from 0.125 inches to 0.117 inches. The resulting yield-point was approximately 70 ksi. The wires were not deformed because slight variations in diameter made it difficult to pull them through the deforming devise.

The reinforcement cage was assembled by positioning the six tensile wires in a jig and tying the stirrups in position with fine brass wire. All crossings between the stirrups and the tensile wires were soldered with a low temperature paste solder. Following assembly, the cage was washed with a 5% hydrochloric acid solution and brushed to remove any unfluxed solder.

Tests by Petri[19] and the writer indicated that no change in the yield point or the ductility of the wire resulted from the heating required to flux the paste solder.

Wire spacers were provided on the sides and bottom of the group of tensile wires to hold it in position in the mould. In addition, the cage was tied through the bottom of the mould to keep it from rising as the concrete was placed. The compressive reinforcement was tied into position prior to the placing of the last lift of concrete.

3.4 Concrete Mixture

To facilitate placement, the design of the concrete was based upon a maximum particle size of #20 sieve. The aggregate gradation was arrived at by scaling down the gradation of a prototype mixture which was based upon Canadian Standards Association[22] and Portland Cement Association[23] recommendations. The scaled results were adjusted to eliminate sizes smaller than the #200 sieve and an envelope of maximum and minimum permissible grading limits drawn. Commercially available silica sand (graded to various sizes) was used as aggregate and the blend of sizes was varied from time to time to keep the mixed gradation as close as possible to the center of the grading envelope.

Several trial mixtures were made to select a mix design. A water/cement ratio of 0.574 was chosen[23] to give a compressive strength of 5000 psi at 28 days, and the cement paste-to-aggregate combination varied to produce the required workability. The mixture chosen is shown in Table 3.2.

Table 3.2

Concrete Mix Design

Aggregate	69% by weight
Cement Paste	31% by weight High-Early Strength Cement
Water/Cement Ratio	0.574
Admixture	Pozzolith LL300 0.4 ml/100 gm. cement

The Pozzolith LL300 admixture is a water-reducing, cement-dispersing type and was used to increase the workability of the mixture. The dosage used was approximately double that recommended for prototype concrete.

Mixing of the concrete was done with a Hobart laboratory mixer operated at its slowest speed. The mixing time was kept constant at three minutes and a sequence was followed for the addition of the various components to maintain consistency from batch to batch.

The results of the strength tests of the concrete used in each of the beam specimens are contained in Appendix A. The compressive strengths varied from 3130 to 6500 psi, depending upon the age at the time of testing. The modulus of rupture varied from $7.5\sqrt{f'_c}$ to $8.5\sqrt{f'_c}$ as compared to the value $7.5\sqrt{f'_c}$ generally used for prototype concrete. The properties of concrete prepared in accordance with the mix design shown on Table 3.2 were measured by Barritt[24]. Four of Barritt's stress-strain curves, representing various ages of concrete, are shown in Figure 3.3. The curves have the same shape as those for prototype concrete but are flatter.

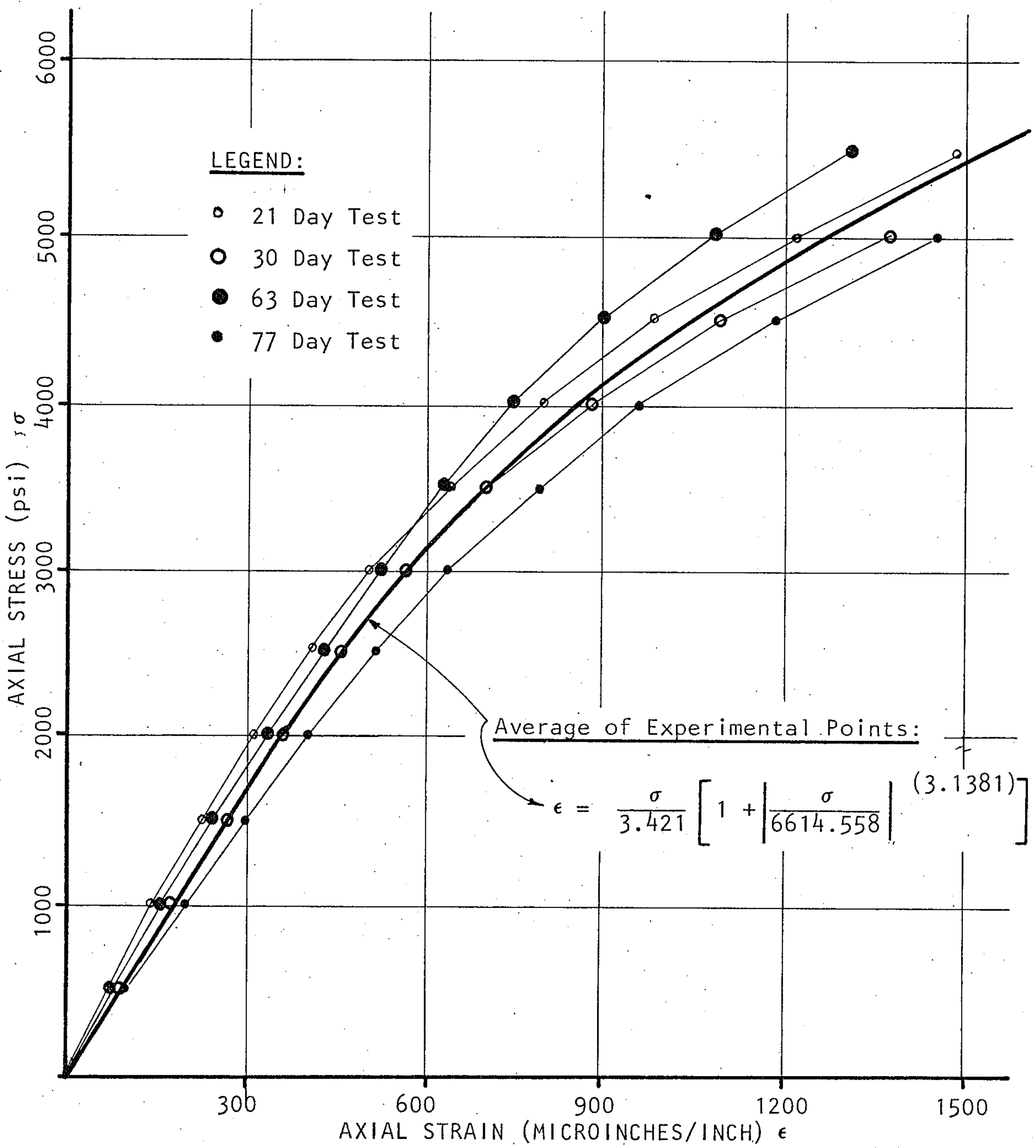

CONCRETE STRESS - STRAIN CURVES

FIGURE 3.3

For analytical use, the average of the four curves was fitted to a Ramberg-Osgood Function[25] of the form:

$$\varepsilon = \frac{\sigma}{3.4201 \times 10^6}\left\{1 + \left|\frac{\sigma}{6614.558}\right|^{3.1381}\right\} \quad \text{-------------------------} \quad (3.1)$$

Using the initial slope of the average stress-strain curve and the initial slope of the average curve for the circumferential strain for the same four samples, the initial Poisson's Ratio was computed as 0.1728. From this, the initial modulus of rigidity of the concrete was computed from the elastic relationship $G = E/2(1 + \nu)$ as:

$$G_c = (3.4201 \times 10^6)/2(1 + 0.1728) = 1.458 \times 10^6 \quad \text{--------------} \quad (3.2)$$

3.5 Casting of the Beam Specimens

The mould was constructed from pieces of 1/4 inch acrylic plastic, fused together with Ethyl Dichloride solvent. Details of the mould are shown in Figure 3.4. The assembled mould was supported on a steel angle frame and braced horizontally to the frame to maintain alignment.

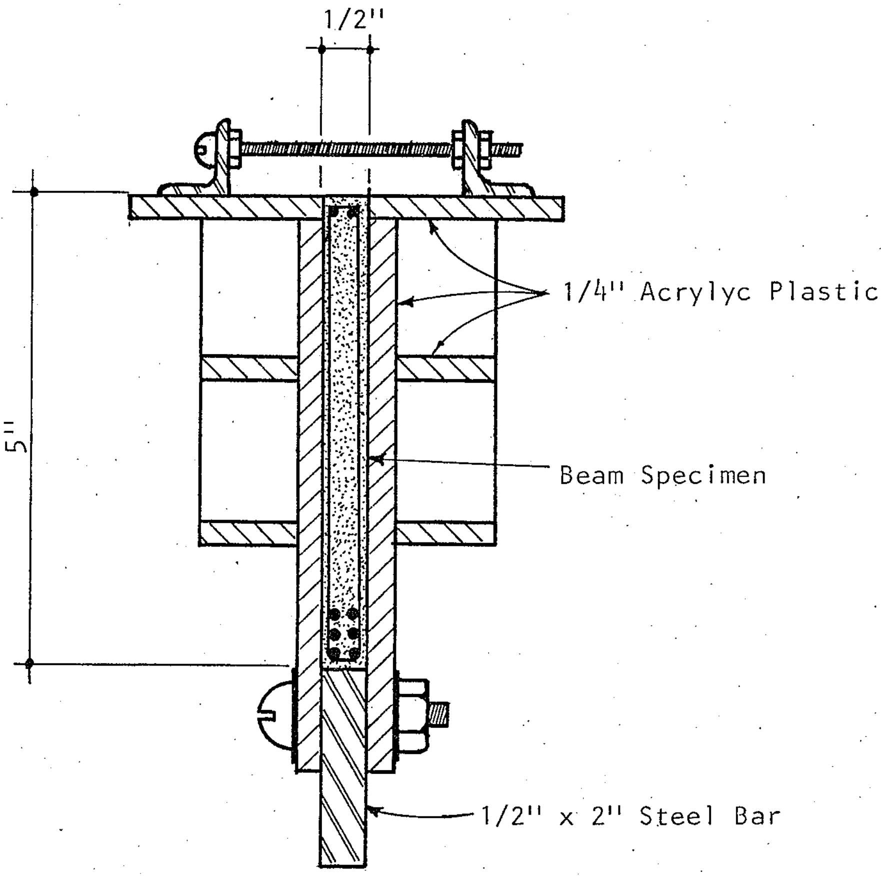

CROSS SECTION OF BEAM SPECIMEN MOULD

FIGURE 3.4

The beams were cast in three lifts, with the first lift filling the mould approximately one-third full, the second to within one-half inch of the top and the third filling the mould. Consolidation of the concrete was achieved through the use of an internal vibrator (1/4 inch outside diameter with an eccentric weight driven at 25,000 rpm). In addition to the vibrator, a small spatula or a piece of wire was used to dislodge air bubbles which collected against the mould surface.

Following casting of the beam and the six test sample cylinders the exposed surfaces were covered with wet paper towels and a layer of polyethylene film. The concrete was then cured at room temperature for forty-eight hours during which time the paper towels were kept wet. After the initial forty-eight hour period, the moulds were stripped and the beam and cylinders placed in a wet room for curing at 75 to 80 degrees Fahrenheit. In preparation for testing, the beams and cylinders were removed from the wet room and allowed to air dry for 24 hours.

3.6 Loading Apparatus

Lateral buckling of the test specimens under load implied that the loading apparatus and reactions had to allow displacement and rotation in specific directions while preventing it in others. To meet the requirements of the various series of tests, a loading head and three support devices were built.

The loading head was to permit rotation about all three mutually orthogonal axes as well as horizontal translation perpendicular to the beam axis (in the "X" direction). In addition, the load was to be

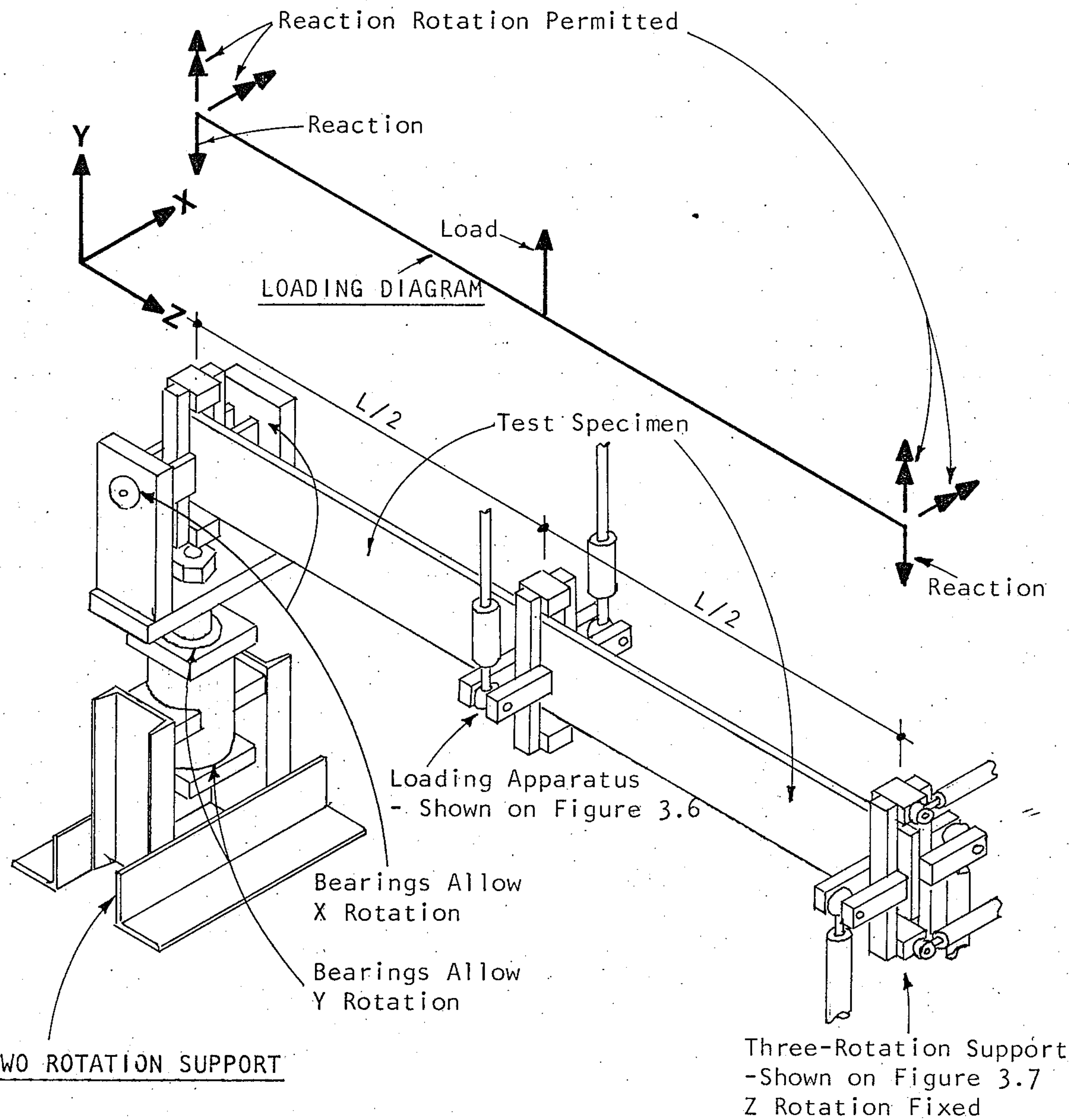

TEST SERIES 1 - SIMPLY SUPPORTED BEAM

FIGURE 3.5

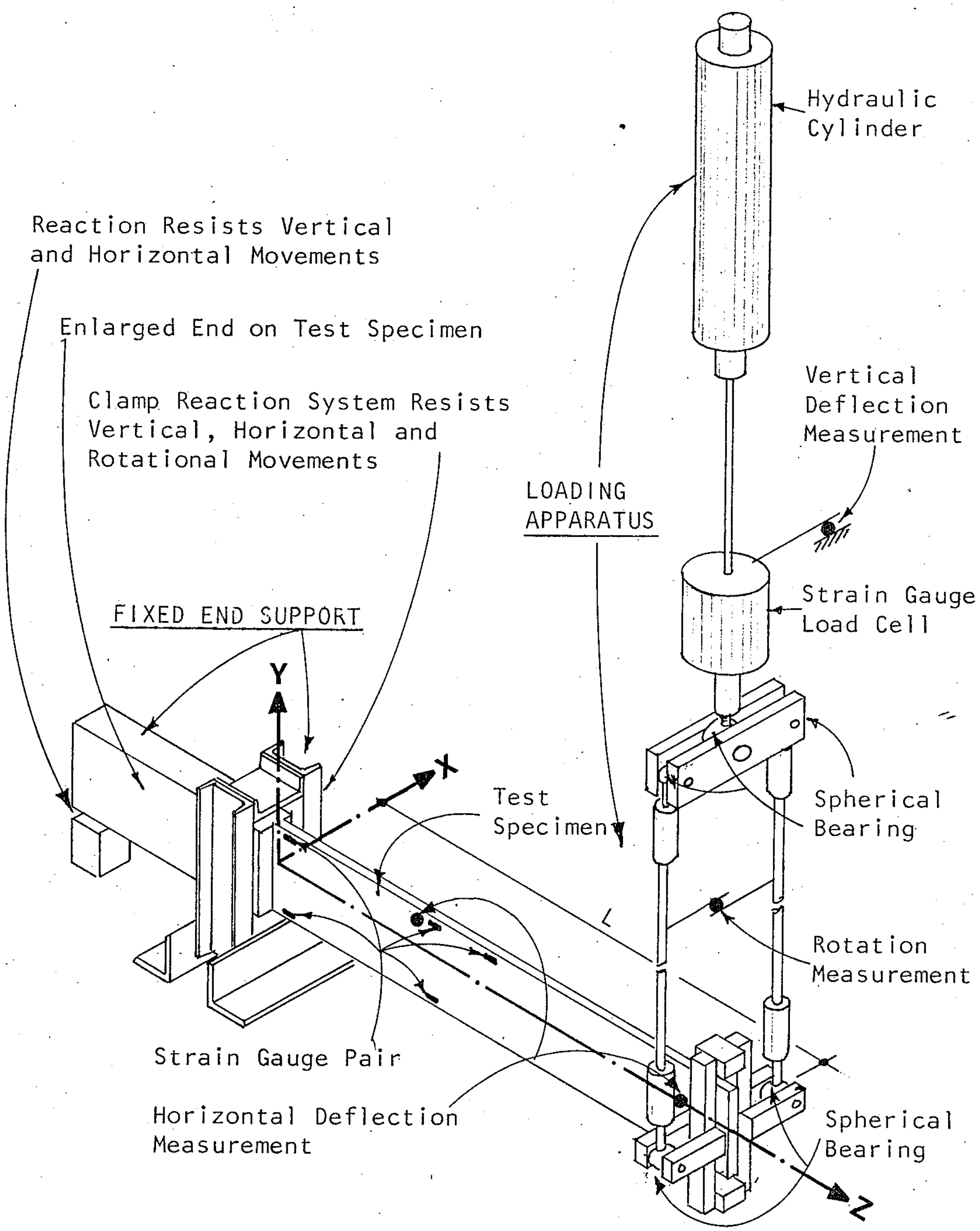

TEST SERIES 2 - UNRESTRAINED CANTILEVERED BEAM

FIGURE 3.6

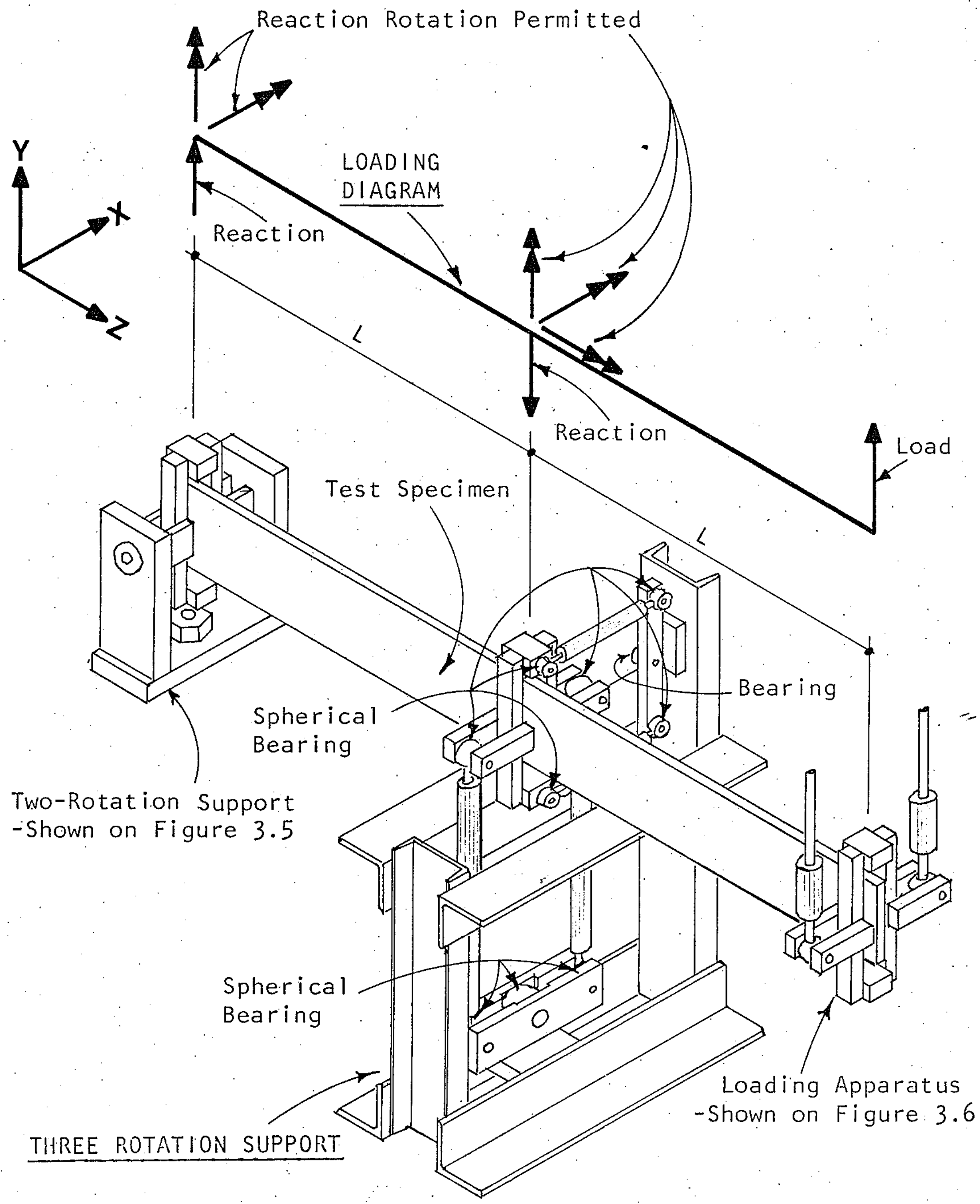

TEST SERIES 3 - OVERHUNG BEAM

FIGURE 3.7

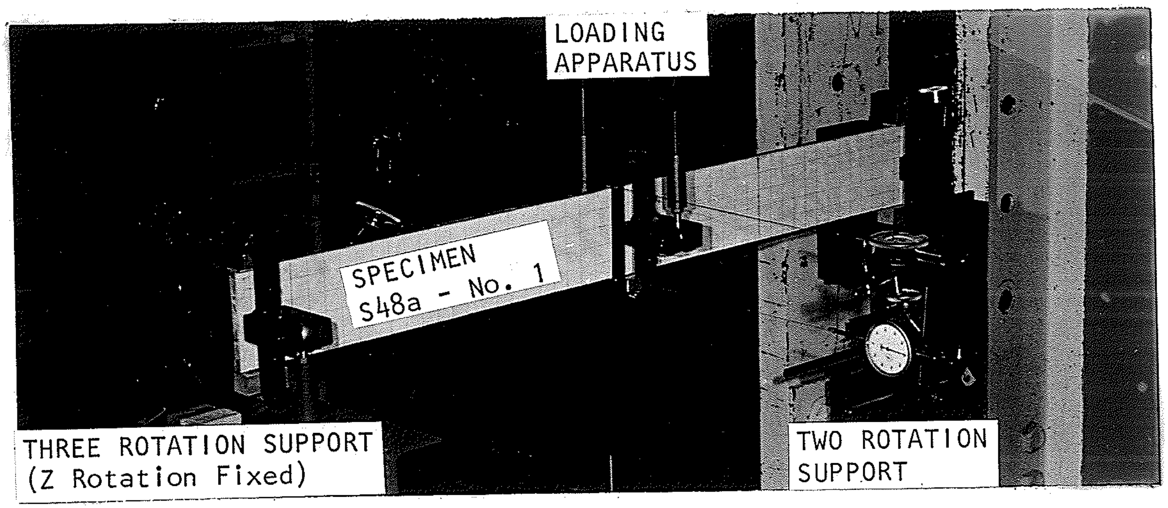

TEST SPECIMEN S48a - No. 1 PRIOR TO TESTING

PHOTO 3.1

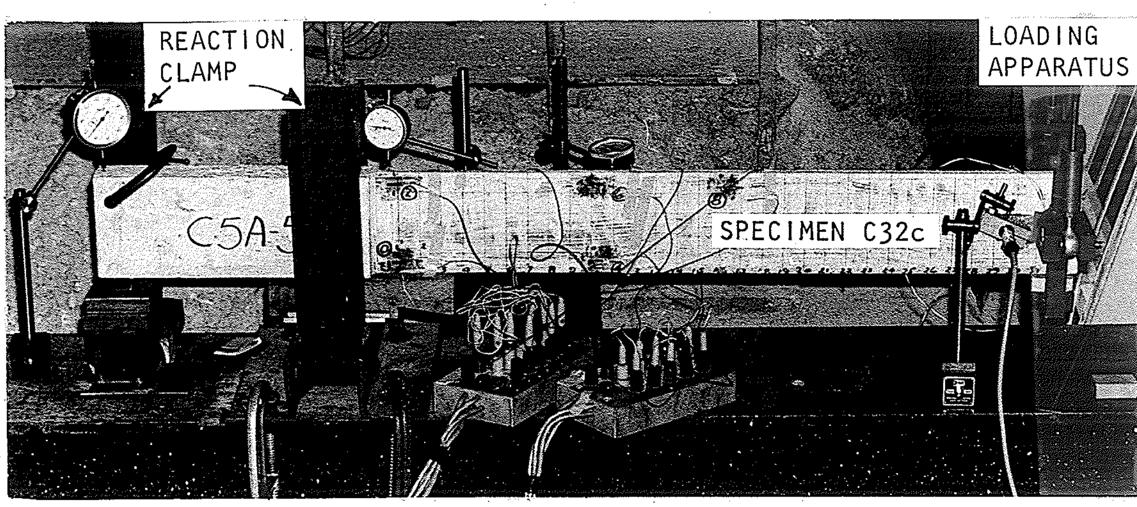

TEST SPECIMEN C32c PRIOR TO TESTING

PHOTO 3.2

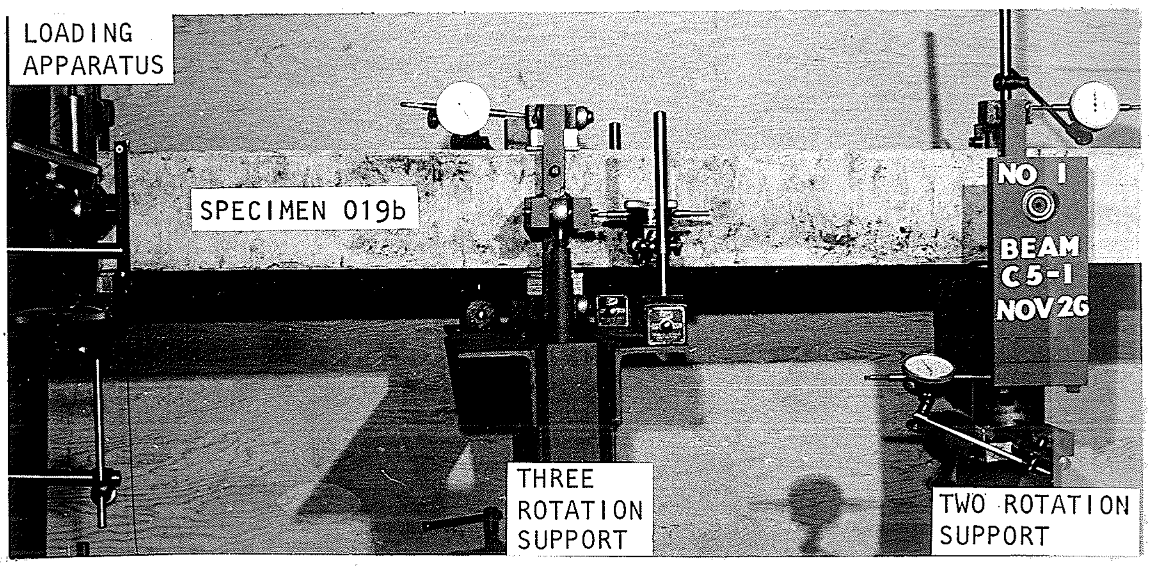

TEST SPECIMEN 019b PRIOR TO TESTING

PHOTO 3.3

vertical (simulating a gravity load) at all times during the lateral deflection. The requirements were closely met by an apparatus consisting of a parallelogram with spherical bearings in the four corners, as shown in Figure 3.6. The beam was clamped at the center of one side and the load was applied through a spherical bearing at the center of the opposite side. The apparatus allowed rotation about all axes and translation in the "X" and "Z" directions, with the only limitation being the frictional force in the bearings. Separate tests of the bearing friction indicated that it was insignificant. Translation was not exactly parallel to the specified directions; rather it was radial about the top bearings. Similarly, the load became inclined to the vertical as lateral deflection occurred. Both of these effects were minimized by making the arms of the parallelogram as long as was practical (approximately 100 inches).

For the simply-supported beams, the supports had to prevent rotation about the longitudinal axis of the beam while allowing it in the two perpendicular directions (i.e. the beam had to remain vertical at the supports and be free to rotate in the other two directions). For the overhung beam, the exterior support had to keep the beam vertical, as in the simply-supported beams, while the interior support allowed rotation in all three directions. The two-rotation support was built as a clamp mounted on a vertical and a horizontal spindle as shown in Figure 3.5. The three-rotation support was built as two parallelograms of the same form as the loading apparatus, as shown in Figure 3.7.

For the simply-supported beams (Test Series 1), the two-rotation support was used at one end of the beam, and the three-rotation support (with the rotation about the beam axis prevented) was used at the other. The loading apparatus was placed at the middle of the beam as shown in Photo 3.1. For the overhung beams (Test Series 3), the two-rotation support was placed at the exterior, the three-rotation support at the center and the loading apparatus at the other end as shown in Photo 3.3.

For the unrestrained cantilevers, the support took the form of clamps which held the beam end in all directions. For this purpose, an enlarged end was cast on the beam specimens. The enlarged end was prevented from twisting by clamps at each end as shown in Photo 3.2 and Figure 3.6.

3.7 Test Instrumentation

Load-deflection data (horizontal, vertical and rotational) were taken at the load point for all tests. In addition, strain measurements were taken on the concrete surface and horizontal deflection was measured at the compression face at one-third span in six of the unrestrained cantilevers. The six specimens were the "c" and "d" type cantilevers. Inspection of the failed configuration of the first set of cantilevers (the type "b"), indicated that the maximum lateral deflection of the top flange in the opposite direction to that of the load point occurred close to the one-third point. As a result, the one-third point was chosen as a site for the second lateral deflection measurement.

In the tests of the unrestrained cantilevers, the load was measured with a strain gauge load cell. For the simply-supported beams and the overhung beams, the expected failure loads were greater than the capacity of the load cell and the load was measured with a pressure gauge on the hydraulic loading cylinder.

Horizontal deflections at the load point and at L/3 were measured with a capacitance transducer, which applied no force to the specimen (and thus had no effect on the lateral buckling). Rotation was measured with a dial gauge between the arms of the loading parallelogram and vertical deflection was measured with a dial gauge at the top of the loading apparatus. Ideally, the vertical deflection should have been measured at the specimen, but this was impractical because of the lateral deflection. With the measurement taken at the top of the parallelogram, several small errors were introduced. (None of these errors were considered serious). Computer programmes were written to reduce the dial-gauge and transducer results to the final form which gave the horizontal, vertical and rotational deflections and their corresponding loads. The rotational deflection was corrected for the apparent rotation which appeared in the parallelogram as the result of lateral deflection. In the case of the unrestrained cantilevers, five dial gauges were used to measure the deflection and rotation of the "fixed" end of the specimen. Only the vertical movements proved to be significant and a correction was made to the load point vertical deflection to account for them.

The concrete strain, parallel to the longitudinal axis of the beam, was measured by electric resistance strain gauges placed in pairs on opposite sides of the beams at five locations. The output from the strain recorder was reduced with a computer programme and the reduced data were plotted with the digital plotter.

CHAPTER 4

TEST RESULTS

4.1 Summary of Test Results

The results of the load tests of the three types of beam specimens are summarized in Table 4.1. The behaviour of each of the types is discussed in later portions of the Chapter and the results of the unrestrained cantilever tests are given in detail in Appendix A.

4.2 Simply-Supported Beam Tests

As discussed previously, the two simply-supported beam specimens were made as models of a larger specimen which was tested by Sant and Bletzacker(9). The first specimen, S48a - No. 1, warped due to uneven drying after the curing period and was crooked at the start of the test. As a result, the failure load was low and the test result was disregarded. The load-deflection results for Specimen S48a - No. 2 are plotted on Figure 4.1. The horizontal deflection was small until the load approached failure; then it increased rapidly and the curve became nearly horizontal. The rotation increased rapidly in the initial stages of the test, then changed more slowly and finally increased rapidly towards failure. The initial period of rapid change in rotation at the beginning of the test was an adjustment to an equilibrium position within the

Table 4.1

Summary of Test Results

SPECIMEN	LENGTH INCHES	FAILURE TYPE	FAILURE LOAD POUNDS	NOTES
Series 1 Simply-Supported Beam				
S48a - No. 1	48	Instability - Lateral buckling.	1031	Crooked specimen, result ignored.
S48a - No. 2	48	Instability	1295	
Series 2 Unrestrained Cantilever Beam				
C44b	44	Instability	355	
C40b	40	Instability	410	
C36b	36	Instability and flexure-reinf. yielding.	461	
C32b	32	Flexure-reinf. yielding.	550	
C48c	48	Instability	355	
C44c	44	Instability	445	
C40c	40	Instability	445	Crooked specimen, result ignored.
C36c	36	Instability	585	
C32c	32	Flexure-Conc. crushing.	590	
C32d	32	Flexure-reinf. yielding.	615	
Series 3 Overhung Beam				
O19b	19	Instability	508	
O14b	14	Instability	743	

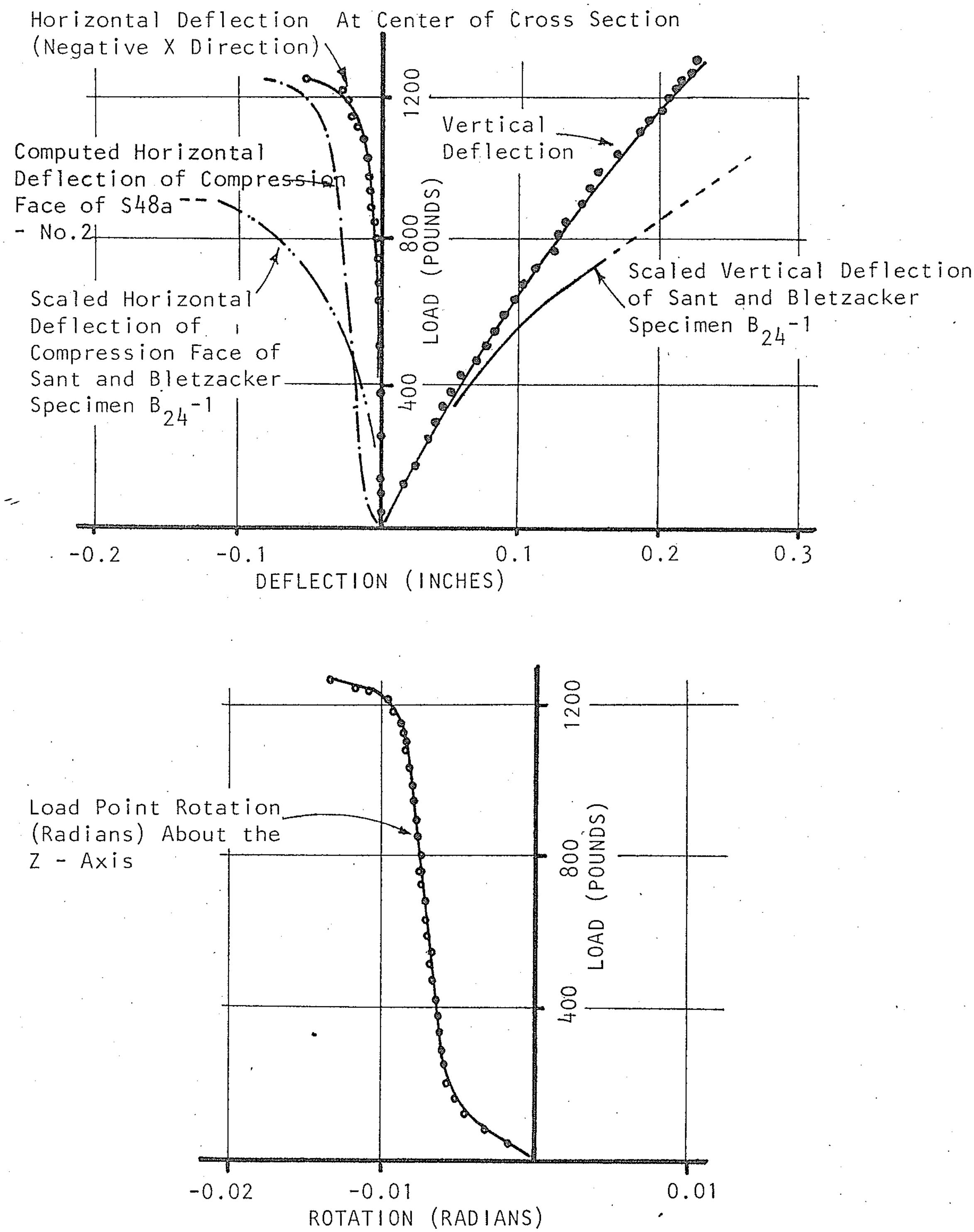

SPECIMEN S48a No. 2 - DISPLACEMENTS AT LOAD POINT

FIGURE 4.1

specimen to compensate for initial crookedness and eccentricities in the test set-up. This behaviour was noted in the lateral deflection and the rotation in all tests to a greater or lesser extent. For the purpose of comparison, the deflections of Sant and Bletzacker's specimen (scaled in accordance with Equations (1.11) and (1.13)) have been shown on Figure 4.1.

Specimen S48a - No. 2 prior to loading and following failure is shown in Photos 4.1 to 4.3. The load was applied upward so that the top face of the beam was in tension.

At failure, the beam deflected laterally, as is shown in Photos 4.2 and 4.3, and rotated at the load point such that the bottom face is closest to the camera in Photo 4.2. Major diagonal cracks occurred at each end as shown in Photo 4.2, with tension on the side facing the camera. Since there was no compressive or shear reinforcement in the specimen, the major cracks at the ends were complete separations across the cross-section with the exception of the immediate area around the tensile reinforcement.

For Specimen S48a - No. 2, the concrete compressive strength f_c' was 5678 psi, and the reinforcement yield strength f_y was 55,600 psi.

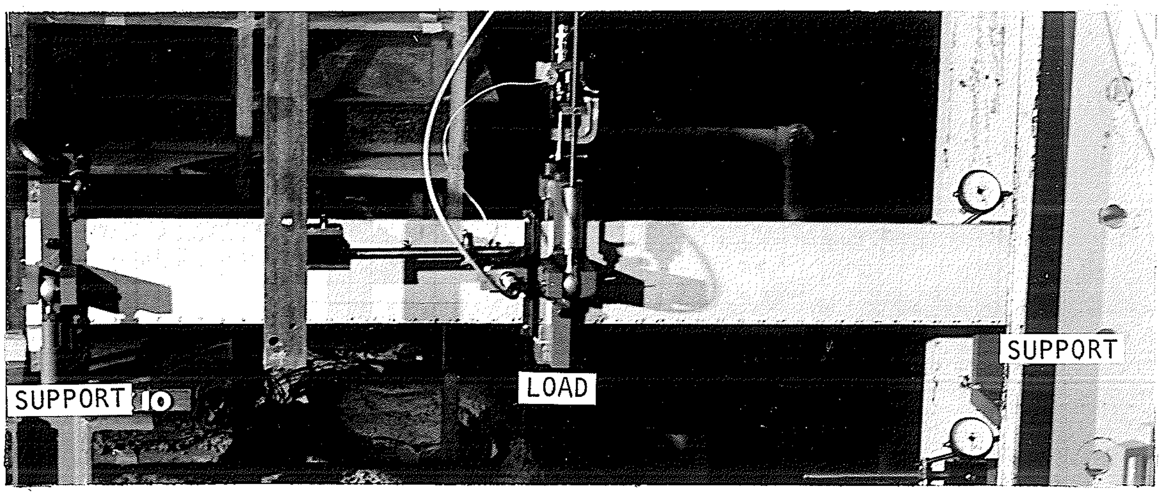

SPECIMEN S48a - No. 2 PRIOR TO TEST

PHOTO 4.1

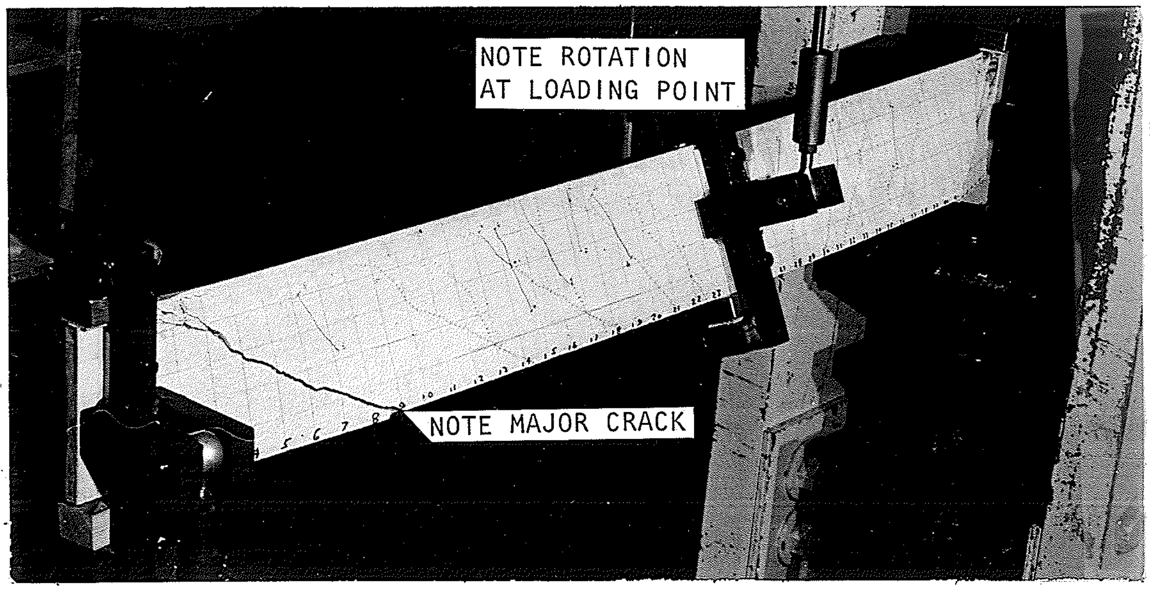

SPECIMEN S48a - No. 2 FOLLOWING FAILURE

PHOTO 4.2

4.3 Unrestrained Cantilever Beam Tests

The failure types and failure loads for each of the ten unrestrained cantilever beam specimens are shown in Table 4.1. Drawings of the failure configurations, plots of the deflection and strain data, and the results of the material tests are given in Appendix A. As an example of the behaviour of an unrestrained cantilever, photographs before loading and after failure and the deflection and strain plots for Specimen C44c are shown here.

Photo 4.3 shows Specimen C44c prior to loading and Photos 4.4 to 4.7 show it following failure. The load-deflection curves are plotted on Figure 4.2 and the load-strain curves are plotted on Figure 4.3. The vertical deflection curve was nearly linear until immediately before failure, at which time it flattened. The horizontal deflections of the load point and the top face 1/3 span from the fixed end were small until approximately 100 pounds below failure load and then increased rapidly in opposite directions. The rotation increased rapidly in the initial stages of loading, then the curve steepened and flattened as failure approached. The initial rapid rotation was due to the adjustment into an equilibrium position, as was the initial reversal of the lateral deflection on the lower portion of the curve.

The load-strain plots on Figure 4.3 show the strain parallel to the longitudinal axis of the specimen. The strain gauges were arranged in pairs on opposite sides of the specimen so that the divergence in the strain in any pair indicated lateral bending. Gauges 0, 1 and 5 failed

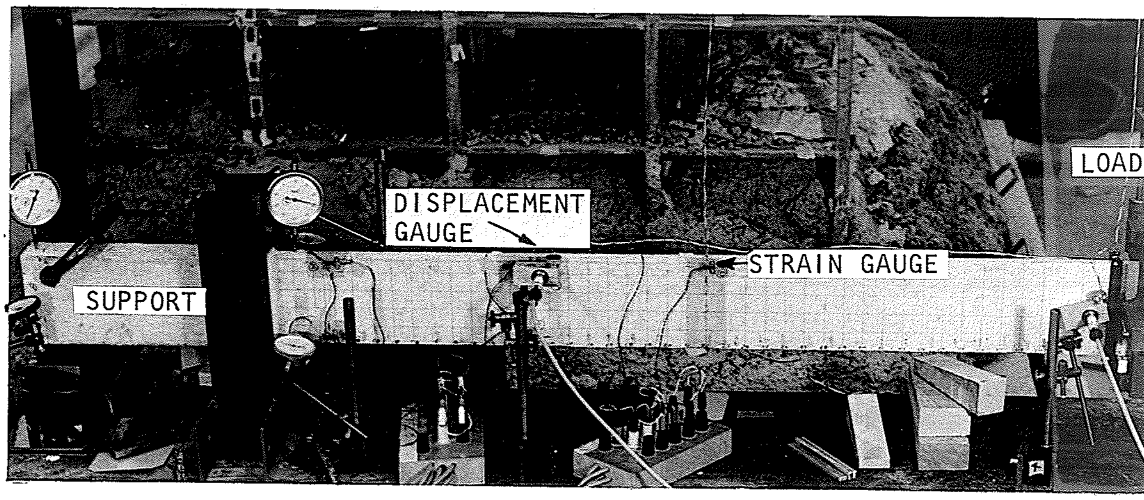

SPECIMEN C44c PRIOR TO TEST (LOOKING AT THE NEGATIVE - X FACE)

PHOTO 4.3

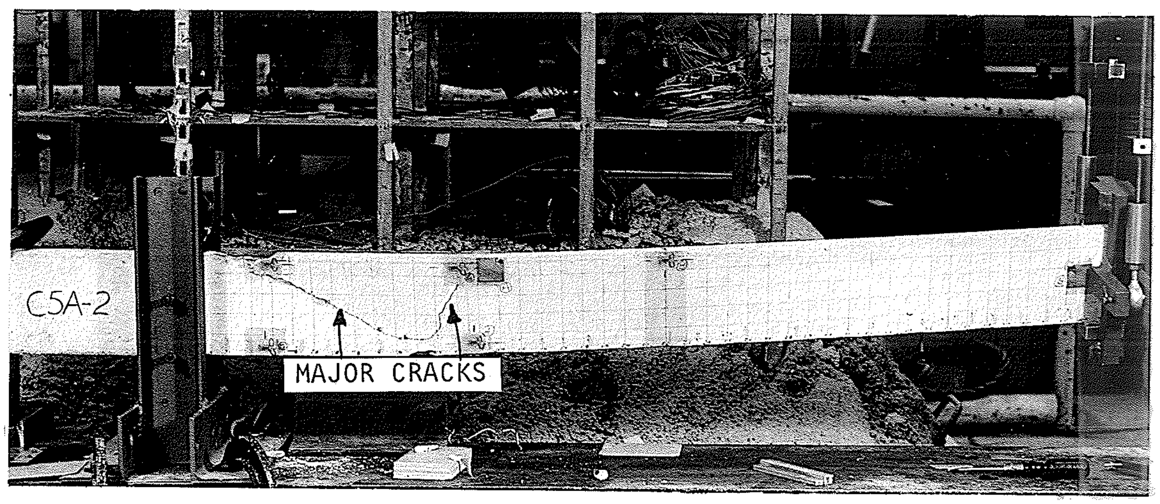

SPECIMEN C44c FOLLOWING FAILURE

PHOTO 4.4

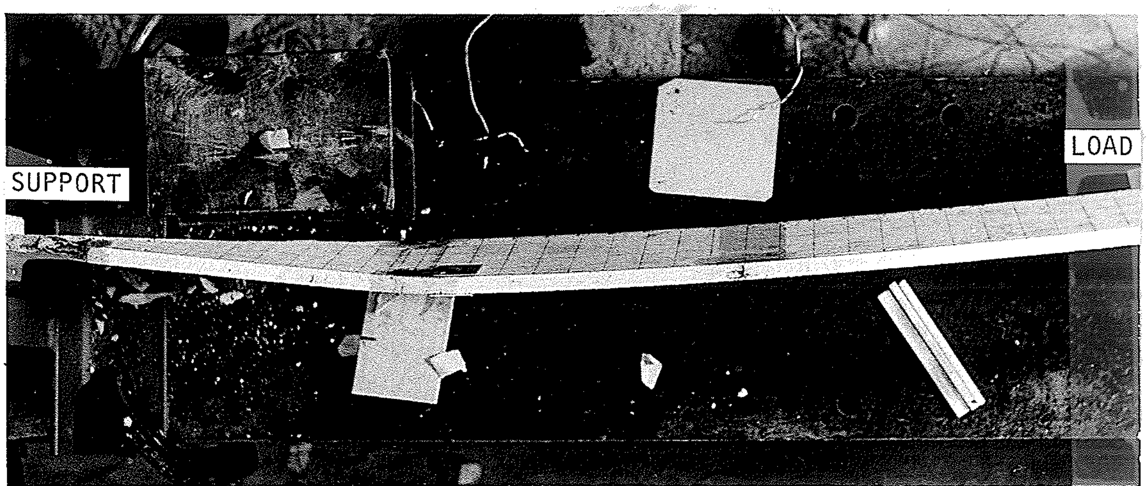

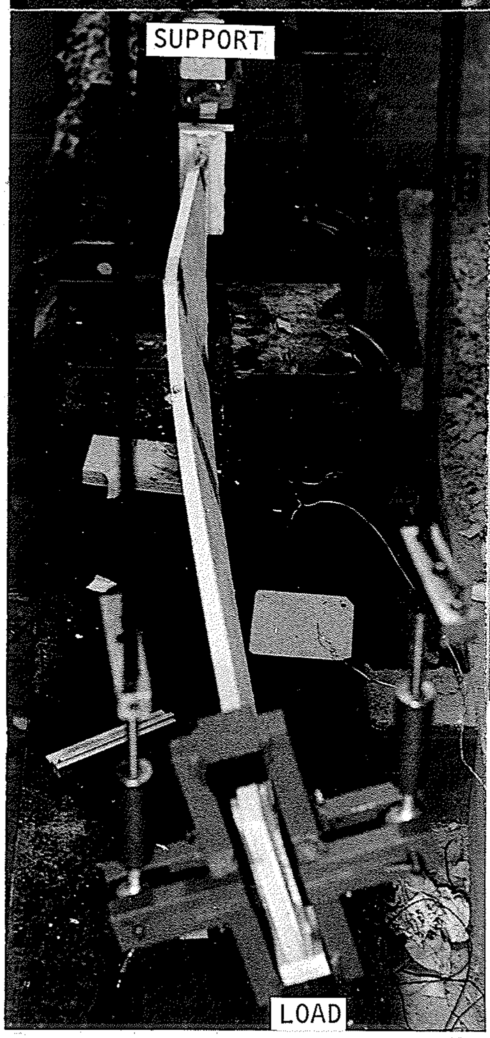

SPECIMEN C44c VIEWED FROM ABOVE

PHOTO 4.5

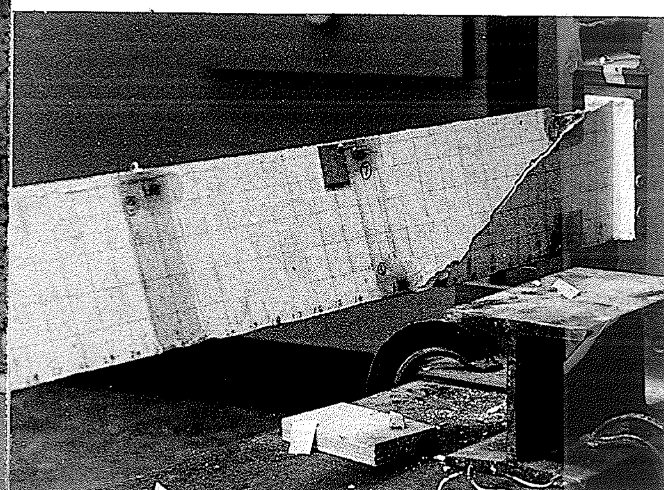

CRACK ON POSITIVE-X FACE OF SPECIMEN C44c

PHOTO 4.6

SPECIMEN C44c VIEWED FROM LOADED END

PHOTO 4.7

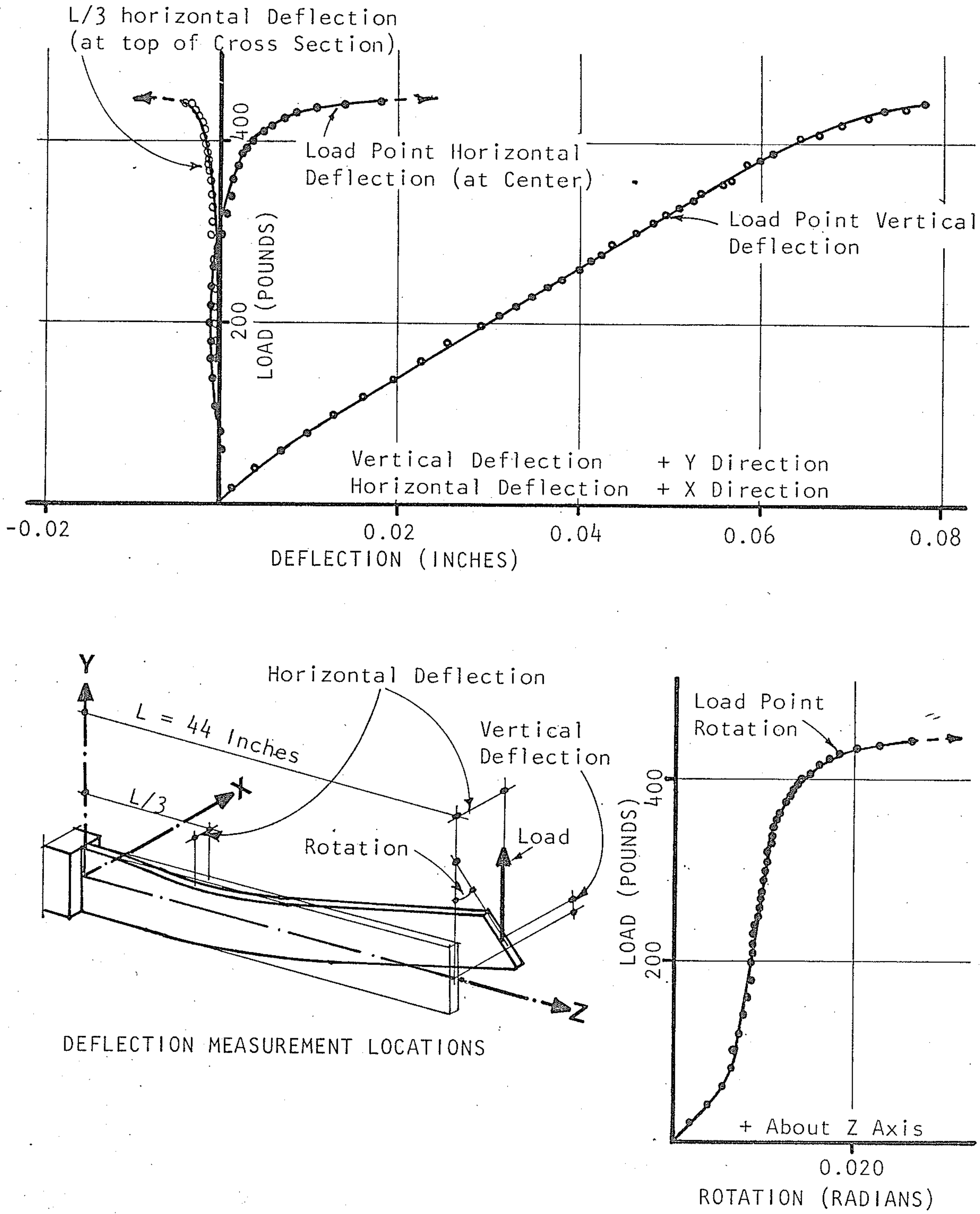

DISPLACEMENT - SPECIMEN C44c

FIGURE 4.2

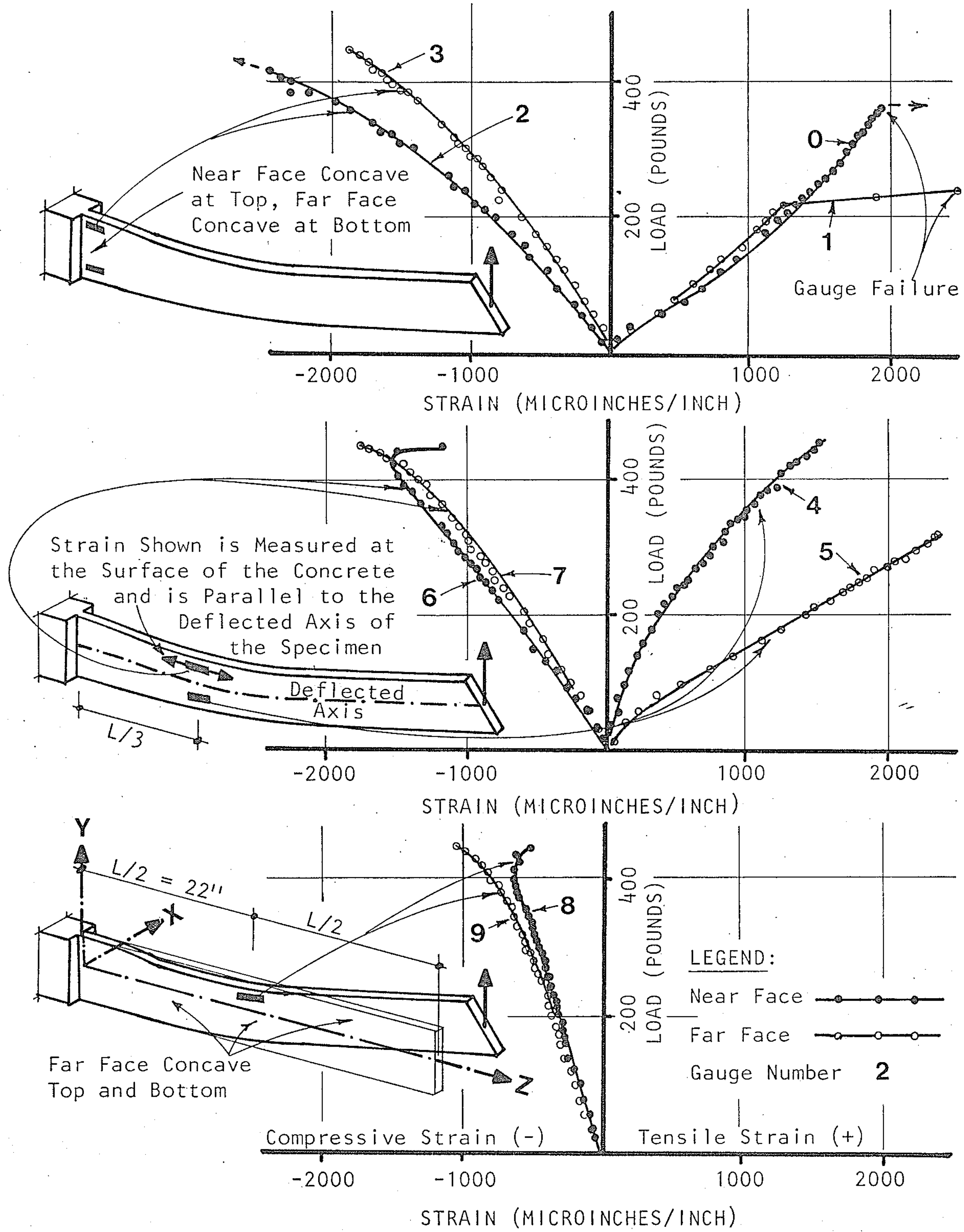

CONCRETE STRAIN - SPECIMEN C44c

FIGURE 4.3

before the test was completed. Gauge pairs 6-7 and 8-9 indicate bending such that the specimen was concave on the side of 7 and 9, which fact is borne out by Photos 4.5 to 4.7 and the lateral deflection curves on Figure 4.2. Gauge pair 2-3 indicates curvature in the opposite direction, which is also shown by the photos and the lateral deflection. Gauge pair 4-5 indicated curvature in the same direction as pair 2-3 and Photo 4.6 shows a crack close to gauge 5 on the outside of the curve. The large divergence of strain at gauge pair 4-5 was not normal and was the result of an initial crookedness or eccentricity.

At failure, the beam deflected laterally very suddenly, from a straight configuration to the one shown in Photos 4.5 to 4.7. In the process of the failure, the specimen developed two large diagonal cracks as shown in Photo 4.4 and 4.7. In Photo 4.4, the crack nearest the fixed end is on the far side of the beam and the concrete is crushed in the photograph. The second crack runs from the tip of the first to the top face. Along this crack, tension occurs on the side facing the camera.

4.3.1 Lateral Buckling Behaviour of an Unrestrained Cantilever Beam

Specimen C44c, discussed previously, exhibited behaviour which was typical of that in all of the unrestrained cantilevers which buckled under load. In general, the lateral deflection and the rotation measured in the tests were slightly erratic as a result of crookedness in the specimen or eccentricity in the test set-up which created unusual bending situations. In general, the lateral deflection and rotation curves exhibited an initial period of rapid movement in either direction, followed by a steepening of the curves to the point at which they were nearly vertical. At failure, the curves flattened as the lateral movement and rotation increased rapidly with load. Before failure, the horizontal deflection at the load was in the range 0.4 to 1.0 inches while the deflection at the 1/3 point was in the range 0.1 to 0.3 inches (and in the opposite direction). Following failure, the load point deflection was in the range 1.0 to 3.0 inches with the 1/3 point deflection approximately one quarter in magnitude. Maximum rotation at the load point prior to failure was in the range of 0.035 radians (about 2 degrees). During the failure, the rotation increased several times to approximately 15 degrees. Vertical deflections at the load point were in the range of 0.7 to 0.9 inches before failure and 1.0 to 1.5 inches following failure. The shape of the vertical deflection curves were very similar to that shown in Figure 4.2.

The shape of the load-strain curves was affected by crookedness and eccentricity in a manner similar to the lateral deflection and the rotation. In most cases, the curves for any pair of strain gauges were close together over most of the loading range, similar to those for pairs 6-7 and 8-9 on Figure 4.3. In some cases, the curves for a pair diverged widely such as those for pair 4-5. As a result, interpretation of the test data was sometimes difficult. The behaviour of the curves for strain gauge pairs 6-7 and 8-9 was typical of the strain observed in all specimens which buckled laterally. Over the lower portion of the loading range, the strains on opposite sides of the beam at any gauge location were nearly equal. As lateral buckling failure approached, the strains diverged indicating lateral bending. Immediately before failure, as lateral bending was increasing rapidly, the change in strain was sufficient to produce a reversal such as occurred at gauges 6 and 8 on Figure 4.3.

Photos 4.8 and 4.9 show the cracking patterns of Specimen C44c on opposite sides of the beam near the fixed end. The major cracks shown developed, during the process of the lateral buckling failure, so rapidly that the sequence of their development could not be determined by observation. One crack began at the top of the beam near the fixed end and ran downward toward the bottom face. The crack formed on the side of the beam toward the direction of the load point deflection. In Photo 4.9, the crack is on the side away from the camera. Crushed concrete is visible in the photograph. In the six specimens which developed the diagonal crack pattern, the slopes of the cracks were in the range of 1.5 : 1 to 2 : 1 (horizontal to vertical).

The second crack extended on a line beginning at the bottom, near the end of the first, and ending at the top near the point of maximum opposite deflection of the top face, about one-third of the beam length from the fixed end. The crack formed on the side opposite the horizontal deflection of the load point (that is on the opposite side to the first crack). In most tests, crushing occurred along the same line on the other face of the beam for both cracks. Photo 4.9 shows pronounced crushing for the crack nearest the fixed end. Slight crushing occurred along the diagonal pencil line on the left side of Photo 4.8.

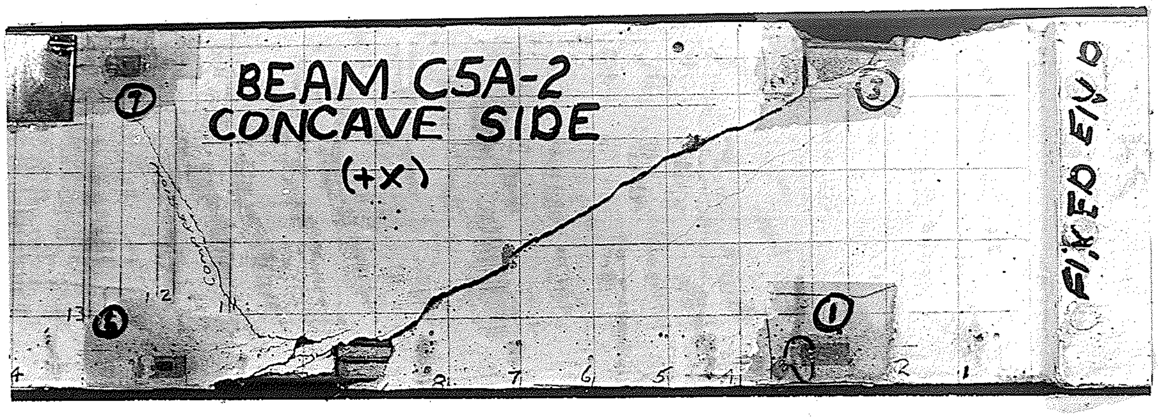

SPECIMEN C44c CRACK PATTERN ON POSITIVE-X FACE

PHOTO 4.8

Note: "Concave Side" Refers to the Curvature of the Failed Specimen
See Photo 4.7

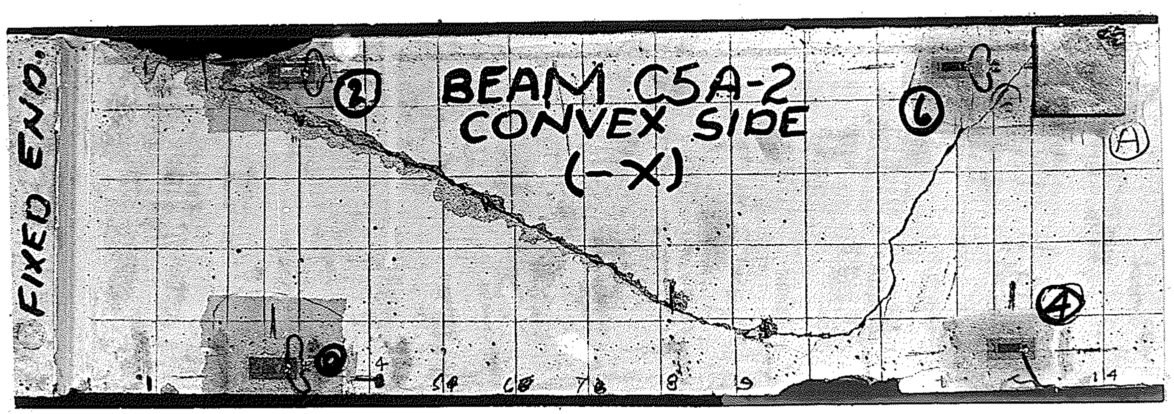

SPECIMEN C44c CRACK PATTERN ON NEGATIVE-X FACE

PHOTO 4.9

Observation during the tests indicated that several hairline cracks formed on each beam prior to failure. These cracks were vertical beginning at or near the bottom and extending upwards. Such cracks were the result of flexural tension and were more numerous on the side of the beam opposite to the horizontal deflection of the load point, (which was the convex side - with the greatest tensile stress). No significant diagonal cracks were observed prior to failure of the beams.

In the early stages of the test, the lateral deflection and rotation of the load point and the remainder of the beam was small. As the load approached failure, the lateral deflection and rotation increased to the point at which the beam was bent into a curved shape such as is shown on Figure 4.4(a). At this point, the lateral deflection and rotation were increasing rapidly and the beam was buckling. The rotation of the beam was the result of twist induced by the lateral displacement of the load. The horizontal position of any point on the beam was the superposition of the horizontal and twisting displacements. Near the fixed end, the twisting displacement was greater than the lateral displacement and thus a horizontal deflection of the top face opposite to that of the deflection of the load point occurred.

At some point in the buckling process, cracking occurred along the two yield lines described previously. It appears that the cracking began at the top of the beam near the point of maximum horizontal curvature (approximately 1/3 span) on the near face of the beam and progressed downward and toward the fixed end as is shown in Figure 4.4(a). The curvature is visible in Photo 4.5 and Photo 4.7. As rotation occurred

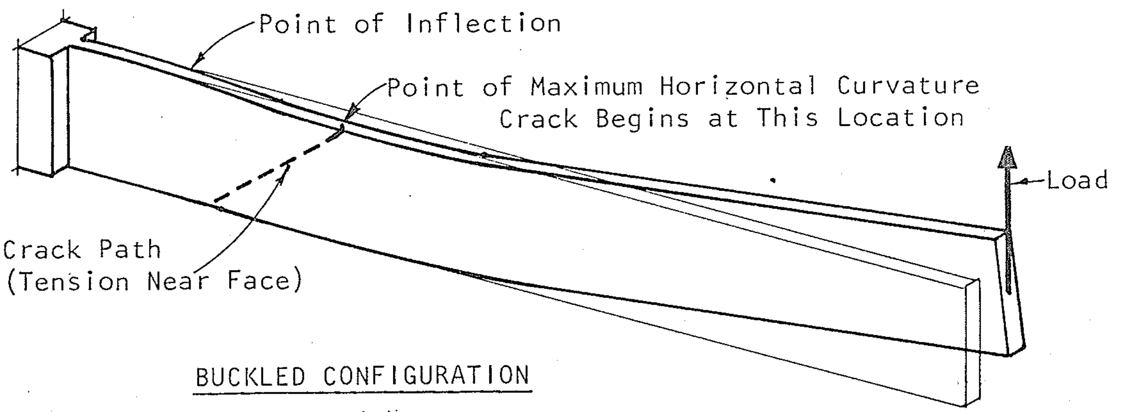

BUCKLED CONFIGURATION

(a)

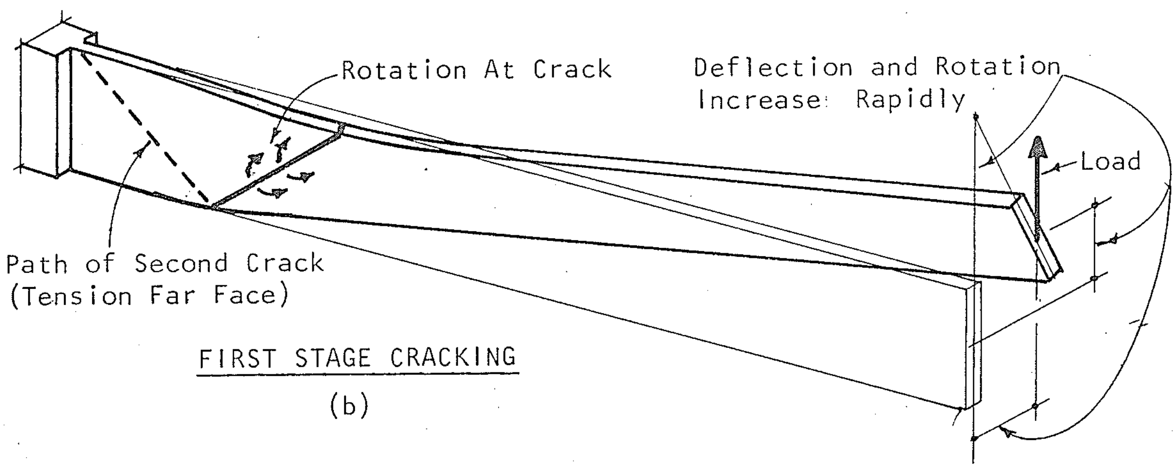

FIRST STAGE CRACKING

(b)

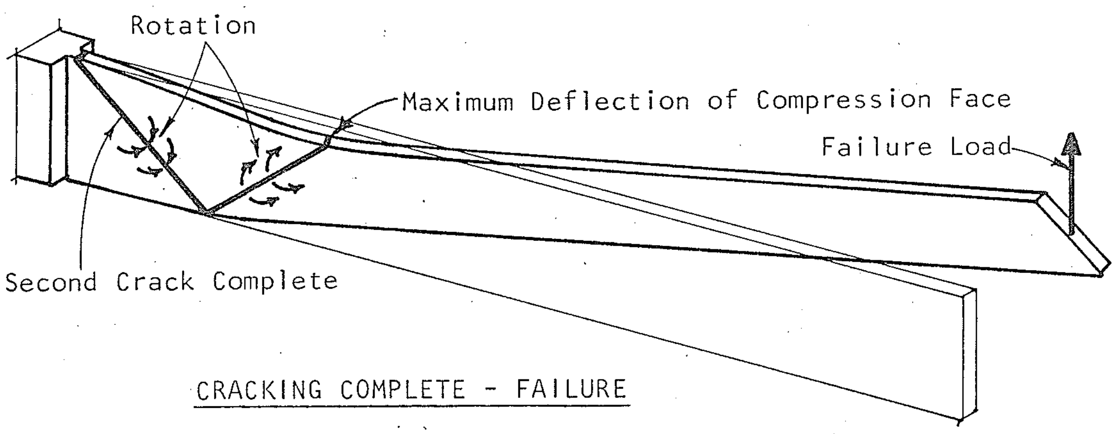

CRACKING COMPLETE - FAILURE

(c)

UNRESTRAINED CANTILEVERED BEAM - SEQUENCE OF LATERAL BUCKLING FAILURE

FIGURE 4.4

along the crack, the load point was allowed to deflect laterally an additional amount with a resulting increase in torsion on the section between the crack and the fixed end, as shown in Figure 4.4(b). A second crack then formed on the opposite face between the tip of the first crack and the top of the beam at the fixed end, as is shown in Figure 4.4(c). The failure was then complete.

4.4 Overhung Beam Tests

The shorter of the two overhung beams, Specimen 014b, is shown in Photo 4.10 prior to testing and Photo 4.11 following failure. The deflections measured during the test are shown on Figure 4.5. The vertical deflection of the load point was nearly linear throughout the test, while the horizontal deflection curve was concave downward. Both the horizontal and vertical deflections were small. The load point rotation was insignificant.

The failure occurred, without warning, in the form of a sudden lateral deflection. A major diagonal crack developed between the two reactions as is shown in Photo 4.11. No cracking was observed prior to the failure.

The development of the long diagonal crack was the result of the freedom of rotation of the front support (closest to the load). All of the torsion induced in the beam was resisted at the back support.

The material properties for the two overhung beams are given in Table 4.2.

Table 4.2

Material Properties for Overhung Beam Specimens

Specimen 014b

Concrete compressive strength	f_c'	= 4533 psi.
Compressive reinforcement yield stress	f_{yC}	= 67,000 psi.
Tensile reinforcement yield stress	f_{yT}	= 66,200 psi.

Specimen 019b

Concrete compressive strength	f_c'	= 4117 psi.
Compressive reinforcement yield stress	f_{yC}	= 67,000 psi.
Tensile reinforcement yield stress	f_{yT}	= 66,200 psi.

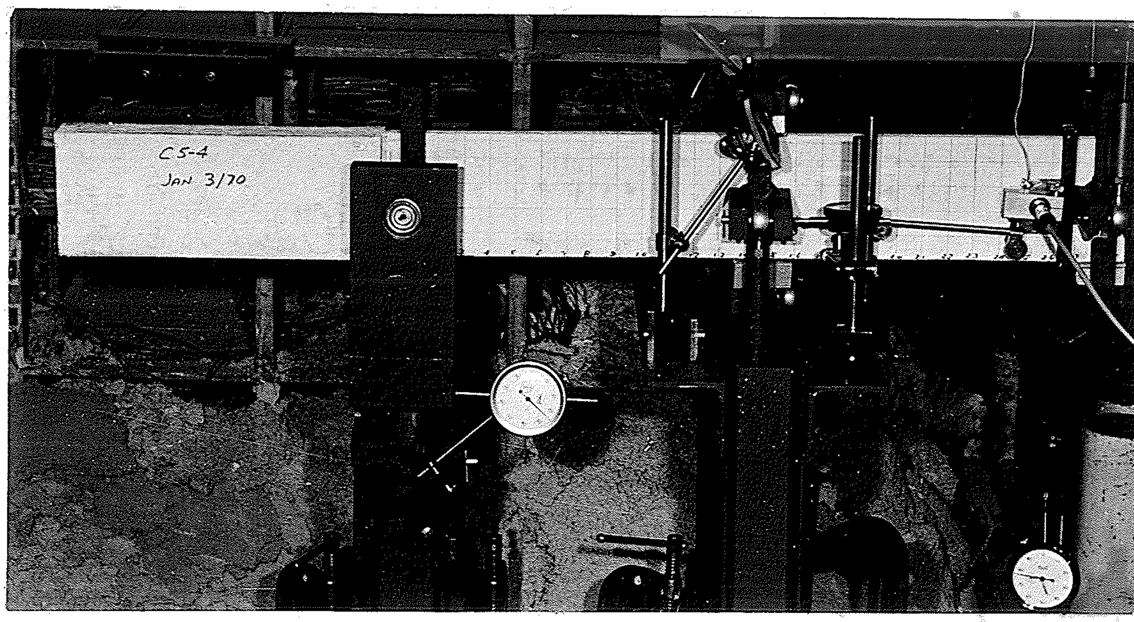

SPECIMEN 014b PRIOR TO LOADING

PHOTO 4.10

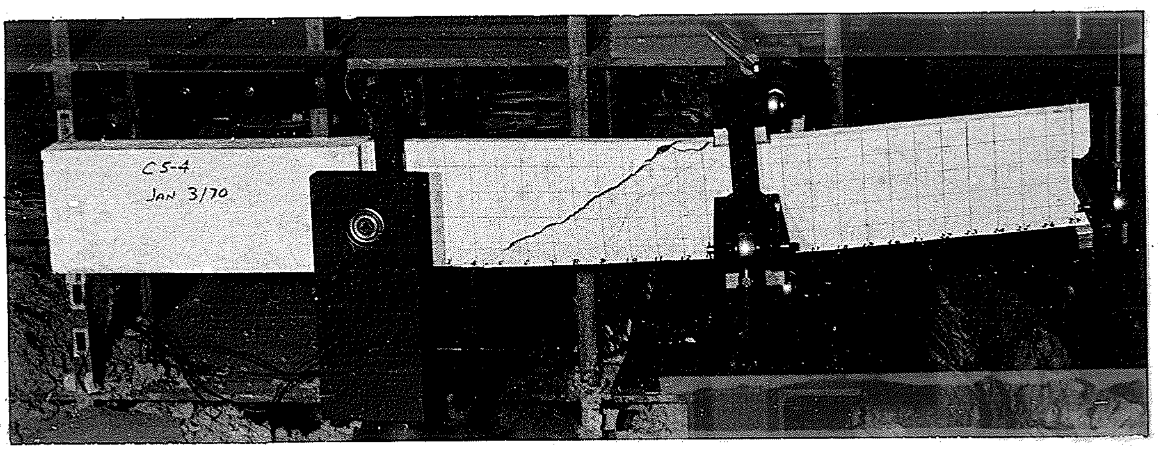

SPECIMEN 014b FOLLOWING FAILURE

PHOTO 4.11

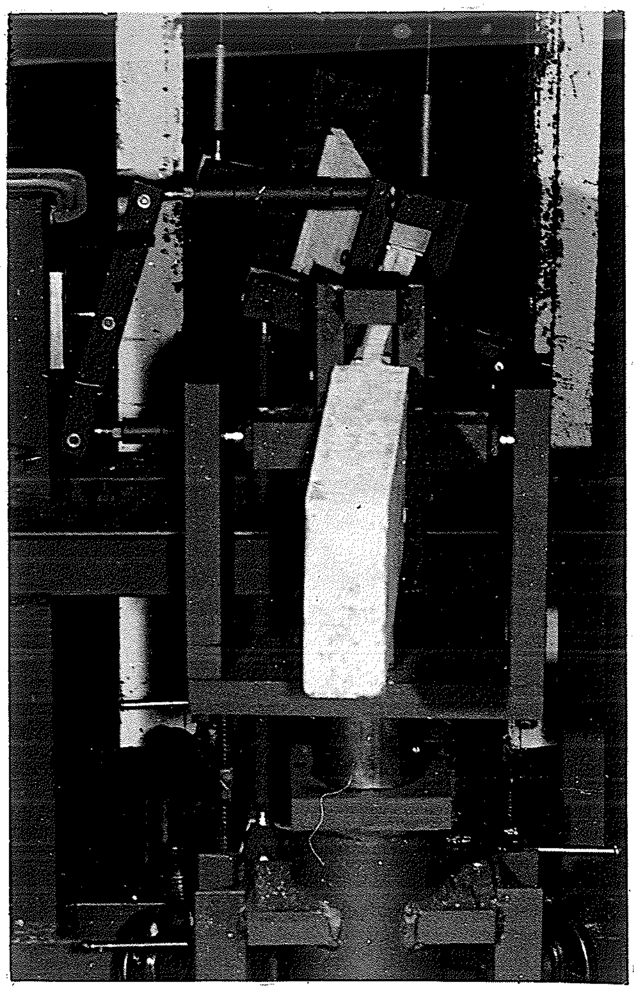

SPECIMEN 014b VIEWED FROM THE REAR

PHOTO 4.12

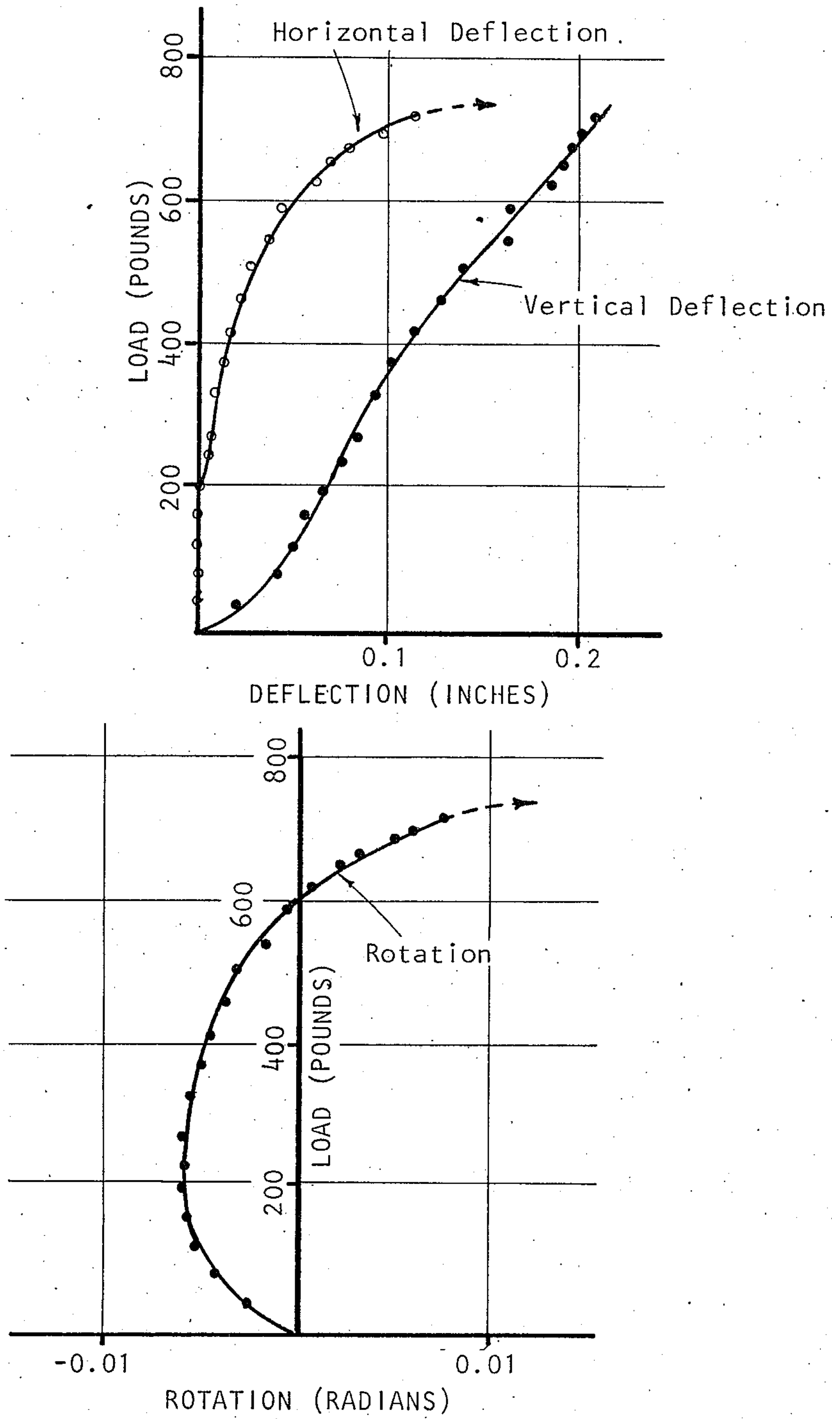

LOAD POINT DISPLACEMENTS - SPECIMEN 014b

FIGURE 4.5

CHAPTER 5

COMPUTATIONS

This Chapter discusses the computation of the ultimate flexural capacity and the lateral buckling capacity of the test specimens, based upon the theoretical discussions in Chapter 2. The results of the computations are summarized and discussed in Chapter 6.

5.1 Ultimate Flexural Capacity

In all cases, except in the type "c" cross-section, the flexural capacity of the test specimens was governed by yielding of the tensile reinforcement. With the high-strength wire for tensile reinforcement, the type "c" cross-section was over-reinforced. In all cases, the compressive reinforcement yielded prior to the development of the full plastic moment. For cross-section types "a", "b" and "d" the ultimate moment was computed by substitution of the cross-section properties from Figure 3.2, into Equation (2.27), with the following results:

For the type "a" cross-section:

A_s = 0.061752 inches^2

A_s' = 0

b = 0.5 inches

d = 4.586 inches

d' = 0

$$M_u = \left\{ 4.586 - \frac{0.061752 f_{yT}}{.85 f_c^{'}} \right\} (0.061752 f_{yT}) \text{ ------------------ } (5.1)$$

For Specimen S48a - No. 2, the values of the reinforcement yield stress, f_{yT} = 55,600 psi, and the concrete compressive strength, $f_c^{'}$ = 5678 psi, were substituted into Equation (5.1) to produce an ultimate flexural moment of 13,300 inch pounds. Corresponding to this moment is an ultimate load, at the mid point, of 1108.3 pounds.

For the type "b" cross-section:

A_s = 0.05946 inches^2

$A_s^{'}$ = 0.0101 inches^2

b = 0.5 inches

d = 4.646 inches

$d^{'}$ = 0.165 inches

$$M_u = \left\{ 4.646 - \frac{(0.05946 f_{yT} - 0.0101 f_{yC})}{.85 f_c^{'}} \right\} (0.05946 f_{yT} -$$

$$0.0101 f_{yC}) + 0.045258 f_{yC} \text{ ---------------------------- } (5.2)$$

The material properties for the overhung beams, which had type "b" cross-section, are given in Table 4.2. The properties for the cantilevered beams are given in Appendix A. The computed ultimate loads corresponding to the ultimate flexural moments are given in Table 6.1.

For the type "c" and "d" cross-sections:

A_s = 0.06451 inches^2 (nominal for 0.117 inch wire diameter)

$A_s^{'}$ = 0.0101 inches^2

b = 0.5 inches

d = 4.60 inches

d' = 0.165 inches

$$M_u = \left\{4.60 - \frac{(0.06451f_{yT} - 0.0101f_{yC})}{.85f_c'}\right\}(0.06451f_{yT} - 0.0101f_{yC}) + 0.044794f_{yC} \quad (5.3)$$

For Specimen C32d, the tensile reinforcement diameter varied from 0.1175 to 0.1185 inches as is shown in Appendix A. For computation of the flexural capacity, the quantity $0.06451f_{yT}$ was replaced with the summation of the yield loads for the test samples taken from the six tensile wires.

For the type "c" cross-section, which was over-reinforced, the analysis was carried out by replacing the term f_{yT}, in Equation (5.3), with a variable reinforcement stress f_T which was the strain times 29 x 10^6. The compressive reinforcement yielded in all specimens so the stress f_{yC} was used. The analysis was carried out by assuming a neutral axis position, setting the concrete strain equal to 0.003 and checking the equilibrium of the section.

5.2 Elastic Section Properties

Computations of the lateral buckling loads were based upon the assumption of linear-elastic behaviour of the concrete cross-section to be consistent with the assumptions made in the development of the expressions for the critical loads, Equations (2.21) and (2.22), and the rigidity parameters, Equations (2.23), (2.24) and (2.25).

For these computations, the elastic section properties of the beam sections were required. The section properties were computed using the classical assumptions of linear behaviour in concrete members, (that is linear strain distribution, linear compressive stress distribution and a modulus of rupture for concrete of zero). The sections were transformed using a modular ratio based upon the secant modulus of the extreme concrete fibre (Section 1.1).

Thus:

$$n = E_{steel}/E_{sec} \quad \text{-----} \quad (5.4)$$

In normal elastic analysis, the transformed area of the compressive reinforcement is computed using one-half the elastic modulus for concrete to account for creep during long term loading. In this case, loading was rapid and creep was not a factor. The compressive reinforcement was, therefore, transformed using a multiplier of (n - 1) rather than the conventional (2n - 1).

For the three cross-sections shown in Figure 3.2, whose key dimensions and reinforcement quantities are given in Section 5.1, the position of the neutral axis of the cracked, transformed, section was located by making the summation of the first moment of area about the neutral axis equal to zero.

For the type "a" cross-section:

$$0 = (0.5\bar{y})(\bar{y}/2) - (4.586 - \bar{y})(0.061752n) \quad \text{-----} \quad (5.5)$$

In which:

$\bar{y}$ = the position of the neutral axis measured from the compression face of the beam.

n = the modular ratio $29 \times 10^6/E_{sec}$

For the type "b" cross-section:

$$0 = (0.5\bar{y})(\bar{y}/2) + (0.0101)(n-1)(\bar{y}-0.165) - (4.646-\bar{y})(0.05946n) \quad \text{---} \quad (5.6)$$

For the type "c" and "d" cross-sections:

$$0 = (0.5\bar{y})(\bar{y}/2) + (0.0101)(n-1)(\bar{y}-0.165) - (4.60-\bar{y})(0.064506n) \quad \text{---} \quad (5.7)$$

For any given value of n, Equations (5.5), (5.6) or (5.7) were solved as quadratics to determine the value of $\bar{y}$. Due to the shape of the concrete stress-strain curve, the value of the secant modulus was variable as a function of the strong axis bending moment applied to the most highly stressed cross-section. For any given moment, the neutral axis was located by an iterative procedure as follows:

Given a value of the bending moment = M:

Step 1:

Assume a value of the extreme fiber stress = σ

Step 2:

Compute the value of the modular ratio = n as follows:

Since $E_{sec} = \sigma/\varepsilon$ --- (5.8)

Combine Equations (3.1), (5.4) and (5.8) to give:

$$n = 8.479(1 + (\sigma/6614.558)^{3.1381}) \quad \text{-------------------------} \quad (5.9)$$

Step 3:

Locate the neutral axis from Equation (5.5), (5.6) or (5.7).

Step 4:

Compute the moment of inertia of the transformed section.

Step 5:

Compute new the extreme fiber stress

$$\sigma_{new} = M\bar{y}/I \quad \text{---} \quad (5.10)$$

The process was repeated until the assumed and computed values of σ converged.

5.2.1 Lateral Flexural Rigidity - B

For the cross-sections of the test beams, shown in Figure (3.2), the values of B were determined by substituting the beam geometry into Equation (2.23).

$$B = (\bar{y}b^3/12)(E_{sec}) + \sum I_{sy}E_s \quad \text{------------------------------------} \quad (2.23)$$

For the type "a" cross-section:

$$B = 0.010416\bar{y}E_{sec} + 35583.2 \quad \text{------------------------------------} \quad (5.11)$$

For the type "b" cross-section:

$$B = 0.010416\bar{y}E_{sec} + 36712.6 \quad \text{------------------------------------} \quad (5.12)$$

For the type "c" and "d" cross-sections:

$$B = 0.010416\bar{y}E_{sec} + 39191.2 \quad \text{------------------------------------} \quad (5.13)$$

Where:

B = The lateral flexural rigidity, in pound inches^2.

E_{sec} = The secant modulus of the extreme concrete fiber at the point of maximum bending.

$\bar{y}$ = The distance from the compression face to the neutral axis.

The value of the quantity B varied with bending as a function of the values of $\bar{y}$ and E_{sec} which were determined using the iterative procedure described previously. The secant modulus was found from Equation (5.9) by taking:

$$E_{sec} = 29 \times 10^6/n \quad \text{--} \quad (5.14)$$

5.2.2 Torsional Rigidity - C

The value of C was computed from the beam cross-sections shown in Figure 5.2:

$$C = \beta b^3 d' G_c' + 1/3(G_s - G_c') \sum b_s^3 t_s$$
$$+ (\gamma b_1{}^2 d_1 A_t E_s)/2\sqrt{2}\, p_s) \quad \text{------------------------------} \quad (2.24)$$

The first term in Equation (2.23) gives the contribution of the concrete in the section. The parameter β is dependent upon the ratio "d'/b". For $d'/b = 10$, Timoshenko and Goodier[26] give $\beta = 0.312$.

Massey[11] determined the value of the reduced modulus of rigidity "G_c'" experimentally for beams with and without compressive reinforcement. He plotted M/M_e vs G_c'/G_c and drew two straight lines to represent the behaviour with and without compressive reinforcement. For the type "a" cross-section, which had no compressive reinforcement, the line had the following equation:

$$G_c'/G_c = 1 - 0.1142M/M_e \qquad (5.15)$$

In Massey's test specimens, the ratio of compressive to tensile reinforcement was approximately 50%, whereas in this study the ratio was 17% and 15.5% for the type "b" and the type "c" and "d" cross-sections respectively. As a result, the actual value of G_c' was most likely somewhere between Massey's two straight lines. For the purpose of these computations, it was assumed that the value of G_c' was the average of the two. In Equation form:

$$G_c'/G_c = 1 - 0.19M/M_e \qquad (5.16)$$

The parameter M_e is defined by Massey[11] as the moment required to produce a stress of $0.85f_c'$ at the extreme concrete fiber of a transformed section having a modular ratio of 15.

The initial modulus of rigidity, from Section 3.4, was:

$$G_c = 1.46 \times 10^6 \text{ psi} \qquad (3.2)$$

The second term in Equation (2.24) is the contribution of the longitudinal reinforcement. The modulus of rigidity for steel is:

$$G_s = 29 \times 10^6/2(1 - 0.3) = 11.15 \times 10^6 \quad \text{----------------------} \quad (5.17)$$

The third term is the contribution due to closed vertical stirrups. The parameter γ is dependent upon the ratio d_1/b_1 (the stirrup dimensions) and is given by Cowan[27]. For the specimens in this study, the ratio d_1/b_1 was 12.7, Cowan (who gives the parameter as λ) gives values to d_1/b_1 = 3.0 only. By extrapolating the values given by Cowan, the value of γ for d_1/b_1 = 12.7 is approximately 0.5.

For the three specimen cross-sections, using the parameters discussed above, Equation (2.23) becomes:

For the type "a" cross-section:

$$C = 0.195G_c' + (11.15 \times 10^6 - G_c')(0.006613) \quad \text{-----------------} \quad (5.18)$$

For the type "b" cross-section:

$$C = 0.195G_c' + (11.15 \times 10^6 - G_c')(0.007221) + 3440 \quad \text{-----------} \quad (5.19)$$

For the type "c" and "d" cross-sections:

$$C = 0.195G_c' + (11.15 \times 10^6 - G_c')(0.007576) + 3440 \quad \text{-----------} \quad (5.20)$$

In which:

C = Torsional rigidity in pound inches^2.

G_c' = Reduced modulus of rigidity of concrete.

Equation (5.18) was combined with Equations (5.16) and (3.2) to give, for the type "a" cross-section:

$$C = 348780 - 31410.1M/M_e \text{ -------------------------------------- } (5.21)$$

Similarly, Equations (5.17) and (3.2) were combined with Equations (5.19) and (5.20) in turn to give:

For the type "b" cross-section:

$$C = 358111.5 - 52089.9M/M_e \text{ ------------------------------------ } (5.22)$$

For the type "c" and "d" cross-sections:

$$C = 361553.1 - 51991.4M/M_e \text{ ------------------------------------ } (5.23)$$

In which:

M = The strong axis bending moment at the cross-section.

M_e = The moment computed as the extreme fiber concrete stress at the section times the section modulus computed for a transformed section having a modular ratio n = 15.

5.2.3 Warping Rigidity - C_w

The warping rigidity was computed for the three cross-sections by substituting the moments of inertia of the reinforcement, shown in Figure 3.2, into Equation (2.25).

$$C_w = E_s h^2 (I_1 I_2)/(I_1 + I_2) \text{ -------------------------------------- } (2.25)$$

The results are as follows:

For the type "a" cross-section:

$C_w = 0$ -- (5.24)

For the type "b" cross-section:

$C_w = 106880.6$ -- (5.25)

For the type "c" and "d" cross-sections:

$C_w = 106171.1$ -- (5.26)

In which:

C_w = Warping rigidity in pound inches^2.

5.3 Computation of the Elastic Lateral Buckling Loads

The buckling loads for the test specimens were computed by substituting appropriate values of the parameters B, C and C_w discussed previously into Equations (2.21) or (2.22).

For the Cantilevered Beams and the Overhung Beams:

$$P_{cr} = \frac{4.013\sqrt{BC}}{\left(1 - \sqrt{C_w/L_3^2 C}\right)^2 L_e^2} \quad \text{------------------------------------} \quad (2.21a)$$

Where:

P_{cr} = The lateral buckling load.

B = The lateral flexural rigidity, computed from Equations (5.12) and (5.13).

C = The torsional rigidity, computed from Equations (5.22) and (5.23).

L_e = The effective length

L_e = 1.0L for the cantilevered beams.

L_e = 2.7L or 2.95L for the overhung beams[20].

For the Simply-Supported Beams:

$$P_{cr} = 16.94 \sqrt{BC}/L^2 \quad \text{--} \quad (2.22)$$

Since the values of B and C were functions of the applied bending moment, they were variable both with respect to the applied load and position along the length of the beam. To simplify the computation, it was assumed that the rigidity values computed at the point of maximum bending applied along the entire length of the beam.

Two approaches were used. In the first, the rigidity terms were determined upon the basis of test data and in the second they were determined upon the assumption of an idealized behaviour.

5.3.1 Lateral Buckling Load - Based Upon Test Measurements

For this approach, the values of the lateral flexural and torsional rigidity were computed for the maximum moment produced by the failure load and for an extreme fiber concrete stress of $0.85f_c'$. As an example, the computation for Specimen C36b follows:

Specimen C36b:

Failure Load = 461 pounds

Beam Length = 36 inches

Concrete Compressive Strength f_c' = 3870 psi

Step 1:

Locate the neutral axis for a stress of $0.85f_c' = 3289.5$ psi.

(a) from Equation (5.9): $n = 9.426$

(b) from Equation (5.6): $\bar{y} = 2.193$ inches

(c) compute the tensile reinforcement stress $(=.85f_c'n(d - \bar{y})/\bar{y}) = 81356$ psi (for information only)

Step 2:

Compute the lateral flexural rigidity:

(a) from Equation (5.14): $E_{sec} = 3.077 \times 10^6$

(b) from Equation (5.13), with the above values of $\bar{y}$ and E_{sec}, $B = 106417.54$ pound inches^2

Step 3:

Compute the torsional rigidity:

(a) from Equation (5.6), with $n = 15$, $\bar{y} = 2.509$ inches; for this value of $\bar{y}$, the moment of inertia of the transformed section is 7.482 inches^4. Then: $M_e = 0.85(3870)(7.482)/2.509 = 9809.5$ inch pounds

(b) for the failure load and beam length, $M = (461)(36) = 16596$ inch pounds

(c) from Equation (5.22): $C = 269977.65$ pound inches^2

Step 4:

Compute the buckling load:

Substitute $B = 106417.65$, $C = 269977.65$ and, from Equation (5.25), $C_w = 106880.6$ into Equation (2.21a) using $L_e = L$.

$$P_{cr} = \frac{4.013\sqrt{(106417.54)(269977.65)}}{\left\{1 - \sqrt{\dfrac{106880.6}{(36^2)(269977.65)}}\right\}^2 36^2} = 535.6 \text{ pounds}$$

The above procedure was repeated for each of the test specimens.

5.3.2 Idealized Lateral Buckling Load

The approach discussed in the previous section is useful only for the analysis of test data and cannot be used as a design procedure. To determine the stability of a member at the design stage, another approach is necessary. In the approach presented here the maximum concrete stress, on the transformed section at the instant of lateral buckling, was defined as $0.85f_c'$. The concrete was assumed to follow the stress-strain curve given in Equation (3.1) and the value of f_c' was assumed to vary as necessary. Since the resulting buckling loads were based upon assumed idealized material behaviour, they were defined as "Idealized Buckling Loads".

The idealized lateral buckling load - P_{cr}^*, for any specimen, was found by an iterative procedure as follows:

Step 1:

Assume a buckling load and compute the maximum moment in the member. - M.

Step 2:

For that moment, determine the corresponding extreme fibre stress by the iterative procedure given in Section 5.2. The stress was, by definition, $0.85f_c'$. This procedure also found the value of the secant modulus E_{sec} and located the neutral axis ($\bar{y}$). The stress in the tensile reinforcement was also computed at this stage as a secondary part of the computation.

Step 3:

Compute the lateral flexural rigidity and the torsional rigidity for the computed values of maximum moment - M, secant modulus E_{sec} and neutral axis location $\bar{y}$ using the procedure discussed in Section 5.3.1 and the appropriate equations for the rigidities, (Sections 5.2.1, 5.2.2 and 5.2.3).

Step 4:

Compute the buckling load using Equation (2.21a) or (2.22) as necessary.

Step 5:

Compare the computed buckling load to the assumed load.

The procedure was repeated until the assumed load and the computed buckling load converged, and the result was the Idealized Critical Load.

The procedure was repeated for a variety of beam lengths, for the three types of loading and for the appropriate cross-sections. The results are presented in Table 6.1. As a secondary computation, the rigidity terms were recomputed on the assumption that the tensile reinforcement had yielded (thus producing $E_s = 0$). The idealized critical loads were then recomputed with the new, reduced, rigidity terms.

CHAPTER 6

DISCUSSION

6.1 Simply Supported Beam Tests and Model Similitude

Test Specimen S48a - No. 2 was a 1/4.7 Scale model of Specimen B_{24}-1 reported by Sant and Bletzacker[9]. Sant and Bletzacker's apparatus was arranged so that rotation of the loading jack was about a point approximately 24 inches above the center of the beam cross-section. The apparatus used in this study was designed to allow rotation about the center of the cross-section.

The load-deflection curves for Speciman S48a - No. 2 and the scaled deflection curves for Specimen B_{24}-1 (from Figure 10[9] using Equations (1.11) and (1.13)) are shown on Figure 4.1. The failure load for Specimen S48a - No. 2 was 1295 pounds, while the scaled failure load for Specimen B_{24}-1 was 996 pounds. The deflection curves of the two tests are similar in shape, with the curves for the model being steeper in each case. The difference in the horizontal deflection curves is due to the difference in loading arrangement (location of the center of rotation). With the load above the centroid, the horizontal deflection of the full size beam was amplified.

To allow for the difference in the center of rotation, Equation (2.22) is modified as follows:[13]

$$P_{cr} = 16.94\sqrt{BC}/L^2 \left\{1 - \frac{1.74h_1}{L\sqrt{B/C}}\right\} \quad \text{------------------------} \quad (6.1)$$

In which:

P_{cr} = the lateral buckling load

B = the lateral flexural rigidity

C = the torsional rigidity

L = length

h_1 = distance above or below the centroid (+ on the compression side)

Using the values for B and C computed for Specimen S48a - No. 2 (Section 5.3.1) and the dimension h_1 = 5.1 inches (24 x 1/4.7) the term in Equation (6.1) in brackets computes to be 0.672. If the failure load of Specimen S48a - No. 2 is multiplied by this value, it becomes 870 pounds. By applying Equation (1.13):

$$P = S^2P' \quad \text{---} \quad (1.13)$$

In which:

P = prototype failure load (=22,000 pounds[9])

P' = computed model failure load (=870 pounds)

S = scale factor = $\sqrt{(870/22{,}000)}$ = 1/5

This computed scale factor based upon the failure load is within 6% of the geometric scale factor. From this it is assumed that models and prototypes will behave in accordance with the laws of model similitude discussed in Section 1.3.

The microconcrete mix design used in this study had a flatter stress-strain curve and a higher modulus of rupture than normal prototype concrete. Since the load-deflection curves shown in Figure 4.1 had similar shapes and obeyed the similitude relationships, it appears that the variations in material properties did not have a major effect on the results.

6.2 Test Apparatus

The loading apparatus allowed for horizontal movement through a long-sided parallelogram, which introduced a slightly inclined load once lateral deflection began. The apparatus could be improved by the provision of a linkage which would allow horizontal movement of the hydraulic cylinder, (the so-called "gravity simulating linkage"). The apparatus would then apply load vertically throughout the test, in accordance with the assumed loading conditions.

An obvious method of applying a gravity load is the use of hanging weight. Such a solution has disadvantages, since the amount of load required is large and smooth application is difficult. (Both of these difficulties could be easily overcome.) The main objection to the use of hanging load is the fact that the specimen is destroyed at failure. With the available data collection equipment, an intact specimen after failure was desirable to determine the mode of failure, and for this reason the use of a hanging load was ruled out.

Some movement occurred in the vertical direction at the fixed end of the beams. This movement was mainly the result of seating of the bearings and crushing of the bearing areas and could be eliminated by decreasing the bearing stress with larger bearing plates or by increasing the length of the enlarged end. Modifications to the clamping apparatus should be considered to increase its stiffness and to decrease the vertical movement.

In spite of the precautions taken to center the specimens in the loading frame, an eccentricity remained somewhere in the apparatus. With the exception of Specimen C44b, all of the specimens (which buckled) deflected in the same horizontal direction. In each case, the parallelogram apparatus was used in the same position except for Specimen C44b, in which case it was rotated 180 degrees horizontally. Thus, all of the specimens buckled in the same relative direction with respect to the loading parallelogram. Such an occurrence was not likely without an initial eccentricity (which was never located). The initial movements seen in the horizontal deflection and the rotation on Figures 4.1, 4.2 and 4.5 were most likely the result of this initial eccentricity.

6.3 Ultimate Flexural Capacity

Of the three specimens which failed as the result of flexure, the failure loads were 7 to 15% higher than the ultimate flexural loads, as shown in Table 6.1. This fact indicates that either the ultimate moment was higher than computed or the failure load was lower than measured.

Since the load was measured by a calibrated load cell, it is not likely to be in error by any significant amount.

The ultimate moment was computed on the assumption of a rectangular stress block and disregarding strain-hardening of the reinforcement. The reinforcement tensile tests, in Appendix A, indicate strain-hardening of the tensile reinforcement in the range of 4% to 7%. The vertical deflection curves for Specimens C32b and C32d show an increase in load following yielding of the reinforcement, by a slight upward slope in the vertical deflection curve. From this, it appears that the reinforcement went into the strain-hardening range with a resulting increase in the ultimate flexural moment.

In the case of Specimen C32c, which was over-reinforced, the computed ultimate load was 9% lower than the failure load. Since the reinforcement did not yield, strain-hardening was not a factor. From this, it is concluded that the concrete compressive zone also produced a higher ultimate than computed. The ultimate moment is a function both of the shape of the compressive stress block, which determines the location of the compressive resultant, and of the strength of the concrete. The difference between the assumed rectangular block and the actual behaviour is not normally significant. There remains, therefore, the compressive strength of the concrete which must have been higher in the body of the beam specimens than it was in the sample cylinders.

It appears, therefore, that the low computed ultimate flexural strengths (as compared to the failure loads) were the result of higher strengths in the concrete within the specimen than those measured in the test samples and of the fact that the strain hardening of the reinforcement was ignored. With the deep cross-section under consideration, the effects of both of these factors were exaggerated.

6.4 Comparison Between the Computed Buckling Loads and the Test Results - Cantilevered Beam Specimens

The test results and the theoretical buckling loads are compared in Table 6.1 and Figure 6.1. The buckling loads were computed from the relationships developed in Chapter 2, using the procedures described in Section 5.3.2.

The buckling loads shown are the "Idealized Buckling Loads", which were computed on the assumption that the concrete strength varied as necessary to give 0.85 f_c' at the instant of buckling. The buckling loads computed from the actual values of f_c' for the test specimens are not shown. All were within 6% of the "ideal" values.

The failure loads for the type "b" cross-section specimens were below the buckling curve while those for the four type "c" specimens, which buckled, were above. Specimens C32c and C32d, both of which failed due to flexure, were below the buckling curve.

The position of the failure load of a buckling specimen with respect to the buckling curve was related to the extent of cracking of the cross-section. For those specimens in which the maximum moment approximated that required to develop a fully cracked cross-section, but without significant yielding, the buckling loads and the failure loads were nearly equal. This was

TABLE 6.1 COMPARISON OF FAILURE, ULTIMATE FLEXURAL AND BUCKLING LOADS

SPECIMEN	LENGTH	FAILURE LOAD (1)	ULTIMATE FLEXURAL LOAD (1)	BUCKLING LOAD (1)
SIMPLY SUPPORTED BEAMS				
S48a - No. 2	48	1295	1108.3	1246.6
CANTILEVERED BEAMS				
C44b	44	355	325.2	354.2
C40b	40	410	382.8	422.4
C36b	36	461 (3)	395.8	512.5
C32b	32	550 (4)	468.1	635.6
C48c	48	355	426.5	307.9
C44c	44	445	441.6	361.7
C36c	36	585	541.7	523.3
C32c	32	590 (5)	537.2	649.0
C32d	32	615 (4)	576.3	649.0
OVERHUNG BEAMS - Effective Length = 2.7L				
O14b	14	743	1081.4	526.8
O19b	19	508	811.5	290.5

NOTES:

(1) All loads are in pounds.
(2) Specimens S48a - No. 1 and C40c are disregarded.
(3) The failure of Specimen C36b was a combination of flexure and lateral buckling.
(4) The failure of Specimens C32b and C32d were by yielding of the reinforcement.
(5) The failure of Specimen C32c was the result of crushing of the concrete.
(6) All specimens except those noted above failed as a result of lateral buckling.

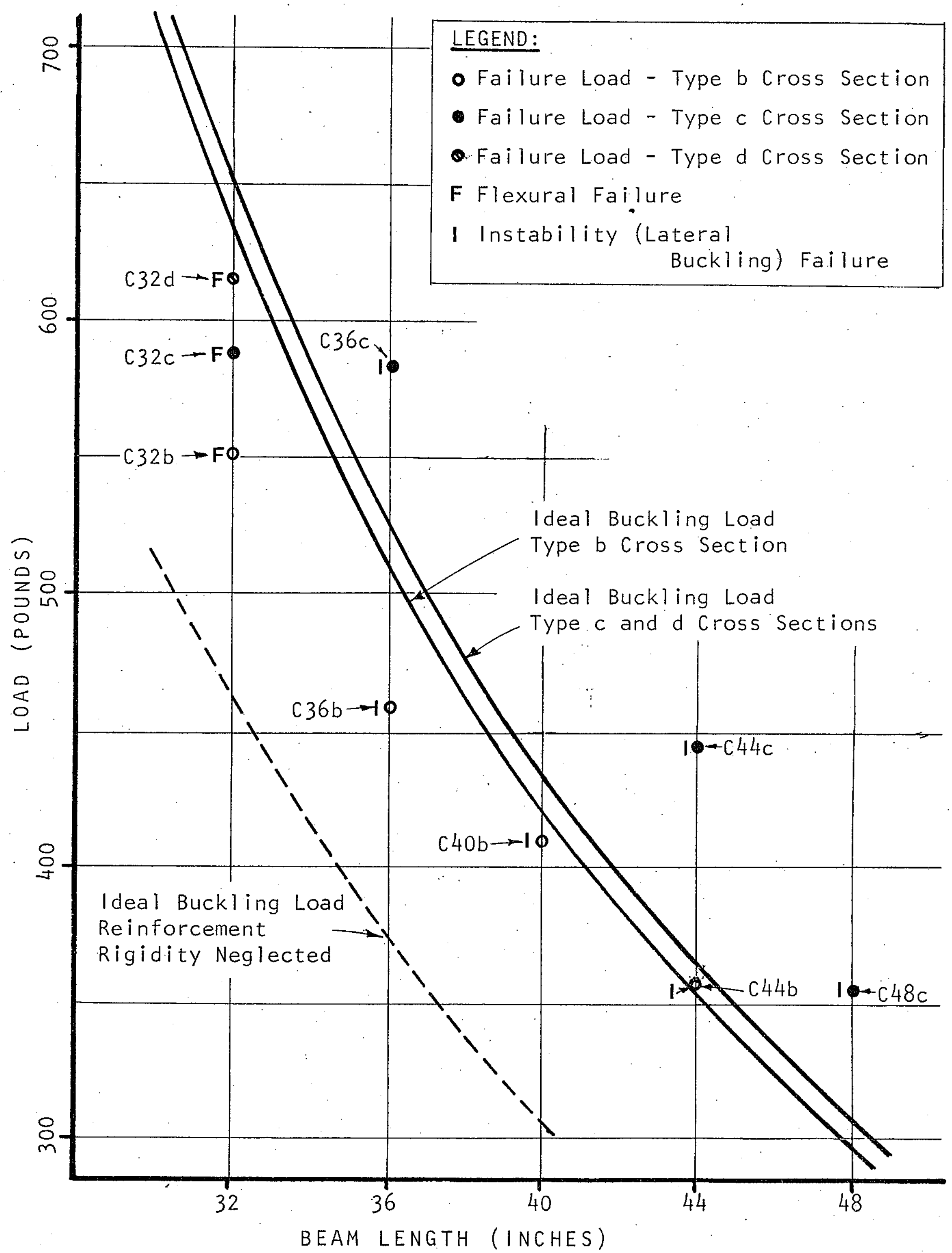

UNRESTRAINED CANTILEVERED BEAMS - COMPARISON BETWEEN FAILURE LOADS AND COMPUTED BUCKLING LOADS

FIGURE 6.1

particularly true in the case of Specimen C44b in which the tensile reinforcement stress, on the transformed cracked section at buckling, was approximately equal the yield stress. At this level of bending, the assumed cracked elastic section was more or less achieved and the conditions assumed in the development of the rigidity terms (Section 2.2) were approximated. At higher bending levels, such as those in Specimen C36b, the elastically computed reinforcement stress was approximately 20% in excess of yield level. As yielding took place, the contribution of the reinforcement to the rigidity terms was reduced with a resulting reduction in the buckling load. In the case of the type "c" cross-section, the reinforcement had a high "yield" stress and no significant yield plateau. As a result, the cracked cross-section could not develop fully prior to buckling. In this case, the lateral flexural rigidity was greater than assumed by virtue of an increase in the uncracked portion of the cross-section and of an increase in the secant modulus resulting from a decrease in the extreme fiber stress (due to the increased section modulus). With the increased lateral flexural rigidity, the buckling load was increased.

Inspection of the vertical deflection curves, for the four type "b" Cantilevers in Appendix A, shows that only the longest, Specimen C44b, did not exhibit yielding of the reinforcement prior to failure. For this specimen, the vertical deflection curve was nearly linear to failure. For Specimens C40b, C36b and C32b, the amount of yielding, indicated by the flattening of the upper end of the vertical deflection curve, increased as the length decreased. Specimens C44b and C40b buckled laterally, and Specimen C32b failed due to flexure. The failure configuration of Specimen

C36b had features both of lateral buckling and of flexure, as shown in Figure A.10. At failure, some diagonal cracks formed but the major cracking was immediately adjacent to the fixed end and was in the form of a separation which occurred on a vertical plane inclined to the longitudinal axis of the specimen.

Since the shorter specimen (C32b) failed as the result of flexure and the longer one (C40b) buckled, it appeared that the failure of Specimen C36b was in the "elasto-plastic" range between. In this range, yielding of the reinforcement produced a reduction in the rigidity of the specimen and a subsequent reduction in the buckling load. To check on the effect of the yielding, the ideal buckling loads were recomputed with the contribution of the longitudinal reinforcement removed from the rigidity equations (Sections 5.2.1, 5.2.2 and 5.2.3). The result is shown as a broken line on Figure 6.1. The failure loads for Specimens C32b and C36b were 18% and 20% respectively above the critical loads indicated by the lower curve. Thus it is concluded that computed buckling loads, which neglect the reinforcement rigidity, underestimate the capacity of specimens in which the reinforcement has yielded. Consideration of the full reinforcement rigidity overestimates the capacity.

The test results have pointed out three types of failure in the unrestrained cantilevered concrete beam specimens.

The probable form of the interaction curve between failure load and beam length is sketched on Figure 6.2. This form is characteristic of that found in most instability problems. For the design of members by ultimate strength, the flexural mode and the elasto-plastic mode of failure are of the most interest.

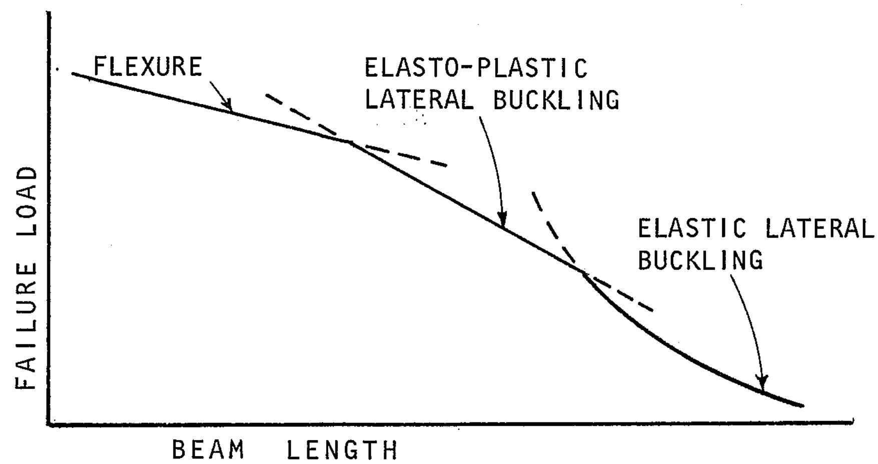

FAILURE MODES OF UNRESTRAINED CANTILEVERED BEAMS OF CONSTANT CROSS-SECTION

FIGURE 6.2

6.5 Comparison Between the Computed Buckling Loads and the Test Results - Simply-Supported Beam Specimens

From Table 6.1, the failure load and the buckling loads agreed closely. In this case, the reinforcement stress computed on the basis of the cracked elastic section was approximately 20% above yield level but the comparison between the loads indicated that the failure was not in the elasto-plastic range. As discussed previously, Specimen C36b buckled in the elasto-plastic range with a cracked section reinforcement stress 20% above yield. The difference between the behaviour of the two lies in the fact that there was considerably more restraint available in the simply-supported beam. In the case of the cantilever, yielding at the fixed end allowed large lateral deflection and rotation to occur while in the case of the simply-supported beam, the torsional restraint was applied at the ends at which points the moment was low.

6.6 Comparison Between the Computed Buckling Loads and the Test Results - Overhung Beam Specimens

As shown in Table 6.1, the computed buckling loads were considerably below the failure loads. Since the tensile reinforcement stresses on the cracked section were less than half the yield stress, the cracked section was not fully developed and the buckling loads were underestimated by 30 to 40%. The results computed for the effective length of 2.95L[20] were somewhat lower.

By comparing the results of the idealized buckling loads for various lengths to the flexural capacity of the members, it appeared that elasto-plastic buckling would take over at approximately 10 inches length with flexural failures at lengths slightly lower. At these lengths, the computed shear in the member exceeded the shear capacity.

6.7 Design Procedure

As discussed in Chapter 1, present codes for the design of concrete structures[1][2] insure ductile failures of flexural members by restricting the tensile reinforcement to 75% of balanced reinforcement. To insure stability of these members, the geometry should be limited in such a way as to allow the development of the ultimate moment prior to lateral buckling. Sant and Bletzacker[9] have argued that the reinforcement should be limited to achieve this end and Equation (1.9) was developed upon this basis. Equation (1.9) was applied to the test data for the five under-reinforced specimens and the results are shown in Table 6.2.

From Table 6.2, the values of k_{10} and of the product $k_{10}E_{sec}$ for Specimen C32b are the lowest for all specimens. Specimen C32d which also failed due to flexure, but which had considerably higher values of f_c' and f_y, produced higher values of k_{10} and $k_{10}E_{sec}$. From these two results, it appears that a single value of k_{10} or of $k_{10}E_{sec}$ is not sufficient to cover the full range of possibilities of concrete and reinforcement strengths and that the numerator in Equation (1.9) is a function both of the loading and restraint geometry (which was assumed in the derivation) and of the material strengths.

For use as a building code provision, it is suggested that the beam slenderness be limited to the point that a member reinforced with 75% of the balanced reinforcement will reach its ultimate moment before buckling. The result for Specimen C32b meets this criterion exactly, while Specimen C32d nearly meets it with the exception that the reinforcement ratio exceeds the $0.75p_b$ limit. These two results provide a first approximation of a set of limits.

For Specimen C32b:

f_c' = 4010 psi

f_y = 66,000 psi

$0.75p_b$ = 0.01872

From Equation (1.9) - Table 6.2

$$0.75p_b f_y = \frac{834720.9}{Ld/b^2} = 0.01872 \times 66000$$

$$Ld/b^2 = 675.6 \quad \text{--} \quad (6.2)$$

For Specimen C32d:

$f_c' = 6920$ psi

$f_y = 70{,}800$ psi

$0.75p_b = 0.01814$

From Equation (1.9) - Table 6.2

$$0.75p_b f_y = \frac{1028816.9}{Ld/b^2} = 0.01814 \times 70800$$

$$Ld/b^2 = 599.3 \quad \text{--} \quad (6.3)$$

Since Equations (6.2) and (6.3) assume $0.75p_b$ in their development, the result is a function both of f_c' and f_y. Equations (6.2) and (6.3) may be thought of as point within a family of curves relating the reinforcement yield stress and concrete compressive strength to the maximum beam slenderness ratio at which the beam will develop its ultimate moment as an unrestrained cantilever without buckling.

For beams with loading and restraint different from the assumed unrestrained cantilever, the concept of effective length discussed previously may be applied. For example, Kerensky, Flint and Brown[20] give an effective length of 0.57L for a cantilever with horizontal deflection prevented at the load point. For the overhung beams, they give an effective length of 2.7L based upon a theoretical analysis and 2.95L based upon experimental work. By substituting these values into Equation (6.2) the

TABLE 6.2 BUCKLING COEFFICIENTS - UNDER-REINFORCED CANTILEVERED BEAMS

$$pf_y = \frac{k_{10}E_{sec}}{\frac{Ld}{b^2}} \text{ -- } (1.9)$$

Where:

pf_y = the tensile reinforcement ratio = $(A_s f_{yT} - A_s' f_{yC})/bd$

$\frac{Ld}{b^2}$ = the governing slenderness ratio

k_{10} = a constant

E_{sec} = the secant modulus of concrete, computed at $0.85f_c'$.

SPECIMEN	$\frac{Ld}{b^2}$	pf_y	$\%p_b$ (1)	k_{10}	$k_{10}E_{sec}$	FAILURE TYPE
C32b	594.7	1403.6	85.3%	0.2745	834720.9	Flexure
C36b	699.0	1312.1	80.3%	0.2853	877854.6	Combination
C40b	743.3	1403.6	75.0%	0.3653	1043493.3	Buckling
C44b	817.7	1406.6	99.4%	0.3615	1147521.9	Buckling (2)
C32d	588.8	1747.3	76.6%	0.5089	1028816.9	Flexure

NOTES:

(1) $\%p_b$ = percent of balanced reinforcement

(2) f_c' for Specimen C44b was low. As a result, the reinforcement ratio and the secant modulus were higher than expected.

critical length for the overhung beams was computed as 13.4 or 12.3 inches (on the assumption of a section at $0.75p_b$). From Section 6.6, the cross-over point was expected at approximately 10 inches.

6.8 Practical Loading Considerations

The commentary to the ACI Code[2] suggests that beams having dimensions normally found in practice will not usually be subject to lateral instability. This comment appears to be valid, so long as reasonable precautions are taken to insure that the beam is prevented from displacing laterally and that the points of support do not rotate. In simple terms, the use of common sense in the detailing of the support and restraint of most concrete beams will usually guarantee stability. The problem of lateral instability should still be studied and understood so that the stability of unusual designs can be assured and so that unnecessary (and often costly) restraint need not be provided.

In practice, cantilevered beams are normally extensions of beams beyond the exterior support. The assumed condition of full fixity (in which the beam is built-in), rarely occurs. Regardless of this fact, if the cantilever is prevented from rotating about the Z-axis at the exterior support, the boundary conditions given in Equations (2.17) to (2.20) remain the same and the buckling load does not change[20].

In the event that rotation is allowed, about the longitudinal axis of the beam at the exterior support, the beam restraint approaches that assumed in the overhung beam tests. With this condition, the beam becomes very unstable and is unsafe at almost any length.

CHAPTER 7

CONCLUSIONS AND RECOMMENDATIONS

7.1 Lateral Buckling of Rectangular Concrete Beams

The results of this study, combined with the data reported in the literature, have demonstrated that lateral buckling will occur in slender reinforced concrete beams. The critical load, at lateral buckling, is a function both of the beam slenderness and of the loading configuration.

The slenderness ratio governing lateral buckling has the form Ld/b^2 in which L is the beam length, d the depth from compression face to centroid of reinforcement and b the width of compression face. In this study, rectangular unrestrained cantilevers with Ld/b^2 in the range of 600 failed due to flexure while those with higher slenderness buckled. The simply-supported beam specimens buckled with $Ld/b^2 = 881$ and the shortest overhung beam buckled with $Ld/b^2 = 260$.

Present building codes[1][2] restrict the slenderness of beams to $L/b = 25$ for cantilevers and $L/b = 50$ for others. The L/b criterion has been proven to be incorrect and should be replaced with a criterion based upon the slenderness ratio Ld/b^2.

The reinforced concrete building codes, currently in use, take the approach that flexural members should fail in a ductile manner and restrict the tensile reinforcement to 75% of balanced. To be consistent with this philosophy, it is recommended that the geometry of beams be restricted so that they will fail in flexure rather than by lateral buckling. To this end, it is proposed that the maximum slenderness ratio Ld/b^2 be limited to the value at which a member reinforced with 75% of balanced reinforcement will not buckle at ultimate moment. Pending further investigation, a maximum value of $Ld/b^2 = 600$ is recommended for cantilevered beams. This value is based upon the behaviour of unrestrained cantilevers, for most other cantilevers, it should be conservative. To account for the variety of loading and restraint conditions, the "effective length" concept is recommended.[20]

To guard against the possibility of very unstable members, such as the overhung beams, the code provisions should require positive rotational restraint at all supports. At this stage, it appears that reasonable precautions to prevent rotation at the supports and to provide lateral support along the beam length (through the attachment of decking or by other means) will stabilize most beams to the extent that lateral buckling will not be a problem.

7.2 Theoretical Consideration of Lateral Buckling

The analysis presented herein was based upon the assumption of elastic buckling of a homogeneous member. The rigidity terms were developed using procedures published by Massey[11], which were based upon research into the behaviour of simply-supported beams under pure moment. For specimens in which the assumed conditions of a fully-cracked elastic section were approximated, the computational procedure gave buckling loads close to the failure loads. For specimens which failed at loads which did not develop the fully-cracked section, the computed buckling loads were lower than the failure loads, while for specimens in which the tensile reinforcement yielded, the failure loads were lower than the computed loads. Computations which neglected the contribution of the reinforcement to the rigidity terms underestimated the failure loads even for specimens in which the reinforcement had yielded completely.

It was, therefore, concluded that the computational procedure developed applied only to the limited range assumed in the derivation, that is, the cracked elastic section. Since present North American building codes for reinforced concrete structures are based upon ultimate strength philosophy, and since beams are required to fail by their tensile reinforcement, the cracked elastic section is of limited usefulness. It is, therefore, recommended that the buckling of reinforced concrete beams, in the plastic range, be investigated theoretically.

Analysis of lateral buckling of a reinforced concrete member in the plastic range is complicated in the extreme. Regardless of this fact, the development of this capability is essential if the many possibilities of loading and restraint are to be analyzed. The number of possibilities makes a complete experimental investigation unrealistic by virtue of its size. The very significant phenomenon of creep was not considered in this investigation since the loading was of short duration. In real structures, creep has the effect of reducing the long term stability and thus it must be considered. For this purpose, an analytical approach is very useful.

7.3 Model Similitude

The experimental portion of this study was carried out using small-scale specimens, which were thought of as scale models of larger prototype members. Tests of a simply-supported beam specimen which was a scale model of a beam test (which buckled) reported in the literature indicated good agreement between the model results and those expected by scaling down the prototype results. It is, therefore, concluded that small-scale test specimens may be used to investigate lateral buckling and that the results obtained may be applied to prototype structures with the appropriate scale factors.

7.4 Future Experimental Investigation

To continue the investigation begun by this study, the testing of additional specimens will be required in conjunction with the theoretical study. This experimental work should concentrate on specimens reinforced with 75% of balanced reinforcement and having concrete and reinforcement strengths in the range found in practice.

The minimum possible width of beam will occur with a single vertical row of reinforcement plus stirrup thickness plus minimum concrete cover each side. This reinforcement configuration also produces the minimum lateral and torsional rigidity. It is, therefore, recommended that the width of test specimen be based upon the width of a single vertical row of reinforcement. This approach will have the added benefit of reducing the time and effort required to assemble the reinforcement cages.

7.4.1 Specimen Materials

To produce absolute flexural similarity between the small test specimens and the prototype members, a microconcrete with properties identical to prototype concrete is necessary. In this study, good agreement between model and prototype results was found even though the concrete properties were somewhat different. Regardless of this fact, the development of a microconcrete with properties identical to prototype concrete is desirable. Strain-hardened reinforcement produced stress-strain curves very similar to prototype reinforcement, but the production of this reinforcement consumed a large amount of time. For this reason, a commercial supply of similar reinforcement should be sought.

Some disagreement between the computed ultimate moment and the failure moment of the test specimen was found. This problem was not explored in this study but it is suggested as an area of future study.

7.4.2 Specimen Construction

Some difficulty was experienced in maintaining the alignment of the acrylic plastic beam mould, partly due to the flexibility of the mould and partly due to creep in the acrylic plastic. Acrylic plastic was chosen as the mould material because of its transparency. It was originally thought necessary to have a transparent mould to insure satisfactory concrete placing but experience indicated that the concrete could be satisfactorily placed without inspecting the surfaces during the casting process. It is, therefore, recommended that future specimens be cast in more rigid moulds, preferably steel.

The use of internal pencil vibrators to place the concrete was satisfactory except that a large amount of time was required for initial setting of the concrete. To decrease the time required to place the concrete, other consolidation techniques should be considered. If practical, the entire mould should be vibrated.

7.4.3 Test Apparatus

The fixed-end support for the cantilevered beams allowed some movement to occur under load. This movement did not have a significant effect on the final results but several deflection measurements and a computational procedure were required to eliminate its effect from the measured load point deflections. To eliminate this added complication, a more rigid reaction system is recommended.

The parallelogram loading apparatus produced an inclined load as lateral deflection occurred. To eliminate this effect, a "gravity simulating" linkage is recommended. As an alternative, a hanging load should be used. The hanging load has the advantage of simplifying the loading apparatus but has the disadvantage of destroying the specimen at failure.

7.4.4 Test Instrumentation

To fully understand the pnenomenon of lateral buckling, knowledge of the deflection, cracking and strain behaviour of test specimens is required. Of most importance are the events which occur during the buckling process. Since the failure is rapid, measurement of the deflection and strain requires high-speed data acquisition equipment and the observation of the cracking requires high speed photographic techniques. Such equipment is costly but its use is desirable.

Since the specimens under load are in a laterally unstable condition, they are very sensitive to lateral force. As a result, the lateral deflection and rotational measurements should be taken with instruments which do not contact the specimen. In this study, capacitance transducers were used with good success.

Some measurement of the deflected shape of cantilevered plastic beams has been done[14]. This type of measurement, or other similar optical techniques provide very useful information and it is recommended that they be considered in future studies.

BIBLIOGRAPHY

1. Canadian Standards Association Code for the Design of Plain or Reinforced Concrete Structures - Standard A23.3 - 1973.

2. American Concrete Institute Building Code Requirements for Reinforced Concrete - Standard 318 - 71.

3. Lee, C.G. A Survey of Literature on The Lateral Instability of Beams Welding Research Council Bull. Ser. 63, Aug. 1960 p. 50-59.

4. Marshall, W.T. The Lateral Stability of Reinforced Concrete Beams Paper 5641 Inst'n of Civil Engineers (London) Journal v.30(6) April 1948 - published in abstract form.

5. Vasarhelyi, D. & Turkalp, I. Lateral Buckling of Slender Reinforced Concrete Beams The Trend in Engineering at The University of Washington v.6(3) July/54.

6. Hansell, W. & Winter, G. Lateral Stability of Reinforced Concrete Beams Journal American Concrete Inst. Sept./59.

7. Smith, R.B.L. Discussion of Paper by Hansell & Winter Journal American Concrete Inst. March/60.

8. Siev, A. The Lateral Buckling of Slender Reinforced Concrete Beams Magazine of Concrete Research v.12 n.36 Nov./60.

9. Sant, J.K. & Bletzacker, R.W. Experimental Study of Lateral Stability of Reinforced Concrete Beams. Journal American Concrete Institute Dec./61.

10. Sant, J.K. & Bletzacker, R.W. Closure to Discussion of Experimental Study of Lateral Stability of Reinforced Concrete Beams Journal, American Concrete Institute, Pt. 2, June/62.

11. Massey, C. Lateral Instability of Reinforced Concrete Beams Under Uniform Bending Moments Journal American Concrete Institute March/67.

12. Marshall, T.W. A Survey of the Problem of Lateral Instability in Reinforced Concrete Beams Proceedings, Institution of Civil Engineers, v43 July, 1969 pg. 397 to 406

13. Timoshenko, S.P. and Gere, J.M. Theory of Elastic Stability 2nd. Ed. McGraw-Hill, Toronto, 1961

14. Piotrowski, R. and Zihrul, J. Lateral Buckling of Cantilever Beams Graduate Thesis, Faculty of Engineering, The University of Manitoba, 1971

15. Swann, R.A. and Godden, W.G. The Lateral Buckling of Concrete Beams Lifted by Cables The Structural Engineer v. 44, n. 1, January 1966.

16. Woolcock, S.T. and Trahair, A.M. Post-Buckling Behaviour of Determinate Beams J. Eng. Mech. Div. ASCE, v. 100, n. EM2, Proc. Paper 10471 pg. 151 to 171

17. Charlton, T.M. Model Analysis of Plane Structures Pergammon Press

18. Harris, Sabnis and White, Small Scale Direct Models of Reinforced and Prestressed Concrete Structures, Cornell University, Department of Structural Engineering Report No. 326, September 1966.

19. Petri, Robert Model Analysis of a Ten Storey Building, M. Sc. Thesis, University of Manitoba, 1966

20. Kerensky, O.A., Flint, A.R., and Brown, W.C., The Basis for Design of Beams and Plate Girders in the Revised British Standard 153. Proceedings, Institution of Civil Engineers, Vol. 5, Part II

21. Canadian Standards Association Standard G30.6 Deformations for Concrete Reinforcement

22. Canadian Standards Association Standard A23.1-1967 Concrete Materials and Methods of Concrete Construction

23. Portland Cement Association Design and Control of Concrete Mixtures EB001.11T, 1968

24. Barritt, W.N. A Study of Brittle Fracture in Concrete M. Sc. Thesis, University of Manitoba, 1973

25. Ramberg, W. & Osgood, W.R. Description of Stress-Strain Curves by Three Parameters, National Advisory Committee for Aeronautics - Technical Note No. 902

26. Timoshenko, S.P. and Goodier J.N., Theory of Elasticity, Second Ed. Chapter 11, McGraw Hill, Toronto

27. Cowan, H.J. The Theory of Torsion Applied to Reinforced Concrete Design, Part 2, Civil Engineering (London), v. 48, n. 568, October 1953, pp 950 - 952

APPENDIX A

TEST RESULTS

Introduction

This Appendix contains the results of the load tests on the three series of cantilevered beams. Included are load-deflection curves and diagrams showing the failure configurations and the cracking patterns of all beams as well as the load-strain curves for the type "c" and "d" specimens.

The failure configuration and cracking pattern diagrams were prepared from photographs taken during and after each test. The failure diagrams are isometric, to 1/6 the actual size of the beam, the cracking patterns are shown on elevations which are 1/3 actual size.

The crack patterns are described in terms of the side of the beam on which they appear as "near side" which indicates the negative X face and "far side". The word "tension" is used to denote a crack (produced by convex bending), and the word "crushing" is used to indicate crushing of the concrete caused by concave bending. The cracks are plotted with respect to a one inch grid, which was drawn on the beams before testing.

Specimen C44b

Concrete Cast January 21, 1970

Specimen Tested February 6, 1970

Concrete Compressive Tests   Age = 16 days

Cylinder	1 (3" x 6")	3460 psi
	2	3552
	3	3310
Average		f'_c = 3442 psi

NOTE: The concrete compressive strength results were lower than expected for no apparent reason.

Reinforcement Tensile Tests - Wire preloaded to 60 ksi and deformed.

Wire Size (Before Preloading)	Yield Stress	Ultimate Strength
#14 (.08 inch)	62.7 ksi	68.9 ksi
#14	62.7	69.6
#14	62.7	68.6
#14	58.7	68.6
Average	f_y = 61.7 ksi	68.9 ksi
.1254 inch	67.2 ksi	70.4 ksi
.1254	67.3	70.4
.1254	64.8	69.6
.1254	64.8	68.8
Average	f_y = 66.0 ksi	69.8 ksi

Beam Length   44 inches

Failure Load   355 pounds

Failure Type   Lateral Instability

At failure, the load point deflected in the negative X direction and rotated negative about the Z-axis as shown in Figure A.1. A diagonal cracking pattern developed with tension on the negative X face near the fixed end and tension on the far face away from the fixed end.

The deflections of the load point are shown on Figures A.2, A.3, and A.4.

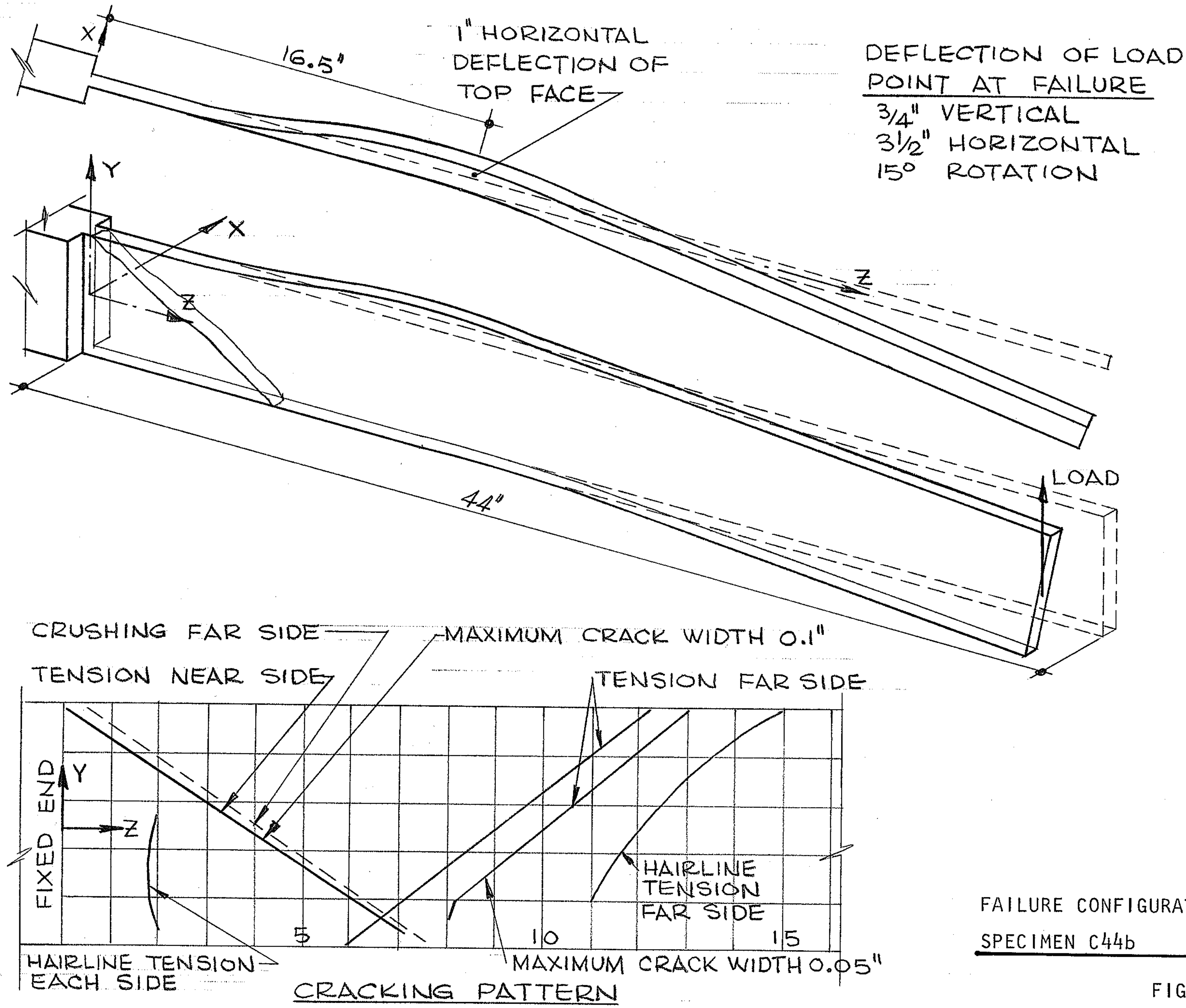

FAILURE CONFIGURATION - SPECIMEN C44b

FIGURE A.1

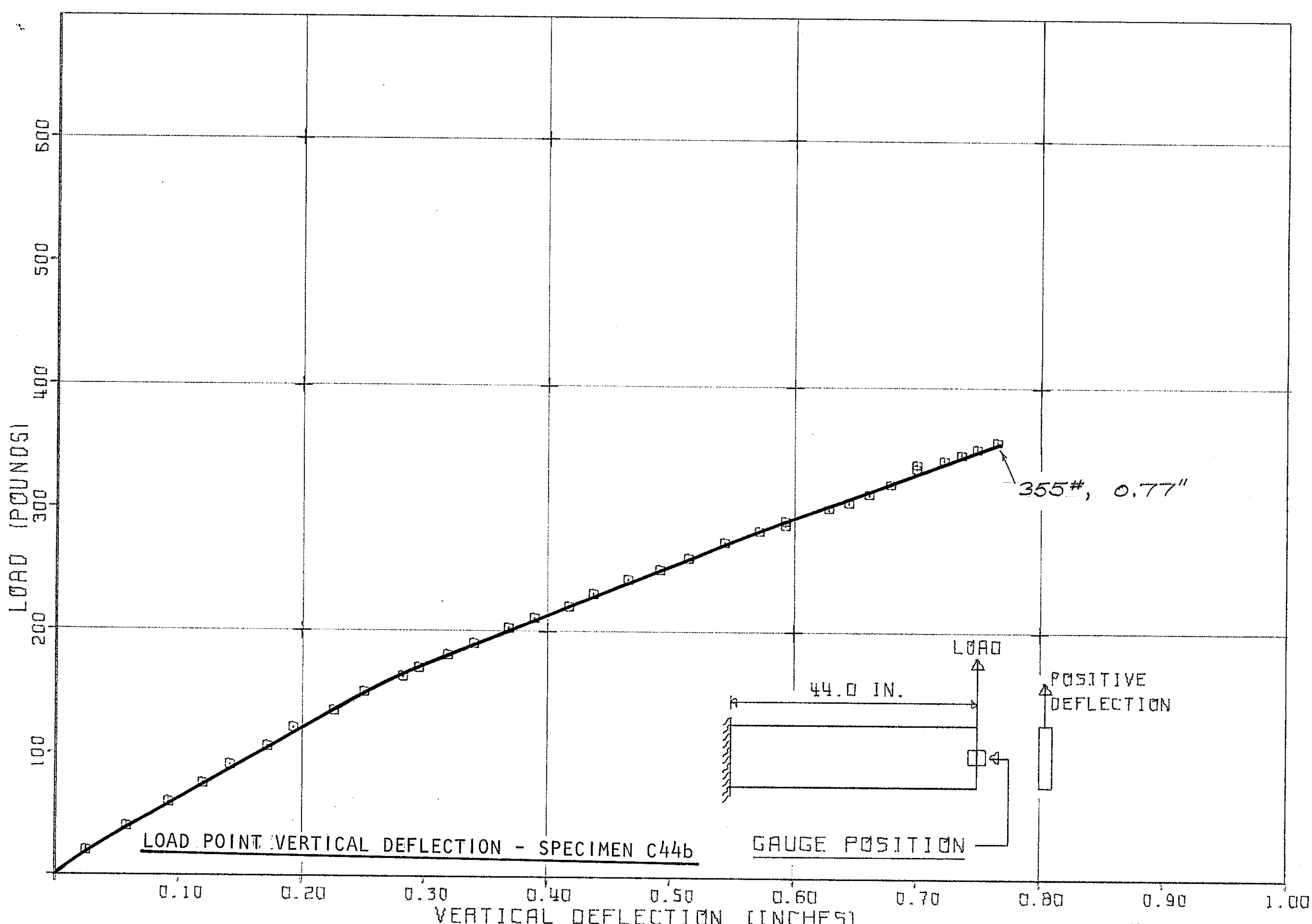

LOAD (POUNDS)
100
200
300
400
500
600
0.10
0.20
0.30
0.40
0.50
0.60
0.70
0.80
0.90
1.00
VERTICAL DEFLECTION (INCHES)
355#, 0.77"
LOAD POINT VERTICAL DEFLECTION - SPECIMEN C44b
LOAD
44.0 IN.
POSITIVE
DEFLECTION
GAUGE POSITION

FIGURE A.2

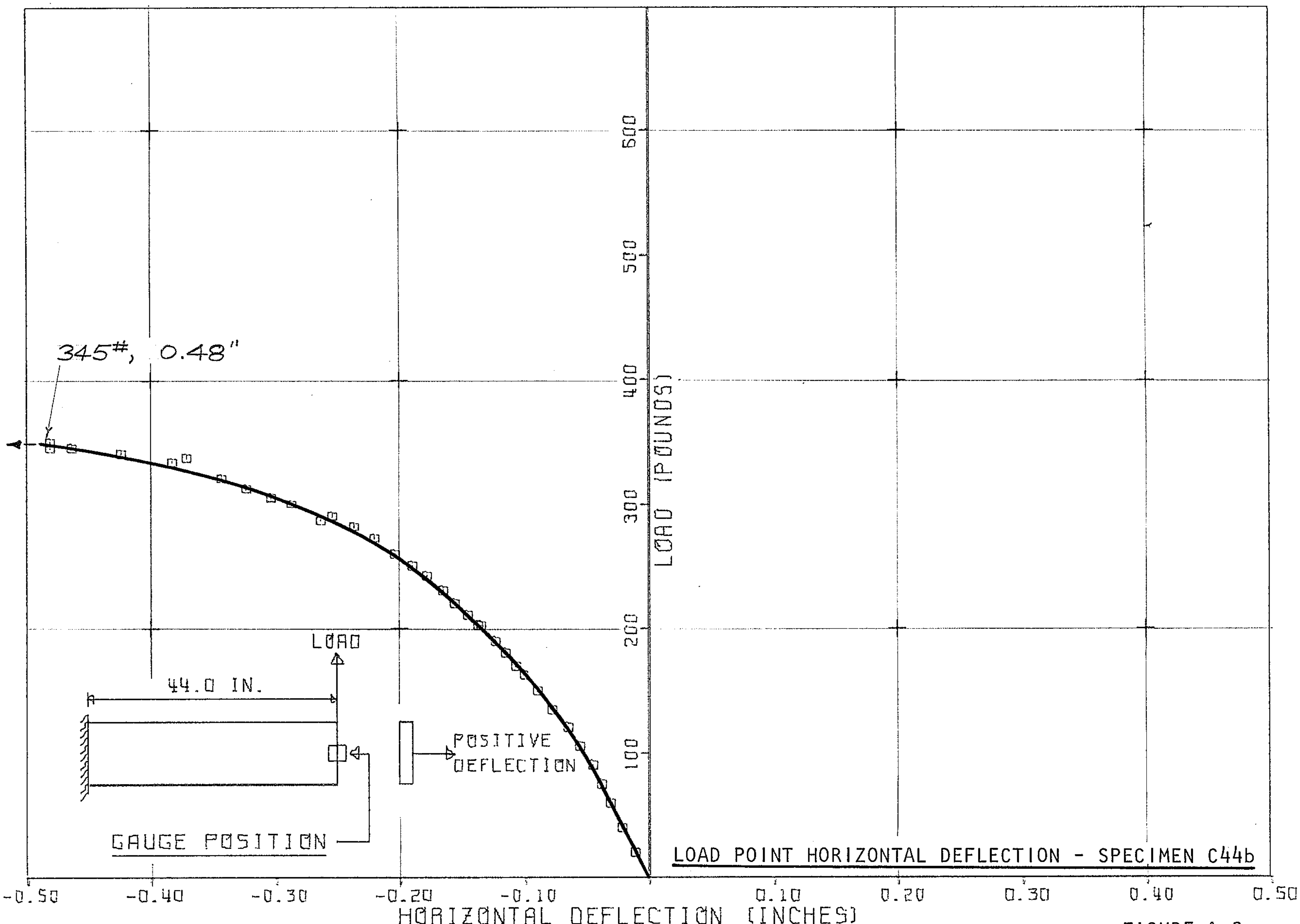

LOAD POINT HORIZONTAL DEFLECTION - SPECIMEN C44b

FIGURE A.3

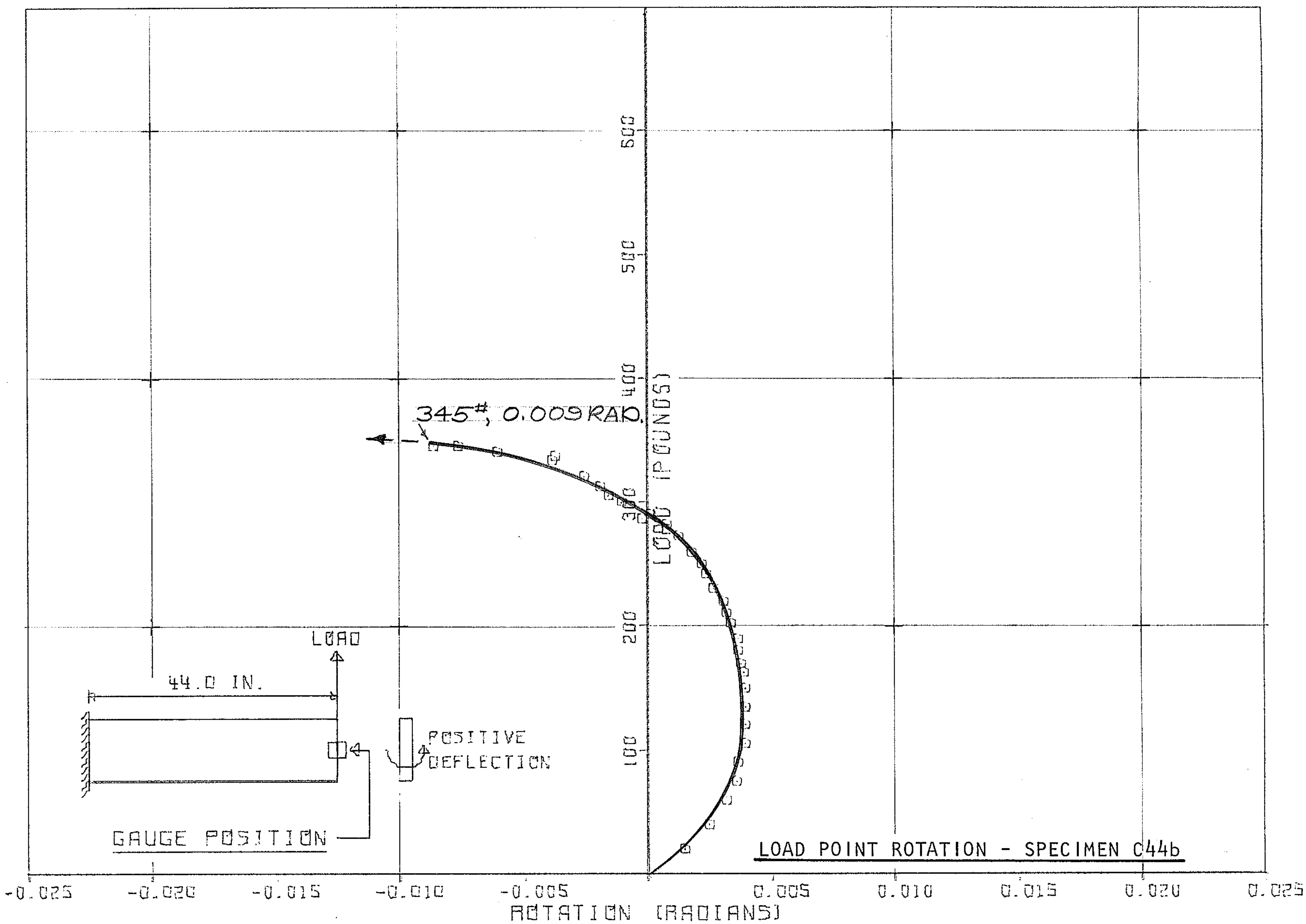
LOAD POINT ROTATION - SPECIMEN C44b
LOAD (POUNDS)
100
200
300
400
500
600
ROTATION (RADIANS)
-0.025
-0.020
-0.015
-0.010
-0.005
0.005
0.010
0.015
0.020
0.025
345#, 0.009 RAD.
LOAD
44.0 IN.
POSITIVE
DEFLECTION
GAUGE POSITION

FIGURE A.4

Specimen C40b

Concrete Cast December 23, 1969

Specimen Tested January 9, 1970

Concrete Compressive Tests   Age = 17 days

Cylinder 1 (3" x 6")		4630 psi
2		4750
3		4580
Average	f_c' =	4640 psi

Reinforcement Tensile Tests - Wire preloaded to 60 ksi and deformed.

Wire Size (Before Preloading)		Yield Stress	Ultimate Strength
#14 (0.08 inch)		67.6 ksi	70.6 ksi
#14		66.6	70.6
#14		67.6	70.6
#14		66.6	71.6
Average	f_y =	66.8 ksi	70.8 ksi
.1254 inch		62.3 ksi	69.6 ksi
.1254		66.4	71.3
.1254		66.4	70.4
.1254		64.8	70.4
Average	f_y =	65.0 ksi	70.4 ksi

Beam Length   40 inches

Failure Load   410 pounds

Failure Type   Lateral Instability

At failure, the beam deflected in the positive X direction at the load point and rotated positive about the Z-axis as is shown on Figure A.5. The cracking pattern which developed at failure was diagonal with tension on the positive X face near the fixed end and tension on the negative X face away from the fixed end.

The vertical deflection of the load point is shown on Figure A.6, the horizontal deflection on Figure A.7 and the rotation on Figure A.8.

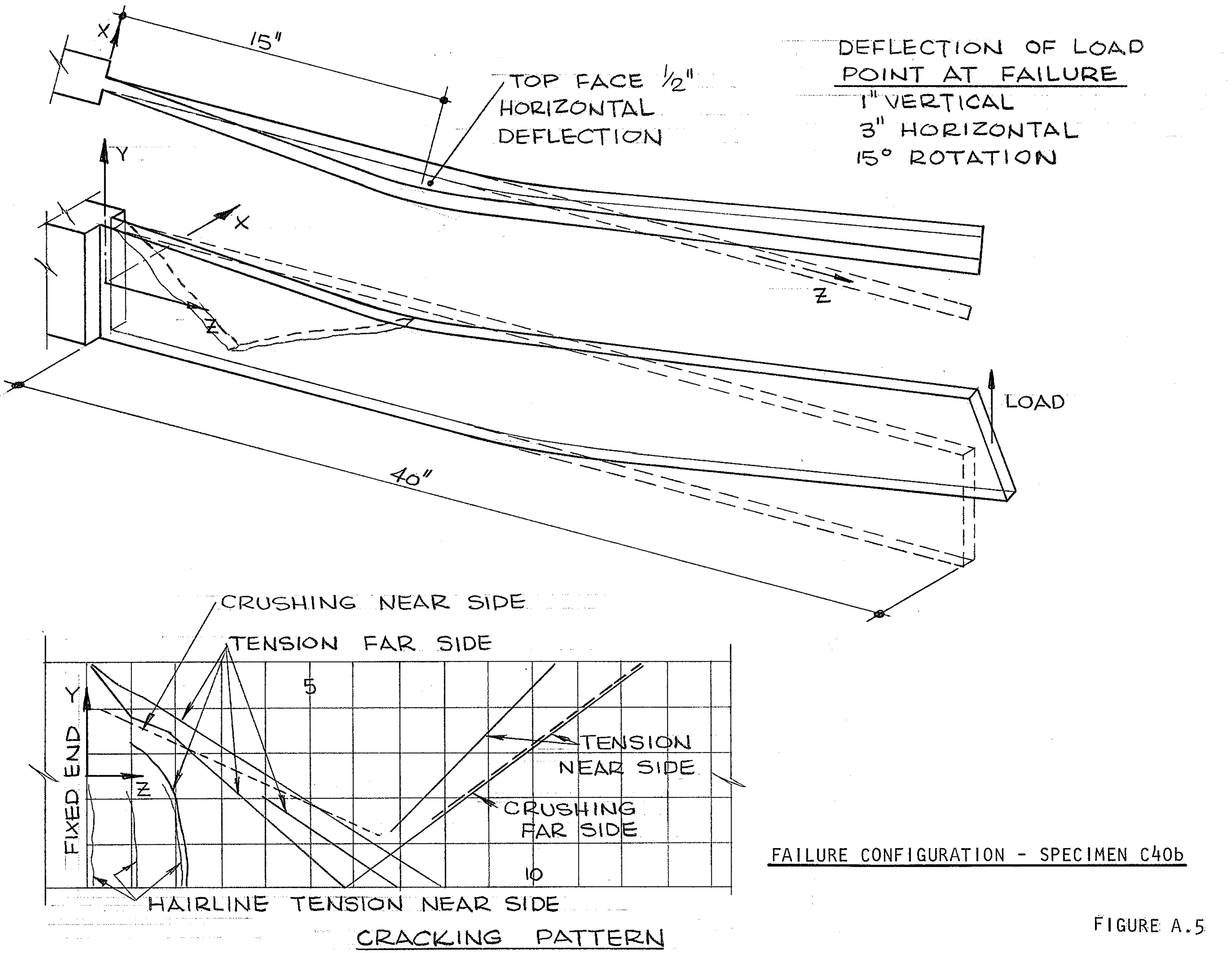

FAILURE CONFIGURATION - SPECIMEN C40b

FIGURE A.5

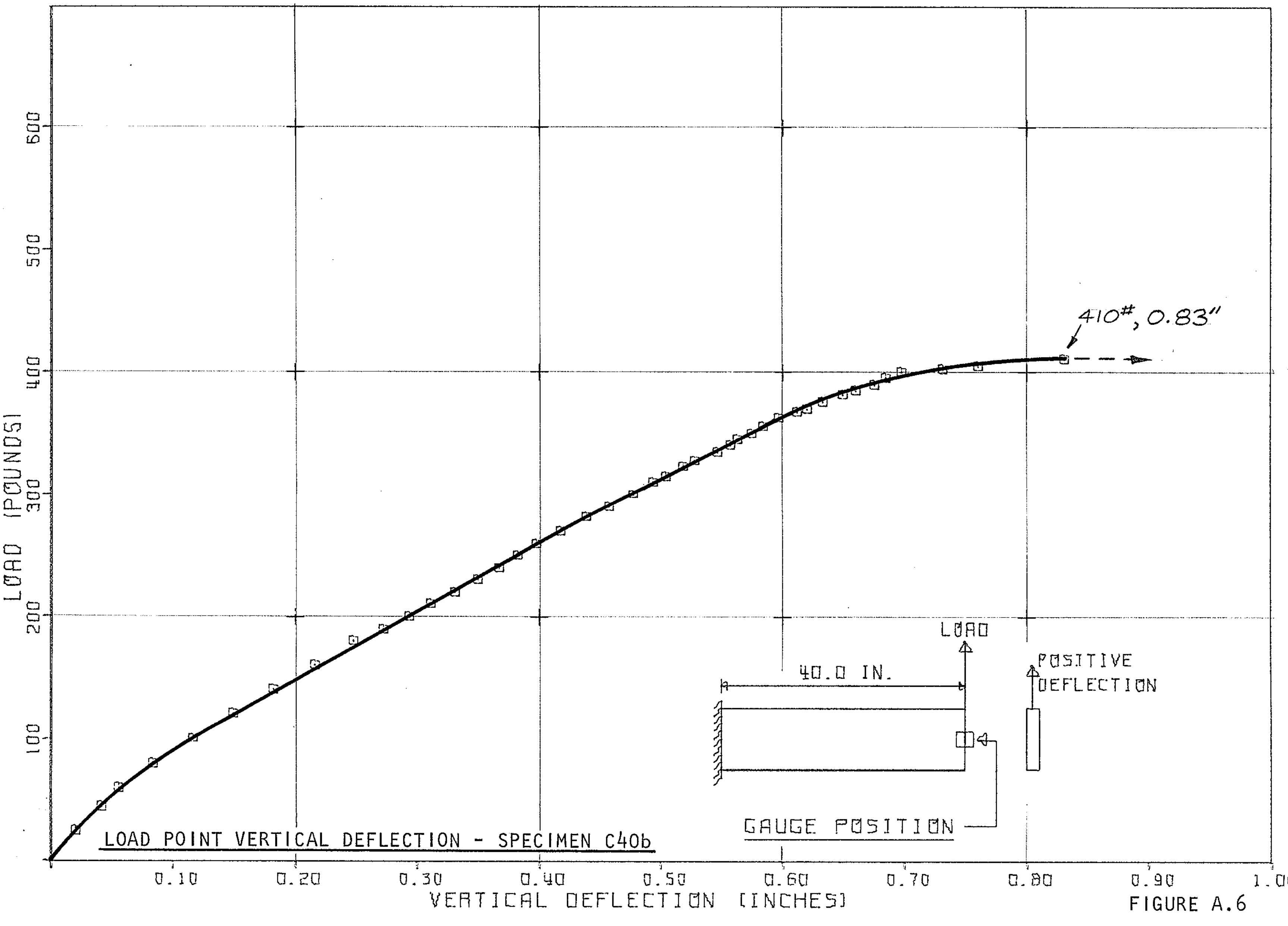
410#, 0.83"
LOAD POINT VERTICAL DEFLECTION - SPECIMEN C40b
LOAD
40.0 IN.
POSITIVE
DEFLECTION
GAUGE POSITION
LOAD (POUNDS)
100
200
300
400
500
600
0.10
0.20
0.30
0.40
0.50
0.60
0.70
0.80
0.90
1.00
VERTICAL DEFLECTION (INCHES)

FIGURE A.6

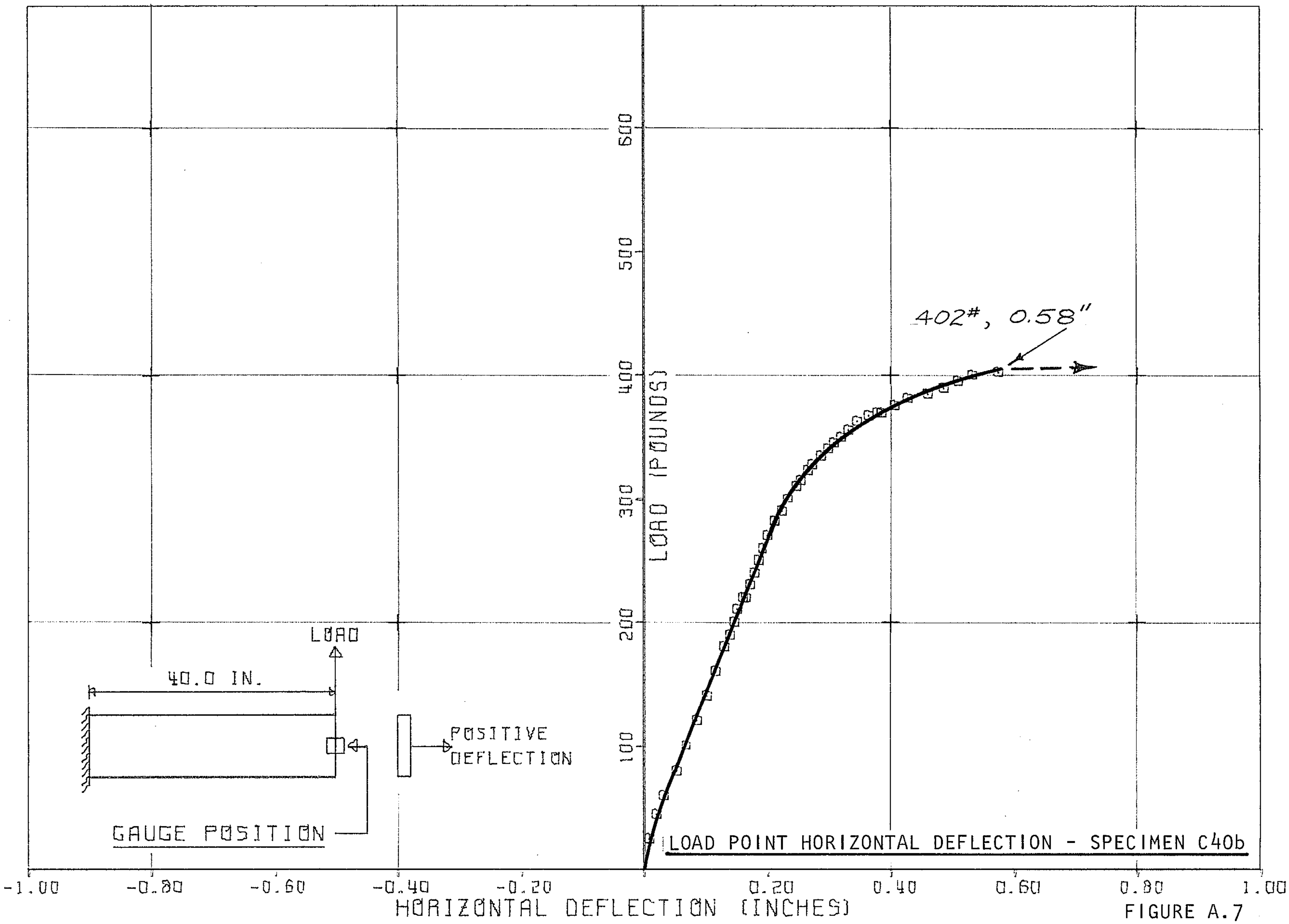

LOAD POINT HORIZONTAL DEFLECTION - SPECIMEN C40b
402#, 0.58"
LOAD (POUNDS)
100
200
300
400
500
600
-1.00
-0.80
-0.60
-0.40
-0.20
0.20
0.40
0.60
0.80
1.00
HORIZONTAL DEFLECTION (INCHES)
LOAD
40.0 IN.
POSITIVE DEFLECTION
GAUGE POSITION

FIGURE A.7

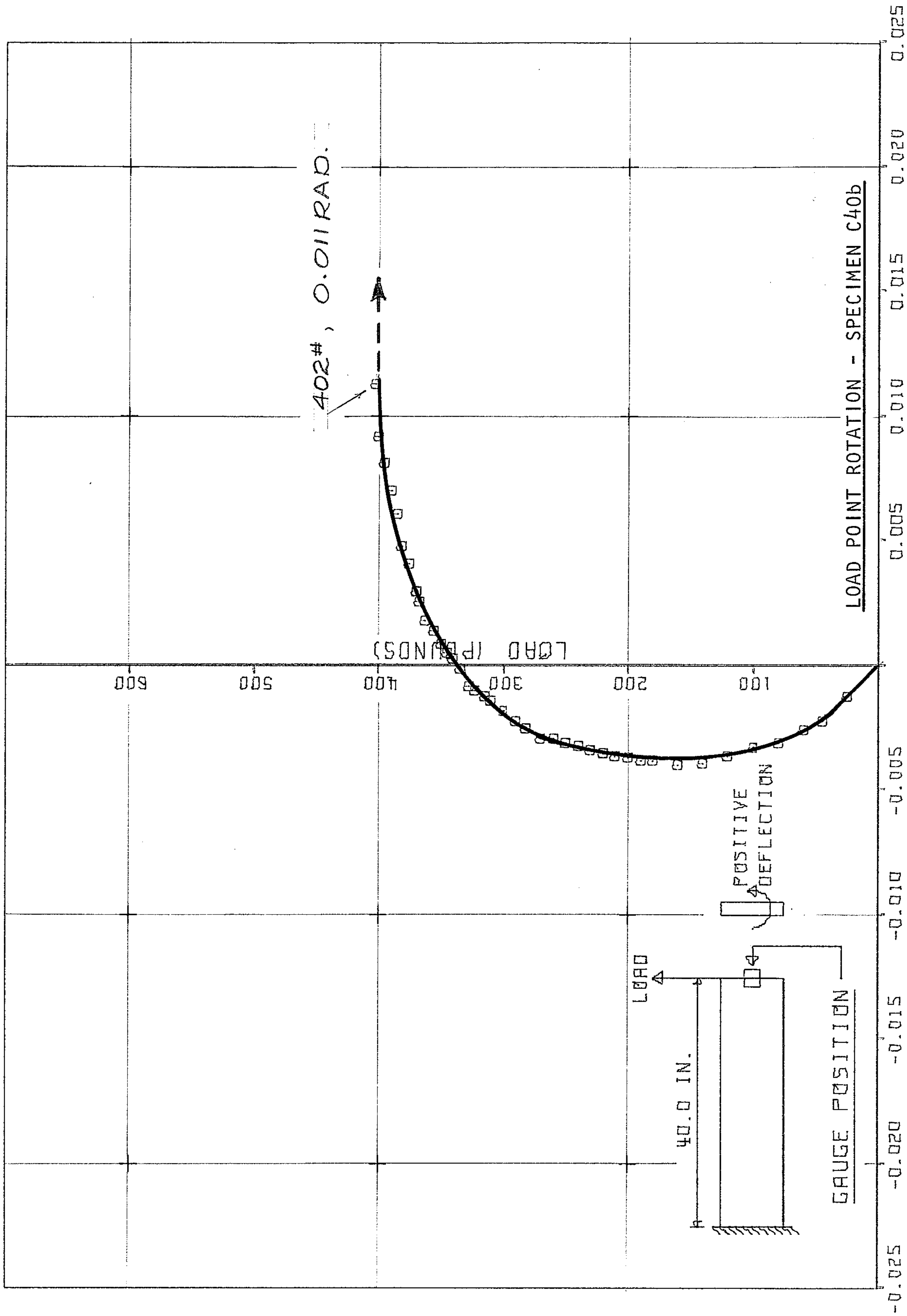
LOAD POINT ROTATION - SPECIMEN C40b
ROTATION (RADIANS)
LOAD (POUNDS)
402#, 0.011 RAD.
POSITIVE DEFLECTION
LOAD
40.0 IN.
GAUGE POSITION
-0.025
-0.020
-0.015
-0.010
-0.005
0.005
0.010
0.015
0.020
0.025
100
200
300
400
500
600

FIGURE A.8

Specimen C36b

Concrete Cast December 4, 1969

Beam Tested December 18, 1969

Concrete Compressive Tests   Age = 14 days

Cylinder 1 (3" x 6")	3900 psi
2	3930
3	3770
Average	f'_c = 3870 psi

Reinforcement Tensile Tests - Wire preloaded to 60 ksi and deformed.

Wire Size (Before Preloading)	Yield Stress	Ultimate Strength
#14 (0.08 inch)	64.6 ksi	67.6 ksi
#14	64.6	67.6
#14	64.6	67.6
#14	64.6	67.6
Average	f_y = 64.6 ksi	67.6 ksi
.1254 inch	61.5 ksi	69.6 ksi
.1254	61.5	69.6
.1254	61.5	71.1
.1254	62.3	68.6
Average	f_y = 61.7 ksi	69.5 ksi

Beam Length   36 inches

Failure Load   461 pounds

The failure was a combination of lateral instability and vertical flexure. The load point deflected laterally in the positive X direction and twisted positive about the Z-axis. Flexural cracks appeared at the bottom of the beam at the fixed end (point of maximum bending) indicating yielding of the tensile reinforcement. In addition, diagonal cracks indicative of a buckling failure developed. The most pronounced feature of the failure was, however, the separation which occurred one inch from the fixed end. The separation is shown cross-hatched on Figure A.9, and was caused by the torsion produced by the horizontal deflection of the load. The sequence of development of the failure is not known; it is most likely that the tensile cracks formed first, followed by the diagonal cracks. The separation most likely developed at the end of the failure process, as an after-effect of the lateral deflection.

The vertical deflection of the load point is plotted on Figure A.10. The horizontal deflection and rotation are plotted on Figures A.11 and A.12 respectively.

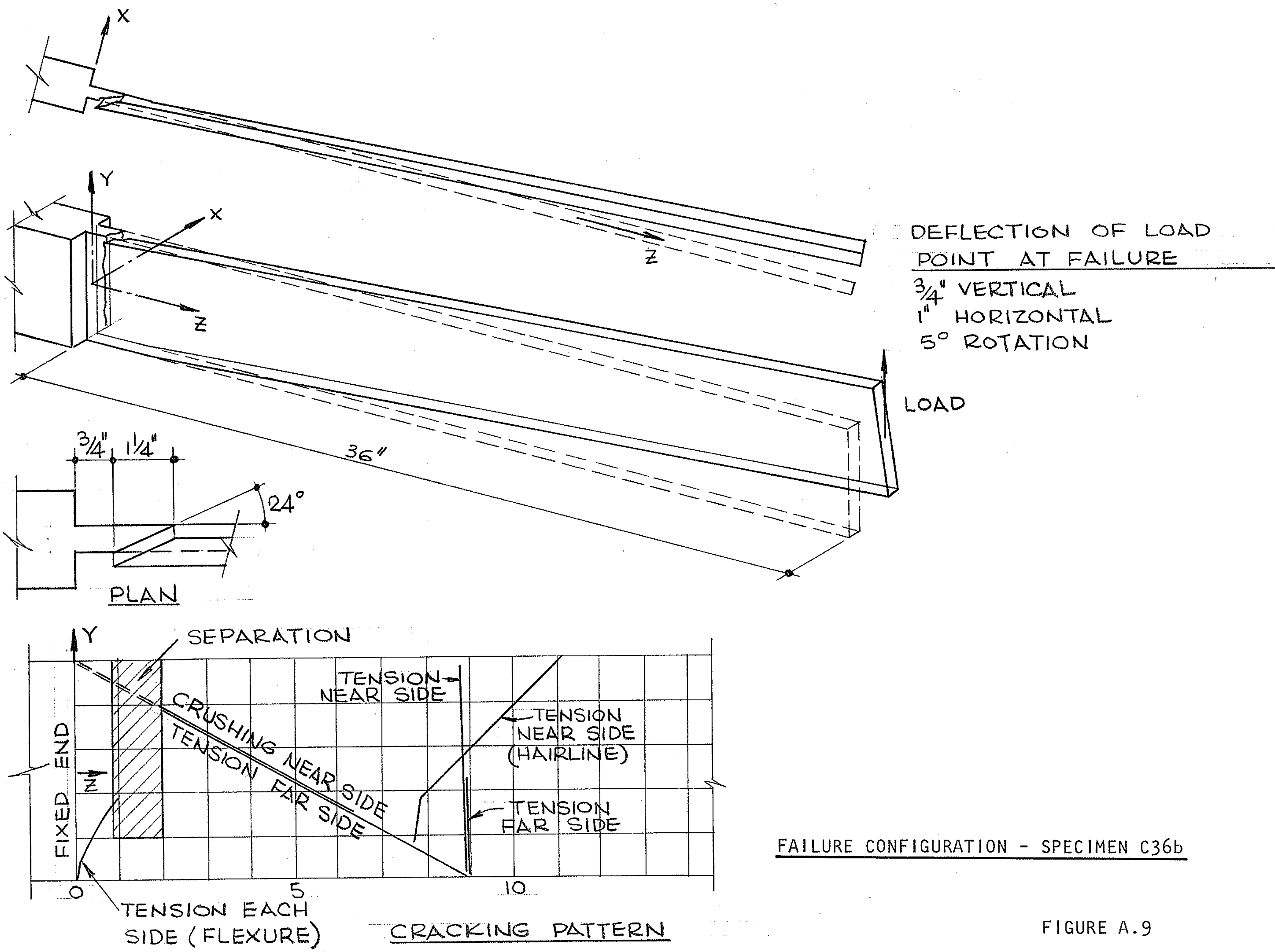

FAILURE CONFIGURATION - SPECIMEN C36b

FIGURE A.9

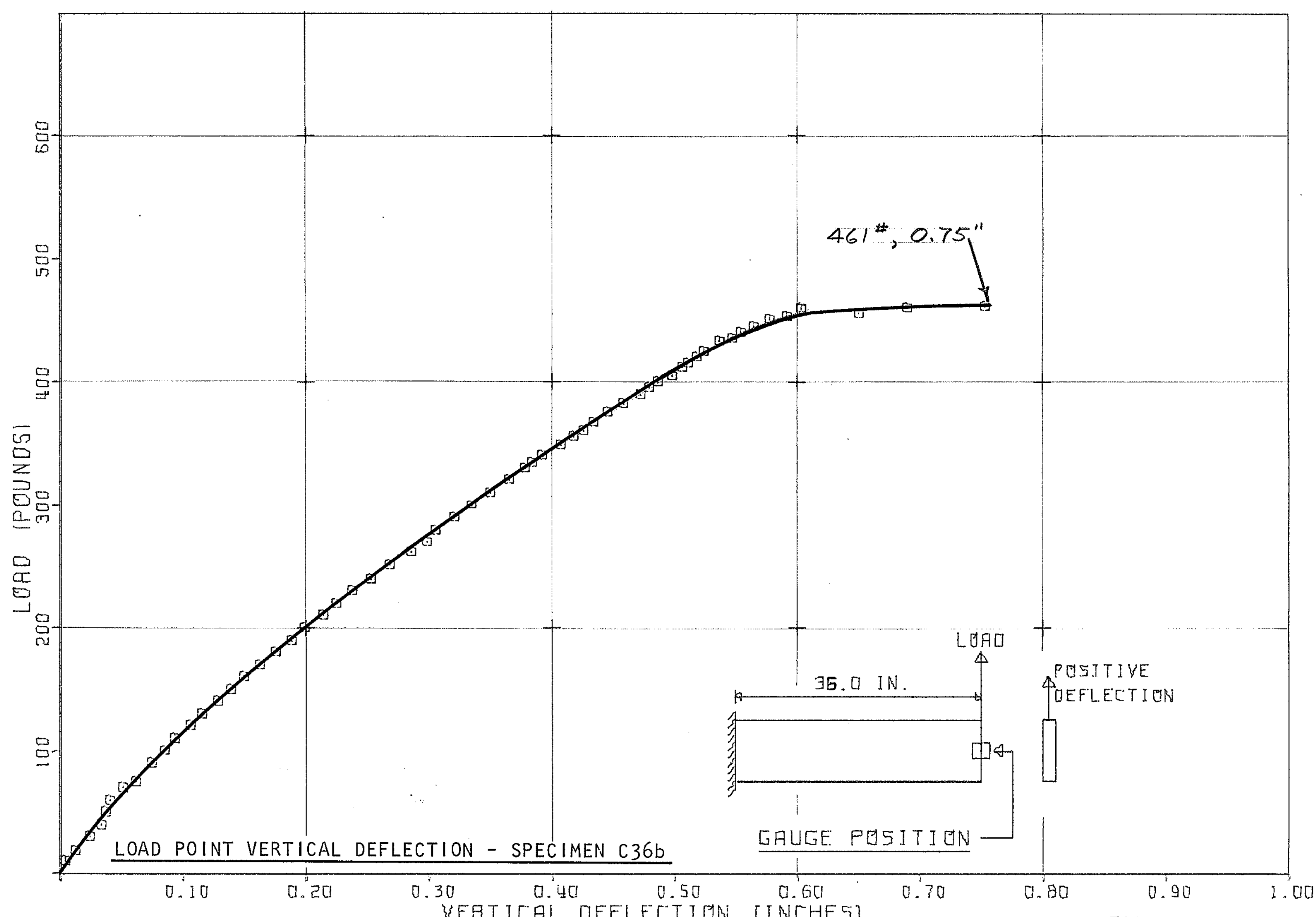

LOAD POINT VERTICAL DEFLECTION - SPECIMEN C36b
461#, 0.75"
LOAD
POSITIVE
DEFLECTION
36.0 IN.
GAUGE POSITION
LOAD (POUNDS)
100
200
300
400
500
600
0.10
0.20
0.30
0.40
0.50
0.60
0.70
0.80
0.90
1.00
VERTICAL DEFLECTION (INCHES)

FIGURE A.10

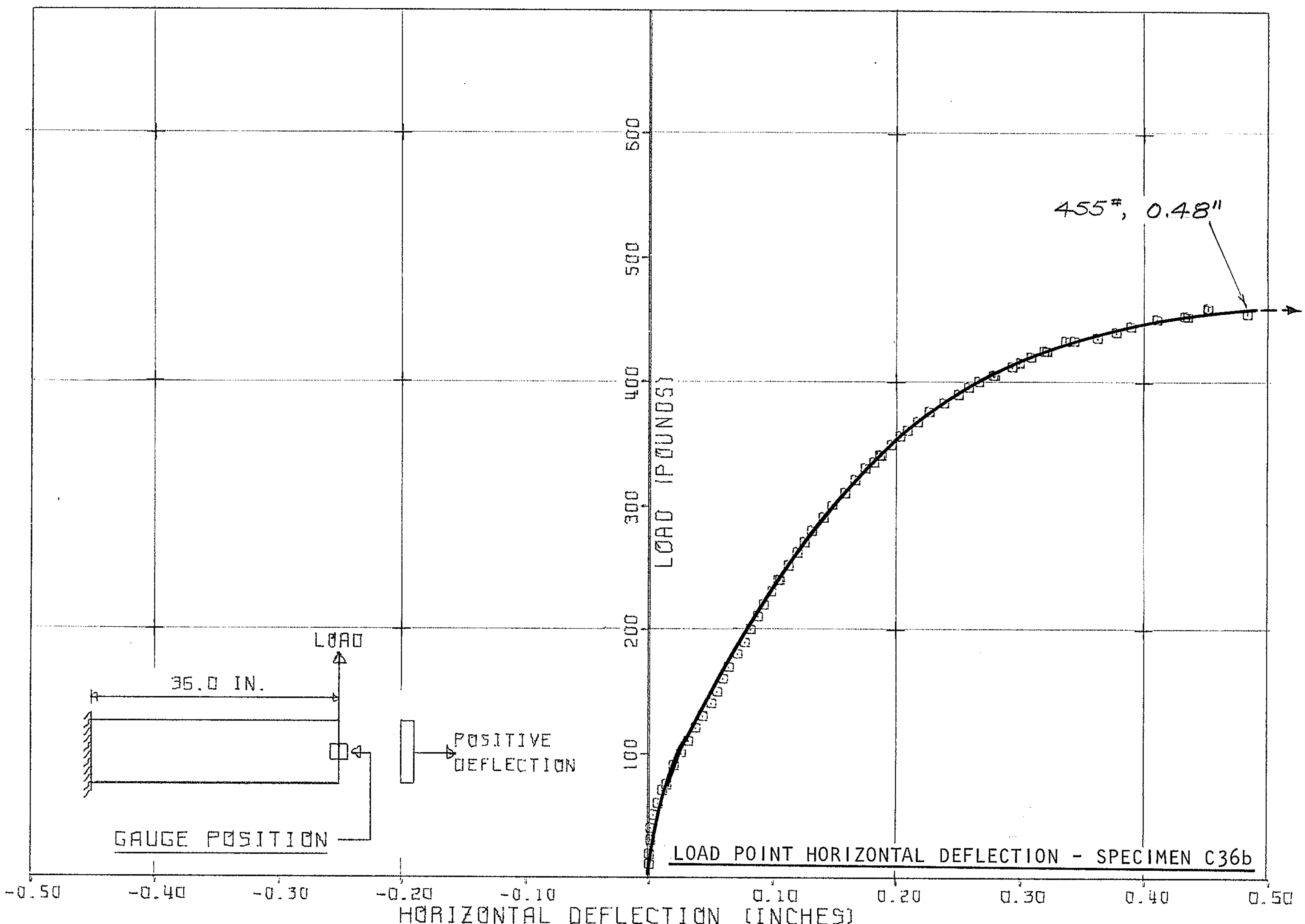

LOAD POINT HORIZONTAL DEFLECTION - SPECIMEN C36b

FIGURE A.11

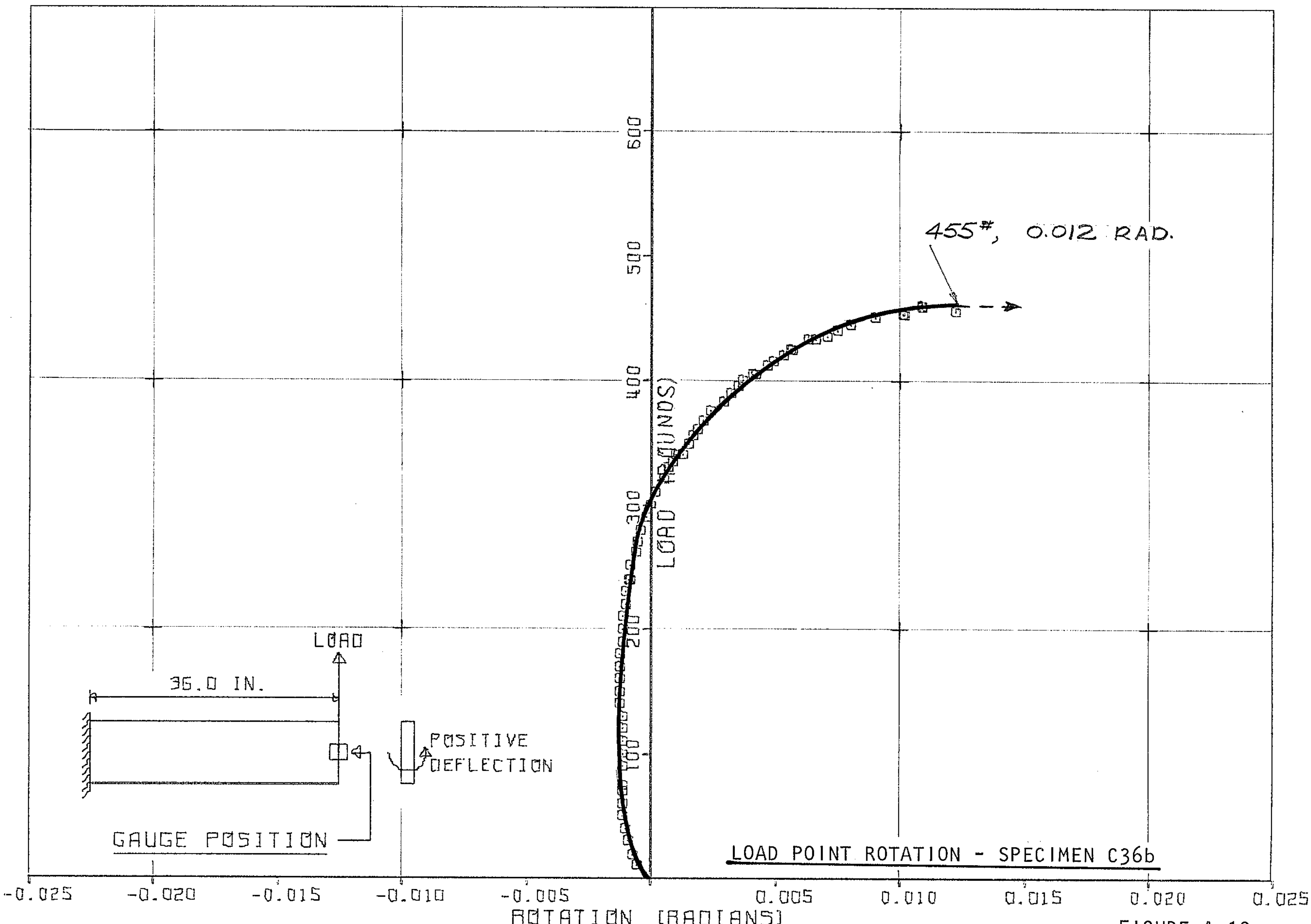
455#, 0.012 RAD.
LOAD (POUNDS)
600
500
400
300
200
100
-0.025
-0.020
-0.015
-0.010
-0.005
0.005
0.010
0.015
0.020
0.025
ROTATION (RADIANS)
LOAD
36.0 IN.
POSITIVE
DEFLECTION
GAUGE POSITION
LOAD POINT ROTATION - SPECIMEN C36b

FIGURE A.12

Specimen C32b

Concrete Cast December 12, 1969

Beam Tested December 31, 1969

Concrete Compressive Tests Age = 19 days

Cylinder	1 (3" x 6")	3980 psi
	2	3890
	3	4150
Average		$f_c' = 4010$ psi

Reinforcement Tensile Tests - Wire preloaded to 60 ksi and deformed

Wire Size (Before Preloading)	Yield Point	Ultimate Strength
#14 (0.08 inch)	63.7 ksi	71.6 ksi
#14	65.6	70.5
#14	67.6	70.5
#14	65.6	70.5
Average	$f_y = 65.6$ ksi	70.8 ksi
.1254 inch	64.0 ksi	70.4 ksi
.1254	66.4	71.2
.1254	67.2	72.1
.1254	66.4	72.9
Average	$f_y = 66.0$ ksi	72.9 ksi

Beam Length 32 inches

Failure Load 550 pounds

Failure Type Flexure (yielding of tensile reinforcement)

The primary failure occurred in the form of a crack beginning at the bottom of the beam at the fixed end and progressing upwards on both sides. At the conclusion of the test, the crack had reached within one-half inch of the top of the beam as is shown on Figure A.13. The test was stopped when it was obvious that the tensile reinforcement had yielded.

The vertical deflection of the load point is shown on Figure A.14. The horizontal deflection and the rotation are shown on Figures A.15 and A.16 respectively. The horizontal deflection was in the positive X direction and was comparatively small.

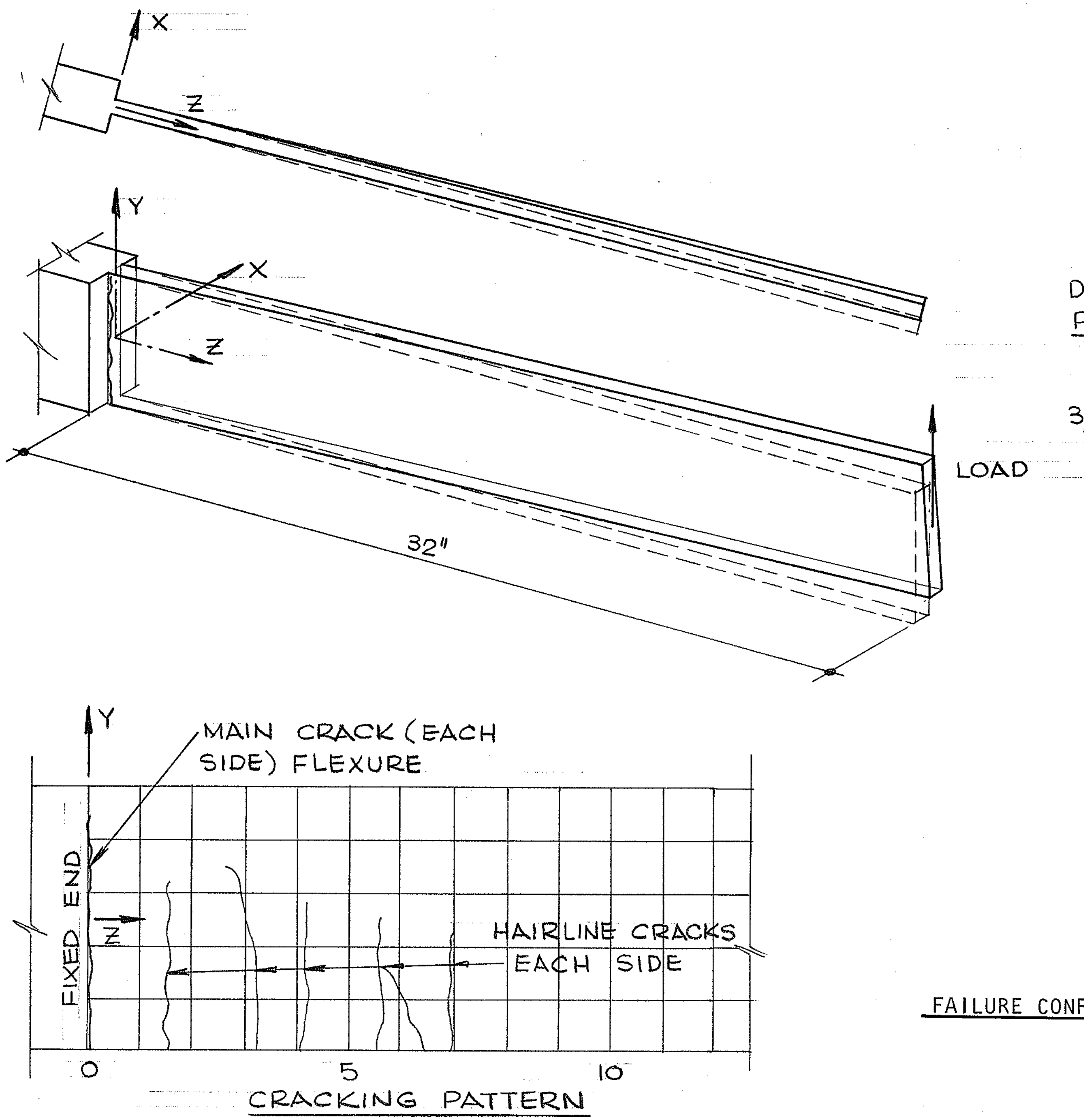

FAILURE CONFIGURATION - SPECIMEN C32b

FIGURE A.13

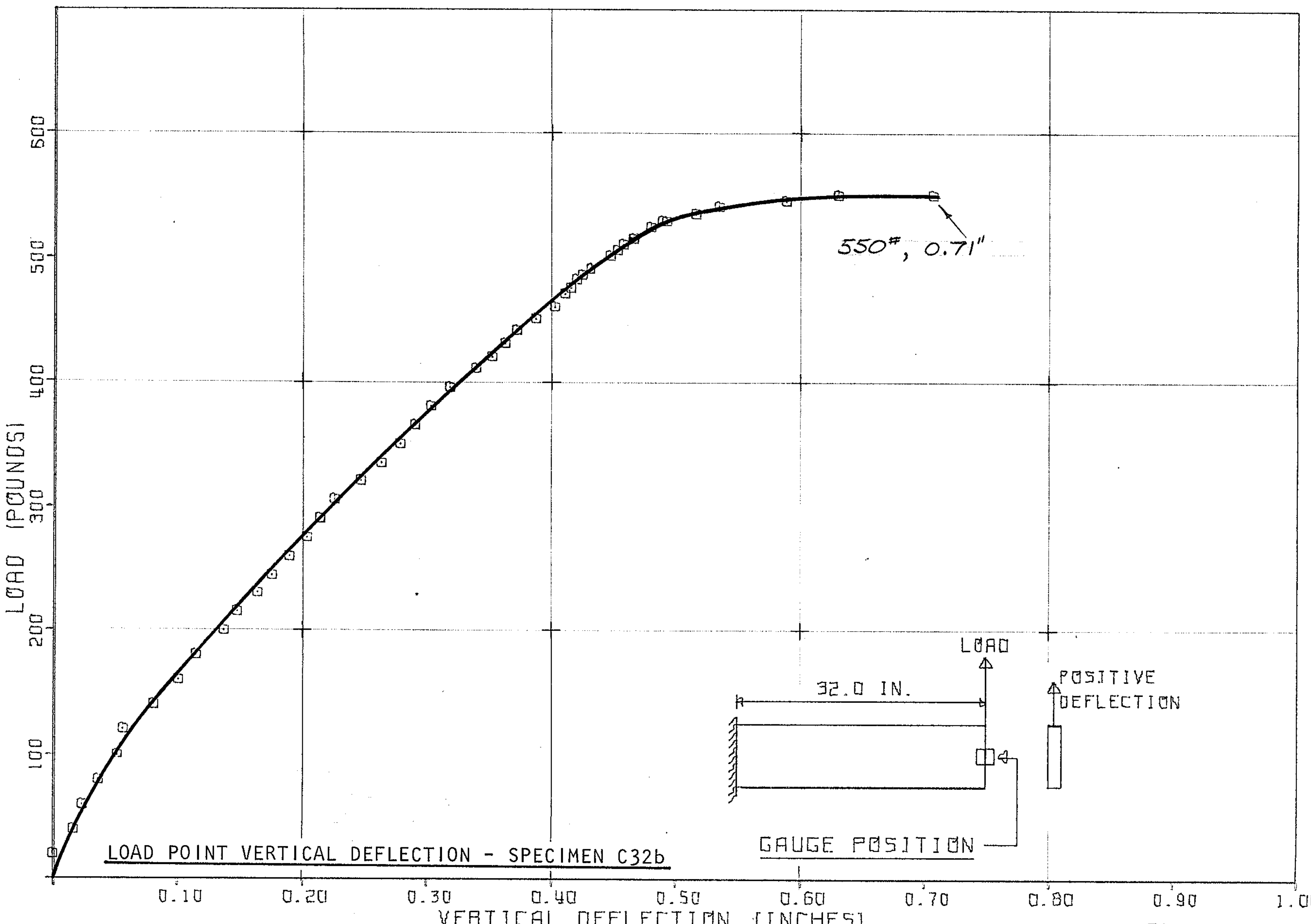

LOAD POINT VERTICAL DEFLECTION - SPECIMEN C32b
550#, 0.71"
LOAD
32.0 IN.
POSITIVE DEFLECTION
GAUGE POSITION
LOAD (POUNDS)
100
200
300
400
500
600
0.10
0.20
0.30
0.40
0.50
0.60
0.70
0.80
0.90
1.00
VERTICAL DEFLECTION (INCHES)

FIGURE A.14

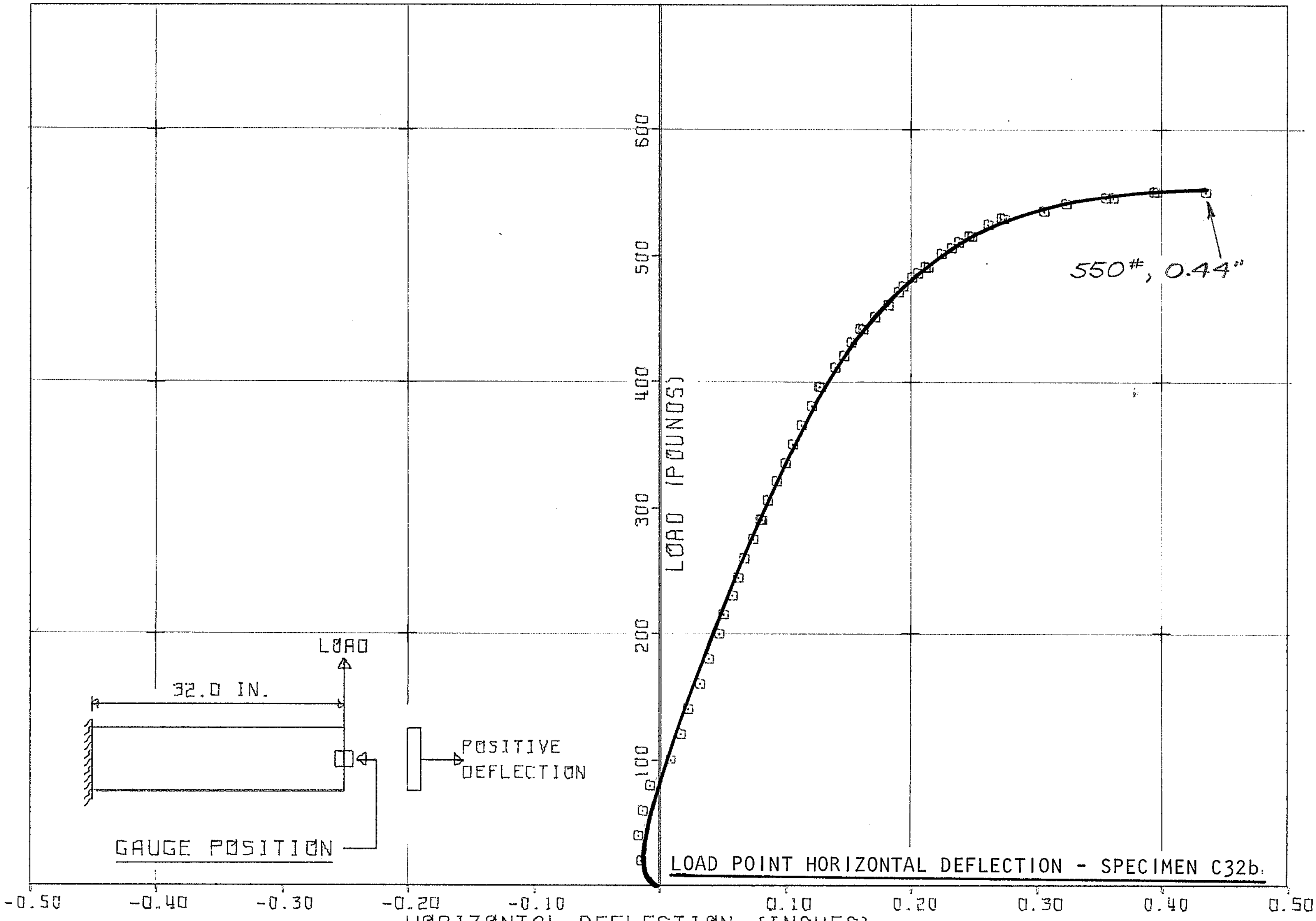

600
500
400
300
200
100
LOAD (POUNDS)
550#, 0.44"
LOAD
32.0 IN.
POSITIVE
DEFLECTION
GAUGE POSITION
LOAD POINT HORIZONTAL DEFLECTION - SPECIMEN C32b.
-0.50
-0.40
-0.30
-0.20
-0.10
0.10
0.20
0.30
0.40
0.50
HORIZONTAL DEFLECTION (INCHES)

FIGURE A.15

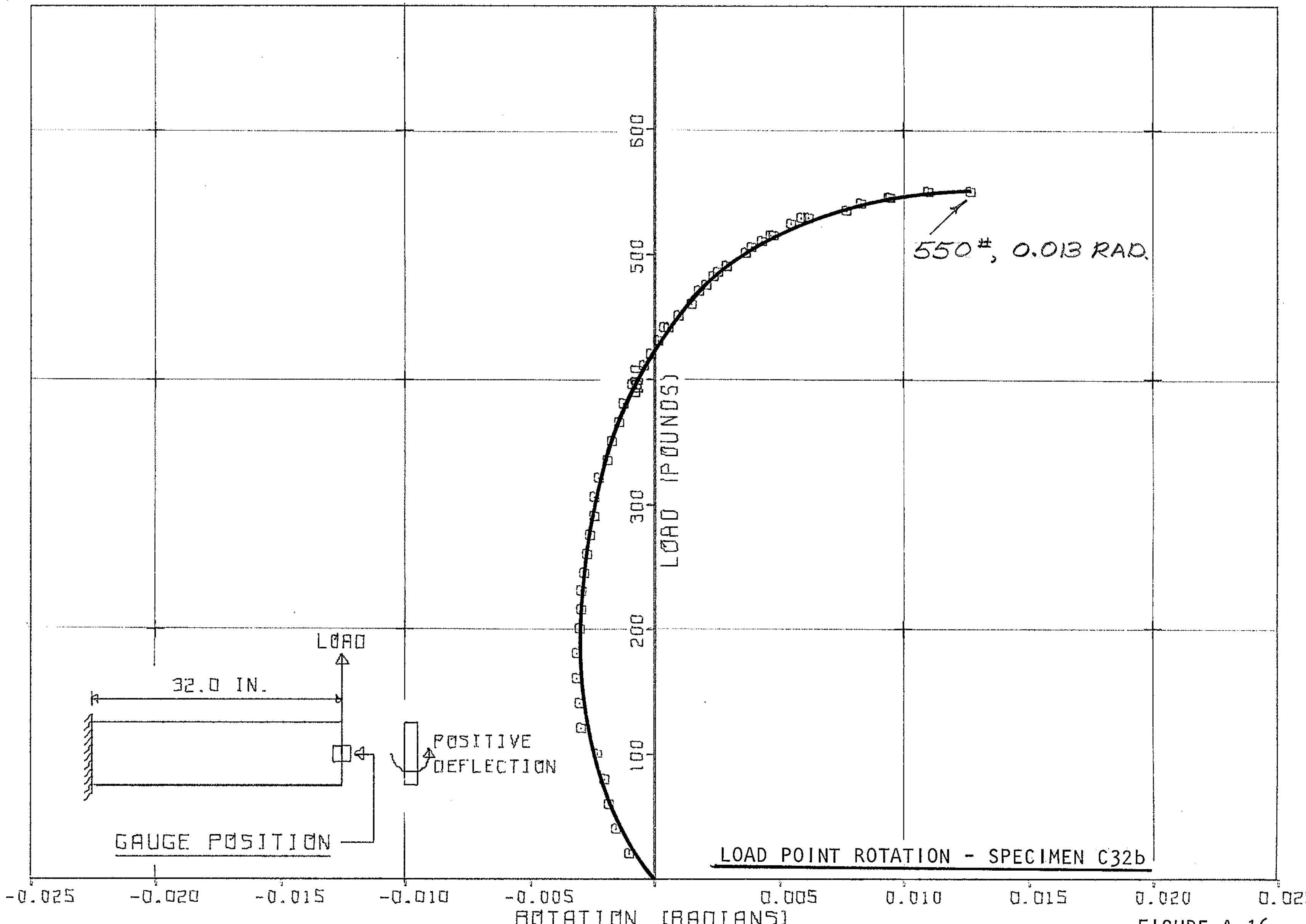
550#, 0.013 RAD.
LOAD (POUNDS)
100
200
300
400
500
600
LOAD
32.0 IN.
POSITIVE
DEFLECTION
GAUGE POSITION
LOAD POINT ROTATION - SPECIMEN C32b
-0.025
-0.020
-0.015
-0.010
-0.005
0.005
0.010
0.015
0.020
0.025
ROTATION (RADIANS)

FIGURE A.16

Specimen C48c

Concrete Cast February 27, 1970

Beam Tested April 20, 1970

Concrete Compressive Tests Age = 51 days

Cylinder	1 (3" x 6")	5850 psi
	2	7040
	3	6760
Average	f'_c =	6500 psi

Concrete Tensile Tests Age = 51 days

(Split-Cylinder Test)

Cylinder	4 (3" x 6")	633 psi
	5	672
	6	625
Average		657 psi

Reinforcement Tensile Tests

Compressive Reinforcement Preloaded to 60 ksi.

Wire Size	Yield Stress	Ultimate Strength
#14 (0.08 inch)	59.7 ksi	67.6 ksi
#14	61.7	65.7
Average	f_y = 60.7 ksi	66.6 ksi

Tension Reinforcement - High-strength Wire

Wire Size	Ultimate Strength
#11 (0.117 inch)	92.3 ksi
#11	98.7

#11	93.3
#11	96.0
#11	94.3
#11	98.7
Average	96.5 ksi

The #11 wires had no pronounced yield plateau and thus no yield point could be determined from the load-deflection curves obtained from the Hounsfield Tensometer. At a stress of approximately 88 ksi, the curves flattened slightly and this stress was called the yield point roughly corresponding to the 0.2% offset yield point.

Of the ten strain gauges placed on the beam three were found to be defective after the beam was positioned in the loading frame. The test was carried out without the three defective gauges since their replacement would have involved dismantling the test (and the risk of damage to the beam). The positions of the remaining gauges are shown on Figures A.21 to A.23.

Beam Length 48 inches

Failure Load 355 pounds

The failure was due to lateral instability, with the load point deflecting in the positive X direction and rotating positive about the Z-axis as shown in Figure A.17. The primary failure occurred in the form of a crack running from Z = 2 at the top to Z = 13 at the bottom. The crack formed on the positive X face, with a maximum width of 0.2 inches. The cracks on the near face beyond Z = 10 were hairline, rather than the single wider crack observed in previous tests.

The horizontal deflection of the load point and the top face at L/3 are shown on Figure A.19. The most significant feature of the L/3 deflection is the fact that it was initially in the same direction as the load point deflection then reversing as failure approached. The load point rotation and vertical deflection are shown on Figures A.18 and A.20 respectively.

The strain at the concrete surface for the seven working gauges is shown on Figures A.21 to A.23. Gauges 3 and 4, at the bottom of the beam near the fixed end, showed rapidly increasing strain and exceeded the limit of the recording equipment early in the test. This was likely the result of a hairline crack in the concrete (as expected in the area of highest tension). The gauges illustrated on Figure A.22 show the behaviour of the strain at failure, with gauges 6 and 8 (on the concave side from Figure A.17) showing a decrease (algebraically) in strain and 5 and 7 showing an increase.

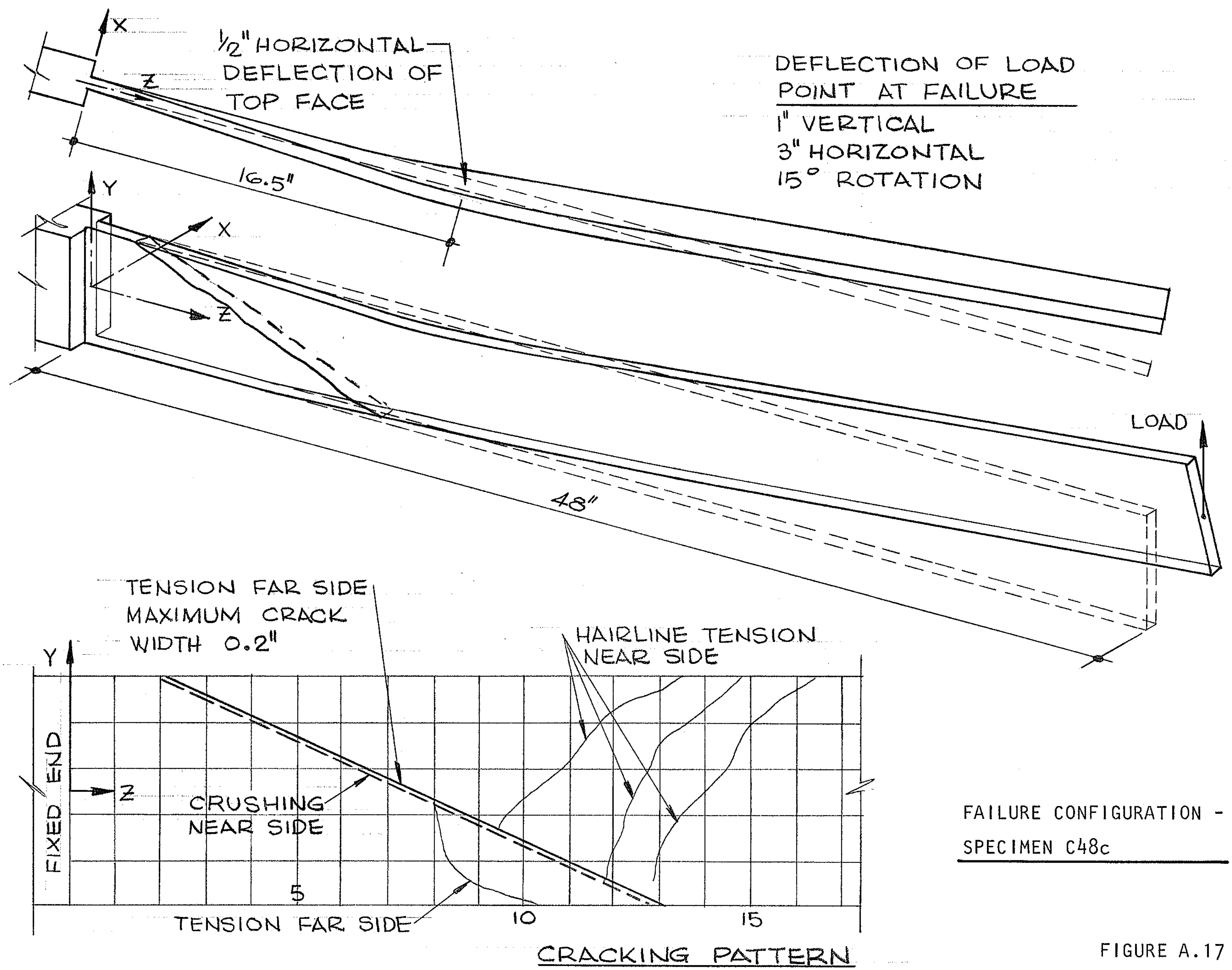

FAILURE CONFIGURATION - SPECIMEN C48c

FIGURE A.17

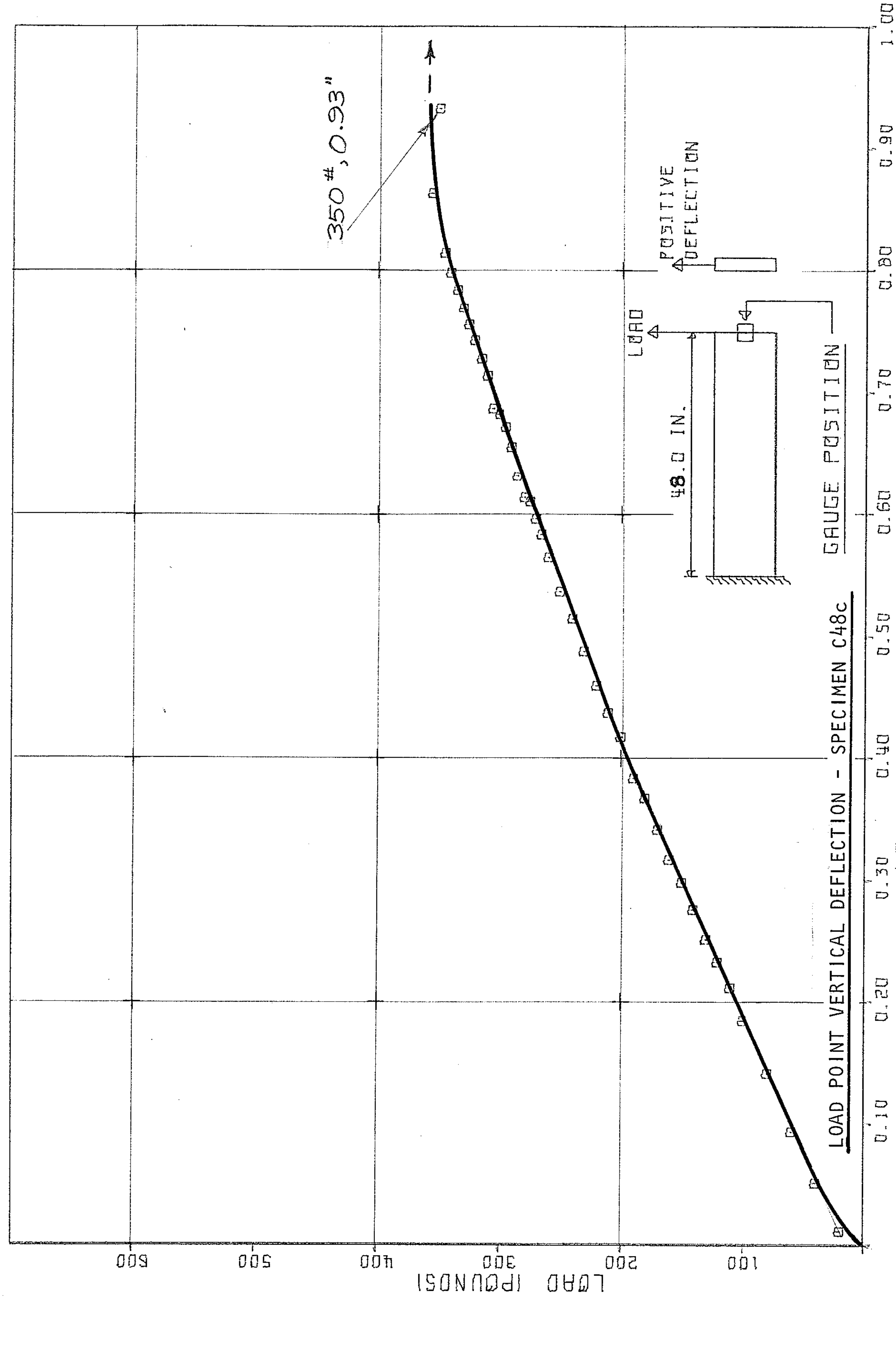

350#, 0.93"
LOAD POINT VERTICAL DEFLECTION - SPECIMEN C48c
POSITIVE DEFLECTION
LOAD
48.0 IN.
GAUGE POSITION
VERTICAL DEFLECTION (INCHES)
LOAD (POUNDS)
0.10
0.20
0.30
0.40
0.50
0.60
0.70
0.80
0.90
1.00
100
200
300
400
500
600

FIGURE A.18

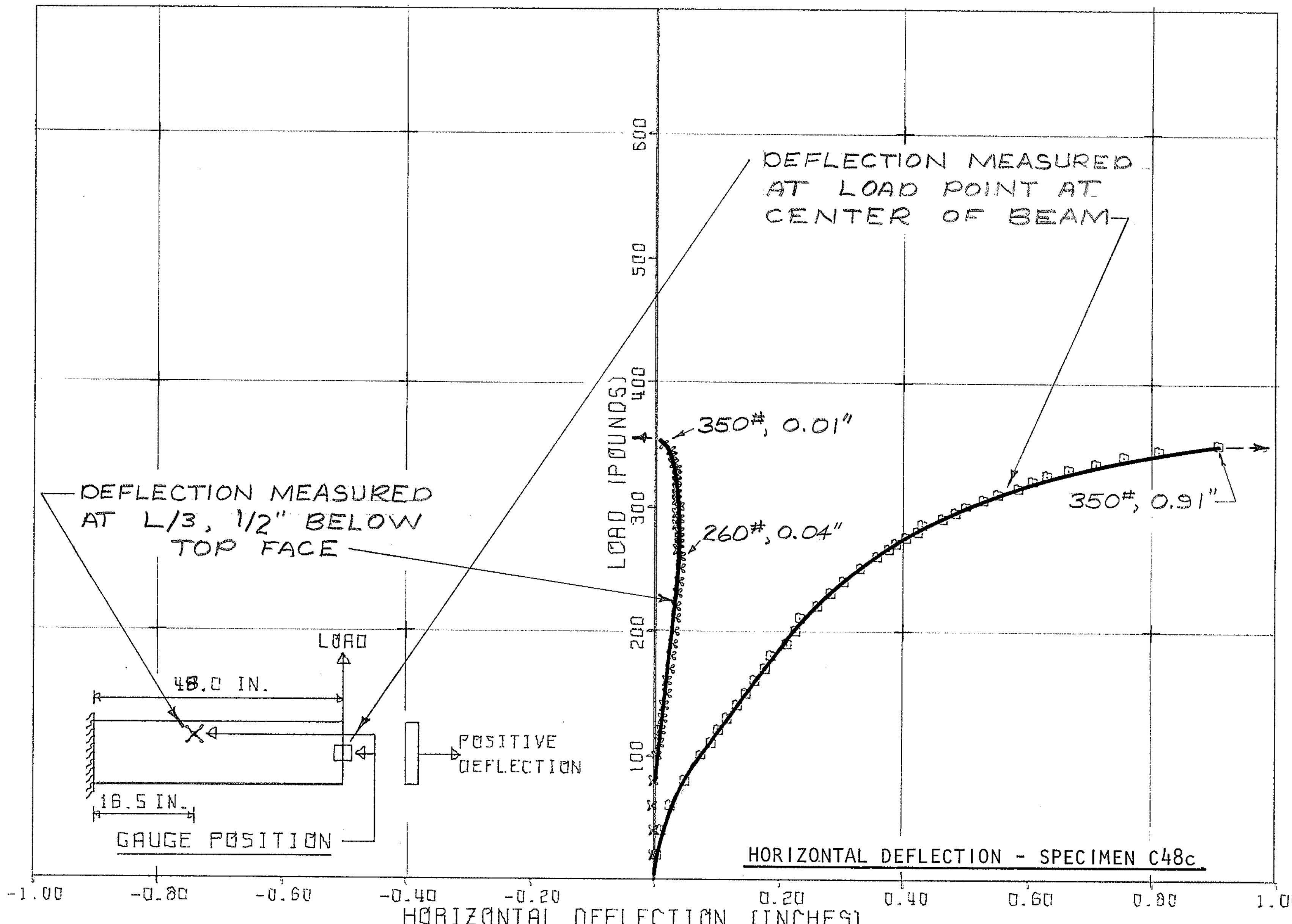
HORIZONTAL DEFLECTION - SPECIMEN C48c
DEFLECTION MEASURED AT LOAD POINT AT CENTER OF BEAM
DEFLECTION MEASURED AT L/3, 1/2" BELOW TOP FACE
350#, 0.01"
260#, 0.04"
350#, 0.91"
LOAD
48.0 IN.
16.5 IN.
GAUGE POSITION
POSITIVE DEFLECTION
LOAD (POUNDS)
100
200
300
400
500
600
-1.00
-0.80
-0.60
-0.40
-0.20
0.20
0.40
0.60
0.80
1.00
HORIZONTAL DEFLECTION (INCHES)

FIGURE A.19

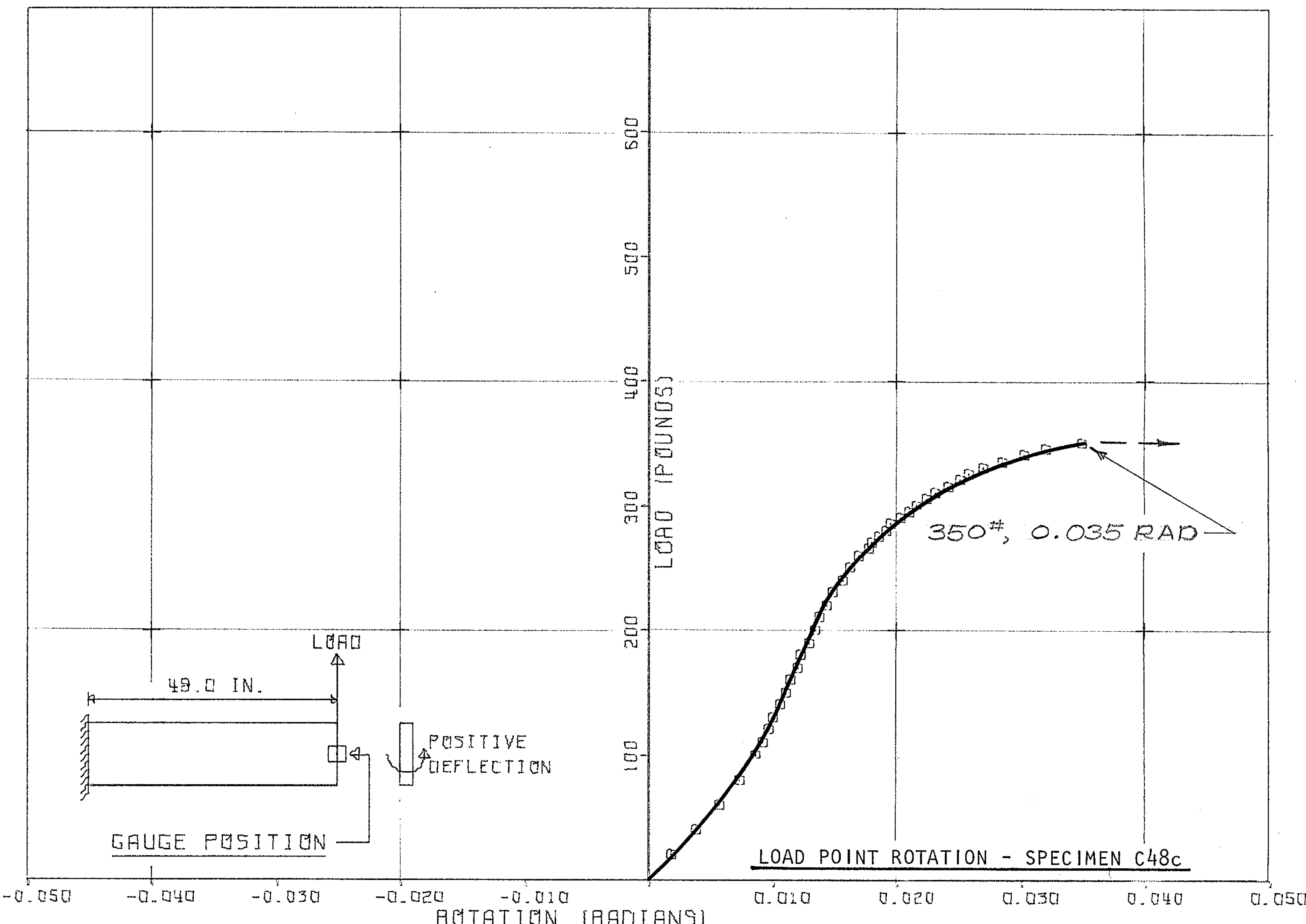

LOAD POINT ROTATION - SPECIMEN C48c
350#, 0.035 RAD
LOAD (POUNDS)
100
200
300
400
500
600
ROTATION (RADIANS)
-0.050
-0.040
-0.030
-0.020
-0.010
0.010
0.020
0.030
0.040
0.050
LOAD
49.0 IN.
POSITIVE DEFLECTION
GAUGE POSITION

FIGURE A.20

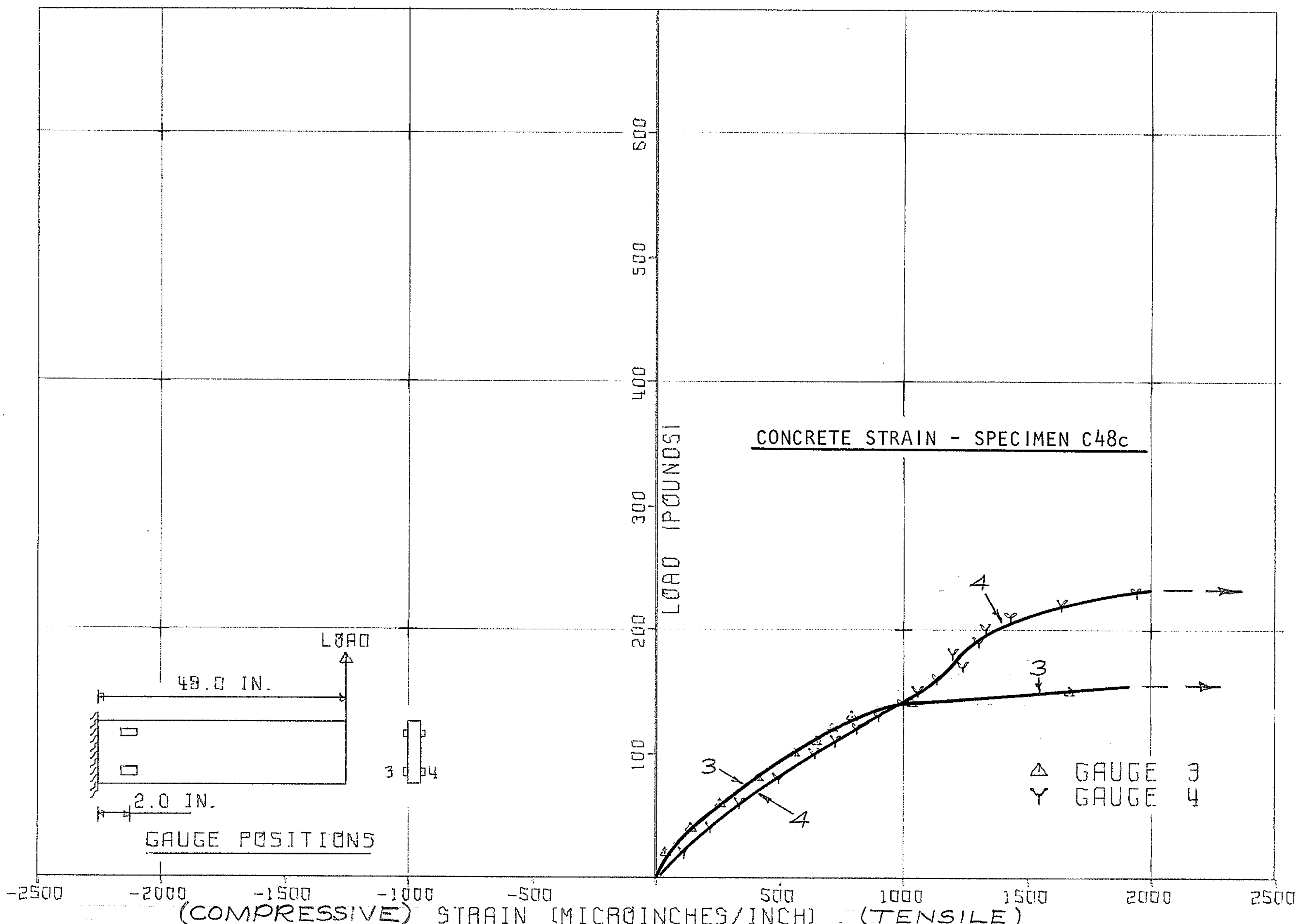
CONCRETE STRAIN - SPECIMEN C48c
LOAD (POUNDS)
100
200
300
400
500
600
-2500
-2000
-1500
-1000
-500
500
1000
1500
2000
2500
(COMPRESSIVE) STRAIN (MICROINCHES/INCH) (TENSILE)
3
4
△ GAUGE 3
Y GAUGE 4
LOAD
49.0 IN.
2.0 IN.
GAUGE POSITIONS

FIGURE A.21

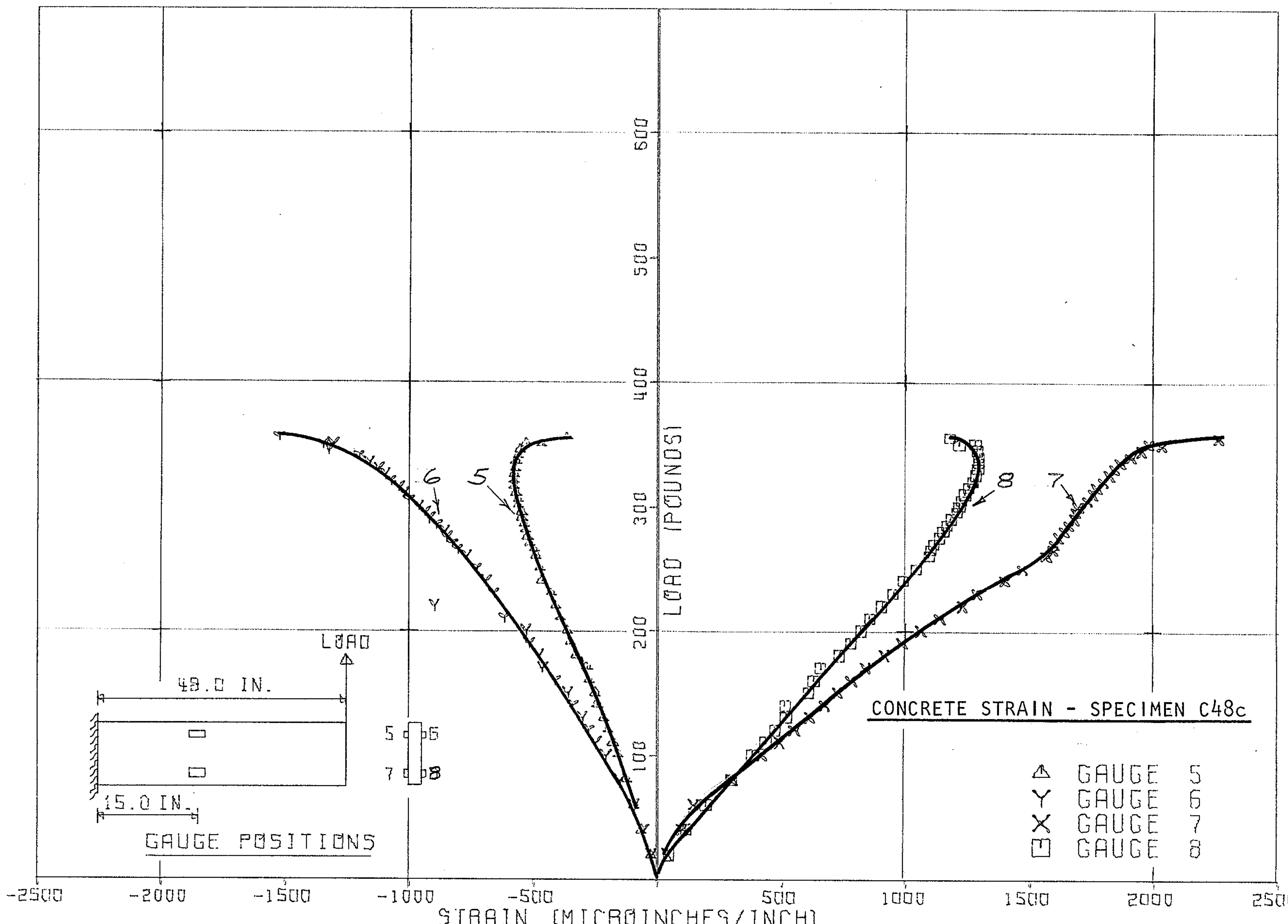
CONCRETE STRAIN - SPECIMEN C48c
GAUGE 5
GAUGE 6
GAUGE 7
GAUGE 8
LOAD (POUNDS)
100
200
300
400
500
600
-2500
-2000
-1500
-1000
-500
500
1000
1500
2000
2500
STRAIN (MICROINCHES/INCH)
LOAD
48.0 IN.
15.0 IN.
GAUGE POSITIONS
5
6
7
8

FIGURE A.22

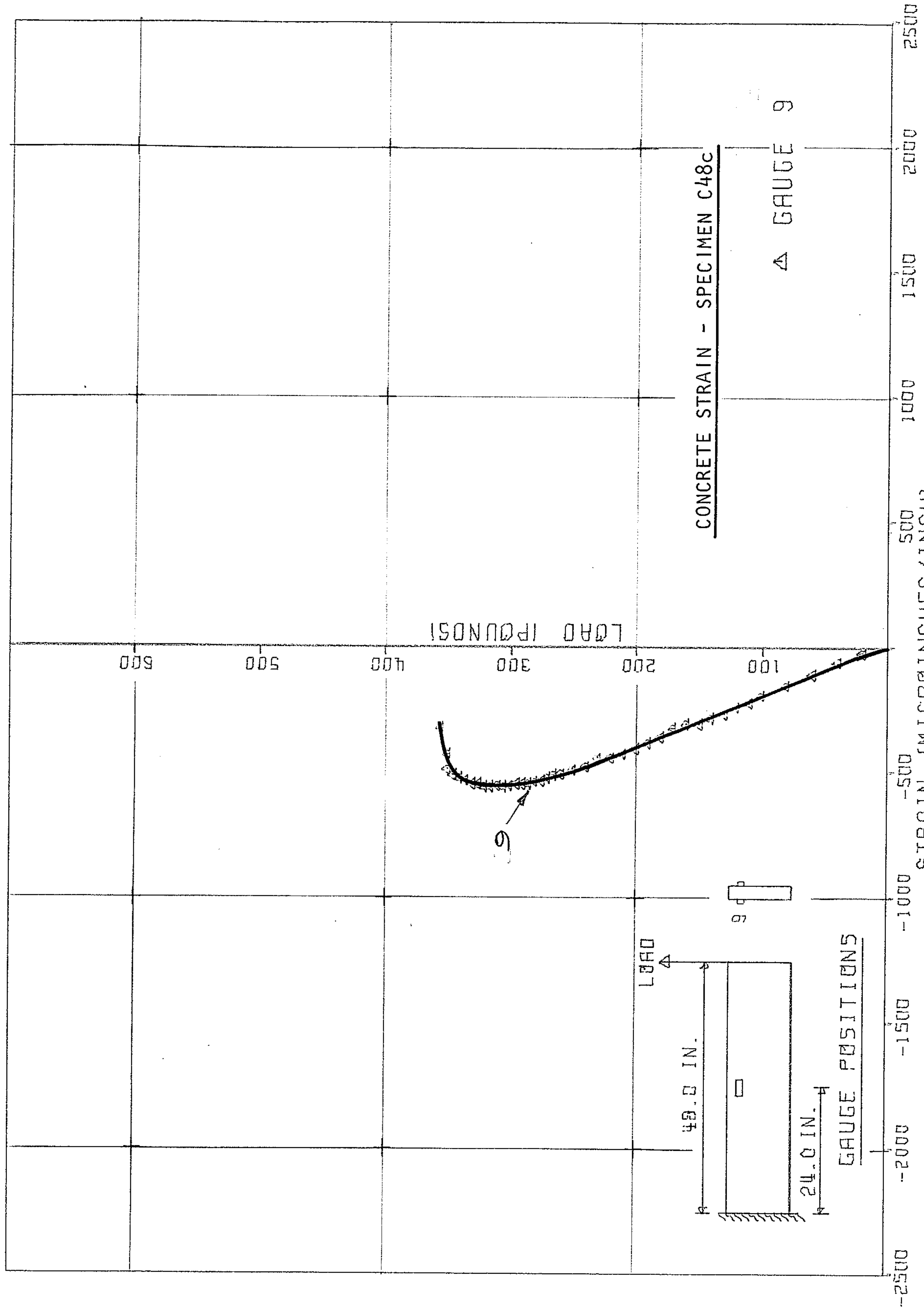

CONCRETE STRAIN - SPECIMEN C48c
△ GAUGE 9
LOAD (POUNDS)
100
200
300
400
500
600
STRAIN (MICROINCHES/INCH)
-2500
-2000
-1500
-1000
-500
500
1000
1500
2000
2500
9
LOAD
49.0 IN.
24.0 IN.
GAUGE POSITIONS

FIGURE A.23

Specimen C44c

Concrete Cast March 4, 1970

Beam Tested April 21, 1970

Concrete Compressive Tests   Age = 48 days

Cylinder	1 (3" x 6")	6030 psi
	2	5790
	3	5520
Average	f_c' =	5820 psi

Concrete Tensile Tests   Age = 48 days

(Split Cylinder Test)

Cylinder	4 (3" x 6")	631 psi
	5	639
	6	650
Average		640 psi

Tensile Reinforcement - 6 #11 High Strength Wires

Compressive Reinforcement - 2 #14 Wires Preloaded to 60 ksi

No tensile tests of the wires were made since the beam was definitely over-reinforced and any flexural failure would occur by crushing of the concrete.

Beam Length   44 inches

Failure Load   445 pounds

The failure type was lateral instability with the load point deflecting in the positive X direction and with rotation positive about the Z axis as is shown in Figure A.24. Two diagonal cracks formed, the first began at approximately Z = 1 at the top face and ran to Z = 9.5 approximately 1 inch above the bottom face with tension on the positive X face. The second crack began at Z = 10.5 approximately 1 inch above the bottom face and ran upward to the top face at Z = 13.5 with tension on the negative X face. The cracks both appeared to end at the top of the tensile reinforcement. The concrete around the reinforcement broke away between Z = 9.5 and Z = 11.5.

The load-deflection curves are shown on Figures A.25 to A.27 and the load-strain curves are shown on Figures A.28 to A.30. These curves are repeated in Chapter 4 as Figures 4.2 and 4.3.

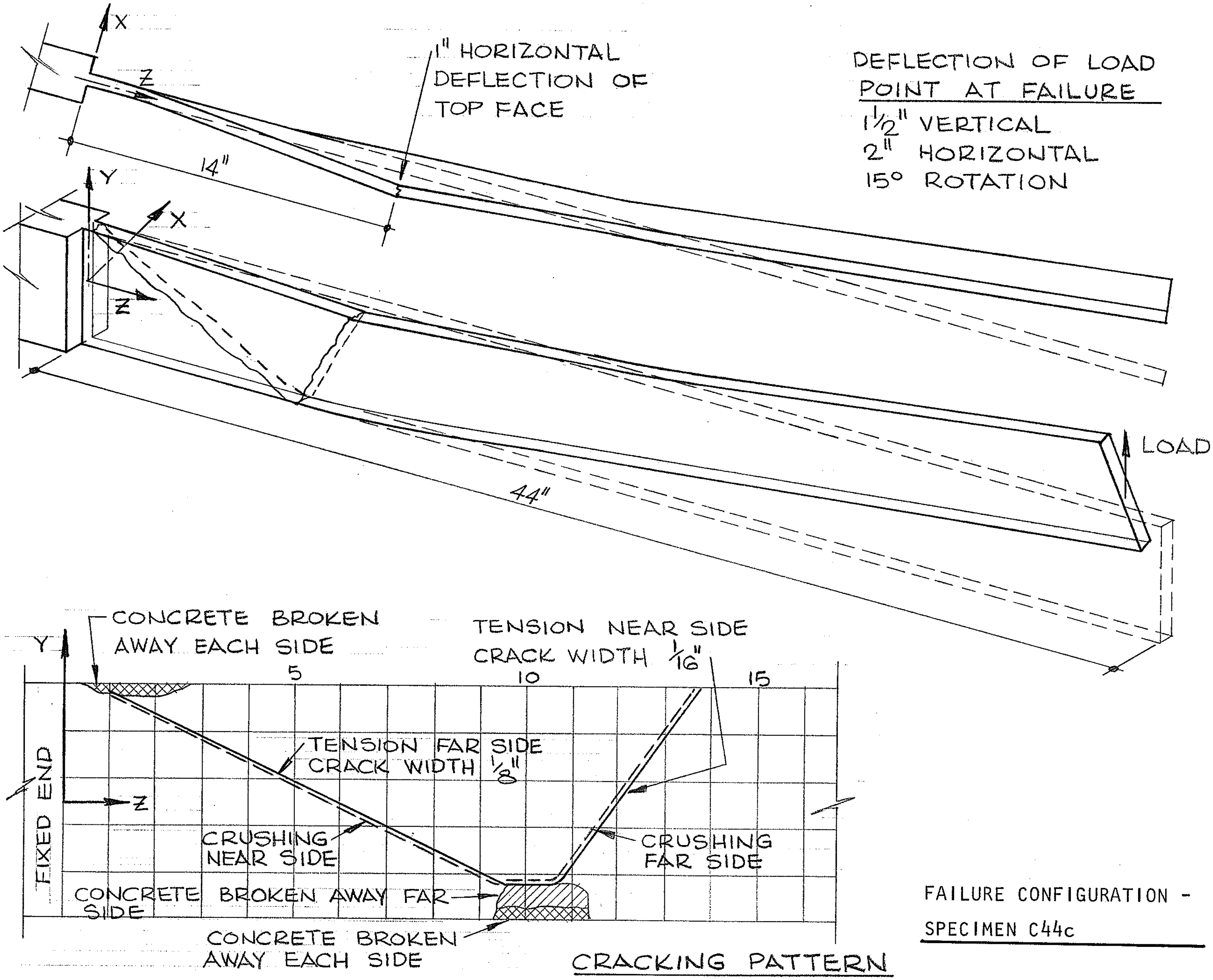

FAILURE CONFIGURATION - SPECIMEN C44c

FIGURE A.24

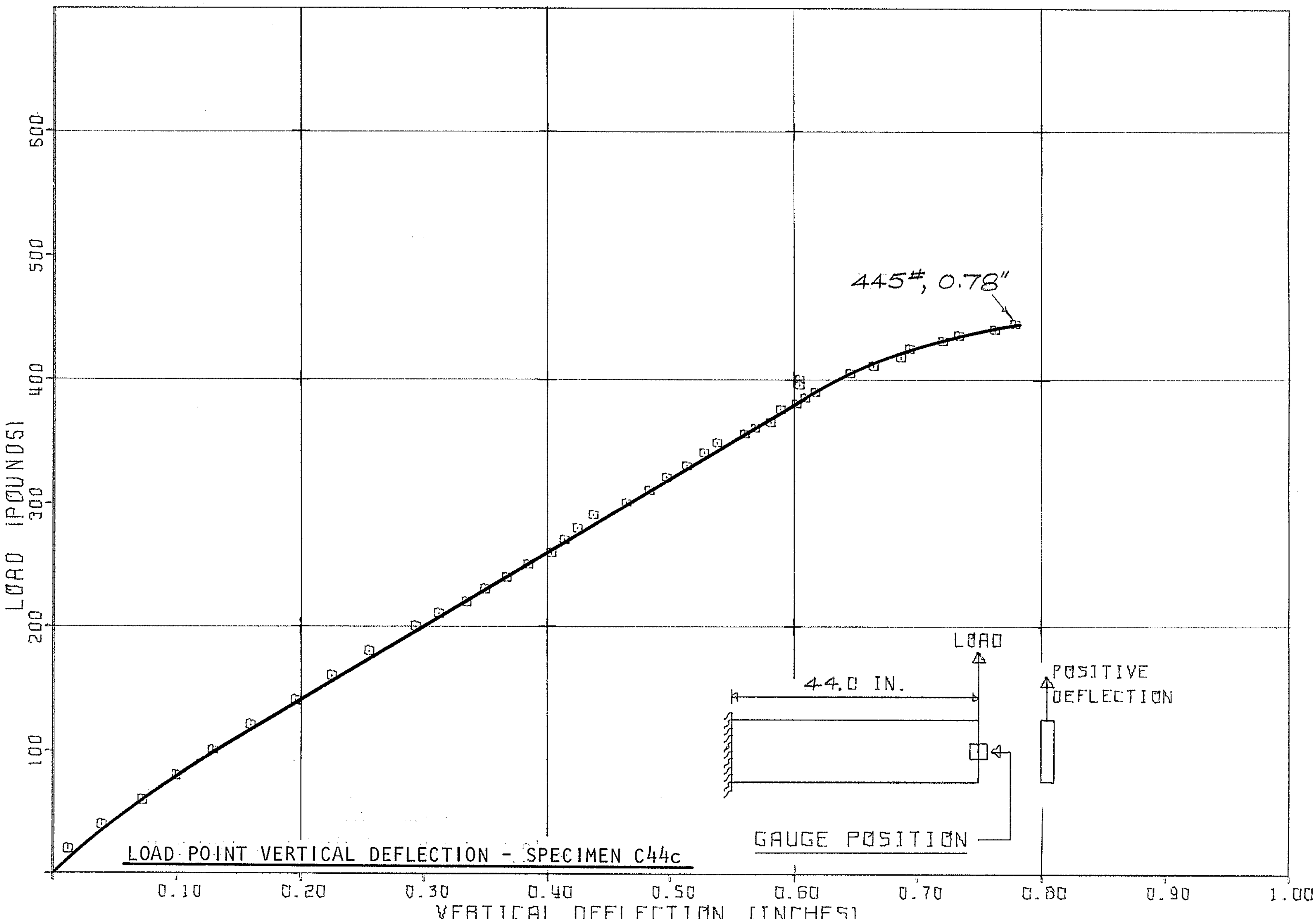
445#, 0.78"
LOAD
44.0 IN.
POSITIVE DEFLECTION
GAUGE POSITION
LOAD POINT VERTICAL DEFLECTION - SPECIMEN C44c
LOAD (POUNDS)
100
200
300
400
500
600
0.10
0.20
0.30
0.40
0.50
0.60
0.70
0.80
0.90
1.00
VERTICAL DEFLECTION (INCHES)

FIGURE A.25

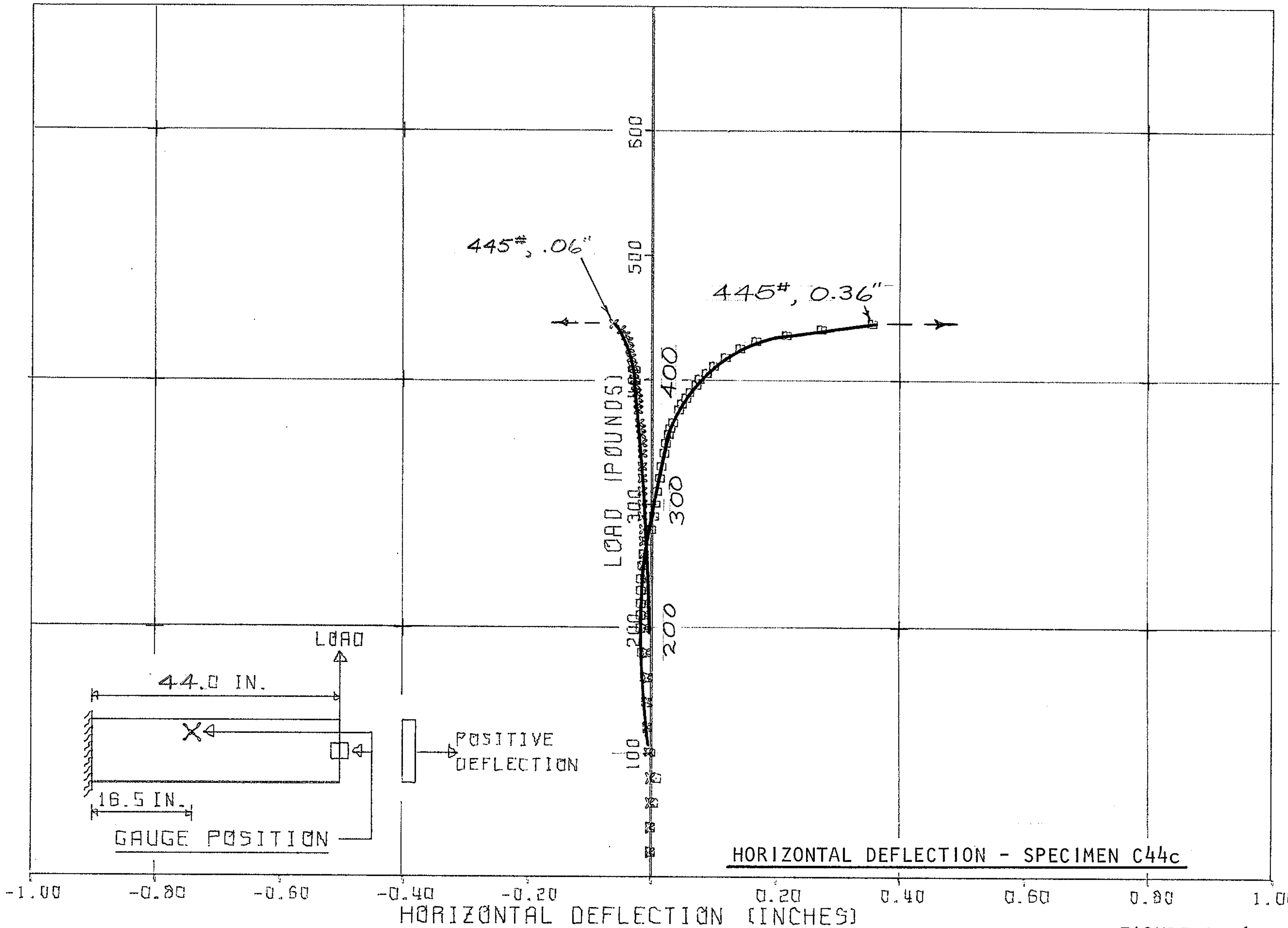
445#, .06"
445#, 0.36"
400
300
200
LOAD (POUNDS)
100
200
300
500
600
LOAD
44.0 IN.
16.5 IN.
GAUGE POSITION
POSITIVE
DEFLECTION
HORIZONTAL DEFLECTION - SPECIMEN C44c
-1.00
-0.80
-0.60
-0.40
-0.20
0.20
0.40
0.60
0.80
1.00
HORIZONTAL DEFLECTION (INCHES)

FIGURE A.26

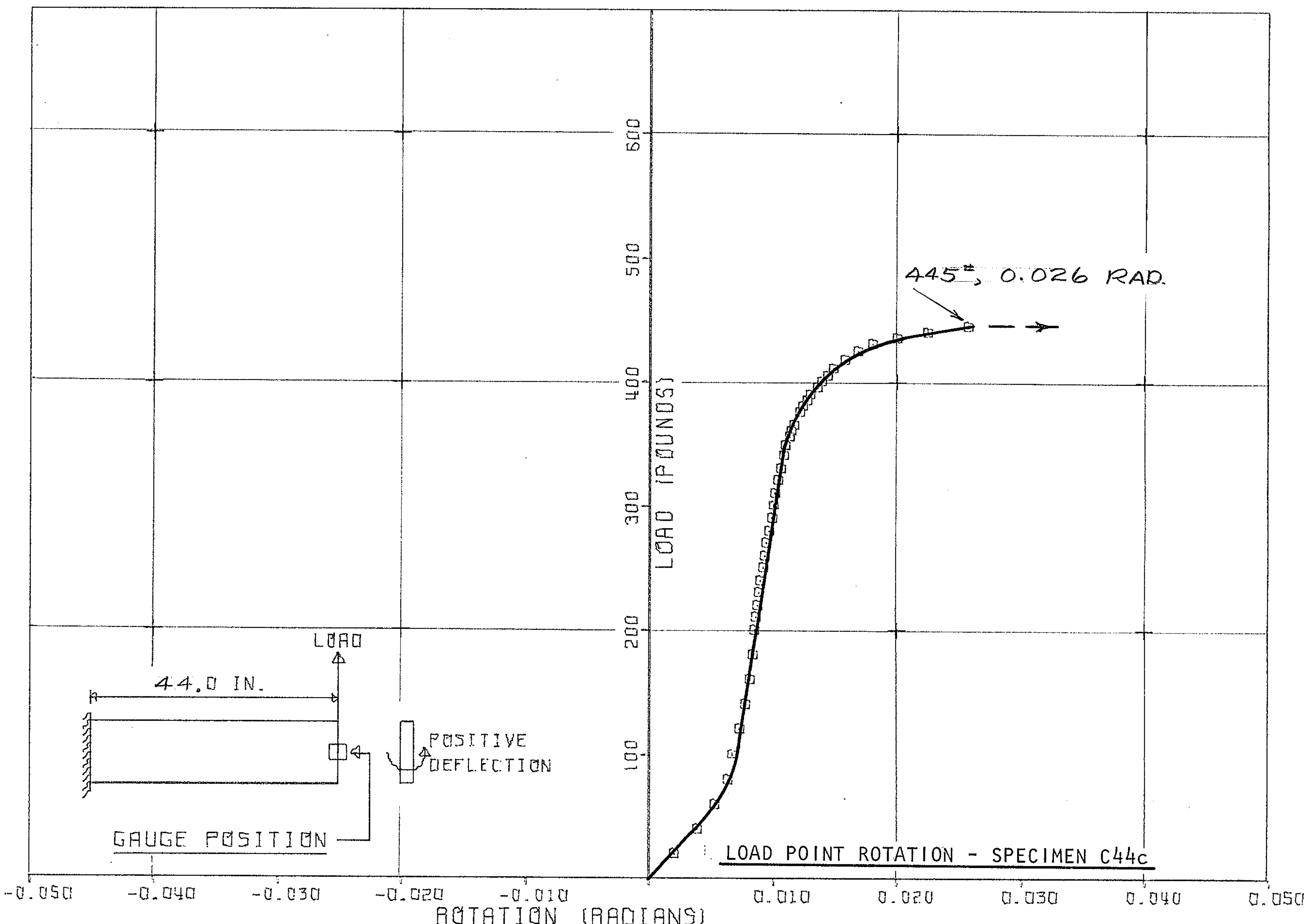

445#, 0.026 RAD.
LOAD POINT ROTATION - SPECIMEN C44c
LOAD (POUNDS)
100
200
300
400
500
600
ROTATION (RADIANS)
-0.050
-0.040
-0.030
-0.020
-0.010
0.010
0.020
0.030
0.040
0.050
LOAD
44.0 IN.
POSITIVE
DEFLECTION
GAUGE POSITION

FIGURE A.27

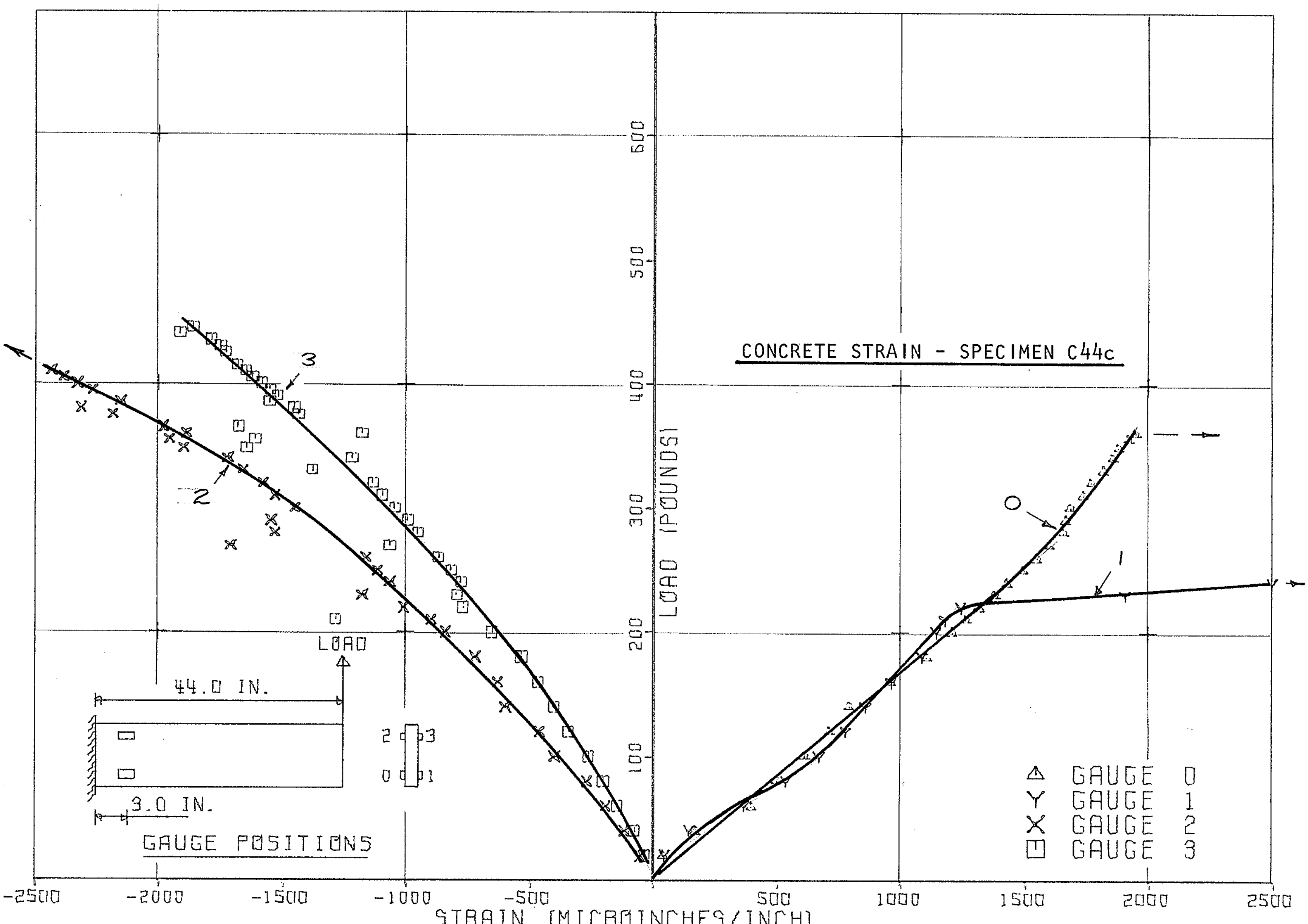
CONCRETE STRAIN - SPECIMEN C44c
LOAD (POUNDS)
STRAIN (MICROINCHES/INCH)
-2500
-2000
-1500
-1000
-500
500
1000
1500
2000
2500
100
200
300
400
500
600
GAUGE 0
GAUGE 1
GAUGE 2
GAUGE 3
0
1
2
3
LOAD
44.0 IN.
3.0 IN.
GAUGE POSITIONS

FIGURE A.28

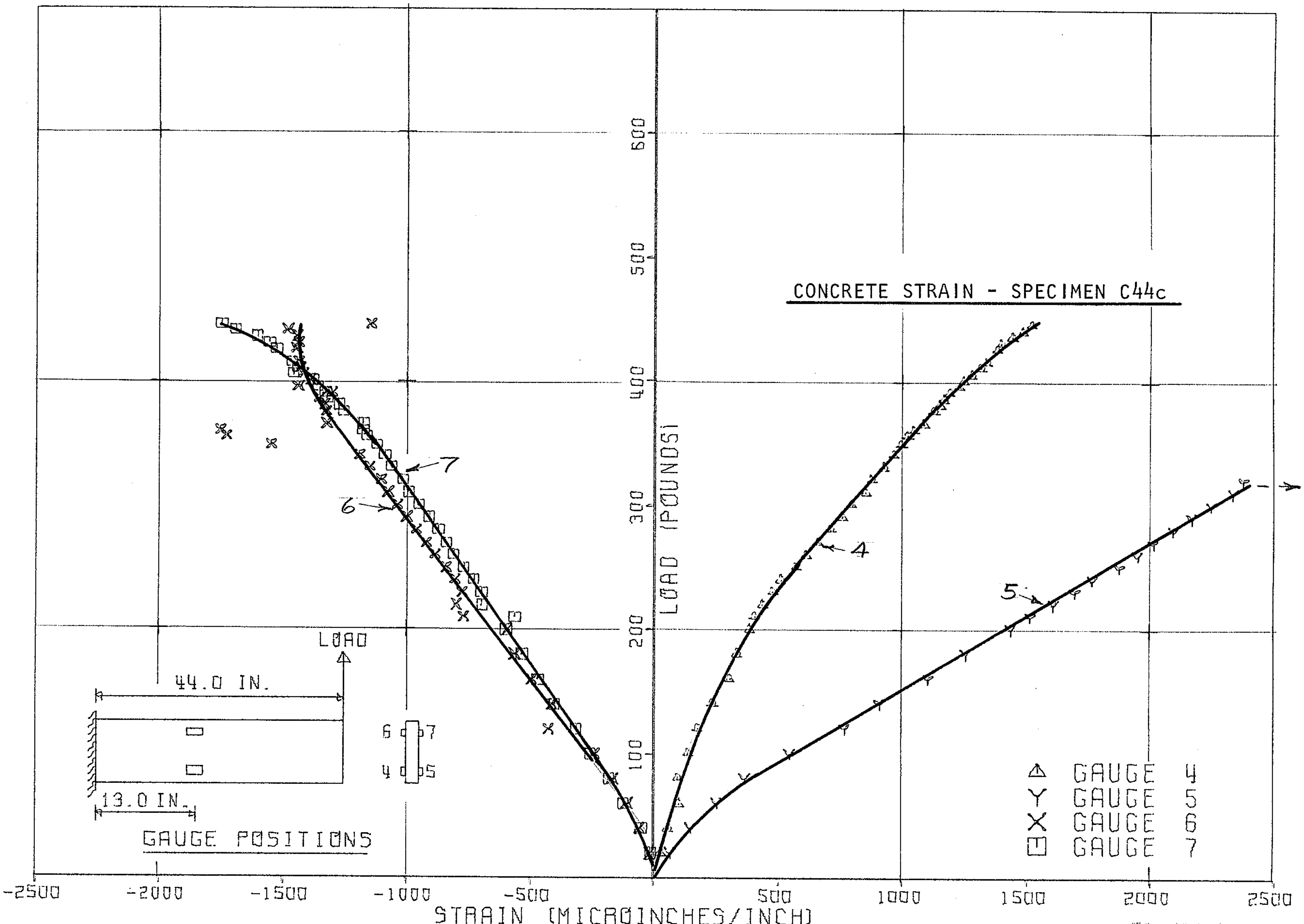
CONCRETE STRAIN - SPECIMEN C44c
LOAD (POUNDS)
STRAIN (MICROINCHES/INCH)
-2500
-2000
-1500
-1000
-500
500
1000
1500
2000
2500
100
200
300
400
500
600
4
5
6
7
GAUGE 4
GAUGE 5
GAUGE 6
GAUGE 7
LOAD
44.0 IN.
13.0 IN.
GAUGE POSITIONS

FIGURE A.29

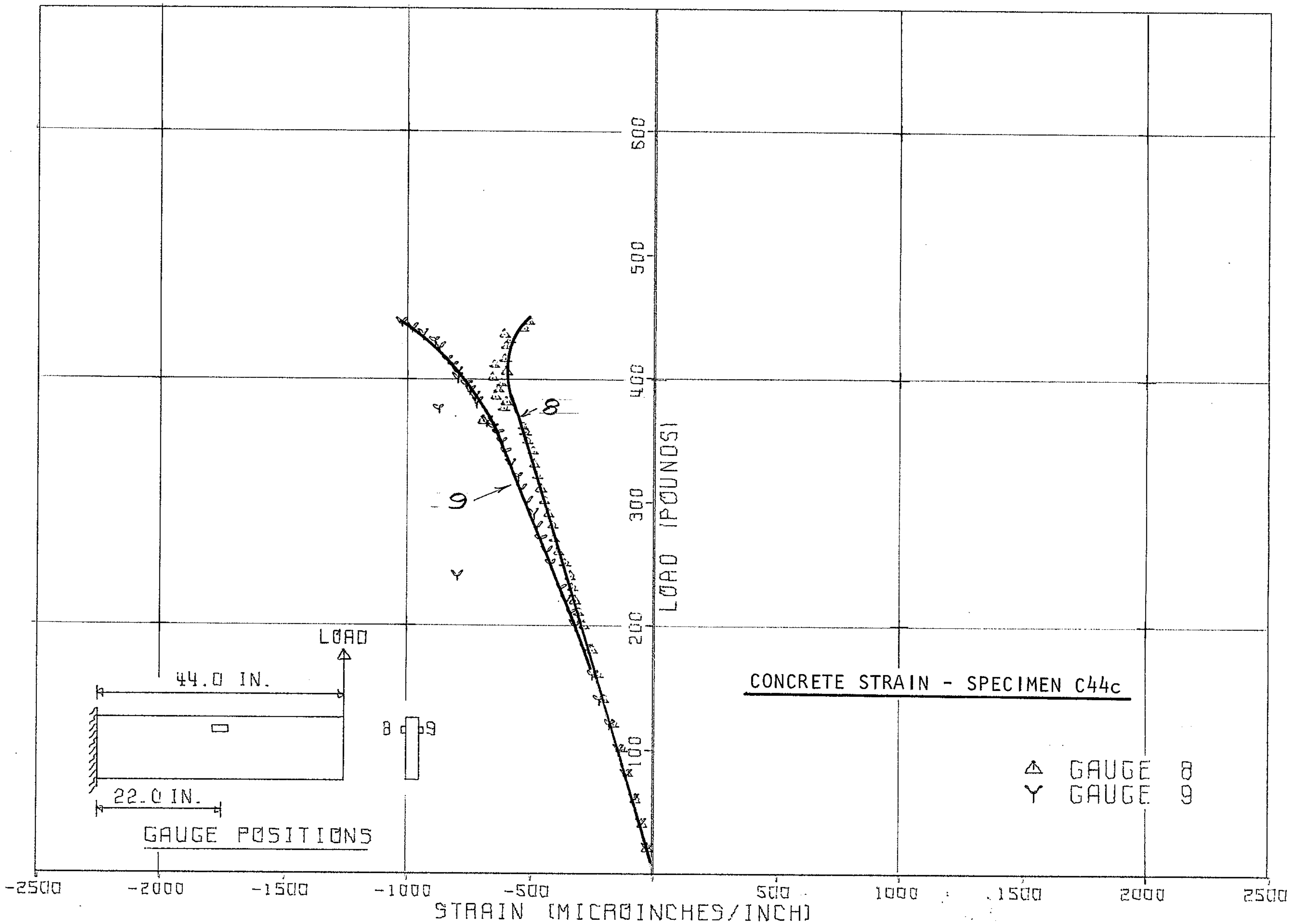
CONCRETE STRAIN - SPECIMEN C44c
LOAD (POUNDS)
100
200
300
400
500
600
STRAIN (MICROINCHES/INCH)
-2500
-2000
-1500
-1000
-500
500
1000
1500
2000
2500
GAUGE 8
GAUGE 9
8
9
LOAD
44.0 IN.
22.0 IN.
GAUGE POSITIONS

FIGURE A.30

Specimen C40c

Concrete Cast March 13, 1970

Beam Tested April 22, 1970

Concrete Compressive Tests   Age = 42 days

Cylinder	1 (3" x 6")	5680 psi
	2	5950
	3	5650
Average	f_c' =	5720 psi

Concrete Tensile Tests   Age = 42 days

(Split Cylinder Test)

Cylinder	4 (3" x 6")	620 psi
	5	640
	6	620
Average		630 psi

Tensile Reinforcement - 6 #11 high-strength wires

Compressive Reinforcement - 2 #14 wires, preloaded to 60 ksi

Beam Length   40 inches

Failure Load   445 pounds

The beam had a slight initial deflection (in the positive X direction), and a slight clockwise twist (negative about the Z axis). The failure load was abnormally low in this test, as a result of the initial crookedness of the beam.

The failure type was lateral instability, with the load point deflecting in the positive X direction and rotating positive about the Z axis as shown in Figure A.31. A crack extended from Z = 0 at the top face to Z = 6.5, 1 inch above the bottom face and then along the top of the tensile reinforcement to Z = 8, with tension on the positive X face. A second crack extended from Z = 8 and 1 inch above the bottom face to Z = 12 at the top with tension on the negative X face.

The deflection curves are shown on Figures A.32 to A.34 and the strain curves are shown on Figures A.35 to A.37. The large horizontal deflection at the load point, shown on Figure A.33 and the strain reversal at the fixed end at the bottom (Gauge 0 on Figure A.35) were the result of the initial crookedness of the specimen.

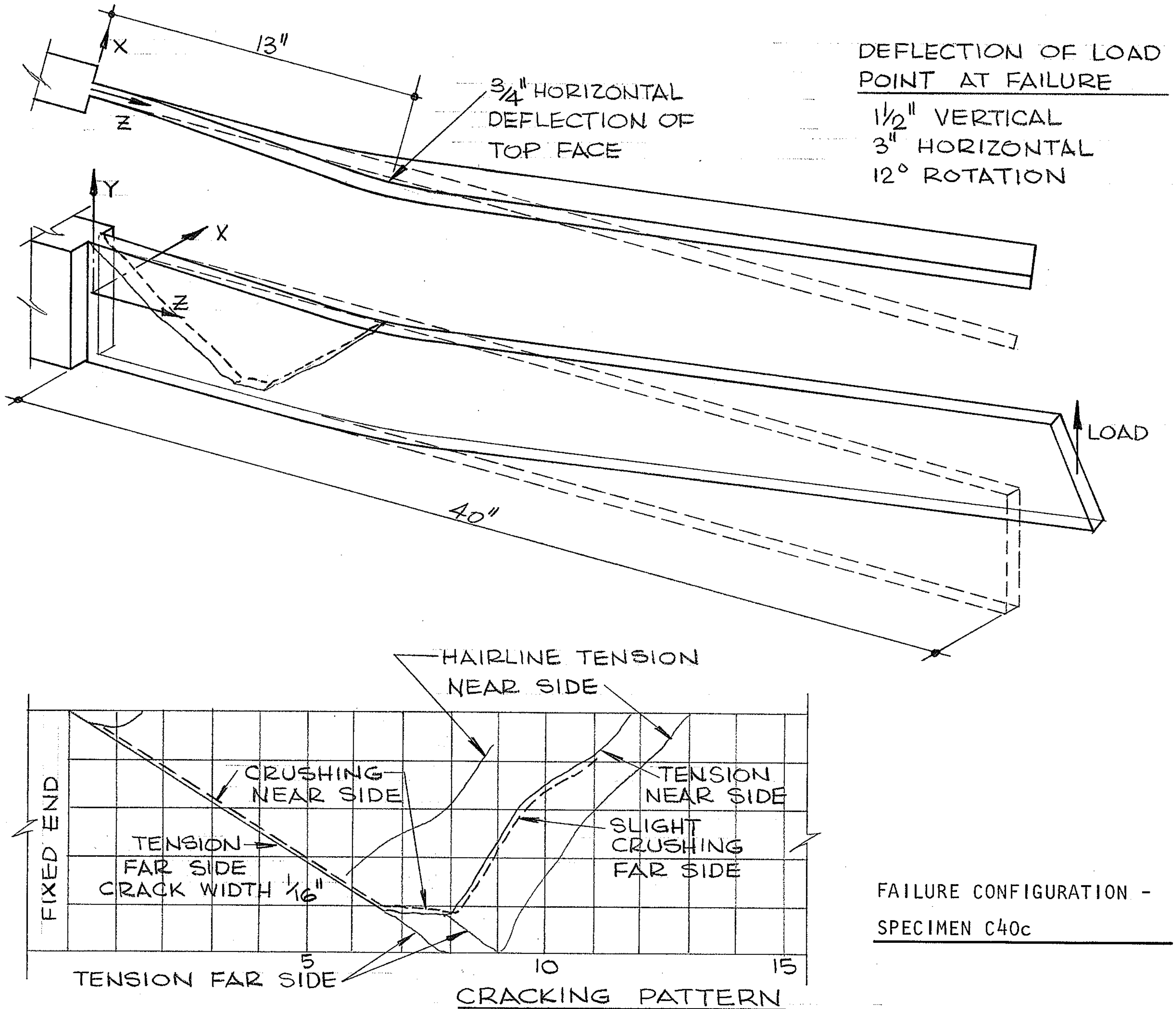

FAILURE CONFIGURATION -
SPECIMEN C40c

FIGURE A.31

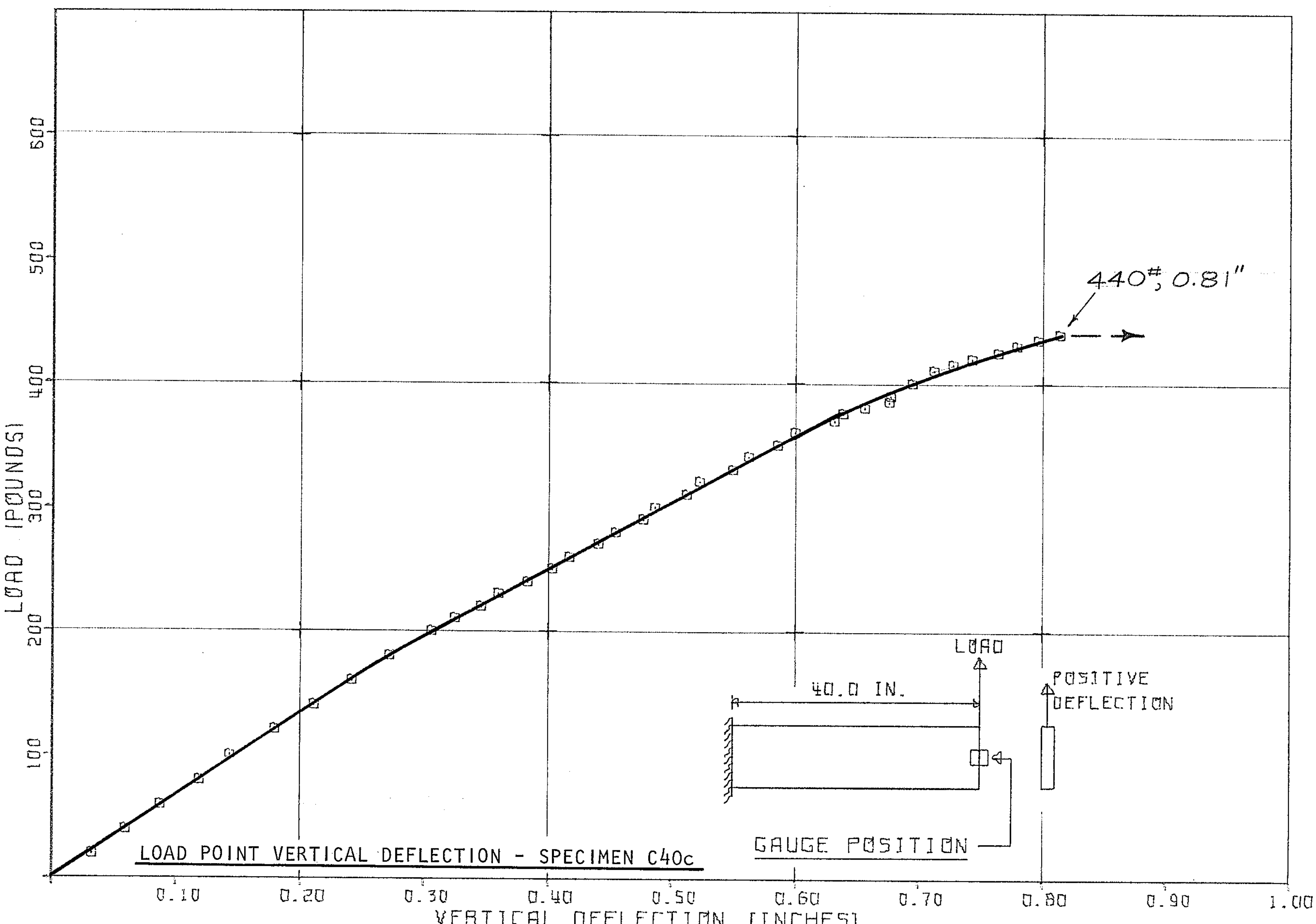
440#; 0.81"
LOAD (POUNDS)
100
200
300
400
500
600
VERTICAL DEFLECTION (INCHES)
0.10
0.20
0.30
0.40
0.50
0.60
0.70
0.80
0.90
1.00
LOAD POINT VERTICAL DEFLECTION - SPECIMEN C40c
LOAD
40.0 IN.
POSITIVE
DEFLECTION
GAUGE POSITION

FIGURE A.32

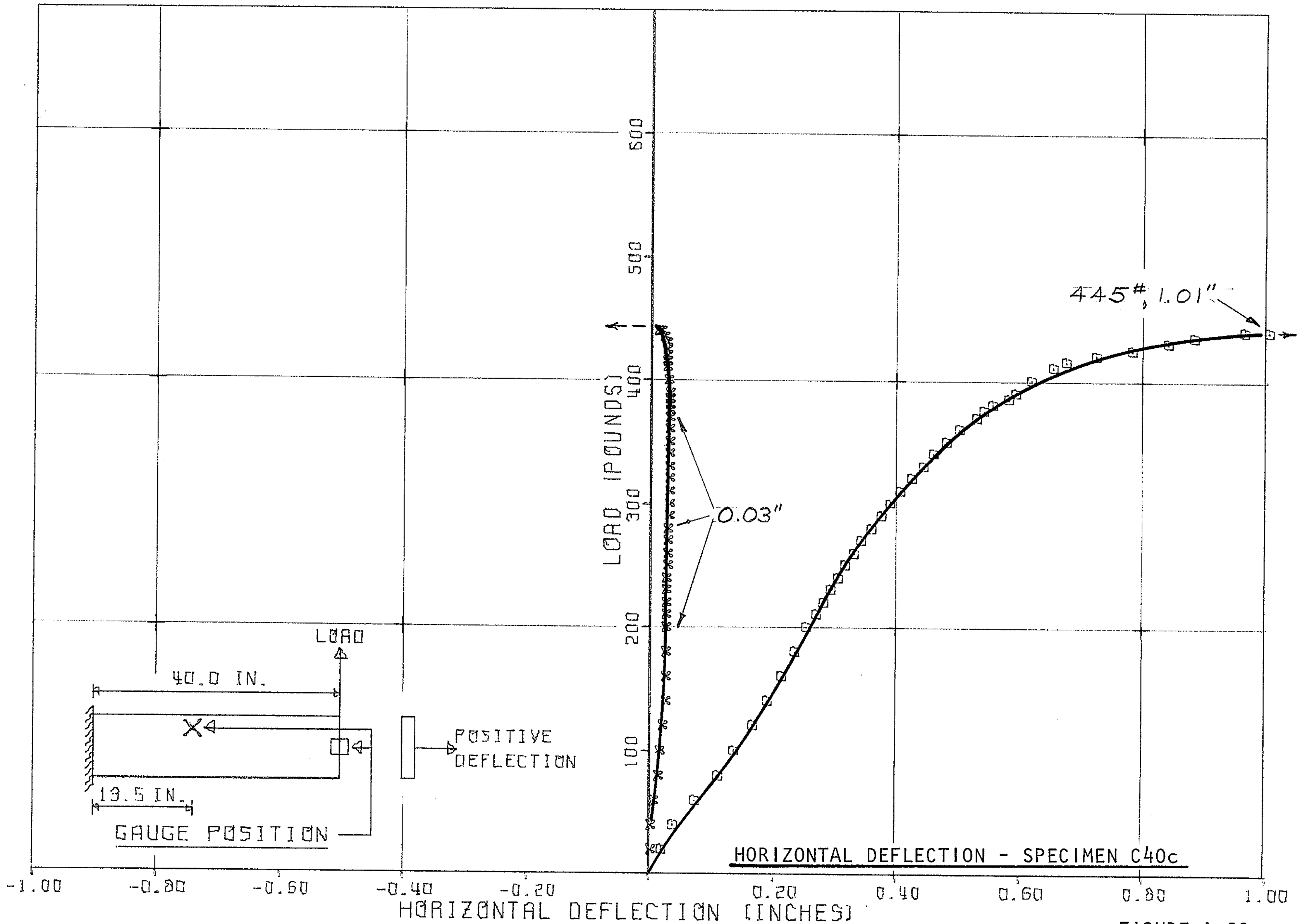

HORIZONTAL DEFLECTION - SPECIMEN C40c
445#, 1.01"
0.03"
LOAD (POUNDS)
HORIZONTAL DEFLECTION (INCHES)
-1.00
-0.80
-0.60
-0.40
-0.20
0.20
0.40
0.60
0.80
1.00
100
200
300
400
500
600
LOAD
40.0 IN.
13.5 IN.
GAUGE POSITION
POSITIVE DEFLECTION

FIGURE A.33

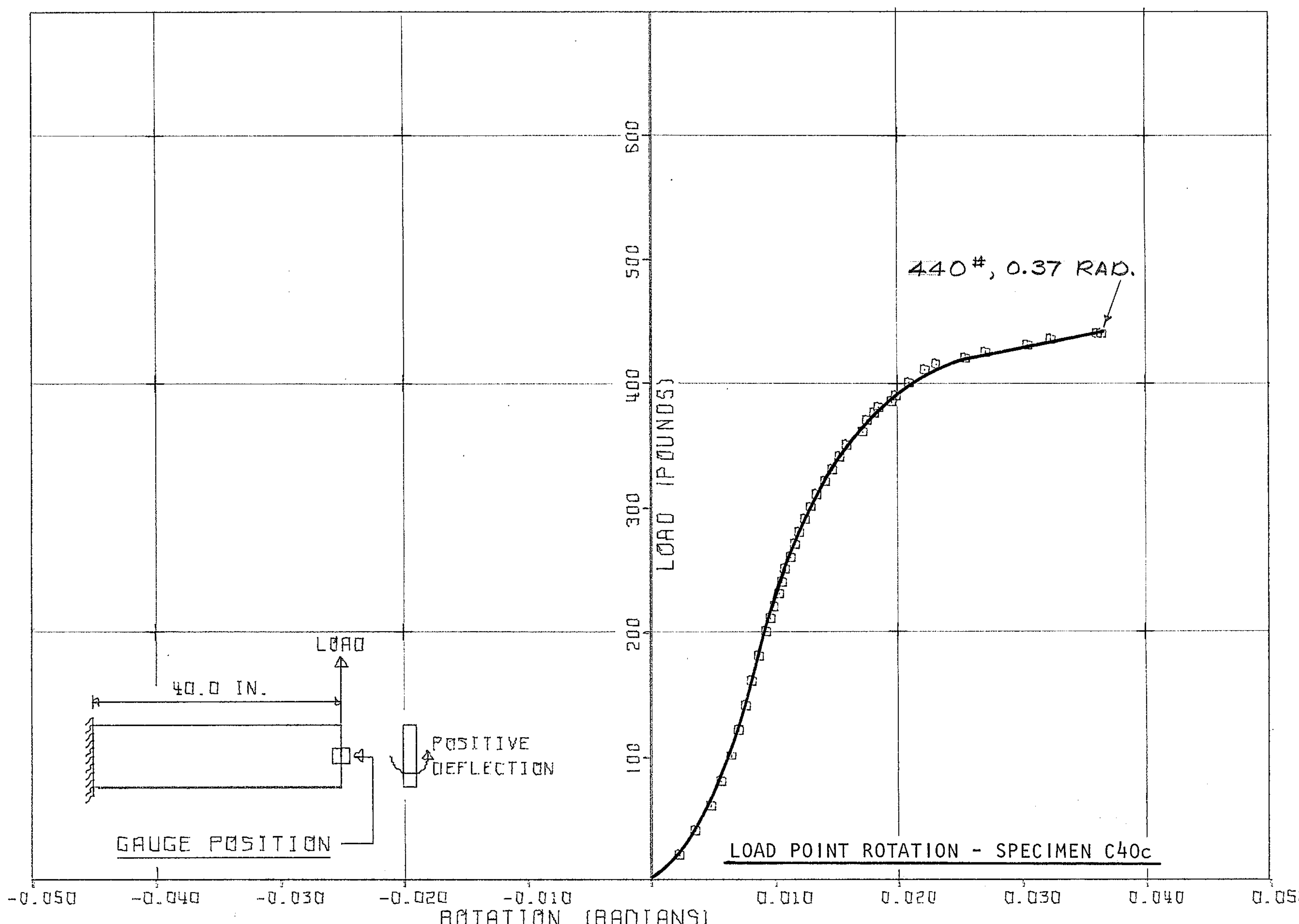
440#, 0.37 RAD.
LOAD (POUNDS)
100
200
300
400
500
600
-0.050
-0.040
-0.030
-0.020
-0.010
0.010
0.020
0.030
0.040
0.050
ROTATION (RADIANS)
LOAD
40.0 IN.
POSITIVE
DEFLECTION
GAUGE POSITION
LOAD POINT ROTATION - SPECIMEN C40c

FIGURE A.34

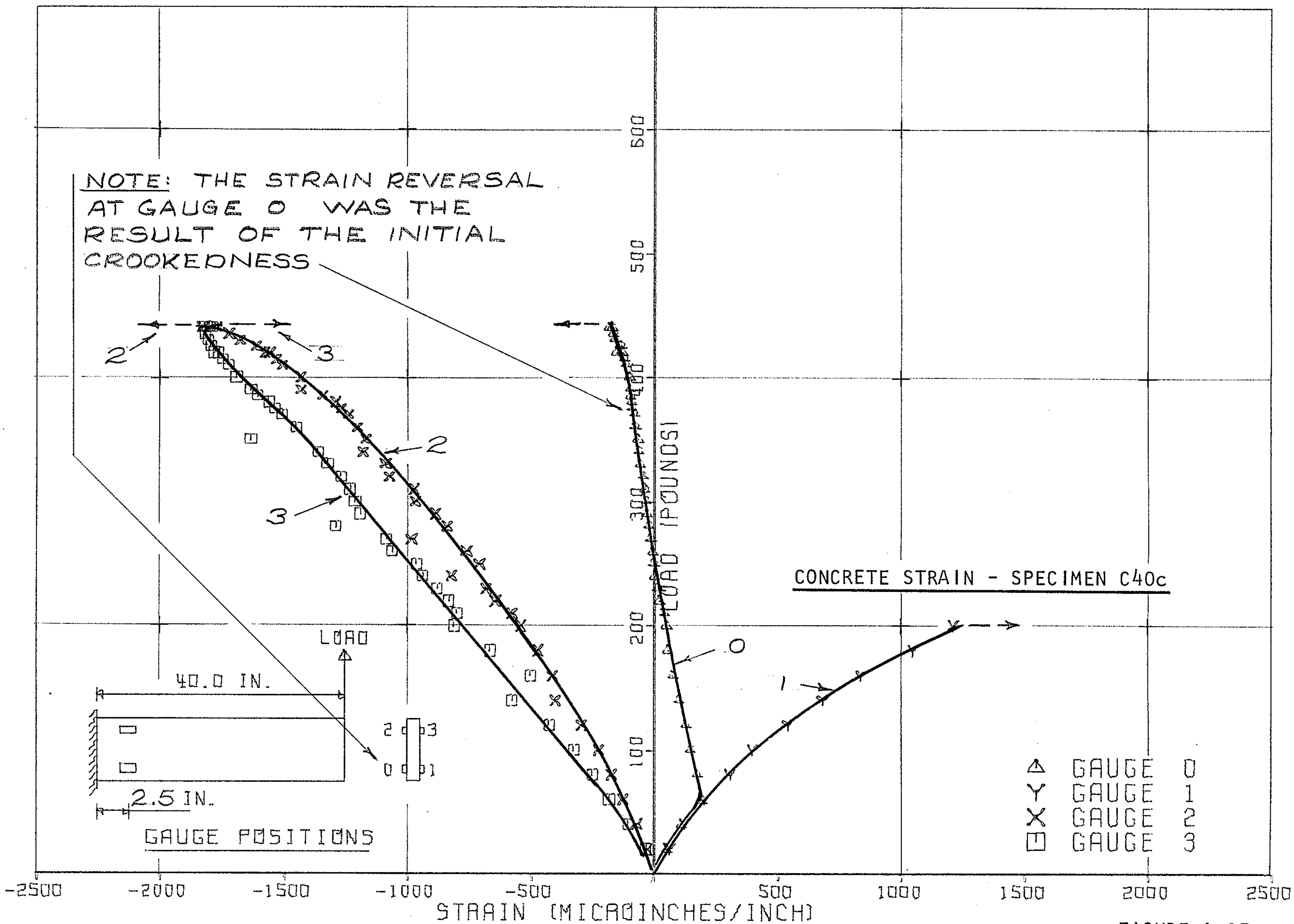
NOTE: THE STRAIN REVERSAL AT GAUGE O WAS THE RESULT OF THE INITIAL CROOKEDNESS
CONCRETE STRAIN - SPECIMEN C40c
LOAD (POUNDS)
STRAIN (MICROINCHES/INCH)
-2500
-2000
-1500
-1000
-500
500
1000
1500
2000
2500
100
200
300
400
500
600
GAUGE 0
GAUGE 1
GAUGE 2
GAUGE 3
LOAD
40.0 IN.
2.5 IN.
GAUGE POSITIONS
0
1
2
3

FIGURE A.35

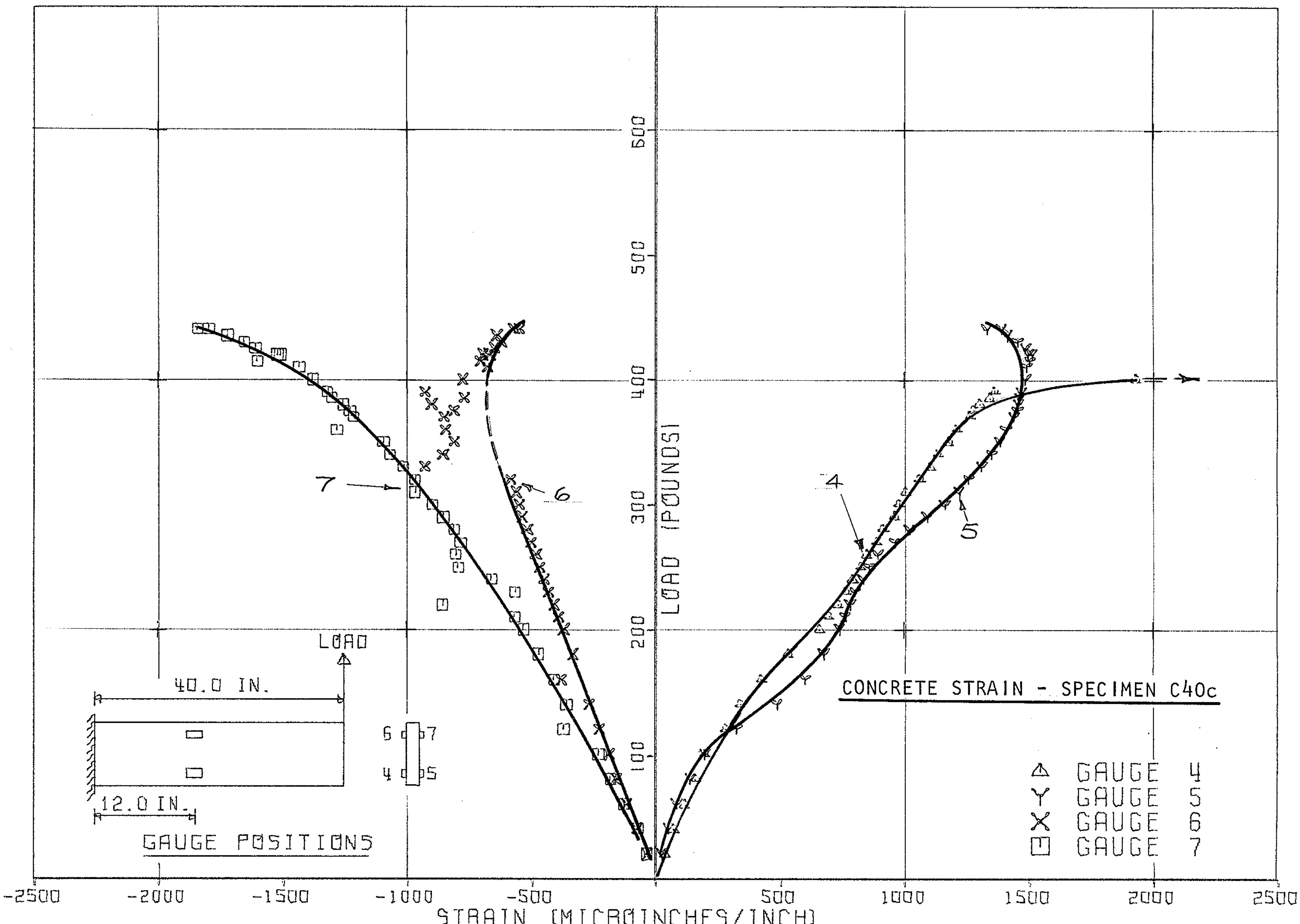
CONCRETE STRAIN - SPECIMEN C40c
GAUGE 4
GAUGE 5
GAUGE 6
GAUGE 7
LOAD (POUNDS)
STRAIN (MICROINCHES/INCH)
100
200
300
400
500
600
-2500
-2000
-1500
-1000
-500
500
1000
1500
2000
2500
4
5
6
7
LOAD
40.0 IN.
12.0 IN.
GAUGE POSITIONS
6
7
4
5

FIGURE A.36

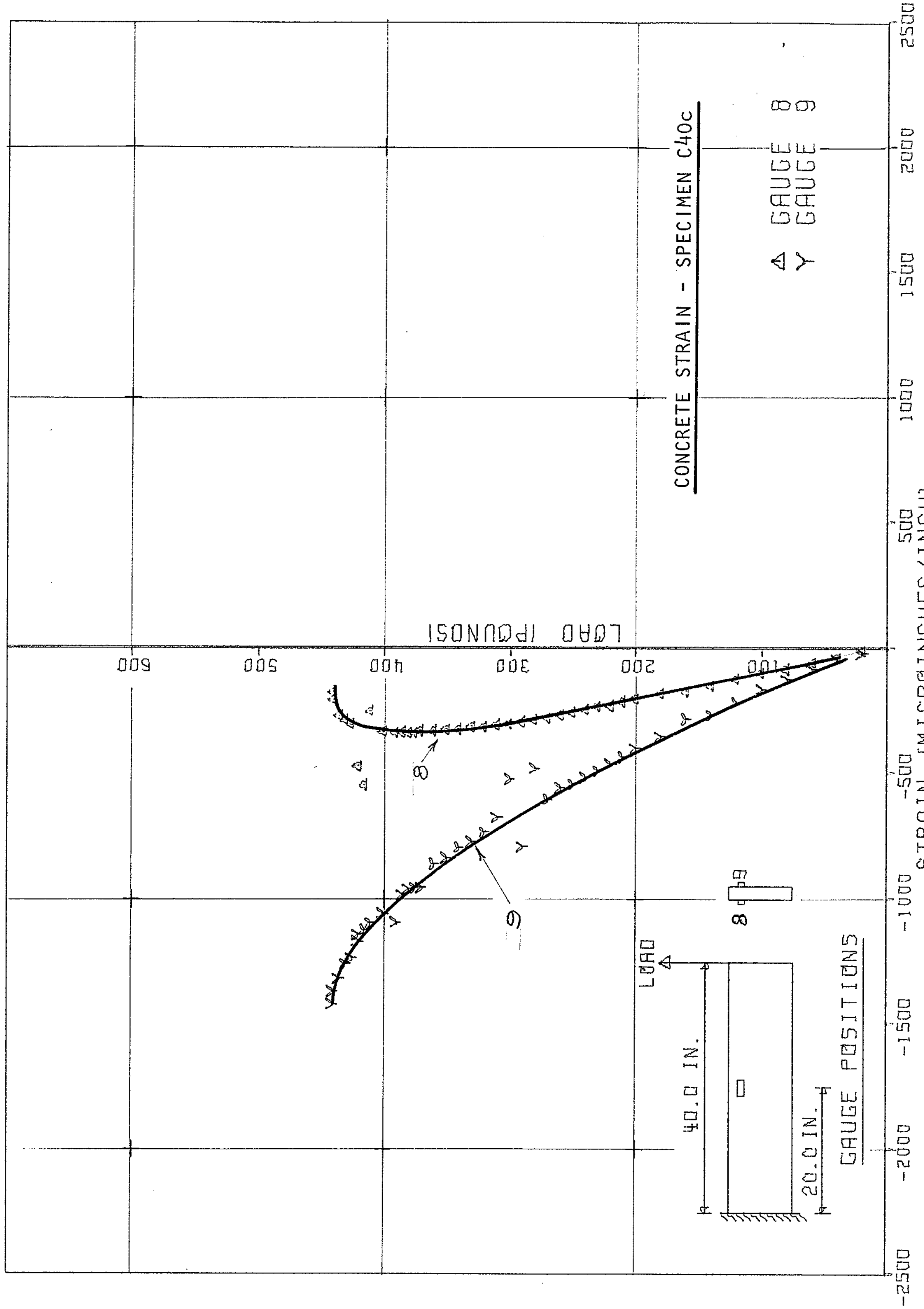
CONCRETE STRAIN - SPECIMEN C40c
Δ GAUGE 8
Y GAUGE 9
LOAD (POUNDS)
100
200
300
400
500
600
STRAIN (MICROINCHES/INCH)
-2500
-2000
-1500
-1000
-500
500
1000
1500
2000
2500
8
9
LOAD
40.0 IN.
20.0 IN.
GAUGE POSITIONS

FIGURE A.37

Specimen C36c

Concrete Cast April 9, 1970

Beam Tested May 20, 1970

Concrete Compressive Tests   Age = 41 days

Cylinder	1 (3" x 6")	5900 psi
	2	6050
	3	5650
Average	f_c' =	5850 psi

Concrete Tensile Tests   Age = 41 days

(Split Cylinder Test)

Cylinder	4 (3" x 6")	596 psi
	5	585
	6	534
Average		572 psi

Tensile Reinforcement - 6 #11 high strength wires

Compressive Reinforcement - 2 #14 wires preloaded to 60 ksi

Beam Length   36 inches

Failure Load   585 pounds

The failure was the result of lateral instability, with the load point deflecting in the positive X direction and rotating positive about the Z axis, as shown on Figure A.32. Two main cracks formed, the first running from Z = 1 at the top to Z = 10 at the bottom with tension on the positive X face. The second crack was vertical at Z = 11 with tension on the negative X face.

The load-deflection curves are shown on Figure A.39 to A.41 and the load-strain curves are shown on Figure A.42 to A.44. Note that the numbering of the strain gauges is reversed from that used on the remainder of the specimens. In this case, the even numbers were on the positive X face.

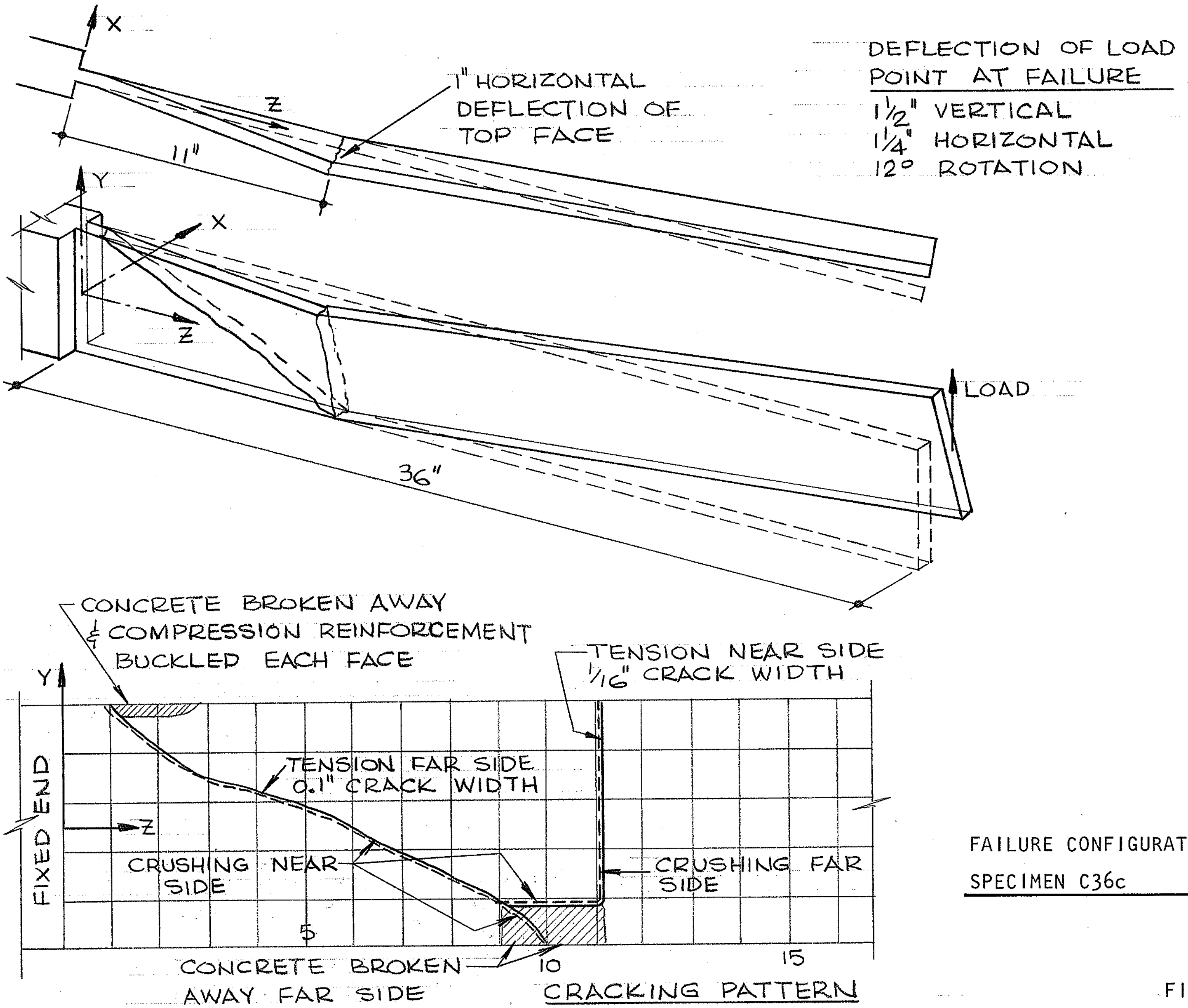

FAILURE CONFIGURATION - SPECIMEN C36c

FIGURE A.38

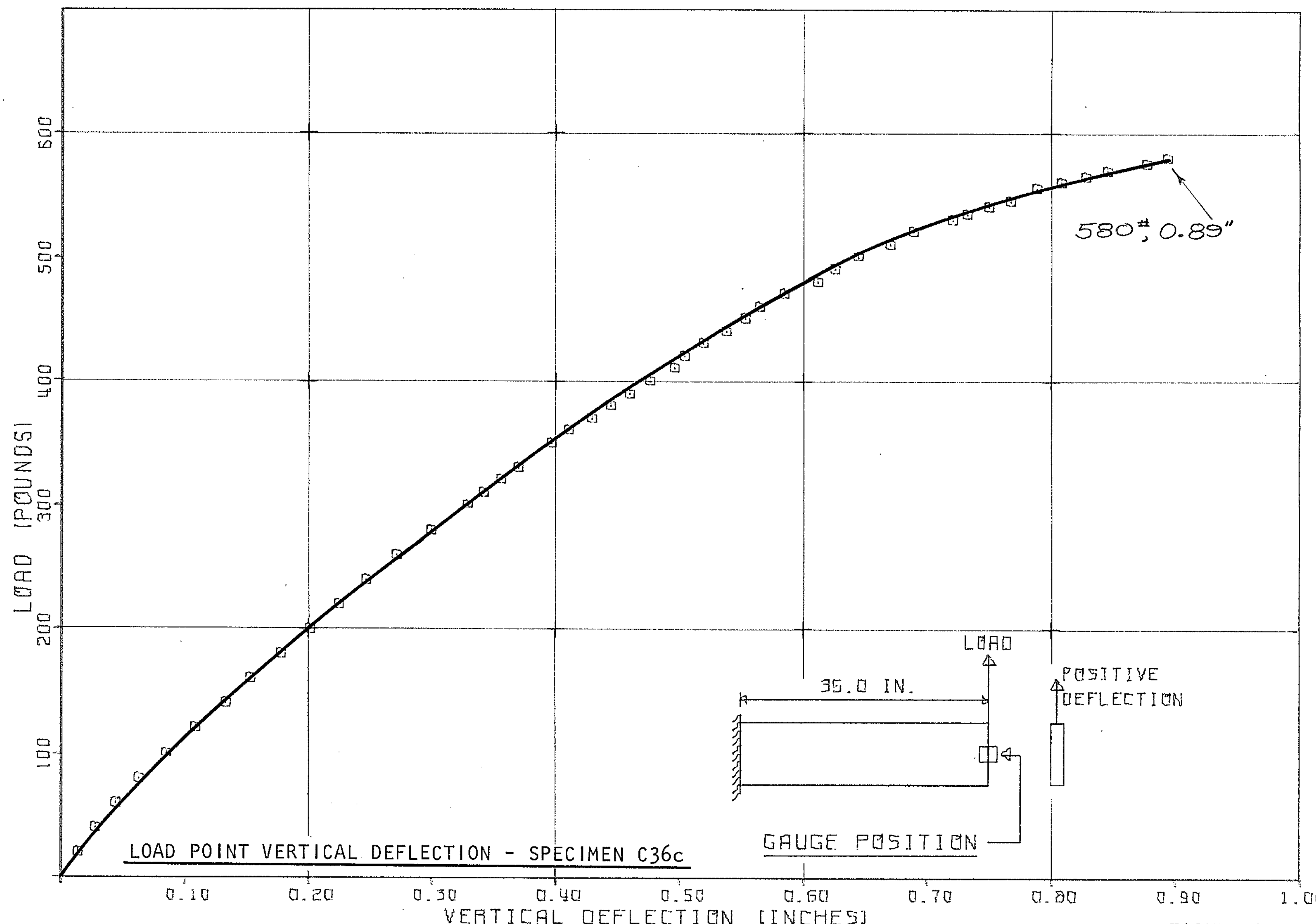
580#, 0.89"
LOAD
35.0 IN.
POSITIVE DEFLECTION
GAUGE POSITION
LOAD POINT VERTICAL DEFLECTION - SPECIMEN C36c
LOAD (POUNDS)
100
200
300
400
500
600
0.10
0.20
0.30
0.40
0.50
0.60
0.70
0.80
0.90
1.00
VERTICAL DEFLECTION (INCHES)

FIGURE A.39

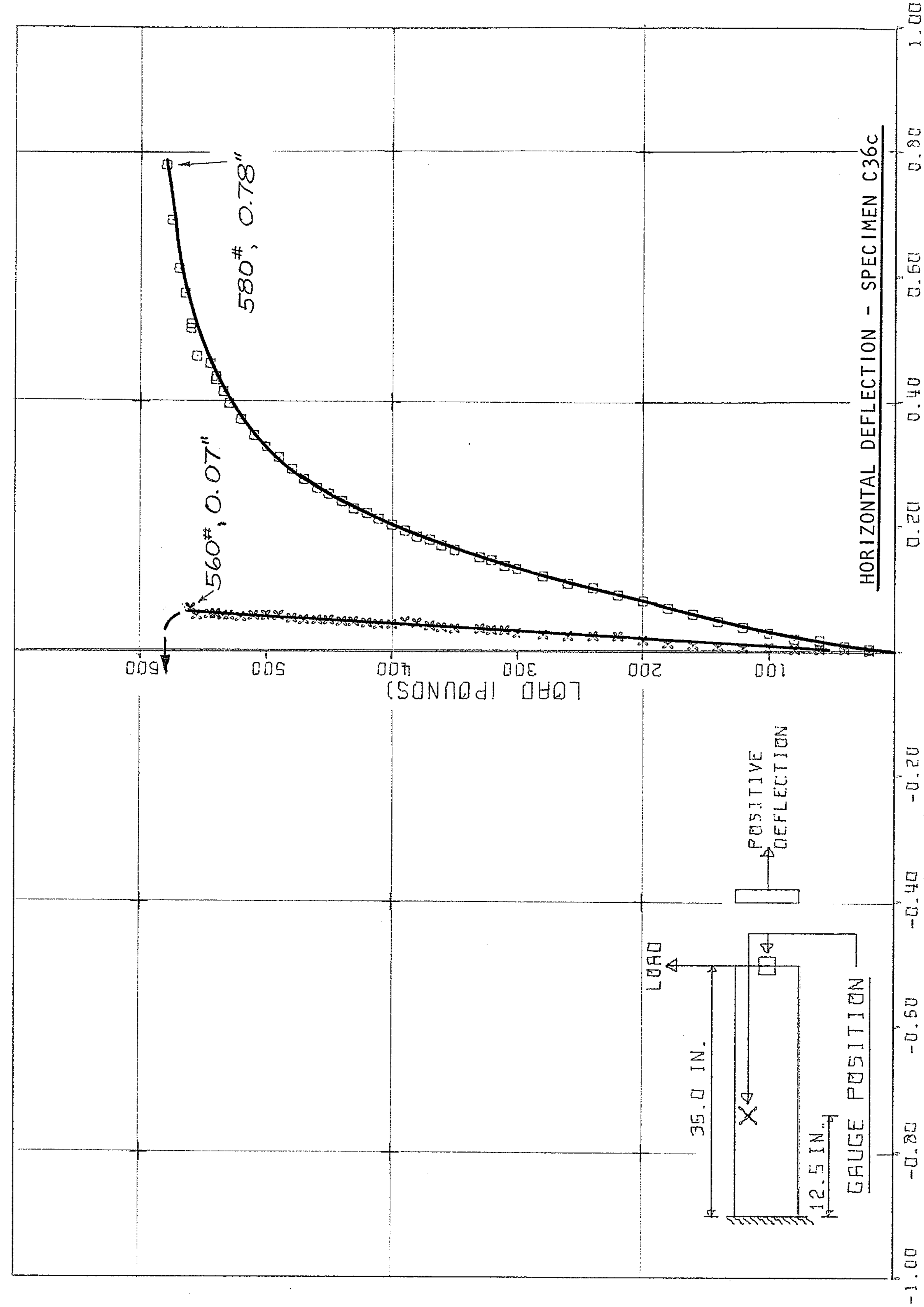
HORIZONTAL DEFLECTION - SPECIMEN C36c
LOAD (POUNDS)
HORIZONTAL DEFLECTION (INCHES)
580#, 0.78"
560#, 0.07"
POSITIVE DEFLECTION
LOAD
35.0 IN.
12.5 IN.
GAUGE POSITION
100
200
300
400
500
600
-1.00
-0.80
-0.60
-0.40
-0.20
0.20
0.40
0.60
0.80
1.00

FIGURE A.40

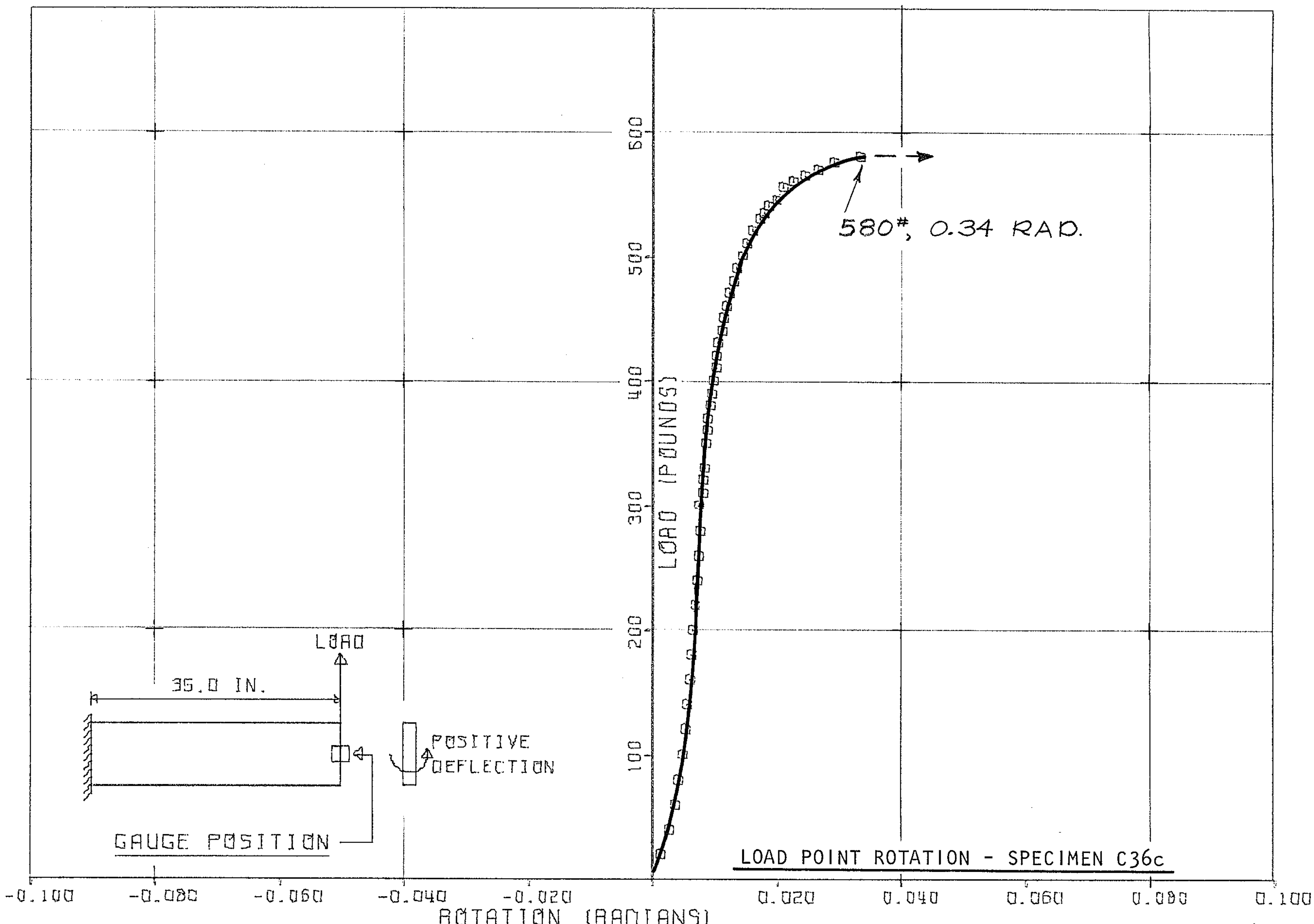
580#, 0.34 RAD.
LOAD (POUNDS)
100
200
300
400
500
600
ROTATION (RADIANS)
-0.100
-0.080
-0.060
-0.040
-0.020
0.020
0.040
0.060
0.080
0.100
LOAD
35.0 IN.
POSITIVE DEFLECTION
GAUGE POSITION
LOAD POINT ROTATION - SPECIMEN C36c

FIGURE A.41

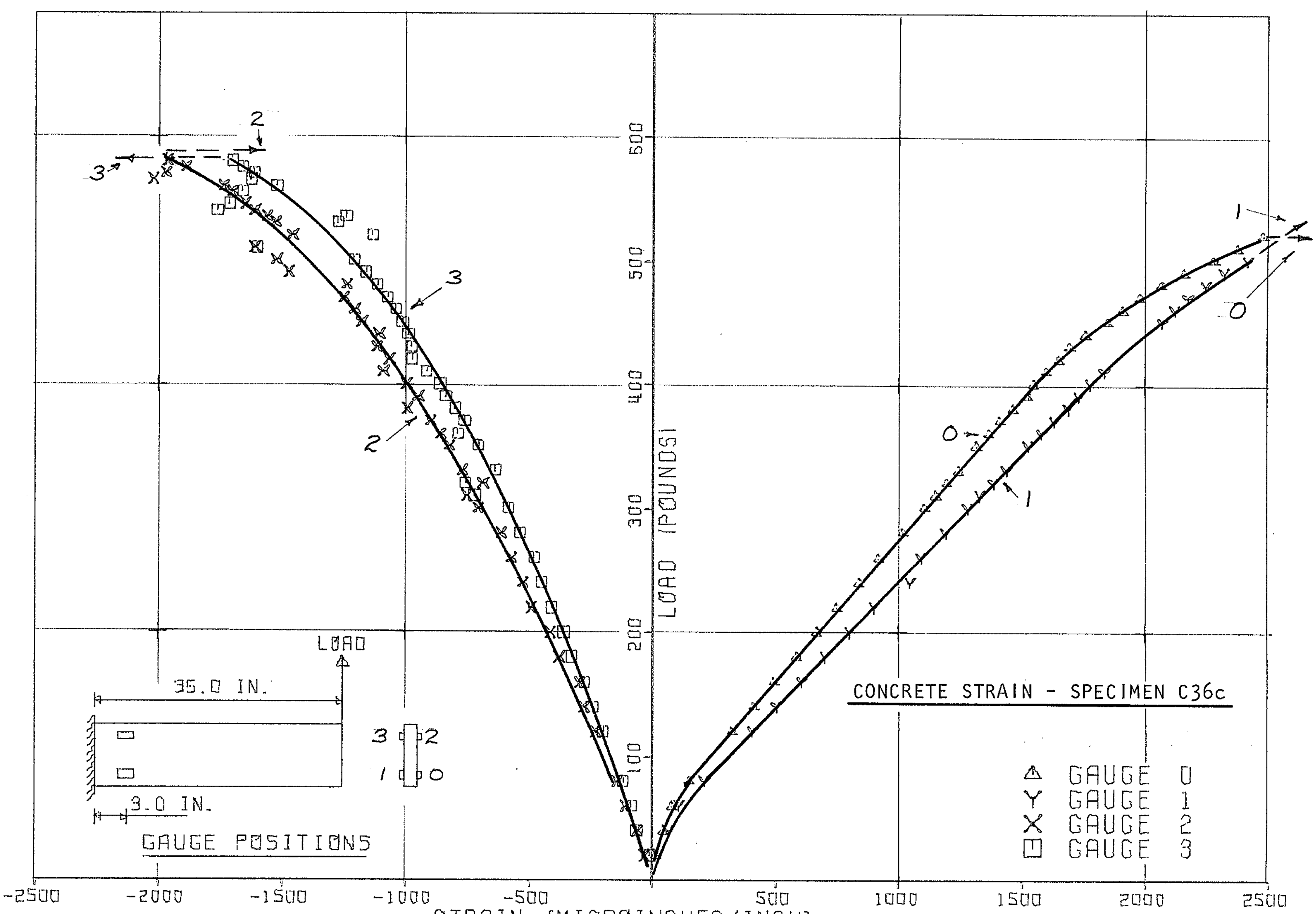
CONCRETE STRAIN - SPECIMEN C36c
LOAD (POUNDS)
STRAIN (MICROINCHES/INCH)
GAUGE 0
GAUGE 1
GAUGE 2
GAUGE 3
GAUGE POSITIONS
35.0 IN.
3.0 IN.
LOAD

FIGURE A.42

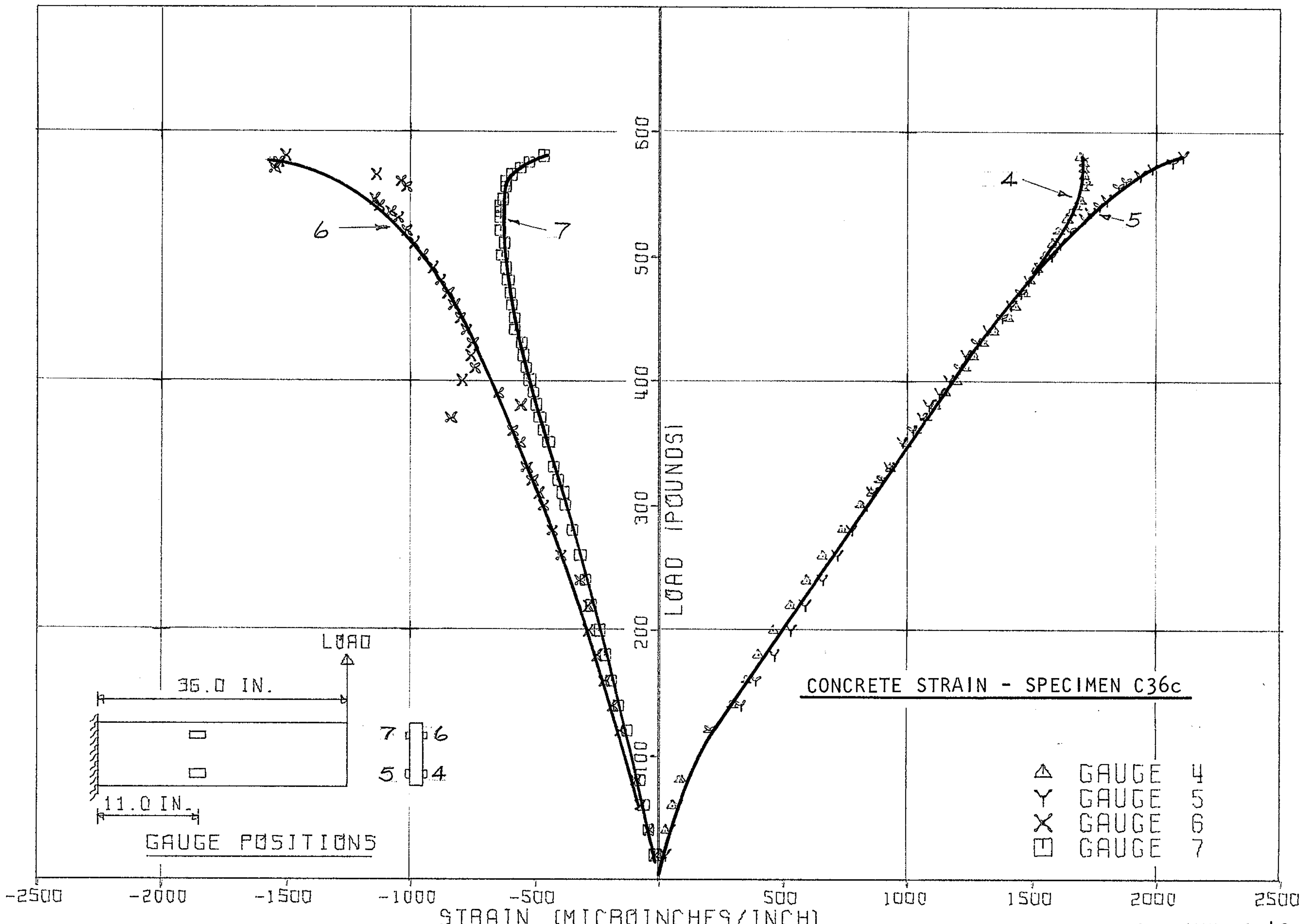

SPECIMEN A.43

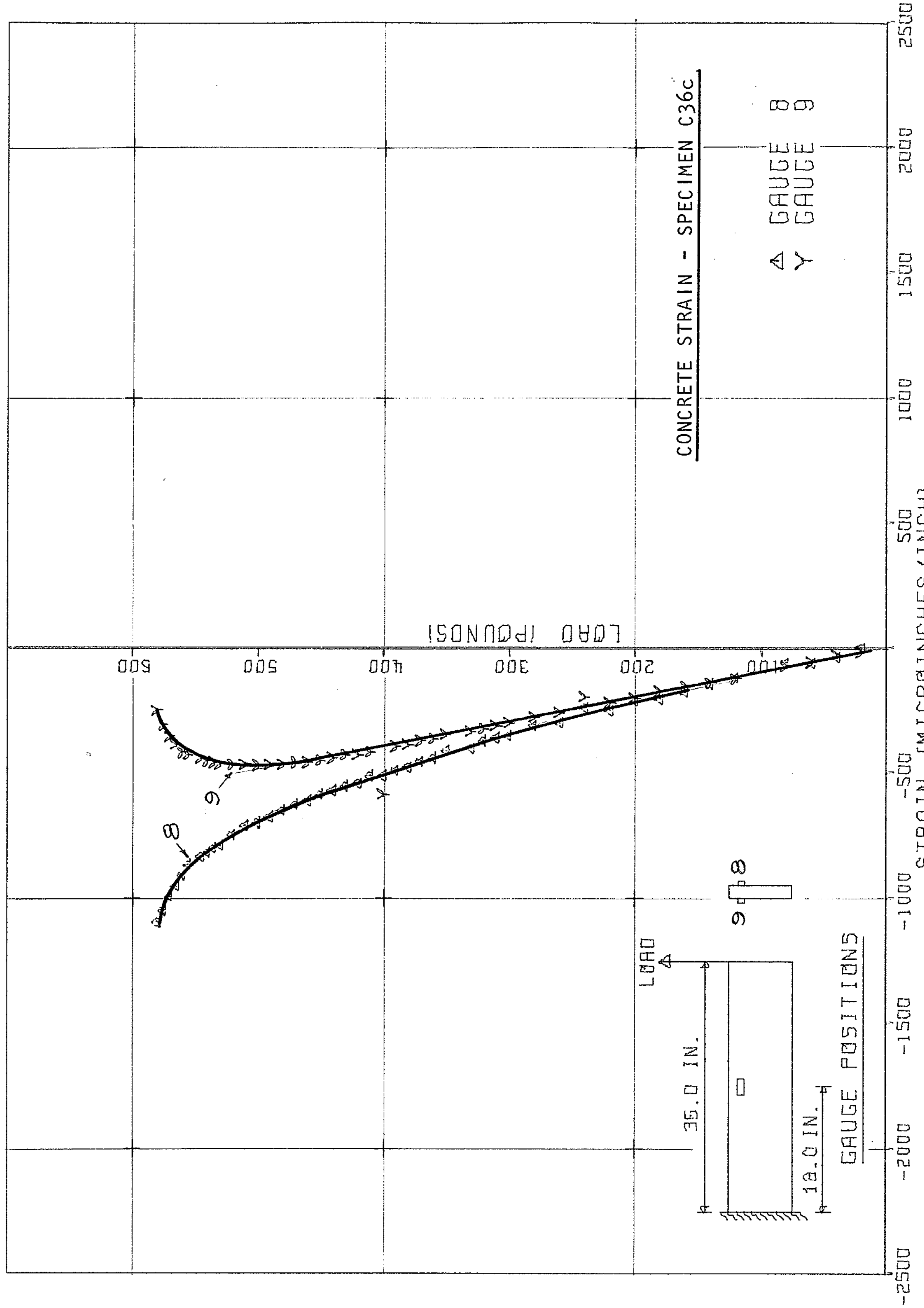
CONCRETE STRAIN - SPECIMEN C36c
△ GAUGE 8
Y GAUGE 9
LOAD (POUNDS)
100
200
300
400
500
600
STRAIN (MICROINCHES/INCH)
-2500
-2000
-1500
-1000
-500
500
1000
1500
2000
2500
8
9
LOAD
35.0 IN.
19.0 IN.
GAUGE POSITIONS

FIGURE A.44

Specimen C32c

Concrete Cast June 1, 1970

Beam Tested July 14, 1970

Concrete Compressive Tests   Age = 43 days

Cylinder	1 (3" x 6")	5000 psi
	2	4400
	3	5100
	4	4400
	5	4450
	6	4590
Average		f'_c = 4660 psi

Tensile Reinforcement - 6 #11 high strength wires

Compressive Reinforcement - 2 #14 wires preloaded to 60 ksi

Beam Length 32 inches

Failure Load 590 pounds

The failure was flexural, with crushing of the concrete occurring near the fixed end as shown on Figure A.45. Portions of the concrete were broken away from each side for the top three inches and the compressive reinforcement buckled. Since the specimen was over-reinforced, the failure was as expected.

The load-deflection curves are shown on Figures A.46 to A.48 and the load-strain curves are shown on Figures A.49 to A.51.

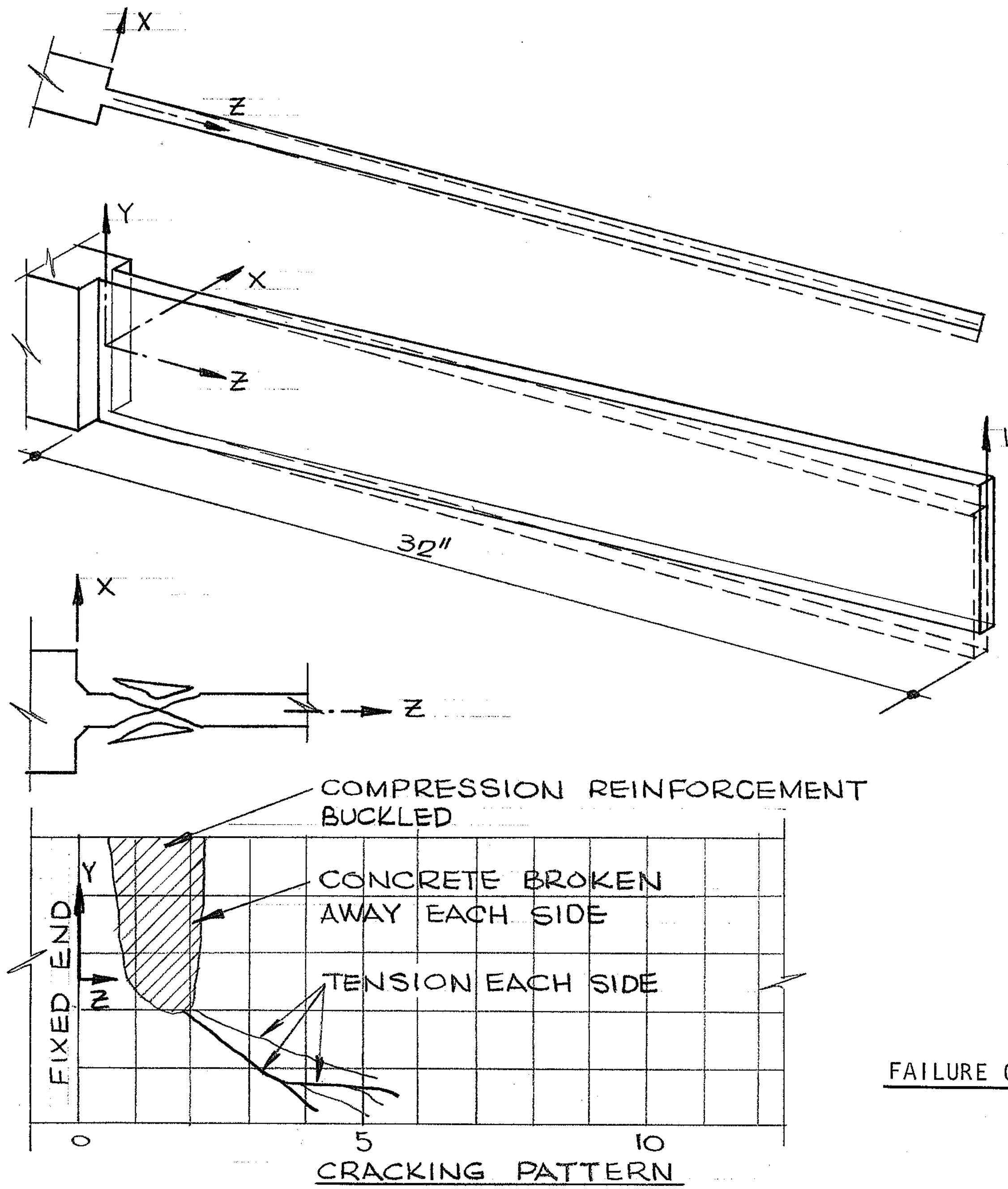

DEFLECTION OF LOAD POINT AT FAILURE

1½" VERTICAL
NIL HORIZONTAL
NIL ROTATION

FAILURE CONFIGURATION - SPECIMEN C32c

FIGURE A.45

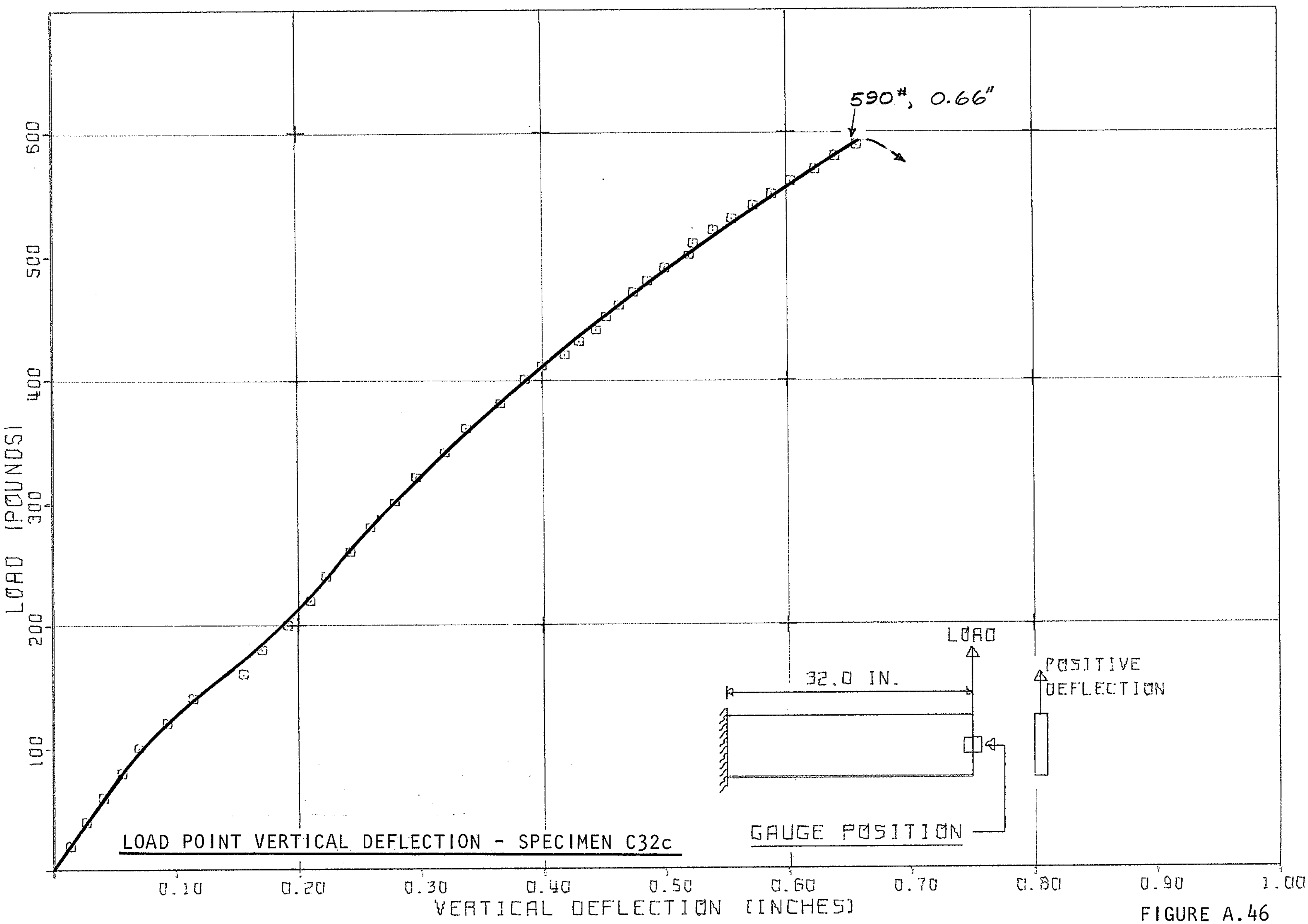
590#, 0.66"
LOAD POINT VERTICAL DEFLECTION - SPECIMEN C32c
LOAD
POSITIVE DEFLECTION
32.0 IN.
GAUGE POSITION
LOAD (POUNDS)
100
200
300
400
500
600
0.10
0.20
0.30
0.40
0.50
0.60
0.70
0.80
0.90
1.00
VERTICAL DEFLECTION (INCHES)

FIGURE A.46

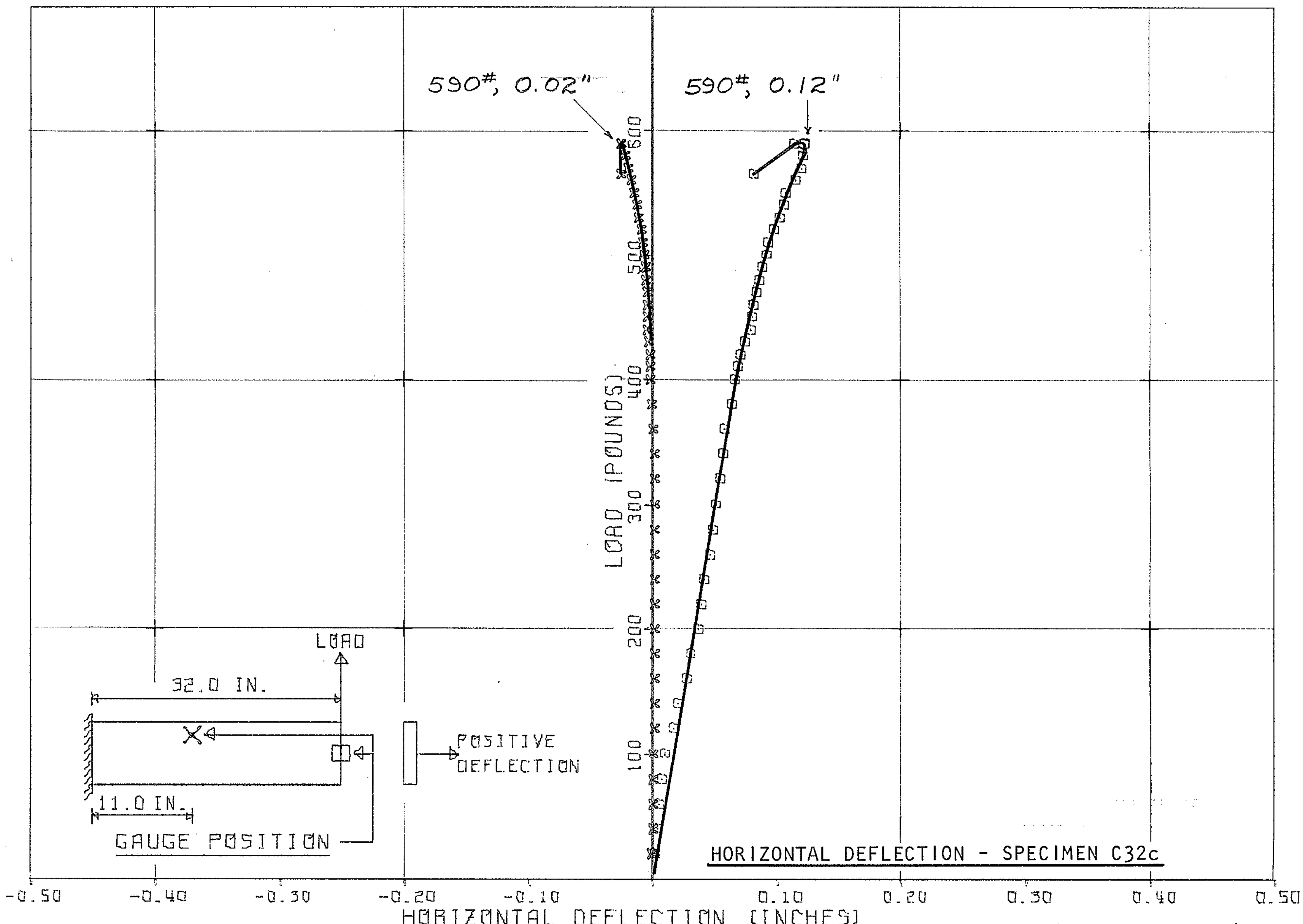
590#, 0.02"
590#, 0.12"
LOAD (POUNDS)
100
200
300
400
500
600
LOAD
32.0 IN.
11.0 IN.
GAUGE POSITION
POSITIVE
DEFLECTION
HORIZONTAL DEFLECTION - SPECIMEN C32c
-0.50
-0.40
-0.30
-0.20
-0.10
0.10
0.20
0.30
0.40
0.50
HORIZONTAL DEFLECTION (INCHES)

FIGURE A.47

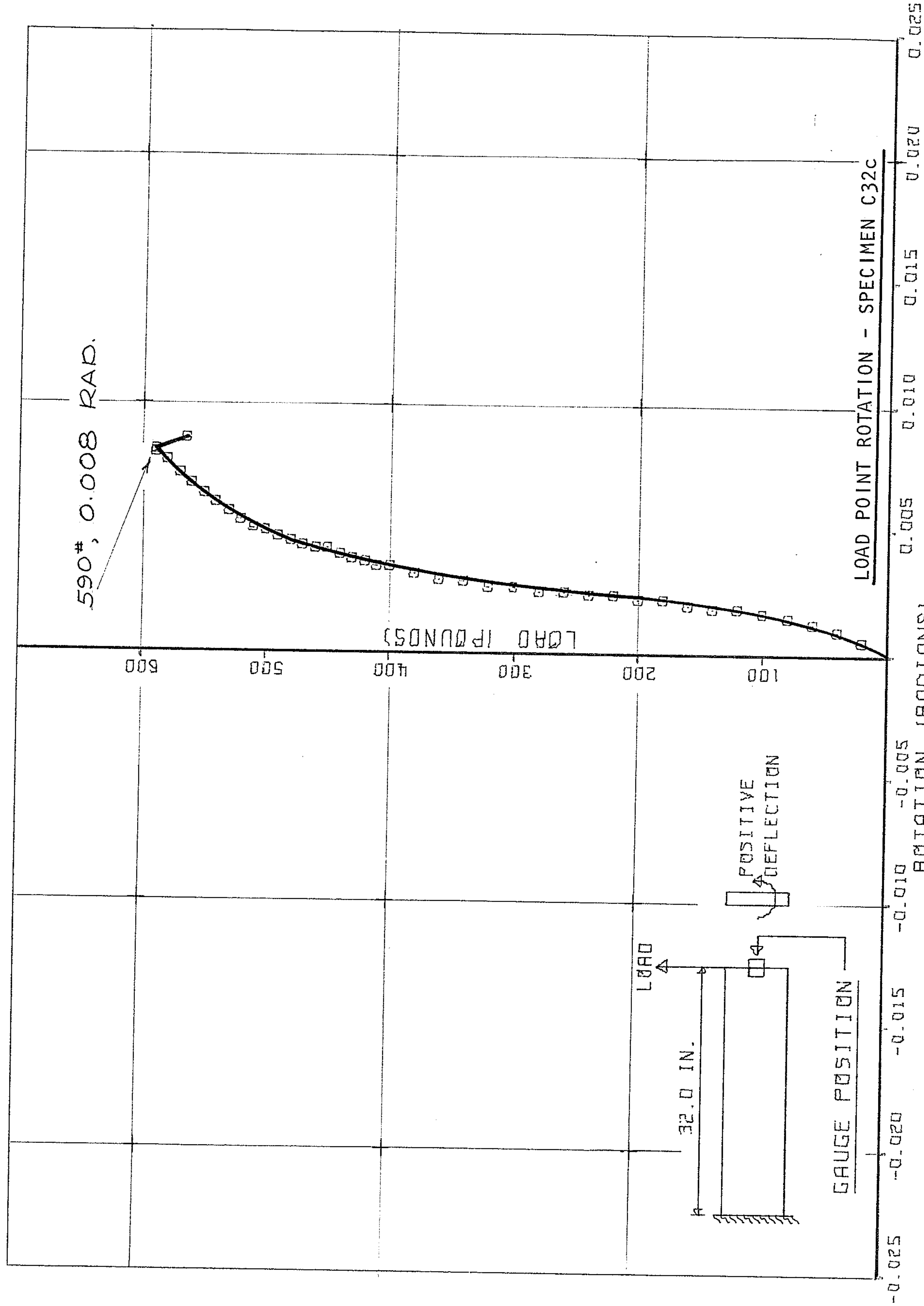
LOAD POINT ROTATION - SPECIMEN C32c
590#, 0.008 RAD.
LOAD (POUNDS)
100
200
300
400
500
600
ROTATION (RADIANS)
-0.025
-0.020
-0.015
-0.010
-0.005
0.005
0.010
0.015
0.020
0.025
POSITIVE DEFLECTION
LOAD
32.0 IN.
GAUGE POSITION

FIGURE A.48

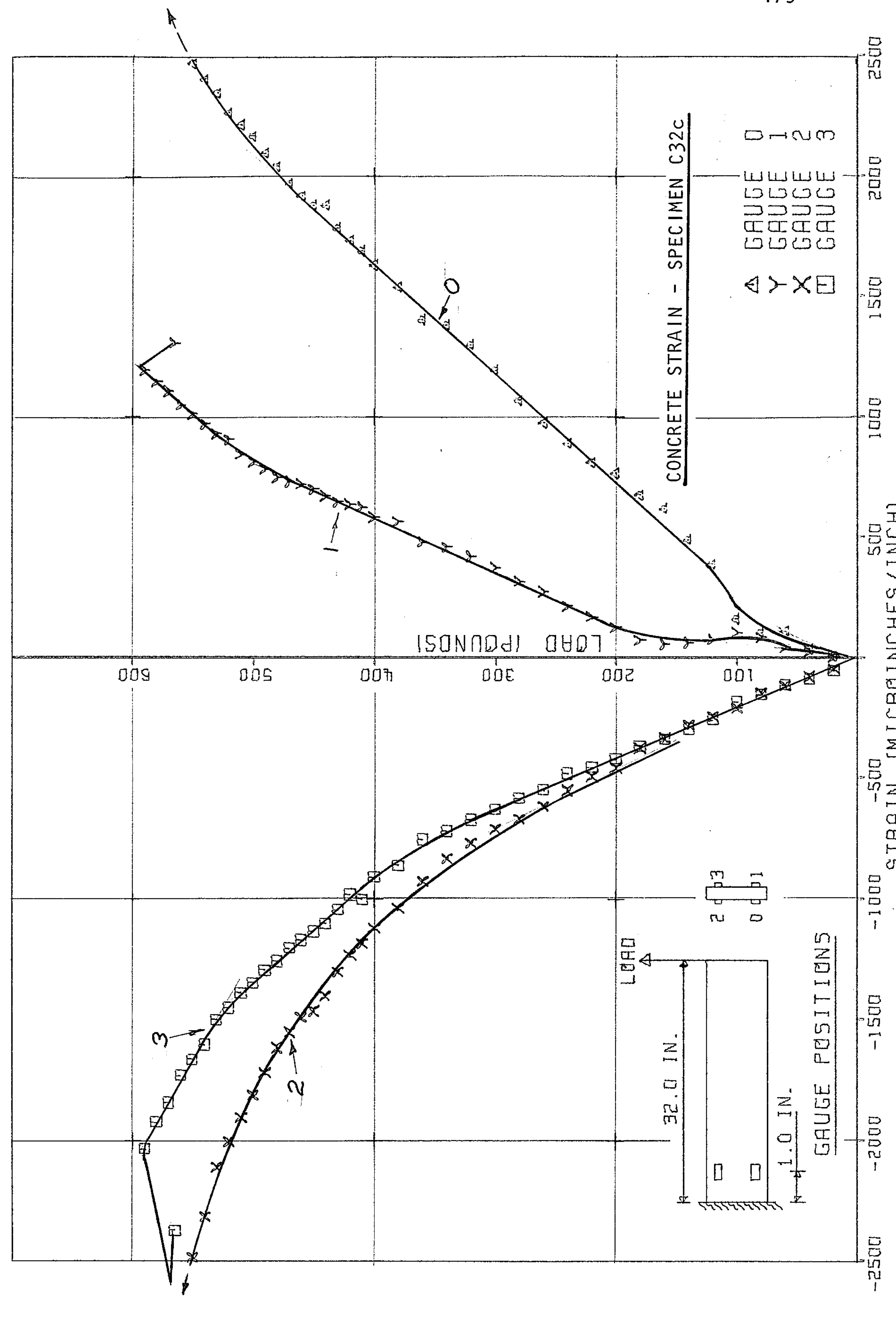
CONCRETE STRAIN - SPECIMEN C32c
GAUGE 0
GAUGE 1
GAUGE 2
GAUGE 3
LOAD (POUNDS)
STRAIN (MICROINCHES/INCH)
LOAD
32.0 IN.
1.0 IN.
GAUGE POSITIONS

FIGURE A.49

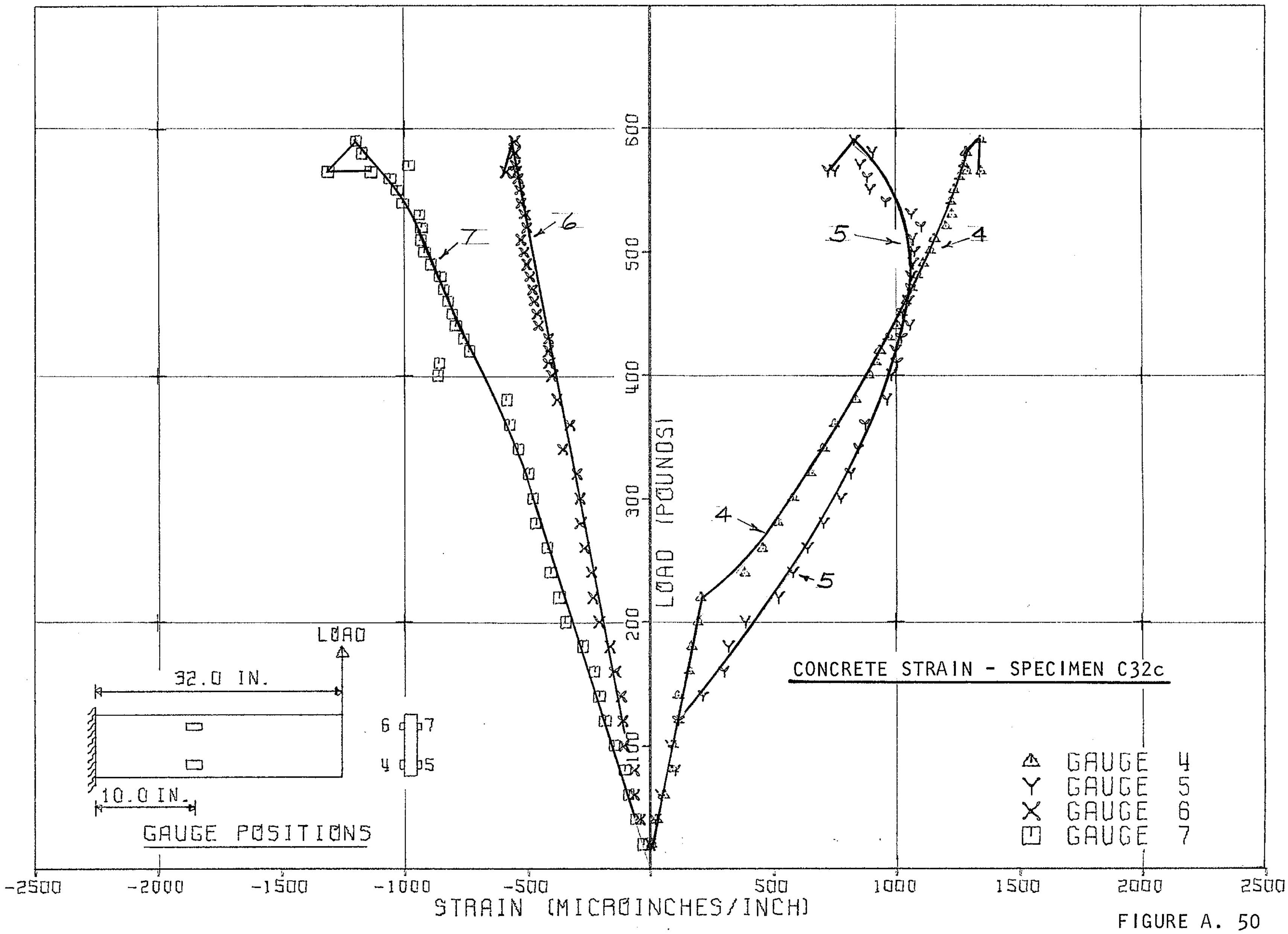
CONCRETE STRAIN - SPECIMEN C32c
LOAD (POUNDS)
100
200
300
400
500
600
STRAIN (MICROINCHES/INCH)
-2500
-2000
-1500
-1000
-500
500
1000
1500
2000
2500
GAUGE 4
GAUGE 5
GAUGE 6
GAUGE 7
4
5
6
7
LOAD
32.0 IN.
10.0 IN.
GAUGE POSITIONS

FIGURE A. 50

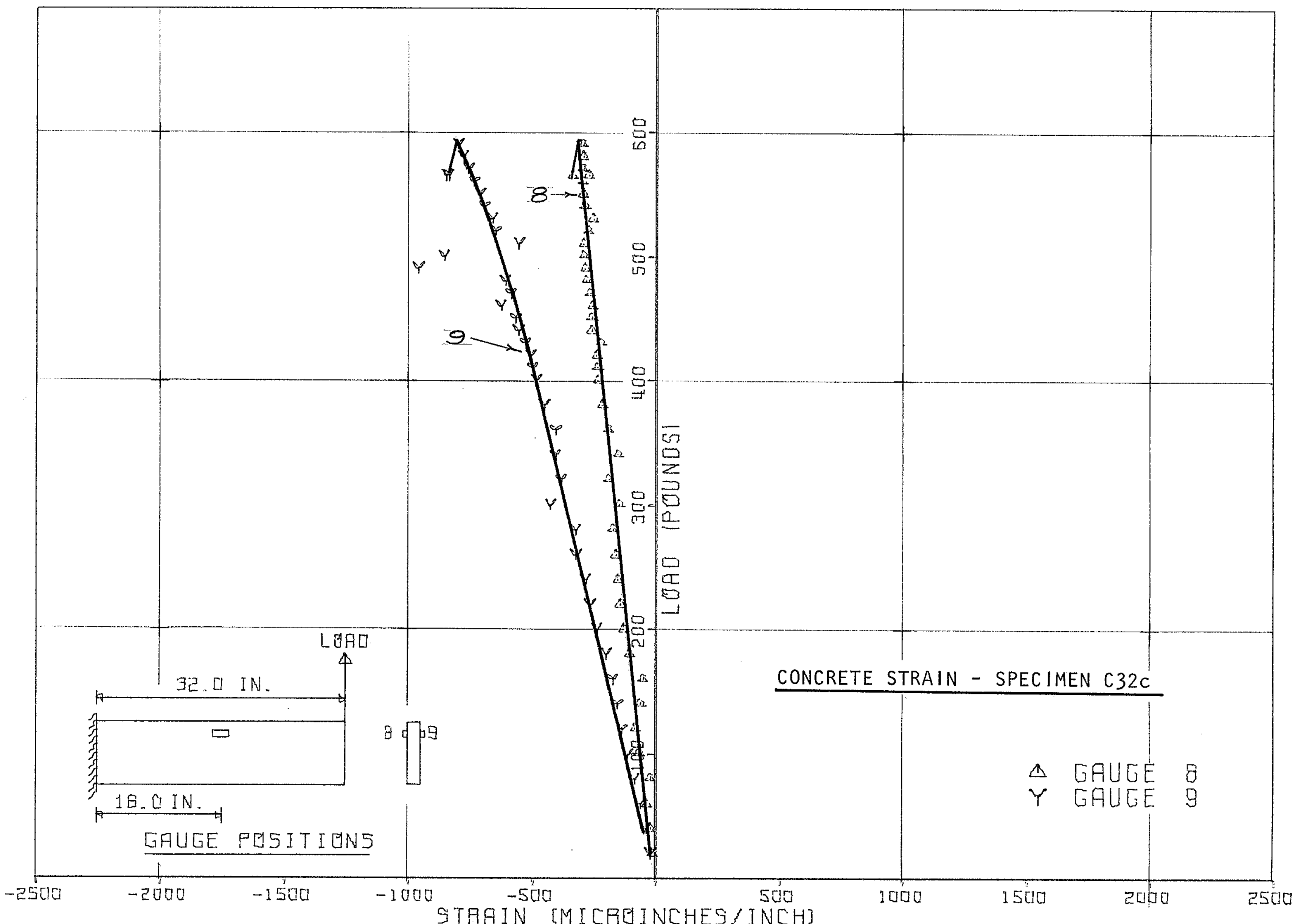
CONCRETE STRAIN - SPECIMEN C32c
GAUGE 8
GAUGE 9
LOAD (POUNDS)
100
200
300
400
500
600
STRAIN (MICROINCHES/INCH)
-2500
-2000
-1500
-1000
-500
500
1000
1500
2000
2500
8
9
LOAD
32.0 IN.
16.0 IN.
GAUGE POSITIONS

FIGURE A.51

Specimen C32d

Concrete Cast June 11, 1970

Beam Tested July 16, 1970

Concrete Compressive Tests   Age = 35 days

Cylinder 1 (3" x 6")		6950 psi
2		6660
3		7140
Average	$f_c^{'}$ =	6920 psi

Concrete Tensile Tests   Age = 35 days

(Split Cylinder Test)

Cylinder 4 (3" x 6")	648 psi
5	666
6	704
Average	673 psi

Reinforcing Wire Tensile Tests - wire deformed

Compressive Reinforcement - preloaded to 60 ksi

Wire Size	Yield Point	Ultimate Strength
#14 (0.08 inches)	63.7 ksi	67.6 ksi
#14	57.7	63.7
Average	f_y = 60.7 ksi	65.7 ksi

Tensile Reinforcement - wire cold-drawn from 1/8" M.S. wire

Wire Diameter	Yield Point	Ultimate Strength
.1175 inch	71.1 ksi	74.2 ksi
.1180	70.3	72.1
.1185	69.7	72.5

.1175	71.5	74.2
.1180	71.3	74.1
.1175	70.6	73.4
Average	f_y = 70.8 ksi	73.4 ksi

The wire diameter was measured at Z = 0 (point of maximum bending)

Beam Length 32 inches

Failure Load 615 pounds

The failure was flexural, as the result of yielding of the tensile reinforcement. Prior to failure, a major crack began at the bottom near the fixed end and progressed upward. At failure, portions of the concrete broke away on the positive X face and above the compressive reinforcement as shown on Figure A.52.

The load-deflection curves are shown on Figures A.53 to A.55 and the load-strain curves are shown on Figures A.56 to A.58.

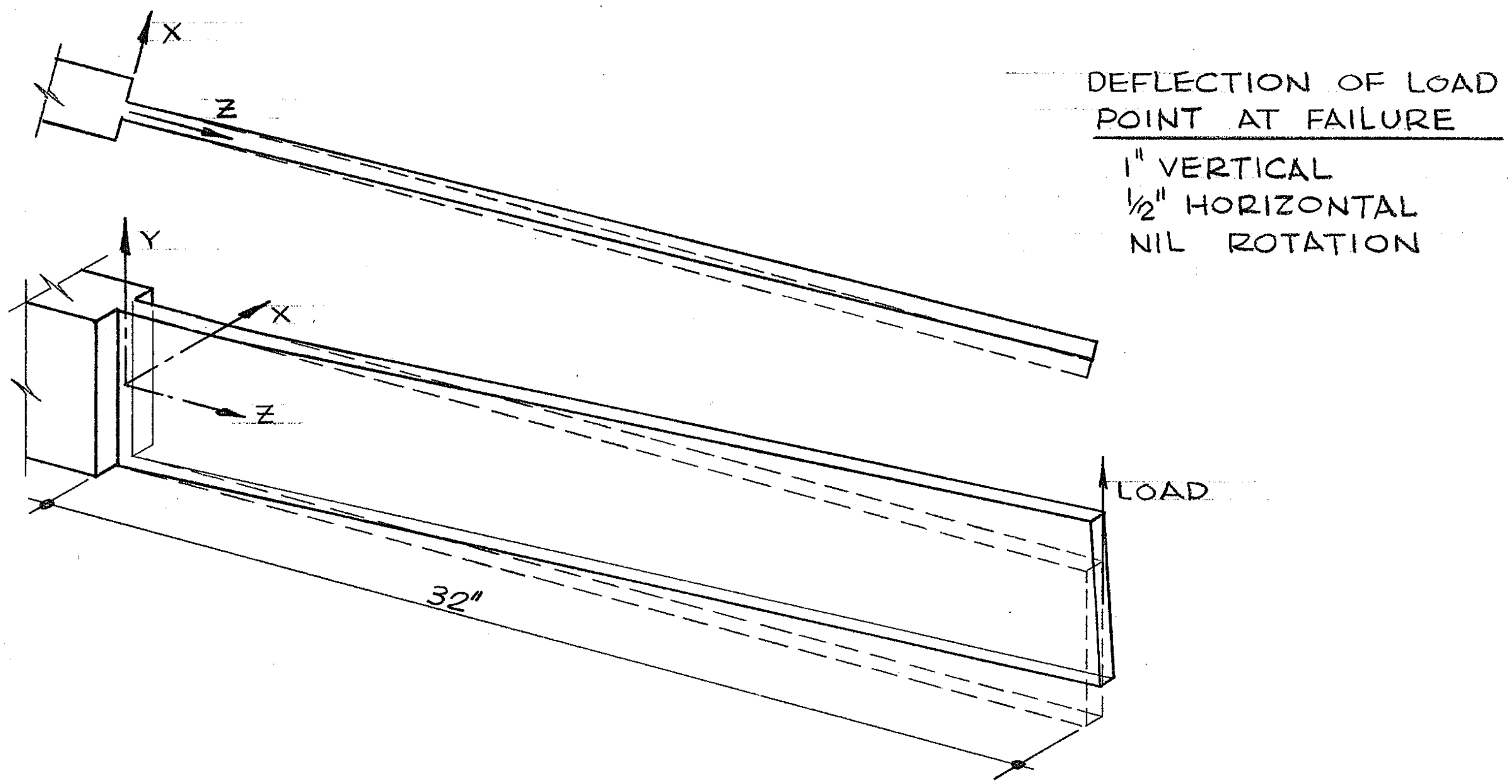

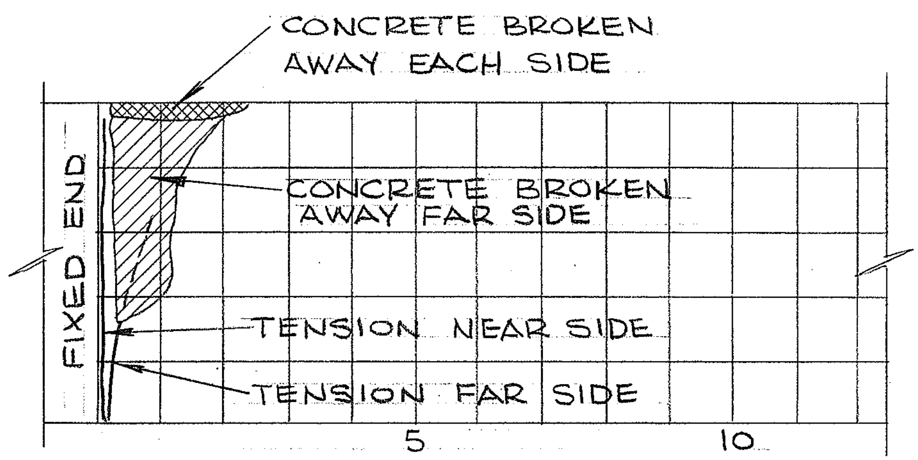

CRACKING PATTERN

FAILURE CONFIGURATION - SPECIMEN C32d

FIGURE A.52

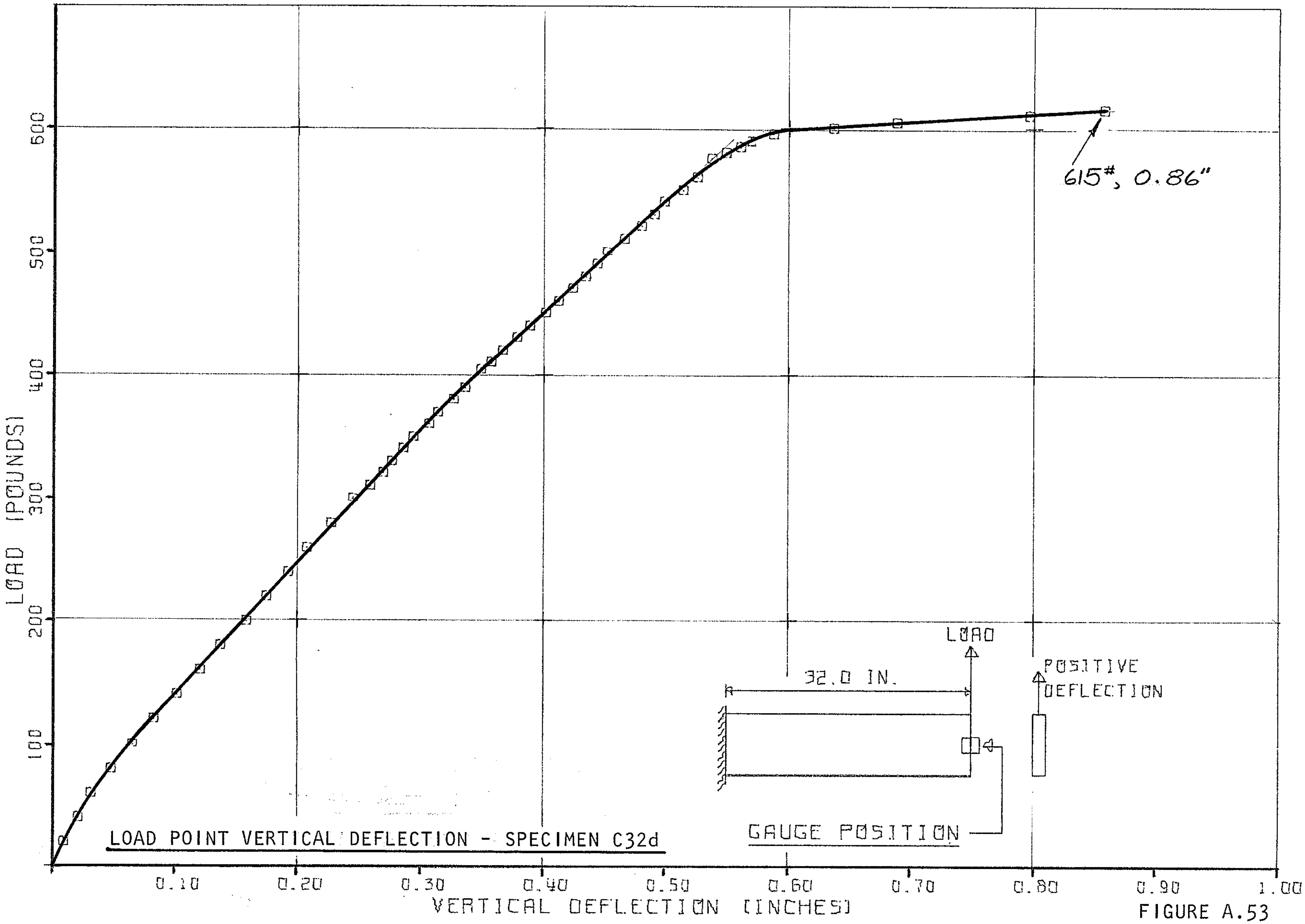
LOAD POINT VERTICAL DEFLECTION - SPECIMEN C32d
LOAD (POUNDS)
100
200
300
400
500
600
0.10
0.20
0.30
0.40
0.50
0.60
0.70
0.80
0.90
1.00
VERTICAL DEFLECTION (INCHES)
615#, 0.86"
LOAD
32.0 IN.
POSITIVE
DEFLECTION
GAUGE POSITION

FIGURE A.53

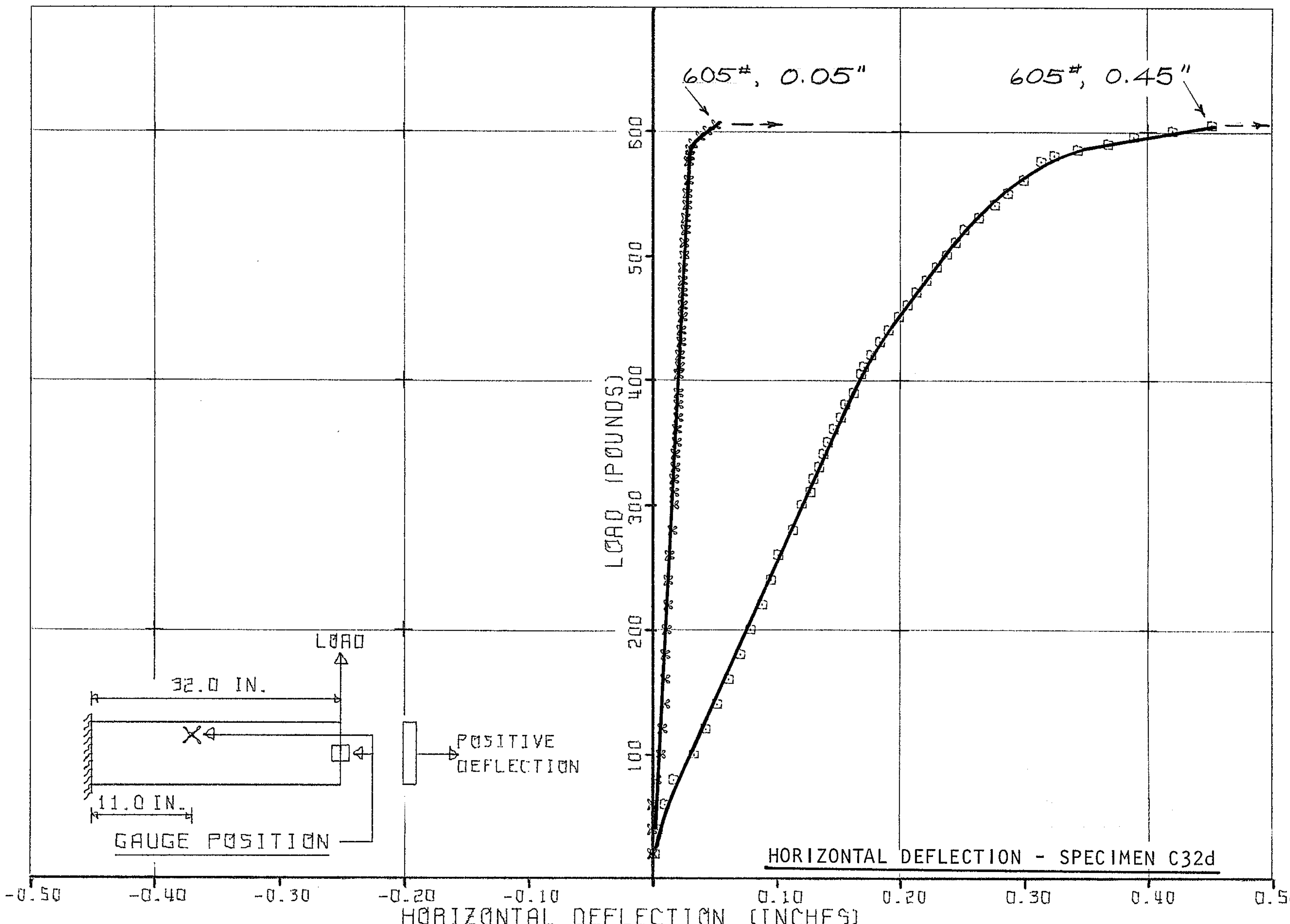
605#, 0.05"
605#, 0.45"
LOAD (POUNDS)
100
200
300
400
500
600
-0.50
-0.40
-0.30
-0.20
-0.10
0.10
0.20
0.30
0.40
0.50
HORIZONTAL DEFLECTION (INCHES)
LOAD
32.0 IN.
POSITIVE DEFLECTION
11.0 IN.
GAUGE POSITION
HORIZONTAL DEFLECTION - SPECIMEN C32d

FIGURE A.54

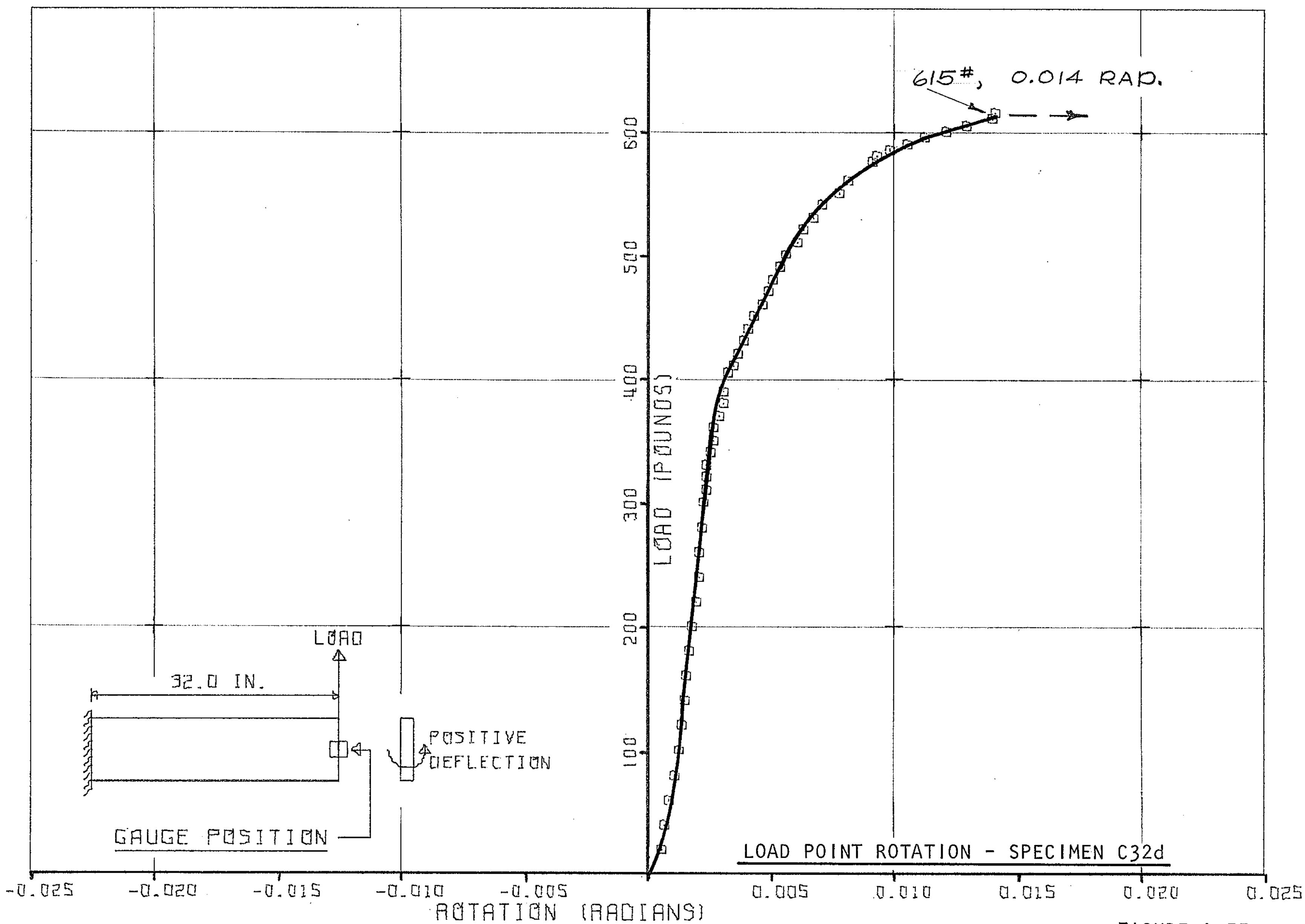
615#, 0.014 RAD.
LOAD (POUNDS)
100
200
300
400
500
600
-0.025
-0.020
-0.015
-0.010
-0.005
0.005
0.010
0.015
0.020
0.025
ROTATION (RADIANS)
LOAD
32.0 IN.
POSITIVE
DEFLECTION
GAUGE POSITION
LOAD POINT ROTATION - SPECIMEN C32d

FIGURE A.55

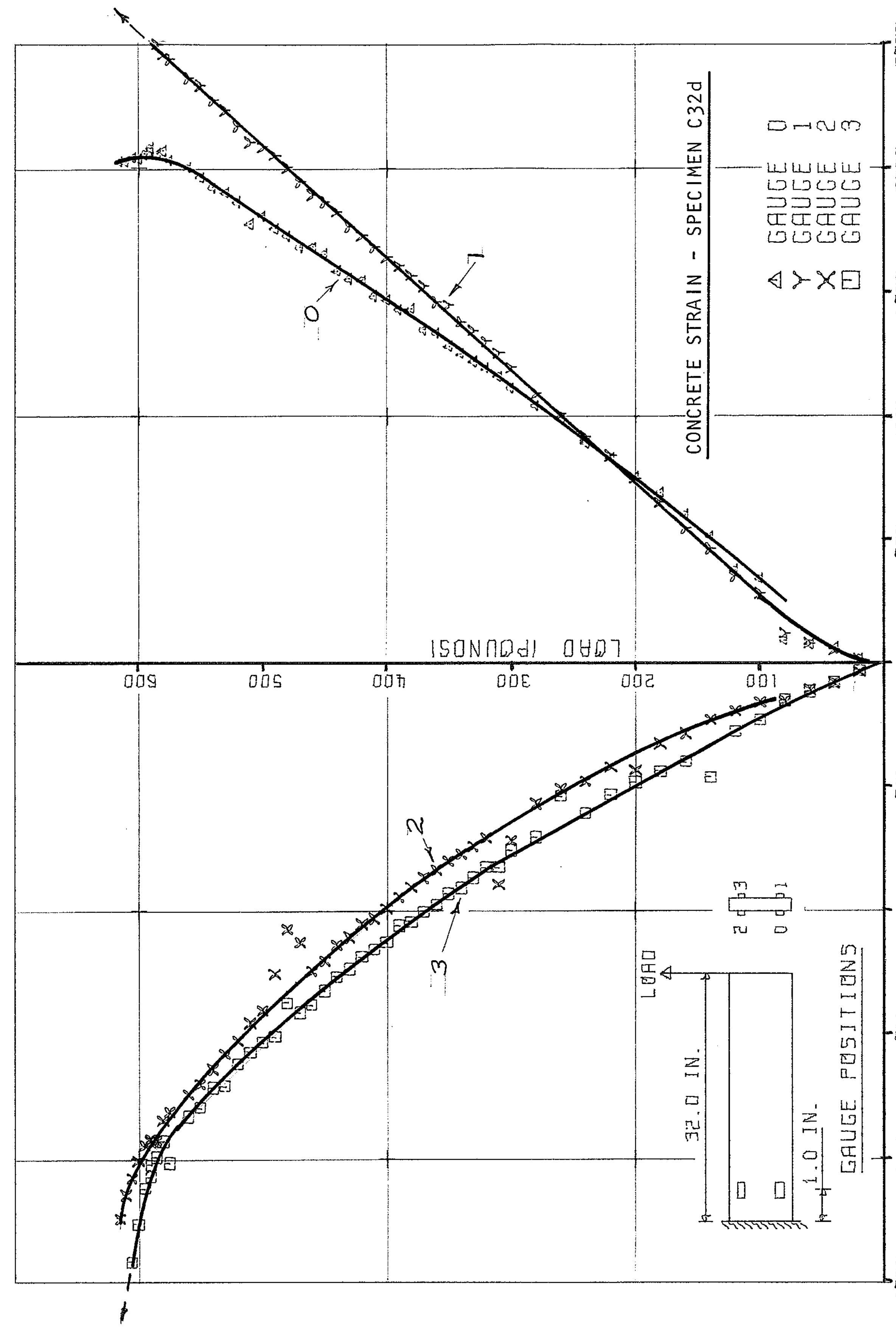
CONCRETE STRAIN - SPECIMEN C32d
GAUGE 0
GAUGE 1
GAUGE 2
GAUGE 3
LOAD (POUNDS)
STRAIN (MICROINCHES/INCH)
600
500
400
300
200
100
-2500
-2000
-1500
-1000
-500
500
1000
1500
2000
2500
0
1
2
3
LOAD
32.0 IN.
1.0 IN.
GAUGE POSITIONS

FIGURE A.56

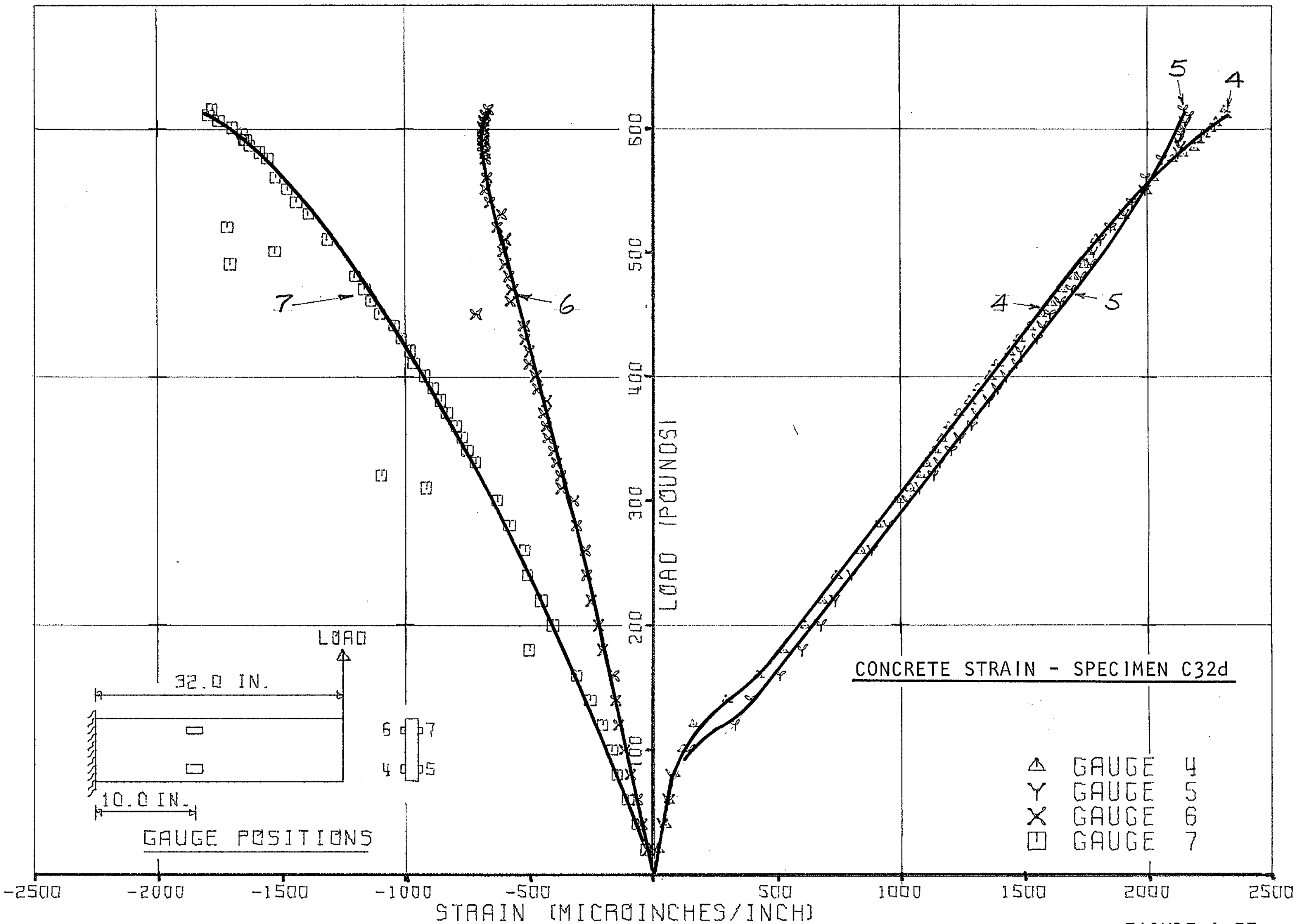
CONCRETE STRAIN - SPECIMEN C32d
LOAD (POUNDS)
STRAIN (MICROINCHES/INCH)
-2500
-2000
-1500
-1000
-500
500
1000
1500
2000
2500
100
200
300
400
500
600
GAUGE 4
GAUGE 5
GAUGE 6
GAUGE 7
GAUGE POSITIONS
LOAD
32.0 IN.
10.0 IN.
6
7
4
5
7
6
4
5
5
4

FIGURE A.57

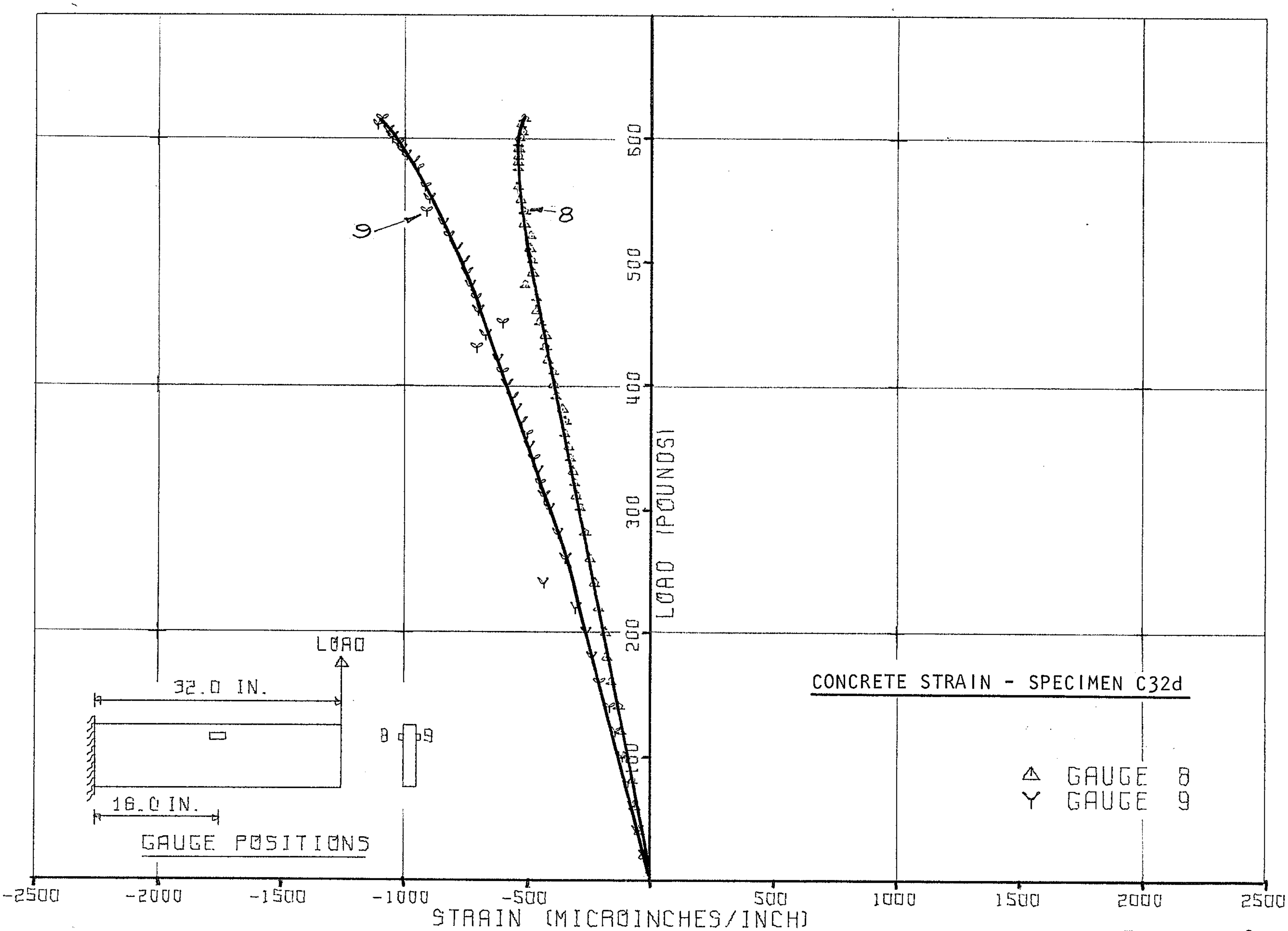
CONCRETE STRAIN - SPECIMEN C32d
GAUGE 8
GAUGE 9
LOAD (POUNDS)
STRAIN (MICROINCHES/INCH)
LOAD
32.0 IN.
16.0 IN.
GAUGE POSITIONS
8
9
-2500
-2000
-1500
-1000
-500
500
1000
1500
2000
2500
100
200
300
400
500
600

FIGURE A.58